

Matrix-Isolation Infrared Spectroscopy and Computational Studies of Diazine Radicals

Mayank Saraswat

*A thesis submitted for the partial fulfillment of
the degree of Doctor of Philosophy*



Department of Chemical Sciences
Indian Institute of Science Education and Research Mohali
Knowledge city, Sector 81, SAS Nagar, Manauli PO, Mohali 140306, Punjab, India.

June 2021

Dedicated to Mummy, Papa, Bhaiya and Jiji for their love and support

Declaration

The work presented in this thesis has been carried out by me under the guidance of Dr. Sugumar Venkataramani at the Indian Institute of Science Education and Research Mohali. This work has not been submitted in part or in full for a degree, a diploma, or a fellowship to any other university or institute. Whenever contributions of others are involved, every effort is made to indicate this clearly, with due acknowledgement of collaborative research and discussions. This thesis is a bona fide record of original work done by me and all sources listed within have been detailed in the bibliography.

Mayank
Saraswat

10-06-2021

Mayank Saraswat

In my capacity as the supervisor of the candidate's thesis work, I certify that the above statements by the candidate are true to the best of my knowledge.



Dr. Sugumar Venkataramani

Acknowledgements

The research work presented in this thesis would not have been possible without the constant encouragement and support of my supervisor Dr. Sugumar Venkataramani during the complete tenure of my Ph.D. I would like to extend my gratitude to my thesis committee members: Dr. Arijit Kumar De, Dr. P. Balanarayan and Prof. K. S. Viswanathan for their crucial suggestions and ideas during the annual review meetings, and their feedback for scientific problems throughout my Ph.D. which increased the quality of this work. I am grateful to the former Director Prof. N. Sathyamurthy and also to the present Director Prof. J. Gowrishankar for the experimental and computational facilities. My sincere thanks to the former and current Head of Department of Chemical Sciences. A special thanks to Prof. K. S. Viswanathan for his immense help and guidance in the initial stages of setting up the low temperature matrix isolation infrared spectroscopy facility which allowed me to learn a lot not only about the technical aspects but also a general researcher's mind approach to solve various problems. I would also like to thank the faculty members of DCS who have been involved during my coursework here at IISER Mohali. Special mentioned to Dr. S. A. Babu, Dr. R Vijaya Anand, Dr. Sanchita Sengupta and Dr. Jino George for their support during these past years.

Apart from the scientific and professional support, I would like to thank Dr. Sugumar Venkataramani, for taking me on to be a member in his group which provided me the unique opportunity to learn a lot in terms of the non-academic life which I'm sure will serve me well in all my future endeavours. A special mention to Mrs. Manju Bashini for making me feel welcome to her home and her warm encouragement during these past years.

No words can do justice to how grateful I am to my family for their encouragement throughout my MS and Ph.D. journey at IISER Mohali. My mother Manjulata Saraswat and father Vijay Kumar Saraswat who always encouraged me, and my elder sisters Ruchi Saraswat and Amita Saraswat and elder brother Rahul Saraswat who always supported me in all my decisions, and all their guidance and teaching during my school days. Special thanks to my brother Rahul Saraswat for introducing, teaching and for developing my interest in chemistry right from my school days.

I greatly benefited from all my previous and current lab members for maintaining a very happy, healthy and supportive environment. My sincere thanks to all the POC lab Ph.D. members with whom I got to share this wonderful journey: Sudha Devi, Chitranjan Sah, Anjali Mahadevan, Surbhi Grewal, Debapriya Gupta, Ankit Gaur, Pravesh Kumar, Himanshu Kumar, Anjali Srivastava and Sapna Singh. A special thanks to Chitranjan, Surbhi, Debapriya, Ankit, Himanshu and Lilit Jacob with whom I shared a lot of scientific projects. I am particularly excited to have shared the lab space with all the MS thesis students of the POC lab over the years and am grateful

to the friendships that developed with Ajit Yadav, Ankit Somani, Virinder Bhagat, Amandeep Singh, Divanshu Gupta, Lincoln, Hunarpreet Kaur and Harjasnoor Kakkar. I am especially grateful to have worked with Virinder Bhagat and Lincoln during their MS thesis. This thesis has a lot less errors courtesy proofreading and valuable suggestions from Debapriya, Surbhi, Harjasnoor and Hunarpreet whom I am thankful towards.

I am thankful to Dr. Satyam Ravi and Dr. K R Shamasundar to have worked on some exciting problems which allowed me to expand my scientific knowledge vastly. I am also grateful to Dr. Jayashree Nagesh (IISc) for the collaboration opportunity and was lucky to share some great intellectual discussions over the past couple of years. I would like to thank Dr. Bhisma K Patel and Suresh R. (IIT Guwahati) for the opportunity to work together allowing me to apply my scientific skills towards understanding exciting problems.

I am thankful to Kaushalendra Patel for his efforts towards the synthesis of precursors used for experiments. I would like to extend my thanks to Prof. K.S. Viswanathan's lab members and Shalender from Dr. Ananth Venkatesan's lab whose help with vacuum accessories and experimental advice is greatly appreciated.

This long journey would have been a lot harder, had it not been for some great friendships with Samridhi Gambhir, Ayushi Singhanian, Jaskaran Singh, Ankit Verma and Anubhav Preet Kaur. All our walks and canteen/restaurant visits will be lifelong memories. I will forever be indebted to your wonderful and fun camaraderie during this amazing journey. I also thank Vikash Mittal and Poulami Choudhuri for their enjoyable company.

This journey was made a lot more fulfilling courtesy a lot of fun trips, walks and conversations with Bhisem, Nagesh and Bhupinder. I will cherish all my memories with you. Special thanks to Pankaj Dubey who never fails to make any conversation livelier and entertaining, and I'm grateful for all the academic discussions we had over the years. I am also thankful to have shared the company of Kaushalendra and express my gratitude for his help during experimental runs, especially during the lockdown period. I am grateful for my friendship with Shradha Sapru during the last couple of years during my Ph.D.

Thank you to the Chemistry PhD cricket team members for helping me feel refreshed every time I needed so.

I would like to thank IISER Mohali for providing the infrastructure and facilities which made this work possible. Additionally, I would like to thank the Library, IISER Mohali, for providing valuable academic resources. I also acknowledge the financial support from CSIR and DST during my Ph.D.

Last but not the least, I am extremely grateful to Divita Gupta for her support and encouragement during my Ph.D.

List of Publications (thesis work)

- **Mayank Saraswat**, Satyam Ravi, K R Shamasundar* and Sugumar Venkataramani* “Photochemistry of 3,6-didehydropyridazine, the traceless para benzyne analogue through combined matrix isolation and computations” (manuscript under preparation)
- **Mayank Saraswat** and Sugumar Venkataramani* “Photochemistry of 2-iodopyrazine and 2-iodopyrimidine using matrix-isolation infrared spectroscopy” (manuscript under preparation)
- **Mayank Saraswat**, Satyam Ravi, K R Shamasundar* and Sugumar Venkataramani* “Electronic structures studies of didehydrodiazine diradicals” (manuscript under preparation)
- **Mayank Saraswat** and Sugumar Venkataramani* “Thermal unimolecular reactivity pathways in dehydro-diazines radicals” *J Phys Org Chem.* **2020**; e4152.
- **Mayank Saraswat** and Sugumar Venkataramani* “Through bond and through space interactions in dehydrodiazine radicals: a case study of 3c-5e interactions” *Phys. Chem. Chem. Phys.* **2018**, 20, 4386–4395.

Publications from contributory projects

- Chitranjan Sah[‡], **Mayank Saraswat**[‡], Lilit Jacob, Sugumar Venkataramani* “Insights on unimolecular and bimolecular reactivity patterns of pyridyl, pyridyl-N-oxide, and pyridinyl radicals through spin density” *Comp. Theo. Chem.* **2020**, 1191, 113025–113035.
- Chitranjan Sah[‡], Lilit Jacob[‡], **Mayank Saraswat**[‡], Sugumar Venkataramani* “Does Nitrogen Lone Pair Lead to Two Centered - Three Electrons (2c-3e) Interactions in Pyridyl Radical Isomers?” *J. Phys. Chem. A.* **2017**, 121, 3781–3791.
- Sudha Devi[‡], **Mayank Saraswat**[‡], Surbhi Grewal[‡], Sugumar Venkataramani* “Evaluation of Substituent Effect in Z-Isomer Stability of Arylazo-1H-3,5-dimethylpyrazoles – Interplay of Steric, Electronic Effects and Hydrogen Bonding” *J. Org. Chem.*, **2018**, 83, 8, 4307–4322.
- Sudha Devi[‡], Ankit Kumar Gaur[‡], Debapriya Gupta[‡], **Mayank Saraswat**[‡], Sugumar Venkataramani* “Tripodal N-Functionalized Arylazo-3,5-dimethylpyrazole Derivatives of Trimesic Acid: Photochromic Materials for Rewritable Imaging Applications” *ChemPhotoChem*, **2018**, 2, 806–810.
- Surbhi Grewal, Saonli Roy, Himanshu Kumar, **Mayank Saraswat**, Naimat K Bari, Sharmistha Sinha*, Sugumar Venkataramani* “Temporal control in tritylation reactions through light-driven variation in chloride ion binding catalysis – A proof of concept” *Catal. Sci. Technol.*, **2020**, 10, 7027–7033.

Book chapter contribution

- Surbhi Grewal[‡], Debapriya Gupta[‡], Ankit Kumar Gaur[‡], **Mayank Saraswat**[‡], and Sugumar Venkataramani* “Azoheteroarene photoswitches – Synthesis, Photoswitching and Utility” book chapter in “Photoisomerization: Causes, Behavior and Effects” Ed.; Diego Sampedro, Nova Publishers, USA, **2019**.

Contents

List of Abbreviations

List of Figures

List of Tables

List of Schemes

Abstract

Chapter 1. Introduction	3
1.1 Free radicals	3
1.2 Classification of free radicals	4
1.3 Importance of free radicals	5
1.3.1 Importance of free radicals in organic synthesis	6
1.3.2 Importance of free radicals in atmospheric chemistry	7
1.3.3 Importance of free radicals in biological process	8
1.3.4 Importance of free radicals in interstellar chemistry.....	9
1.4 General methods for generating free radicals	10
1.4.1 Photolysis	10
1.4.2 Flash vacuum pyrolysis (FVP)	11
1.5 General methods for characterization of free radicals	11
1.6 Importance of <i>N</i> -heterocyclic radicals	13
1.7 Diazines	13
1.8 Literature reports on diazines	14
1.8.1 Experimental reports on diazines	14
1.8.2 Computational reports on diazines	17
1.9 Aim of the thesis	19
1.10 Structure of the thesis	19
1.11 References	23
 Chapter 2. Electronic structure and reactivity studies dehydrodiazine radicals	30
2.1 First C-H bond dissociation energy of dehydrodiazine radicals	31
2.2 Relative thermodynamic stability diazines and dehydrodiazine radicals	32
2.3 Radical stabilization energy of dehydrodiazine radicals	35
2.4 Geometrical parameters of dehydrodiazine radicals	36
2.5 Spin densities of dehydrodiazine radicals	38

2.6	Electrostatic potential of dehydrodiazine radicals	39
2.7	Natural bond orbital analysis of dehydrodiazine radicals	40
2.8	Molecular orbitals analysis of dehydrodiazine radicals	43
2.9	Proton affinities of dehydrodiazine radicals	45
2.10	AIM analysis of dehydrodiazine radicals	46
2.11	Isotropic hyperfine coupling constants of dehydrodiazine radicals	47
2.12	Summary of electronic structure of dehydrodiazine radicals	48
2.13	Reactivity studies of isomeric dehydrodiazines radicals	51
2.14	Isomerization through 1,2-H shift in dehydrodiazine radicals	52
2.15	Unimolecular decomposition channels of dehydrodiazine radicals	53
2.15.1	Unimolecular decomposition channels of 2-dehydropyrimidine (1a)..	53
2.15.2	Unimolecular decomposition channels of 4-dehydropyrimidine (1b)..	55
2.15.3	Unimolecular decomposition channels of 5-dehydropyrimidine (1c) ..	56
2.15.4	Unimolecular decomposition channels of 2-dehydropyridazine (2a) ..	58
2.15.5	Unimolecular decomposition channels of 3-dehydropyridazine (2b) ..	59
2.15.6	Unimolecular decomposition channels of 2-dehydropyrazine (3a)	61
2.16	Overall reactivity of dehydrodiazine radicals (1a–c , 2a–b and 3a)	62
2.17	Summary of reactivity studies of dehydrodiazine radicals	65
2.18	References	66

Chapter 3. Matrix-isolation FTIR spectroscopic studies of 2-iodopyrazine (46) and 2-iodopyrimidine (48)	67
3.1 Introduction	67
3.2 Matrix isolation FTIR spectroscopic study of 2-dehydropyrazine radical (3a)	68
3.3 Deposition of 2-iodopyrazine (46)	68
3.4 Photochemistry of 2-iodopyrazine (46)	68
3.5 Photochemistry of 2-dehydropyrazine radical (3a), ring-opening and ring-fragmentation	72
3.6 Matrix-isolation FTIR spectroscopic study of 2-dehydropyrimidine radical (1a)	75
3.7 Deposition of 2-iodopyrimidine (48)	75
3.8 Photochemistry of 2-iodopyrimidine (48)	75
3.9 Photochemistry of 2-dehydropyrimine radical (1a), ring-opening and ring-fragmentation	78

3.10	Analysis of ring-opening species (Z)/(E)- 17 , (Z)/(E)- 26 and (Z)/(E)- 42 (diazine analogues of enediyne)	79
3.11	Ring-opening and ring-fragmented products and radical intermediates from 2-dehydropyrimidine (1a)	83
3.11.1	Formation of first ring-opening radical intermediate 50 from 2-dehydropyrimidine radical (1a)	83
3.11.2	Formation of ring-opening products (Z)/(E)- 17 from of ring-opening radical intermediate 50	83
3.11.3	<i>Cis-trans</i> (Z-E) isomerization in (Z)/(E)- 26 and (Z)/(E)- 17 obtained from 2-dehydropyrimidine radical (1a) upon irradiation at 254 nm.	85
3.11.4	Formation of ring-opening radical intermediate 41 from 50 via HCN elimination.	85
3.11.5	Formation of ring-fragmented small molecules HCCNC, HCCCN, HCCH and CN radical from the ring-opening radical intermediate 41	87
3.11.6	Formation of second ring-opening radical intermediate 4 from 2-dehydropyrimidine radical (1a).	88
3.11.7	Formation of ring-opening products (Z)/(E)- 10 from of ring-opening radical intermediate 4	88
3.12	Ring-opening and ring-fragmented products and radical-intermediates from 2-dehydropyrazine radical (3a)	89
3.12.1	Formation of ring-opening products (Z)/(E)- 42 from 2-dehydropyrazine radical (3a).	89
3.12.2	Formation of first ring-opening radical intermediate 40 from 2-dehydropyrazine radical (3a).	90
3.12.3	Formation of ring-opening products (Z)/(E)- 42 from the ring-opening radical intermediate 40	91
3.12.4	Formation of ring-opening radical intermediate 41 from 40 via HCN elimination.	92
3.12.5	Formation of second ring-opening radical intermediate 38 from 2-dehydropyrazine radical (3a).	92
3.12.6	Formation of ring-opening products (Z)/(E)- 37 from the ring-opening radical intermediate 38	93
3.12.7	Formation of ring-opening radical intermediate 19 from 38 via HCN elimination.	93
3.13	Summary of photochemistry of 2-iodopyrimidine	95
3.14	Summary of photochemistry of 2-iodopyrazine	97
3.15	References	99
 Chapter 4 Matrix Isolation FTIR Spectroscopic studies of 3,6-diiodopyridazine and 4,6-diiodopyrimidine		
4.1	Deposition of 3,6-diiodopyridazine (52)	101

4.2	Photochemistry of 3,6-diiodopyridazine (52)	101
4.3	Computational analysis and mechanistic aspects	104
4.4	Photoisomerization of (<i>Z</i>)- 26 to (<i>E</i>)- 26	110
4.5	Summary of photochemistry of 3,6-diiodopyridazine (52)	115
4.6	Deposition of 4,6-diiodopyrimidine (63)	116
4.7	Photochemistry of 4,6-diiodopyrimidine (63)	116
4.8	Summary of photochemistry of 4,6-diiodopyrimidine (63)	117
4.9	References	118
Chapter 5. Electronic structure of didehydrodiazine biradicals		119
5.1	Introduction	119
5.2	Didehydrodiazine biradicals and nomenclature used	120
5.3	Active space for CASSCF calculations	121
5.4	Singlet-triplet energy gaps through vertical excitation and adiabatic energies gaps	121
	5.4.1 Vertical excitation energy gaps	122
	5.4.2 Adiabatic excitation energy gaps	123
5.5	Geometrical parameters of didehydropyrimidine and didehydropyridazine biradicals	125
5.6	Molecular orbitals analysis of didehydrodiazines	129
5.7	Spin densities of triplet didehydrodiazines	134
5.8	Atoms-in-molecules analysis of didehydrodiazines	134
5.9	Summary of electronic structure of didehydrodiazine biradicals	138
5.10	References	139
Chapter 6 Summary and outlook		140
	6.1 Summary	140
	6.2 Outlook for future	144
Chapter 7 Materials and methods		146
7.1	General introduction of matrix-isolation	146
	7.1.1 Matrix-isolation experiment procedure and set-up	147
	7.1.2 Gas phase generation of unstable species	147
	7.1.3 <i>In situ</i> generation of unstable species	147

7.1.4	Host materials for matrix-isolation spectroscopy	148
7.1.5	Deposition of precursor (guest) molecules	148
7.1.6	Photochemistry and detection of unstable species	149
7.1.7	Matrix-isolation FTIR spectroscopy set up in our lab at IISER Mohali	149
7.2	Computational details	154
7.2.1	Basic quantum chemistry approach	154
7.2.2	Levels of theory (methods) used in this work	154
7.2.3	Basis sets used in this work	155
7.2.4	Geometry optimization and frequency calculations	155
7.2.5	Spin density and molecular orbitals	155
7.2.6	Natural bond orbital (NBO) Analysis	156
7.2.7	Atoms in molecules (AIM) Analysis	157
7.2.8	Multireference Methods	157
7.3	References	158
Appendix		160

List of Abbreviations

AE	Adiabatic Excitation Energy
AIM	Atoms in Molecules
BDE	Bond Dissociation Energy
B3LYP	Becke, 3-parameter, Lee–Yang–Parr Functional
cc-pVTZ	Correlation Consistent Polarized Valance Triple-Zeta Basis set
CIs	Configuration Interactions
CASSCF	Complete Active Space Self Consistent Field
CCSD	Coupled Cluster Singles and Doubles
CSF	Configuration State Functions
DFT	Density Functional Theory
ESP	Electrostatic Potential
FVP	Flash Vacuum Pyrolysis
HF	Hartree-Fock
HOMO	Highest Occupied Molecular Orbital
IRC	Intrinsic Reaction Coordinate
LUMO	Lowest Unoccupied Molecular Orbital
MCSCF	Multi Configuration Self Consistent Field
MECI	Minimum Energy Conical Intersection
M06-2X	Minnesota functional released in 2006 with 54 % of HF exchange
NBO	Natural Bond Orbital
PA	Proton Affinity
PES	Potential Energy Surface
RSE	Radical Stabilization Energy
SOMO	Singly Occupy Molecular Orbital
TS	Through Space
TB	Through Bond
VE	Vertical Excitation Energy
ZPVE	Zero Point Vibrational Energy

List of Figures

Figure 1.1	National historic chemical landmark for the isolation and discovery of the first ‘free radical’ by Moses Gomberg.....	3
Figure 1.2	Representative description of photolysis method for generating free radicals.....	11
Figure 1.3	Representative description of flash vacuum pyrolysis (FVP).....	11
Figure 2.1	Bond dissociation energies corresponding to the first C–H bond of the isomeric diazine molecules (1–3) leading to the dehydrodiazine radicals (1a–c , 2a–b and 3a)	32
Figure 2.2	Optimized geometries of three parent diazines (1–3) and their respective six dehydrodiazine radical isomers (1a–c , 2a–b and 3a). The most important bond distances (in Å units) and the bond angles (in degrees) at the radical centres are mentioned.....	37
Figure 2.3	Spin densities of dehydropyrimidine (1a–c), pyridazine (2a–b) and pyrazine (3a) radicals	38
Figure 2.4	Electrostatic potential mapping of three parent diazines (1–3) and their respective six dehydrodiazine radical isomers (1a–c , 2a–b and 3a)	39
Figure 2.5	Natural and Mulliken charges of three parent diazines (1–3) and their respective six dehydrodiazine radical isomers (1a–c , 2a–b and 3a)	40
Figure 2.6	Molecular orbitals of six dehydrodiazine radical isomers (1a–c , 2a–b and 3a) using multiconfigurational CASSCF method	44
Figure 2.7	Proton affinities of three parent diazines (1–3) and their respective six dehydrodiazine radical isomers (1a–c , 2a–b and 3a)	46
Figure 2.8	AIM analysis at (U)B3LYP/cc-pVTZ level of the three parent diazines (1–3) and their respective six dehydrodiazine radical isomers (1a–c , 2a–b and 3a) showing bond critical and ring critical points	47
Figure 2.9	Isomerization through 1,2-H shift in isomeric (a) dehydropyrimidine (1b and 1c), (b) dehydropyrazine (3a), and (c) dehydropyridazine (2a and 2b) radicals	52
Figure 2.10	Unimolecular decomposition channels of 2-dehydropyrimidine (1a) radical	54
Figure 2.11	IRC analysis for 2-dehydropyrimidine (1a) radical unimolecular dissociation channels	54
Figure 2.12	Unimolecular decomposition channels of 4-dehydropyrimidine (1b) radical	55
Figure 2.13	IRC analysis for 4-dehydropyrimidine (1b) radical unimolecular dissociation channels	56
Figure 2.14	Unimolecular decomposition channels of 5-dehydropyrimidine (1c) radical	57
Figure 2.15	IRC analysis for 5-dehydropyrimidine (1c) radical unimolecular dissociation channels	57
Figure 2.16	Unimolecular decomposition channels of 3-dehydropyridazine (2a) radical	58

Figure 2.17	IRC analysis for 3-dehydropyridazine (2a) radical unimolecular dissociation channels	59
Figure 2.18	Unimolecular decomposition channels of 4-dehydropyridazine (2b) radical	60
Figure 2.19	IRC analysis for 4-dehydropyridazine (2b) radical unimolecular dissociation channels	60
Figure 2.20	Unimolecular decomposition channels of 2-dehydropyrazine (3a) radical	61
Figure 2.21	IRC analysis for 2-dehydropyrazine (3a) radical unimolecular dissociation channels	62
Figure 2.22	Summary of the unimolecular ring decomposition and fragmentation channels of six isomeric dehydro-diazine radicals (1a-c , 2a-b and 3a) ...	64
Figure 3.1	Matrix-isolated IR spectrum of 2-dehydropyrazine radical (3a) (Ar, 4K).	69
Figure 3.2	Matrix-isolated IR spectrum of 2-dehydropyrimidine radical (1a) (Ar, 4K)	76
Figure 3.3	Ring-opened species (<i>Z</i>)/(<i>E</i>)- 17 , (<i>Z</i>)/(<i>E</i>)- 26 and (<i>Z</i>)/(<i>E</i>)- 42 from 2-dehydropyrazine radical (3a) and 2-dehydropyrimidine radical (1a)	82
Figure 3.4	Photochemistry of 2-dehydropyrimidine radical (1a) (Ar, 4 K) in the region of 2050–2205 cm ⁻¹	86
Figure 3.5	Photochemistry of 2-dehydropyrimidine radical (1a) and 2-dehydropyrazine radical (3a) in acetylenic C-H stretching region (Ar, 4 K)	94
Figure 3.6	Photochemistry of ring-opened and ring-fragmented products, and intermediates from of 2-dehydropyrimidine radical (1a) at 254 nm irradiation	96
Figure 3.7	Photochemistry of ring-opened and ring-fragmented products, and intermediates from of 2-dehydropyrazine radical (3a) at 254 nm irradiation.....	98
Figure 4.1	Photochemistry of 3,6-diiodopyridazine 52 (Ar, 4 K)	102
Figure 4.2	Optimized geometry (B3LYP/cc-pVTZ) and molecular orbitals (CASSCF/cc-pVDZ) of pyridazine 2 , dehydropyridazine radical 2a and didehydropyridazine biradical 56	105
Figure 4.3	Optimized geometry and molecular orbitals of maleonitrile (<i>Z</i>)- 26 at B3LYP/cc-pVTZ level of theory	106
Figure 4.4	Potential energy surfaces involving biradical 56 and the two possible ring-opening products (<i>Z</i>)- 57 , and (<i>Z</i>)- 26 at B3LYP/cc-pVTZ level of theory	107
Figure 4.5	Thermal ring-opening channels in 2,5-didehydropyridine (60) and <i>p</i> -benzyne (58) at (U)B3LYP/cc-pVTZ and (U)M06-2X/cc-pVTZ levels of theory	109
Figure 4.6	CASSCF(6,5)/cc-pVDZ geometries (in Å) for the S ₀ - <i>Z</i> - 26 , S ₁ - <i>Z</i> - 26 and S ₁ /S ₀ -MECI- <i>Z</i> - 26	111

Figure 4.7	The gradient difference (g) and derivative coupling (h) vectors of S_1/S_0 -MECI-(Z)- 26 , around the minimum energy conical intersection (MECI), at CASSCF(6,5)/cc-pVDZ level of theory	113
Figure 4.8	Potential energy curves along the isomerization of (Z)- 26 into (E)- 26 at CASSCF(6,5)/cc-pVDZ level of theory	114
Figure 4.9	Relative energies of S_0 and S_1 states with respect to FC structures towards the MECI geometry	115
Figure 4.10	Photochemistry of 4,6-diiodopyrimidine 63 (Ar, 4 K)	117
Figure 5.1	Representation of vertical and adiabatic excitation energies gap	121
Figure 5.2	Energy profiles of optimized geometries in singlet and triplet state corresponding to didehydropyrimidine and didehydropyridazine biradicals at CASSCF (12,10)/cc-pVTZ level of theory	123
Figure 5.3	Optimized geometries of the triplet states of didehydropyrimidine biradical isomer 1-m-(2,4) and didehydropyridazine biradical isomer 2-p-(3,6) at (U)B3LYP/cc-pVTZ, (U)M06-2X/cc-pVTZ and CASSCF/cc-pVTZ level of theory	126
Figure 5.4	Optimized geometries of the didehydropyrimidine biradical isomers and its parent compound pyrimidine at (U)B3LYP/cc-pVTZ, (U)M06-2X/cc-pVTZ and CASSCF/cc-pVTZ level of theory	127
Figure 5.5	Optimized geometries of the didehydropyridazine biradical isomers and its parent compound pyridazine at (U)B3LYP/cc-pVTZ, (U)M06-2X/cc-pVTZ and CASSCF/cc-pVTZ level of theory	128
Figure 5.6	Molecular orbitals corresponding to the active space (12 electron, 10 orbitals) of the didehydropyrimidine biradical isomers (1-m-(2,4) triplet state and 1-p-(2,5) in singlet and triplet state) using multiconfigurational CASSCF/cc-pVTZ level of theory	130
Figure 5.7	Molecular orbitals corresponding to the active space (12 electron, 10 orbitals) of the didehydropyrimidine biradical (1-o-(4,5) and 1-m-(4,6) in singlet and triplet state) isomers using multiconfigurational CASSCF/cc-pVTZ level of theory	131
Figure 5.8	Molecular orbitals corresponding to the active space (12 electron, 10 orbitals) of the didehydropyridazine biradical isomers (2-o-(3,4) and 2-m-(3,5) in singlet and triplet state) using multiconfigurational CASSCF/cc-pVTZ level of theory	132
Figure 5.9	Molecular orbitals corresponding to the active space (12 electron, 10 orbitals) of the didehydropyridazine diradical isomers (2-p-(3,6) triplet state and 2-o-(4,5) in singlet and triplet state) using multiconfigurational CASSCF/cc-pVTZ level of theory	133
Figure 5.10	Spin densities of didehydropyrimidine and didehydropyridazine biradicals in their triplet state at (U)B3LYP/cc-pVTZ and (U)M06-2X/cc-pVTZ levels of theory	134

Figure 5.11	AIM analysis of the pyrimidine and didehydropyrimidine biradical isomers with bond critical and ring critical points at (U)B3LYP/cc-pVTZ level of theory	135
Figure 5.12	AIM analysis of the pyridazine and didehydropyridazine biradical isomers with bond critical and ring critical points at (U)B3LYP/cc-pVTZ level of theory	136
Figure 5.13	AIM analysis of the pyrazine and didehydropyrazine biradical isomers with bond critical and ring critical points at (U)B3LYP/cc-pVTZ level of theory	137
Figure 6.1	Summary of electronic structure and unimolecular ring decomposition channels of six-dehydrodiazine radicals	141
Figure 6.2	Overall summary of the work	144
Figure 7.1	Images of each component of matrix-isolation setup.....	151
Figure 7.2	Remaining parts of matrix-isolation setup	152
Figure 7.3	Matrix-isolation FTIR facility in our lab at IISER Mohali	153

List of Tables

Table 2.1	Relative energies of all the diazines (1–3) at different levels of theory	33
Table 2.2	Relative energies of dehydrodiazine radical isomers (1a–c , 2a–b and 3a) at different levels of theory	34
Table 2.3	Radical stabilization energies (RSEs in kcal/mol) of the isomeric dehydrodiazines radicals (1a–c , 2a–b and 3a) through isodesmic reactions at different levels of theory	36
Table 2.4	The second order perturbation energies (in kcal/mol) from the natural bond orbital (NBO) analysis of dehydrodiazine radical isomers (1a–c , 2a–b and 3a)	42
Table 2.5	Isotropic hyperfine coupling constant (in Gauss) of two ¹⁴ N atoms and ¹³ C radical centres for all the six isomeric dehydrodiazine radicals (1a–c , 2a–b and 3a) at (U)B3LYP/EPR-III level of theory	48
Table 2.6	Free energy, enthalpy and entropy of activation (ΔG^\ddagger , ΔH^\ddagger and ΔS^\ddagger) at 298 K for all the reaction steps in the unimolecular dissociation channels.	63
Table 3.1	Computed harmonic vibrational frequencies (U)B3LYP/cc-pVTZ) and experimental IR spectroscopic data (Ar and N ₂ matrices, 4 K) of 2-dehydropyrazine radical (3a)	70
Table 3.2	Computed harmonic vibrational frequencies (U)B3LYP/cc-pVTZ) and experimental IR spectroscopic data (Ar and N ₂ matrices, 4 K) of 2-dehydropyrimidine radical (1a).	77
Table 3.3	Characteristic vibrational normal modes of ring-opened products (<i>Z</i>)/(<i>E</i>)– 17 , (<i>Z</i>)/(<i>E</i>)– 26 and (<i>Z</i>)/(<i>E</i>)– 42 and their intensities	81
Table 4.1	Change in thermodynamic parameters of thermal ring-opening channels in 2,5-didehydropyridine (60) and <i>p</i> -benzyne (58) at (U)B3LYP/cc-pVTZ and (U)M06-2X/cc-pVTZ levels of theory	109
Table 4.2	The vertical excitation energies of maleonitrile and fumaronitrile at different levels of theory	111
Table 4.3	Bond angles and dihedral angles (in deg) corresponding to the S ₀ , S ₁ , and S ₁ /S ₀ -MECI geometries of (<i>Z</i>)– 26 from the CASSCF(6,5)/cc-pVDZ level of theory	112
Table 5.1	Vertical excitation and adiabatic energy gaps of didehydrodiazines biradicals (in kcal/mol) at CASSCF(12,10)/cc-pVTZ level of theory	124

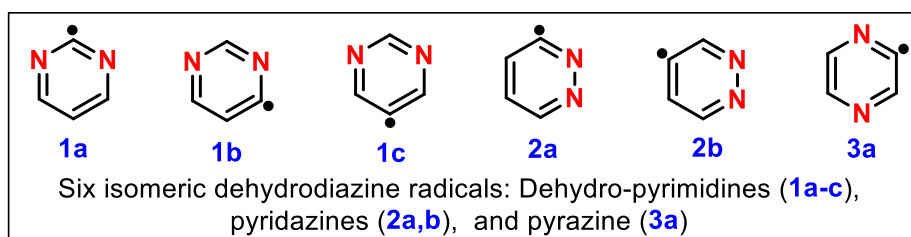
List of Scheme

Scheme 1.1	Classification of free radicals based on (a) orbitals occupancy, (b) number of unpaired electrons, (c) radical reactivity, and (d) spin polarization	5
Scheme 1.2	Representative examples for the characterization of reactive intermediates and unstable species	12
Scheme 1.3	Diazine based molecules relevant to biological and medicinal chemistry.....	14
Scheme 1.4	Three isomeric diazines (1–3) and six-isomeric dehydrodiazine (1a–c , 2a–b and 3a) radicals	19
Scheme 1.5	Organization of the thesis	22
Scheme 2.1	Three parent diazines (1–3) and their respective six dehydrodiazine radical isomers (1a–c , 2a–b and 3a)	30
Scheme 2.2	Illustration of possible reaction channels in isomeric dehydrodiazine radicals (1a–c , 2a–b and 3a)	51
Scheme 3.1	Isomerization under photochemical condition: (a) transposition of pyrazine into pyrimidine; (b) Isomerization of methyl pyrazine to methyl pyrimidines; (c) 2-iodopyrazine into iodopyrimidines; and (d) 2-dehydropyrazine radical into dehydropyrimidines radicals	72
Scheme 3.2	Possible ring-opening channels in 2-dehydropyrazine radical (3a)	73
Scheme 3.3	Possible ring-opening channels in 2-dehydropyrimidine radical (1a) ..	78
Scheme 3.4	Possible common ring-opened products of 2-dehydropyrazine radical (3a) and 2-dehydropyrimidine radical (1a)	80
Scheme 3.5	Formation of first ring-opened radical intermediate 50 from 2-dehydropyrimidine radical (1a)	83
Scheme 3.6	Formation of ring-opened products (<i>Z</i>)/(<i>E</i>)– 17 from of ring-opening radical intermediate 50	83
Scheme 3.7	<i>Cis-trans</i> (<i>Z-E</i>) isomerization in ring-opened products obtained from <i>m</i> -benzyne, <i>p</i> -benzyne and 3,5-pyridyne	84
Scheme 3.8	<i>Cis-trans</i> (<i>Z-E</i>) isomerization in (<i>Z</i>)/(<i>E</i>)– 26 and (<i>Z</i>)/(<i>E</i>)– 17 obtained from 2-dehydropyrimidine radical (1a) upon irradiation at 254 nm	85
Scheme 3.9	Formation of ring-opened radical intermediate 41 from 50 via HCN elimination	85
Scheme 3.10	Formation of ring-fragmented small molecules HCCNC, HCCCN, HCCH and CN radical from the ring-opening radical intermediate 41 .	87
Scheme 3.11	Formation of second ring-opened radical intermediate 4 from 2-dehydropyrimidine radical (1a)	88
Scheme 3.12	Formation of ring-opened products (<i>Z</i>)/(<i>E</i>)– 10 from of ring-opening radical intermediate 4	88
Scheme 3.13	Formation of ring-opened products (<i>Z</i>)/(<i>E</i>)– 42 from 2-dehydropyrazine radical (3a)	89

Scheme 3.14	Formation of first ring-opened radical intermediate 40 from 2-dehydropyrazine radical (3a)	90
Scheme 3.15	Formation of ring-opened products (<i>Z</i>)/(<i>E</i>)– 42 from the ring-opening radical intermediate 40	91
Scheme 3.16	Formation of ring-opened radical intermediate 41 from 40 via HCN elimination	92
Scheme 3.17	Formation of second ring-opened radical intermediate 38 from 2-dehydropyrazine radical (3a)	92
Scheme 3.18	Formation of ring-opened products (<i>Z</i>)/(<i>E</i>)– 37 from the ring-opening radical intermediate 38	93
Scheme 3.19	Formation of ring-opened radical intermediate 19 from 38 via HCN elimination	93
Scheme 3.20	Observed photochemistry and ring-opened channels in 2-dehydropyrimidine radical (1a)	95
Scheme 3.21	Observed photochemistry and ring-opened channels in 2-dehydropyrazine radical (3a)	97
Scheme 4.1	The <i>meta</i> -and <i>para</i> -benzyne and their pyridine and diazine analogues with various possible orbital interactions	100
Scheme 4.2	Bergman cyclization and retro-Bergman cyclization in (a) <i>para</i> -Benzyne, (b) 2,5- didehydropyridine, (c) 3,6-didehydropyridazine.....	103
Scheme 4.3	Photochemistry of 3,6-diiodopyridazine 52	103
Scheme 4.4	Photochemistry of 4,6-diiodopyrimidine 63	117
Scheme 5.1	Diazines (pyrimidine 1 , pyridazine 2 and pyrazine 3), and their possible biradicals	120
Scheme 5.2	Ring-opening of 2,4-didehydropyrimidine 1-m-(2,4) and 3,6-didehydropyridazine 2-p-(3,6) biradicals in their singlet state	123
Scheme 5.3	Didehydropyrimidine and didehydropyridazine biradicals and possible interactions which influence the stability of singlet and triplet state	138

Abstract

Free radicals, in general, are highly reactive and short-lived chemical entities (intermediates) containing one or more unpaired electrons. Their importance is felt in many fields such as organic synthesis, biochemistry, medicinal chemistry, polymer chemistry, atmospheric chemistry, and interstellar chemistry, etc. Various strategies and methods have been adapted to tune and control the stability and in turn, reactivity of radicals that include the introduction of various heteroatoms that can be stabilizing/destabilizing the radicals. Recently, the studies on nitrogen-based heterocyclic radicals gained importance, as these moieties constitute the main building block of several biological systems (like nucleobases, amino acids, etc.), biologically active drug molecules, and are also potential precursors in prebiotic chemistry. Among the various *N*-heterocycles, diazines are those containing two nitrogen atoms that can be classified as pyridazine (1,2-diazine), pyrimidine (1,3-diazine), and pyrazine (1,4-diazine) depending on the relative position of the two nitrogens. Of all these diazine derivatives, pyrimidine (1,3-diazine) moiety has a significant role in biological compounds specifically in nucleobases such as cytosine, thymine, and uracil, which are the key building blocks of DNA and RNA.



Given their biological implications and their relevance in radical damage, systematic studies on diazine-based radicals are quite insightful, and equally intriguing from the fundamental point of view. Since all these radicals have one unpaired electron and two nitrogen lone pairs, the nature and strength of possible “3-centered – 5 electrons” (3c-5e) interactions may play a crucial role in their existence or non-existence, and also their inherent reactivity. To address these, we investigated the electronic structure and unimolecular reactivity aspects of these six-isomeric dehydrodiazine radicals using quantum chemical calculations, which provided the importance of through space (TS) and through bond (TB) interactions between the unpaired electron and the lone pair(s). Attempts have also been made towards the experimental characterization of such transient species using the matrix-isolation (MI) technique in combination with infrared spectroscopy and computations. Under photochemical conditions, we have successfully generated dehydro-diazine radicals (2-dehydropyrimidine

and 2-dehydropyrazine radicals from their respective iodo-precursors) in an inert gas matrix at cryogenic conditions (4 K). Moreover, the photochemistry of these diazine radicals has led to the ring-opening and ring-fragmented products, which have relevance in astrochemistry. Interestingly, several nitrogen rich ring-opened products with a molecular formula $C_4H_2N_2$ have been characterized, which are relevant to aza-enediyne antibiotics. Similarly, 4,6-diiodopyrimidine and 3,6-diiodopyridazine have been used to generate didehydrodiazines, which essentially led to ring-opened products. To shed further light on this, electronic structure of didehydrodiazine biradicals (4c-6e interaction) has also been investigated. Overall, the theoretical insights on the dehydro- and didehydrodiazine radicals, and the experimental results including the design of matrix isolation experimental set up will be presented.

Chapter 1. Introduction

1.1 Free radicals

According to IUPAC, free radicals are molecular entities possessing one or more unpaired electron(s) in their atomic orbital.^[1] In the context of physical organic chemistry, the term ‘free’ refers to those species that are not part of radical pairs. In general, free radical species are highly reactive and short lived or transient in nature and share common properties and reactivities. Free radicals can be generated by the homolytic bond dissociation of a covalent bond, in which both the atoms share at least one electron. Such free radicals are considered as the reactive intermediates in many chemical and biological processes.^[2] These radical species can either accept an electron or donate an electron to other molecules, therefore free radical species can also behave like reductants and oxidants.^[3]

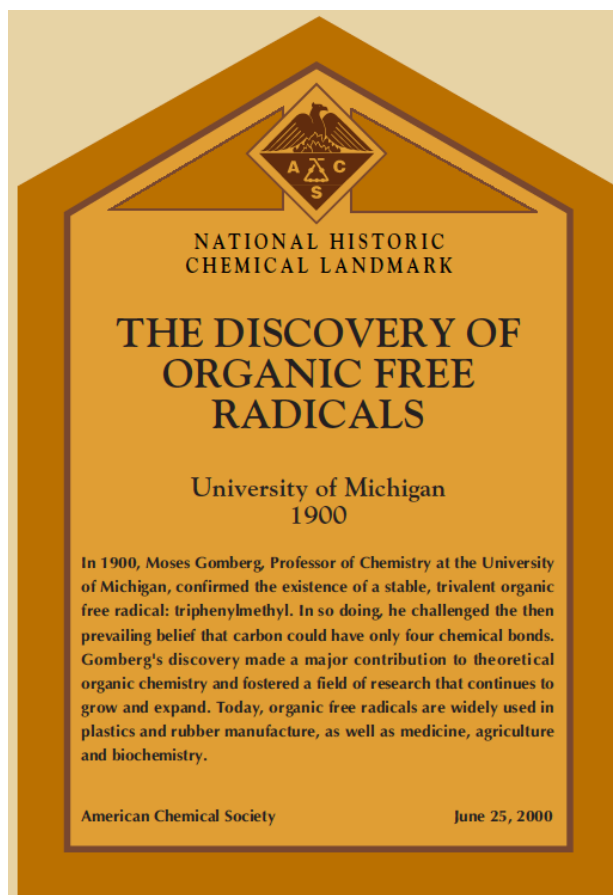


Figure 1.1 National Historic Chemical Landmark for the isolation and discovery of the first ‘free radical’ by Moses Gomberg.

<http://www.acs.org/content/acs/en/education/whatischemistry/landmarks/freeradicals.html>

In 1900, Professor Moses Gomberg discovered the first organic radical, triphenylmethyl (TPM) radical while attempting to prepare the hexaphenylethane from triphenylmethyl chloride via the Wurtz coupling reaction.^[4] Indeed, Gomberg referred to the triphenylmethyl radical as 'Ph₃C', not the familiar 'Ph₃C dot'. (Figure 1.1) Remarkably, the discovery of trivalent carbon radical commenced the fields of electronic structure theory as this was the first reported molecule in which carbon had three valency. This important milestone was declared as a historic chemical landmark by American Chemical Society.

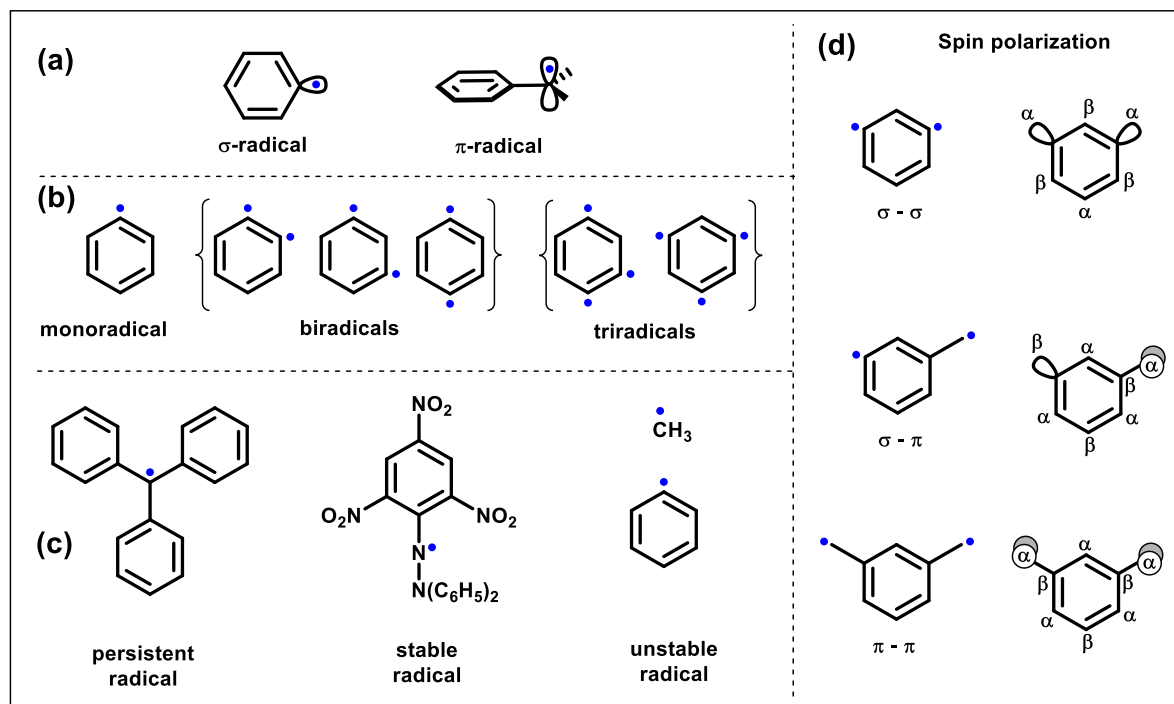
1.2 Classification of free radicals

Since the discovery of TPM radical, the chemistry of free radicals has progressed extensively over the period of time. The generation, understanding, and studies on these reactive species led to the deeper insights in the field of radical chemistry. There are many types of classifications that can be considered for describing the free radicals. For instance, radicals can be classified based on the number of unpaired electrons, unpaired electron orbital occupancy and, also on their reactivity.^[5]

If the unpaired electron occupies an in-plane molecular orbital (within the molecular plane), it is known as σ -radical e.g., phenyl radical. (Scheme 1.1a) On the other hand, if the unpaired electron occupies out-of-plane molecular orbital (perpendicular to the molecular plane) it is classified as π -radical e.g., benzyl radical. Generally, π -radicals are more stable compared to σ -radical due to extra delocalization of unpaired electrons.^[6]

Also, the radical intermediate can be classified based on the number of unpaired electrons. For e.g., radical species with one unpaired electron are known as monoradicals, with two unpaired electrons as biradicals, with three unpaired electrons as triradicals, and, with more than three unpaired electrons are classified as polyradicals.^[7] (Scheme 1.1b) This classification is quite intriguing particularly as the resulting bi-, tri- and polyradicals can attain high spin or low spin depending on the spin-spin interactions, coupling units or spacers between the radical centers, etc.^[8] Species with more than one unpaired electrons can have choice of multiplicity in the ground state such as singlet and triplet in case of biradicals. The low energy or more stable ground state depends upon various factors which include the interaction between two unpaired electrons or orbitals. Several methods have been proposed such as spin polarization to identify or guess the possible ground state in biradical, triradical and polyradicals. (Scheme 1.1d)

In addition to that, radicals can be classified based on their reactivity as persistent, stable and unstable radicals.^[9] Persistent radicals have a significantly high life-time and considerable kinetic stability due to the presence of steric groups present around the radical centre e.g., TPM radical. (Scheme 1.1c)



Scheme 1.1 Classification of free radicals based on (a) orbital occupancy, (b) number of unpaired electrons, (c) radical reactivity, and (d) spin polarization.

Stable radicals have reduced chemical reactivity as they are stabilized due to the extended delocalization of unpaired electrons within molecules e.g., diphenylpicrylhydrazyl radical (DPPH). On the other hand, unstable radicals do not have sufficient kinetic and thermodynamic stability and react very rapidly, and the majority of radicals belong to the class of unstable radicals. (e.g., phenyl radical)

1.3 Importance of free radicals

Based on the wide range of reactivity, selectivity in reactions and stability, radicals are very important in many chemical processes that include biochemical reactions^[10], atmospheric chemistry^[11], combustion chemistry^[12], plasma chemistry^[13] and polymerization reactions^[14] etc., and their importance in few areas have been highlighted separately in the following sections.

1.3.1 Importance of free radicals in organic synthesis

Free radicals are one of the important classes of reactive intermediates from the organic synthesis perspective, which emerged after the first report on “triphenylmethyl (TPM) radical” in 1900.^[4] Indeed, TPM radical had been obtained while attempting to prepare hexaphenylethane from triphenylmethyl chloride via a Wurtz coupling reaction. Since then, numerous reactions have been reported involving free radicals as reactive intermediates, which constituted the radical chemistry. The radical as a reactive intermediate provides various tunable properties and templates desired by synthetic organic chemists. The experimental reaction conditions in radical chemistry are generally neutral and mild, and the reactions are compatible with numerous functional groups, especially polar entities such as alcohols, carboxylic acids, etc., that often require protections under other reaction conditions. Even though radicals are considered highly reactive species, the reaction rates span several orders of magnitude, and a remarkable chemoselectivity can be achieved under radical reaction conditions.^[15] Organic chemists extensively use free radical based reactions in simplifying the complex natural products synthesis.^[16a] In general, generation of radicals requires various strategies that include exploiting bond dissociation energies (BDEs) or the redox properties of the precursors and the excited state chemistry under photochemical conditions.^[16b] The radical chemistry associated with several functional groups allows a wide range of intermolecular or intramolecular cross-coupling and cyclization reactions. Particularly, processes such as hydride reductive methods using Bu_3SnH or $(\text{Me}_3\text{Si})_3\text{SiH}$, atom transfer radical cyclization and addition reactions (ATRA/ATRC), Cu(I) or Ru(II) mediated reactions, single electron transfer (SET) mediated radical cyclization processes promoted by Sm, Fe, Mn, Ti, Ni, and Ag, etc. are quite popular.^[17] Despite their high reactivity and instability, several approaches have been considered in tuning these properties of radicals by utilizing factors such as incorporation of heteroatoms, stereo electronic factors, resonance, and their steric environments, etc.^[18] In recent times, radical based reactions have been reported to achieve various complex molecular architectures with regioselective and stereoselective control under appropriate conditions.^[19] Stabilized radicals can react in predictable manifolds and persistent radicals provide means to improve selectivity for reactions involving transient radicals that are otherwise difficult to access. In fact, better understanding of radical chemistry, their stability and reactivity, synthetic methodology based on radical chemistry continues to expand the toolbox for complex natural product synthesis.^[20]

1.3.2 Importance of free radicals in atmospheric chemistry

Our atmosphere (considered as blanket of our earth) has helped in the advancement and sustainment of life. This atmosphere seems very simple, just like the air we breathe, however it is unimaginably complex if we consider the chemistry within it. In other words, the atmosphere can be considered as the biggest natural photochemical reactor where thousands of chemical transformations take place at every moment and the majority of these chemical transformations are dependent on free radical reactions. Largely, atmospheric chemistry is driven by very complex sets of chain reactions which include ozone, NO_x radicals, OH radical, OOH radical, alkoxy and peroxy radicals.^[21] Solar radiation (particularly in the UV region) is the main driving force behind these reactions involving free radicals. In recent times, various human activities and global industrialization are responsible for increment in pollutants from atmospheric chemistry point of view and have changed various chemical compositions in the atmosphere. The most important atmospheric free radical is the OH (hydroxyl radical) which acts as an oxidant in the atmosphere and removes the extra pollutants from the atmosphere by oxidizing them. Therefore, these free radicals play a major role in balancing the oxidizing power of our atmosphere. Various free radical species (mainly oxidizing agents) have been known as the “atmospheric detergents” which help in the removal of various hydrocarbons, NO_x and other minor constituents.^[22] The free radicals in atmosphere chemistry are solely responsible for maintaining the oxidizing strength of the atmosphere to clean itself off the pollutants with the help of various free radicals such as OH, NO_x and other species. In addition, various radical-catalysed pathways are responsible for the destruction of ozone from the stratosphere.^[23a,b] Chlorofluorocarbons (CFCs) had long been used as refrigerants, until their role in ozone layer depletion was suggested in 1974^[23c], and then a hole in the ozone layer was first seen in 1985. Chlorofluorocarbons can diffuse up into the upper reaches of the atmosphere where they are exposed to intense ultraviolet light dissociating the carbon-chlorine bond. The chlorine free radical generated then starts a radical chain process with the ozone (O₃) which is self-propagating, making CFCs very dangerous leading to ozone depletion. The use of CFCs in various appliances has since been banned. This makes radical chemistry very interesting to study and understand various reactions along with the selective product formation. Thus, the foundation of atmospheric chemistry depends a lot on the detailed study and understanding of free radicals, their stability, their reactivity, product selectivity and, also the rate kinetics of various radical initiated reactions.

1.3.3 Importance of free radicals in biological processes

The study of free radicals has gained enormous importance in the life sciences due to their major role in the various pathological and physiological processes as well as their implications in various diseases.^[24] The involvement of free radicals in biological systems requires interdisciplinary skills for the full investigation of various radical processes for the better understanding in the biological environment along with the knowledge for understanding the various mechanisms of chemical transformations. The crucial role of free radicals studies span from the physical, biological, analytical, bioinorganic and bioorganic chemistry to medicinal chemistry.^[25] In this regard, oxygen and nitrogen based free radicals, known as reactive oxygen species (ROS) and reactive nitrogen species (RNS), have been recognized for playing a dual role (beneficial as well as toxic) in the biological environment.^[26] These free radical species (ROS and RNS) are produced from both endogenous sources (*in-situ* normal cell metabolisms in mitochondria, endoplasmic reticulum, peroxisomes, phagocytic cells, etc.) and exogenous sources (cigarette smoking, pollution, radiation, transition metals, alcohol, pesticides, industrial solvents, etc.).^[27] The presence of free radicals in the biological environment can affect the various biological functions as well as some important biological molecules such as lipids, proteins, and nucleic acids.^[28] The increasing (overload) concentration of free radicals and their accumulation in the body leads to the phenomena known as oxidative stress, upon altering the situation of normal redox status. This free radical induced oxidative stress plays a major role in the development of various diseases such as, aging, cancer, autoimmune disorder, neurodegenerative and cardiovascular disease. The human body has several methods for balancing the concentration of free radicals by producing antioxidants within the body (naturally produced *in-situ*) or by external supply through food and supplements.^[29a] In addition, Tryptophan (Trp) is one of the essential amino acids in animals and has been recognized as a precursor to many active molecules like serotonin, melatonin, etc. Trp can act as an effective scavenger to clear free radicals, like reactive oxygen and active chlorine species, which alleviates cellular damage caused by free radicals.^[29b] Trp has also been shown to be an important antioxidant in certain foods like eggs and potatoes.^[29b] Therefore, understanding free radicals reactivity and mechanism of each chemical step can provide the various strategies for controlling various diseases originated from free radicals. The study of free radicals in chemistry is more of fundamental interest but this can help us in understanding free radical reactions in a biological environment.

1.3.4 Importance of free radicals in interstellar chemistry

After the discovery of simple diatomic species CH, CH⁺, CN and OH radicals in the 1930s, the discovery and detection of new molecules in the interstellar medium (ISM) picked up a steady pace from the start of the 1960s. So far nearly 200 molecules have been detected in the interstellar medium from diatomic molecules to polyaromatic hydrocarbons, neutral to radical species along with some charged molecules.^[30] Molecules with more than 5 atoms have been defined as the complex organic molecules (COMs) as they bring a lot of complexity in the chemistry occurring in the ISM. It is believed that most of the COMs have formed with the help of radical reactions as the radical species can easily react with neutral molecules in the ISM environment.^[31] In ISM, radicals can be generated either by the homolytic dissociation of neutral molecules or by the hydrogenation of unsaturated iced molecules in the presence of UV-radiation and cosmic rays. Some of the simplest detected radicals in the ISM are CH (methyldiyne radical), CN (cyanogen radical), OH (hydroxyl radical), NH (imidogen radical), HCC (ethynyl radical), OOH (hydroperoxyl radical), NH₂ (amino radical), CH₃ (methyl radical), HCO (formyl radical), etc.^[32] Most of these radicals have a lifetime of the order of a few seconds/microseconds in the laboratory, however in the ISM, these radical species may have a lifetime of several days/months due to intermittent collisions in the environment of ISM.^[33] Therefore, the study or the detection of radicals in ISM is not only useful for the interstellar processes, but these radicals also play a major role in the formation of various interstellar molecules such as COMs with various reactions between radicals or with neutral species in the ISM.^[34] As we know the reaction between two identical or different radical species has to be barrier less, which makes this reaction suitable and feasible in any environment given that these two species are in close proximity. On the other hand, some recent reports suggest the possibility of fast and even barrier less reactions between radicals and neutral molecules in a vast temperature range of 10 – 295 K in laboratory experiments that mimic ISM conditions. For instance, the reactions of CN radical with CH₃OH and C₆H₆, and the reaction between OH radical and CH₃OH have been reported to be barrierless.^[35] In addition to that, radical species can also initiate a polymerization reaction with unsaturated molecules to form a stable product in the ISM environment such as CH₃OH from HCO radical.^[36] One of the major challenges in the detection of various species (ions and radicals) is to identify the species using the astrophysical data in ISM without prior laboratory measurements. This makes the generation and characterization of various radical species necessary in the laboratory and to identify the various possibilities of product formation in reactions involving free radicals.

1.4 General methods for generating free radicals

Generally free radicals can be generated by the homolytic cleavage of weak bonds in any given molecule under thermal^[37] (higher temperature) or photochemical^[38] (using irradiation of appropriate wavelength of light) conditions. However, the use of radical initiators drastically reduced the complexity associated with such conditions in the organic synthesis perspectives. The recent advancements in the redox and photoredox reaction conditions further ease them out and equally demonstrate the utility of several radicals.^[39] However, the major challenge in obtaining the structural information on the radical chemistry is not only to generate them but also to stabilize them until direct characterization by various methods. In general, the reactive intermediates can be studied or characterized by using techniques that can detect very fast. (e.g.) time-resolved spectroscopic techniques.^[40] Alternatively, the kinetic stability can be enhanced by preventing the intermolecular interactions and providing cryogenic conditions for such studies (e.g.) organic glasses and matrix isolation technique.^[41] Since the current investigation is mainly focused on the matrix isolation technique, the methods relevant to it are explained. The common ways of generating such transient species are the following: (a) photolysis,^[42] (b) flash vacuum pyrolysis (FVP),^[43] (c) microwave discharge,^[44] and (d) laser ablation.^[45] However, photolysis and pyrolysis are the more generally used techniques for synthesis/generation of radicals. Here, we have described the photolysis and pyrolysis in detail.

1.4.1 Photolysis:

This is the most frequently used method for obtaining free radicals. A chemical reaction in which the molecule is broken down by photons (light) under steady state irradiation condition is known as photolysis. This reaction can be initiated by visible light, ultraviolet light, X-rays or gamma rays. During photolysis, the molecules absorbing light undergo electronic excitation to the excited state at which changes in geometrical, physical and chemical properties may lead to the bond breaking, fragmentation, ring-opening, rearrangement or transposition of the atoms. (Figure 1.2) Such processes depend on the potential energy surfaces of the excited states and the possible involvement of conical intersections.^[46] The photolysis of suitable photolabile precursors under matrix-isolated condition can lead to radical formation under irradiation of appropriate wavelength of light. Photolysis usually leads to high yields of the radicals because of minimization of side reactions based on the chosen wavelength. On the other hand, this technique has some disadvantages too. One of the drawbacks of this method is that the radicals formed/synthesized are always in close proximity of other products during photolysis. As a result, molecules in the close proximity can either lead to spectral shifts and

line broadening due to intermolecular interactions or it may lead to the recombination of the radical products.^[47]

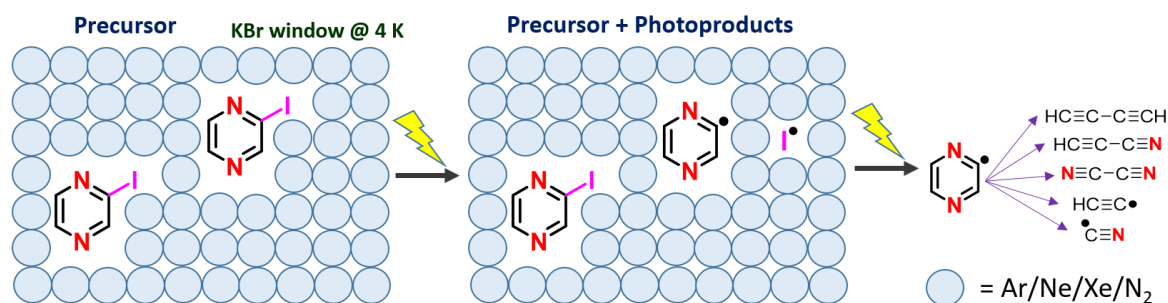


Figure 1.2 Representative description of photolysis method for generating free radicals.

1.4.2 Flash vacuum pyrolysis (FVP):

In this technique, bond scission or fragmentation of molecules can be initiated by passing the gaseous sample under vacuum through a hot channel followed by the trapping of these pyrolysis products in a low temperature inert matrix.^[47] Typically, molecules are allowed to pass through a hot quartz (pyrolysis) tube (600-1000 °C) which results in the collision of the molecules with hot quartz surface (wall) leading to molecular fragmentation. (Figure 1.3) These gas phase fragmented pyrolysis products are trapped individually in matrix cages, which overcomes the drawbacks of photolysis method where recombination can happen. So, the radical (pyrolysis products) recombination is highly unlikely in the FVP method assuming the diffusion of matrix is prevented. Due to the collision in hot quartz tubes, molecules can dissociate in many ways leading to several products from side reactions, which depend on various parameters such as temperature, vacuum, diameter and length of the hot zone, etc. By controlling these parameters, the yields of radicals in the pyrolysis method can be varied.

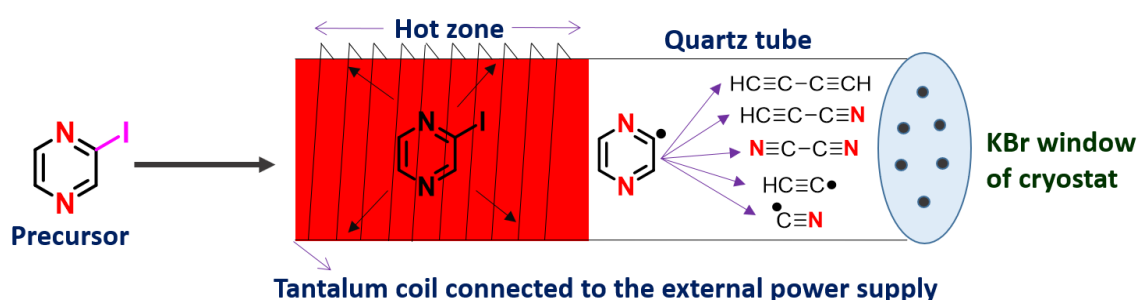


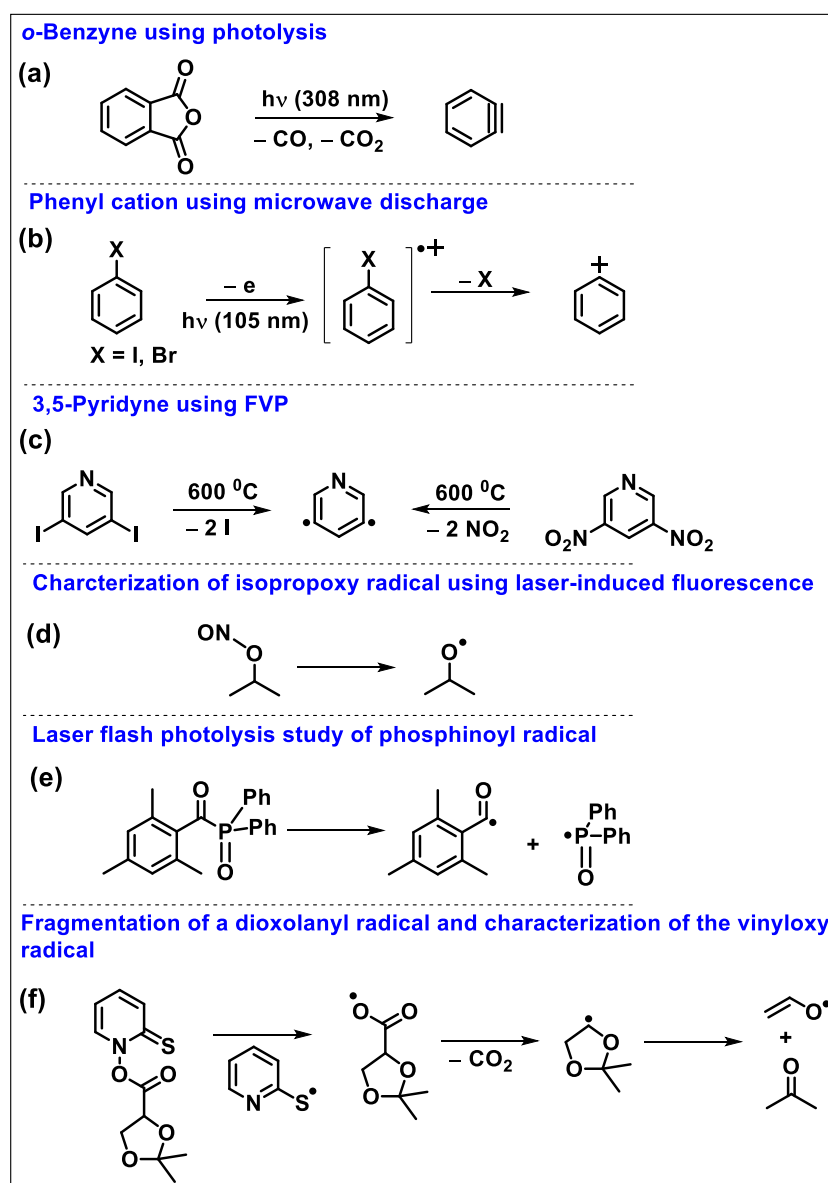
Figure 1.3 Representative description of flash vacuum pyrolysis (FVP).

1.5 General methods for characterization of free radicals

Mostly free radicals are very short-lived species. These species can react very quickly with other species or can undergo dimerization. In addition to that, these reactive free radical species can also react with the molecules present in the atmosphere such as O₂, H₂O, CO, CO₂ etc. The characterization of these highly reactive or unstable radicals is only possible with

techniques which have fast detection such as (a) various time resolve techniques with suitable spectroscopic methods,^[48] (b) laser flash photolysis,^[49] (c) laser induced fluorescence^[50] (LIF) or with techniques by which kinetic stability can be increased by (a) cooling, (b) preventing intermolecular interactions, (c) trapping in condensed phase at low temperature which is matrix-isolation technique we have used in our studies.^[51] (Scheme 1.2) Setting up of matrix-isolation technique and its importance is mentioned in chapter 6.

Also, quantum chemical calculations play a major role in analysing the results obtained from the above-mentioned technique and methods by simulating various computed spectra.^[52]



Scheme 1.2 Representative examples for the characterization of reactive intermediates and unstable species: (a) photolysis^[53a]; (b) microwave discharge^[44]; (c) flash vacuum pyrolysis^[53b]; (d) laser induced fluorescence^[54]; (e) laser flash photolysis^[55]; (f) time-resolved nanosecond photolysis^[48].

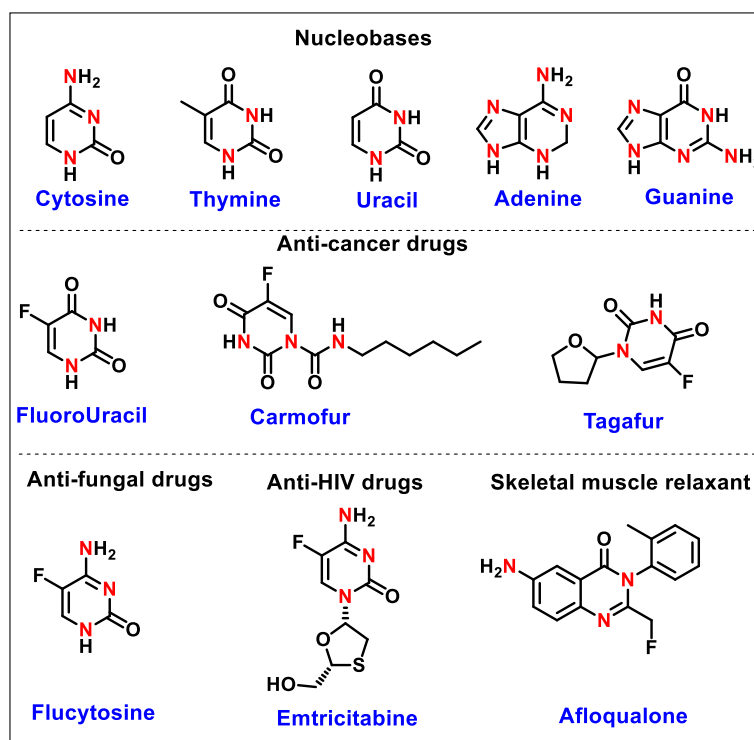
1.6 Importance of *N*-heterocyclic radicals

Nitrogen based heterocyclic molecules have emerged as the attractive and effective scaffolds in the discovery and developments of new pharmaceuticals, natural product synthesis, biological chemistry, and agrochemicals.^[56] Also, *N*-heterocycles are very important in astrochemical environments and diazines based nucleobases were detected in carbonaceous meteorites which suggests the possibility of their formation and survival outside the Earth.^[57] Over the last few decades, the number of stable *N*-heterocyclic radicals has dramatically increased as heteroatoms stabilize the unpaired electron. These *N*-heterocyclic radicals have been used for various applications that include reagents in synthesis, polymerization initiators, redox active ligands, spin active probes analysis, and in material sciences for their potential use in electronic and data storage devices.^[58]

1.7 Diazines

Six membered aromatic rings with two nitrogen atoms are known as the diazine moiety. Based on the relative position of two nitrogens, diazines are classified as 1,2-diazine (pyridazine), 1,3-diazine (pyrimidine) and 1,4-diazine (pyrazine). The diazine moiety and its derivatives remain central for various chemicals due to their ubiquitous chemical properties, and applications in pharmaceutical drugs, dyes, pesticides, and semiconductors and biological investigations.^[59] Pyrimidine (1,2-diazine) is the most important among all diazines as the naturally occurring deoxyribonucleic acid (DNA) and ribonucleic acid (RNA) bases such as uracil, thymine, and cytosine contain the pyrimidine moiety as well as several other natural products and drugs contain this pyrimidine moiety. (Scheme 1.3)

On the other hand, pyrazine moiety (1,4-diazine) is a very useful monodentate bridging ligand and has been utilized in optoelectronic materials widely. In addition to that, diazine *N*-heterocycles are suspected to be present in the ISM and have been searched for a long time as the detected *N*-heterocycles molecules increased rapidly.



Scheme 1.3 Diazine based molecules relevant to biological and medicinal chemistry.^[60]

1.8 Literature reports on diazines

1.8.1 Experimental reports on diazines

Recently, Wilhelm et al. reported the photolysis of pyrazine at 308, 248 and 193 nm, and examined the product analysis using nanosecond time-resolved Fourier transform infrared emission spectroscopy. They have demonstrated that no photolysis products were detected at 308 and 248 nm. However, they identified the vibrationally highly excited pyrazine at 308 and 248 nm irradiation using time-resolved IR emission spectra analysis. On the other hand, HCCH, HCN and HNC photofragmentation products have been observed at 193 nm from the vibrationally highly excited pyrazine in the ground electronic state. This study provided the evidence for the wavelength dependence of the pyrazine UV photolysis.^[61] Boggs and co-workers, have studied the structural and vibrational behaviour of 3,6-dichloropyridazine and 3,4,5-trichloropyridazine using computational and infrared and Raman spectroscopy in solid phase.^[62] Since, diazines have two nitrogen atoms, and both the nitrogen lone pairs can interact with electron deficient species and can also form the H-bond. In this regard, Favero and co-workers studied the 1:1 complex between pyridazine and H₂O using stark and pulse modulated free jet absorption millimetre-wave spectrometer and investigated the H-bond complexes between nitrogen of the aromatic rings and water molecule in which one hydrogen is bound to a nitrogen atom.^[63] Also, O. Kasende et al. studied the hydrogen-bonded complexes of all

diazines pyridazine, pyrimidine, and pyrazine with H₂O using the infrared spectroscopy and investigated the strength of interaction based on thermodynamic data (formation constant K, ΔH , ΔS) as follows: pyridazine > pyrimidine > pyrazine.^[64] Kiefer et al. have investigated the thermal decompositions of pyrimidine, pyridazine and pyrazine initiated by ring C-H fission in shock waves using laser-schlieren (LS) densitometry and time-of-flight (TOF) mass spectrometry (1600-2300 K, 150-350 Torr). They also have estimated the experimental barriers corresponding to the C-H fission for all the possibilities in diazines and compared them with ab initio calculation results.^[65] Livingston and co-workers have studied the solutions of 1,3-dihydropyrimidine, 1,2-dihydropyridazine, and 1,4-dihydropyrazine cation radicals using EPR.^[66] Kinichi Obi and co-workers have studied the hydrogen atom abstraction reactions of triplet pyrazine at low temperature and estimated the activation energy of hydrogen atom abstraction reaction by triplet pyrazine around 2.1–2.3 kcal/mol.^[67] E. R. Bernstein and co-workers have performed the pyrazine spectroscopic studies in cryogenic solutions. In their contribution, they have investigated first excited singlet and triplet states (¹B_{3u} and ³B_{3u}), ¹B_{3u} – ¹A_{lg} absorption, fluorescence, lifetime and ³B_{3u} – ³A_{lg} phosphorescence as a function of concentration and temperature.^[68] Trimble and co-workers have reported the *pK_a* values corresponding to the acid dissociation of protonated (mono- and di-) pyrazine, 2,6-dimethylpyrazine, 2,5-dimethylpyrazine and tetramethyl pyrazine using UV- absorption spectra in sulfuric acid.^[69] Also, Zeng et al. have explored the effect of solvent on the molecular and ionic spectrum of pyridazine in water in its ¹(n, π^*) excited state.^[70] Lahmani et al. have studied the photoisomerization of diazines. They have investigated mercury sensitization isomerization of pyrimidine into pyrazine and vice-versa. Quantum yields of the sensitized isomerization are $(3.8 \pm 0.4) \times 10^{-2}$, $(5.2 \pm 0.5) \times 10^{-2}$, $(3.6 \pm 0.4) \times 10^{-2}$, $(2.08 \pm 0.2) \times 10^{-2}$, and $(2.1 \pm 0.2) \times 10^{-2}$ for pyrimidine, 5-methylpyrimidine, 4,6-dimethylpyrimidine, pyrazine, and 2,5-dimethylpyrazine, respectively.^[71] Also, Fausto and co-workers reported the matrix isolated infrared spectra of each diazine (pyrazine, pyrimidine and pyridazine) and investigated the UV-induced photoisomerization of pyrazine into pyrimidine under matrix-isolation conditions.^[72] Dopfer and co-workers have studied the structure and fragmentation of pyrimidine cation (Pym⁺, C₄H₄N₂, *m/z* 80) using infrared photodissociation (IRPD) spectroscopy in NH and CH stretch ranges and DFT calculations. It has been shown that, pyrimidine cation fragmentation led to HCN and C₃H₃N⁺ (*m/z* 53). Also, they have investigated the percentage contribution of each isomers in C₃H₃N⁺ fragmentation products as follows: *cis*-/*trans*-HCCHNCH⁺ ions (~90%) and *cis*-/*trans*-HCCHCNH⁺ isomers (~10%). Further,

$C_3H_3N^+$ fragmentation formed HCN and $HCCH^+$ (acetylene cation, m/z 26).^[73] Corral and co-workers have explored the photostability of pyrimidine using femtosecond transient absorption spectroscopy and *ab initio* calculations, and demonstrated the electronic relaxation mechanism of pyrimidine from $S_1(n, \pi^*)$ state.^[74] Recently, Samir et al. reported the gas phase UV absorption spectrum of pyridazine, pyrimidine and pyrazine between 200 and 380 nm, and found out that the absorption of these species is significant above 290 nm. The obtained results suggested that these diazine species could be removed in the troposphere using photolysis methods.^[75] Ward et al. have reported the EPR investigations on the diazines negative ions (pyridazine and pyrazine anions).^[76] Knoth et al. have reported the pyrimidine gas phase two-photon excitation spectrum for S_0 to S_1 transition.^[77] Navarro et al. have demonstrated the vibrational analysis of pyrimidine using inelastic neutron scattering spectrum (INS) along with quantum chemical calculations at various levels of theory.^[78] Bierbaum and co-workers have investigated the reaction of pyrazine, pyridazine and pyrimidine anions with N and O- atoms in their ground state using tandem flowing afterglow-selected ion flow tube (FA-SIFT) mass spectrometry and computational methods.^[79] Choi et al. have characterized the S_1 $^1(n, \pi^*)$ excited state of pyridazine using computation and mass-analysed threshold ionization (MATI) spectroscopy.^[80] Patwari and co-workers have investigated and characterized the π -complex between pyrazine and phenylacetylene using IR-UV double resonance spectroscopy and computation.^[81] Pino et al. have investigated the photofragmentation spectra of protonated 1,2-, 1,3- and 1,4-diazines (pyridazine, pyrimidine and pyrazine) along with the excited state lifetimes using a cryogenically cooled quadrupole-ion-trap (QIT) time-of-flight mass spectrometry. These experimental studies are complemented by *ab initio* calculations on the ground and electronically excited states.^[82] Kwon and co-workers have studied the conformational preference of 2-methylpyrazine and its cation using NBO analysis and high-resolution one-photon vacuum ultraviolet mass-analyzed threshold ionization (VUV-MATI) spectroscopy.^[83] Nakamura et al. have studied the emission of pyrazine in gas phase and it has been shown that pyrazine exhibits both phosphorescence and fluorescence and their estimated yields are $(1.70 \pm 0.08) \times 10^{-3}$ and $(1.74 \pm 0.08) \times 10^{-3}$ at 313 nm, respectively.^[84] Taft et al. have investigated the relative solution and gas phase basicities of pyrimidine and pyridazine experimentally.^[85] Verevkin et al. have obtained and reported the thermochemical data and properties of pyridazine, pyrimidine, and pyrazine using combustion calorimetry and vapor pressure measurements. The enthalpies of formation in the condensed and gas phase of the diazines have been re-evaluated in this study and the results were compared with currently

available high accurate composite methods in computational chemistry.^[86] Bent et al. have studied the chemistry of diazines triplet state in organic and aqueous solvent using laser spectroscopy. Also, the kinetic absorption spectrophotometry was used to investigate and study the very short-lived transient species and they reported the lifetime of triplet states in water at 25 °C of pyrazine and pyrimidine as 4.5 and 1.4 μ sec, respectively.^[87] Wren et al. have investigated the role of nitrogen heteroatom in C-H bond strength and their acidities in aromatic species. Negative ion photoelectron spectroscopy has been used to obtain electron affinities (EA) and tandem flowing afterglow-selected ion tube (FA-SIFT) mass spectrometry to obtain deprotonation enthalpies (ΔH_{298}). The C-H bond dissociation energy (BDE) has been obtained for pyridazine, pyrimidine and pyrazine experimentally.^[88] Lifshitz et al. have investigated the decomposition channels of 4-methylpyrimidine and its first order rate constant using computational chemistry and single-pulse shock tube over the temperature range 1160-1330 K.^[89] Ribeiro et al. have studied the fragmentation and ion desorption of pyrimidine in ice phase using time-of-flight mass spectrometry (TOF-MS) and identified several fragmentation products such as $C_2H_2^+$, HCN^+ , $C_3H_3^+$, CHN_2^+ , $C_2H_2N_2H^+$, and $C_4H_4N_2H^+$.^[90]

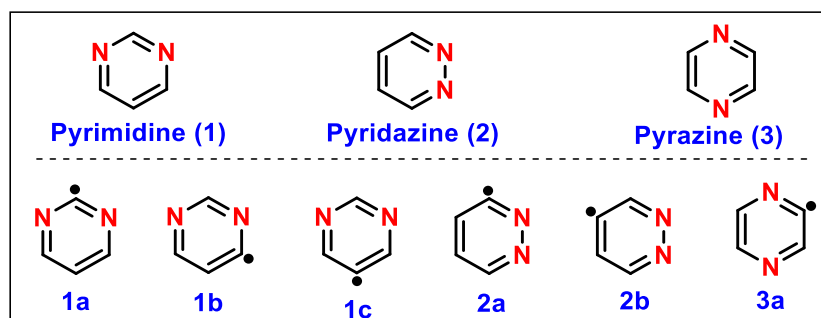
1.8.2 Computational reports on diazines

Maclagan et al. reported the proton affinities, polarizabilities, and ionization energies of 31 polycyclic aromatic nitrogen heterocycles (1-5 rings) (PANHs) including the diazines using quantum chemical calculations at M06-2X/6-311+g**//B3LYP/6-31g* level of theory and investigated that the proton affinities increase with increasing molecular size and show a linear correlation with polarizabilities in *N*-heterocycles.^[91] Alkorta et al. have explored the bonding pattern in the complexes of diazines (pyridazine, pyrimidine and pyrazine) with CO₂ and also investigated the presence of N-C tetrel-bonds in complexes using second order perturbation MP2 theory.^[92] Hadad and co-workers estimated the C-H and N-H bond dissociation energies of small aromatic hydrocarbons including diazines and also explored the potential surface of reactions between dehydro-diazine radicals and O₂ using density functional theory.^[93,94]

Wang et al. have investigated the π -complex of benzene with pyrimidine using various computational methods and demonstrated the π - π interaction between them.^[95] Hahn et al. have provided the computational scheme for predicting the femtosecond time-resolved photoelectron spectrum of pyrazine.^[96] Werner and co-workers have explored the excited states of pyrazine using extended multi-state complete active space second-order perturbation theory

(XMS-CASPT2).^[97] Gadre and co-workers have developed a molecular electrostatic potential (MESP) topography for describing the weak interaction between lone pair containing species and p-deficient molecules such as pyrazine with hexafluorobenzene.^[98] Gatti and co-workers have investigated the radiationless decay of pyrazine from its photoexcited state to ground electronic state with the help of multireference electronic structure and quantum dynamic calculations.^[99] Scheiner and co-workers have explored the σ -hole and π -hole complexes of diazines with AeOF₂ (Ae = Kr, Xe).^[100] Wang et al. have reported the NICS and RE (resonance energy) of diazines using computational chemistry approach.^[101] Hoffmann demonstrated the orbital interactions between two nitrogen lone pairs in the pyrazine, pyrimidine and pyridazine.^[102] Wiberg et al. have studied the p-electron delocalization in benzene and diazine theoretically using the first π - π^* transition, hydrogenation energies and an analysis of wave-function.^[103] Reimers and co-workers have studied the pyrazine vibrational structure in its singlet and triplet excited states using DFT, CASSCF, MRCI and CASPT2 methods^[104] along with few other reports on the geometry and properties of pyrazine lowest triplet states.^[105] The presence of two nitrogen lone pairs in diazine makes it suitable for the study of various possible complex formations. In this regard diazine and water complexes with different H-bonding in the complex have been investigated extensively using experiments and computational methods in ground state as well as in their excited states.^[106-110] Also, few reports are available on the complex of diazine and CO₂ using computations.^[111] In addition to that, Ming-der Su explored and investigated the mechanism of photochemical transposition reactions of pyrazines to form pyrimidine using MP2-CAS methods with the 6-311G(d) basis set. Their study suggests the role of minimum energy conical intersections in explaining photoisomerizations of pyrazines (also methyl derivative) which initiates from its first excited state ¹(π - π^*) to form pyrimidine (and methyl derivatives).^[112] Recently, Gagliardi and co-workers explored the electronic structure of pyrazine biradicals (both singlet and triplet states) using multireference *ab initio* study and estimated the singlet-triplet energy gaps using vertical excitation and adiabatic excitation energies. Also, Chattopadhyay et al. reported the electronic structure of singlet and triplet pyrazine biradicals using improved virtual orbital-based multireference (MR) *ab initio* methods.^[113, 114]

1.9 Aim of the thesis



Scheme 1.4 Three isomeric diazines (**1–3**) and six-isomeric dehydrodiazine (**1a–c**, **2a–b**, **3a**) radicals.

The main objectives of this thesis are to explore some of the key questions related to the diazines, dehydro- and didehydrodiazines using low temperature matrix-isolation infrared spectroscopy in combination with computational methods which include the following:

- Understanding the thermodynamic stability of six isomeric dehydrodiazine radicals.
- Deciphering the role of nitrogen atoms in the kinetic stability of six isomeric dehydrodiazine radicals.
- Understanding the nature and mode of interaction between radical centre and nitrogen lone pairs (3c-5e interaction in dehydrodiazine radicals and 4c-6e interaction in didehydrodiazine biradicals).
- Generation and characterization of selected dehydro- and didehydrodiazine radical isomers using matrix-isolation infrared spectroscopy.
- Photochemistry of dehydrodiazine radicals using matrix-isolation infrared spectroscopy.
- Electronic structure of didehydrodiazine biradicals.

1.10 Structure of the thesis

This thesis work involves both the experimental as well as computational results on the dehydrodiazine and didehydrodiazine radicals as briefly discussed here.

The first part of the thesis involves exploration on the electronic structure studies of six isomeric dehydro-diazine radicals, in which 3c-5e interaction between nitrogen lone pairs and radical centre play a major role in determining the relative thermodynamic stability of these diazine radicals. Various density functional theory-based quantum chemical calculations have been used to estimate bond dissociation energy (BDE), radical stabilization energy (RSE),

localization and delocalization of spin densities, natural bond orbitals (NBO) analysis, proton affinity (PA) estimations, electrostatic potential mapping (ESP), atoms-in-molecules (AIM) analysis, and also multireference calculations for molecular orbital analysis. Based on this analysis, the significant role of 3c-5e interaction in dictating the thermodynamic stability of dehydrodiazine radicals, and also the mode of orbital interaction such as through bond and through space interaction have been demonstrated.

In addition to that, the work has been extended to obtain the information on kinetic stability of dehydrodiazines radical isomers using various reaction channels such as isomerization via 1,2-H shift and thermal unimolecular decomposition channels. We obtained the kinetic stability order of six isomeric dehydrodiazine radical isomers based on unimolecular decomposition channels and observed various ring-opening products (diazine analogue of enediyne with a molecular formula $C_4H_2N_2$) and ring-fragmented products of astrochemical interest.

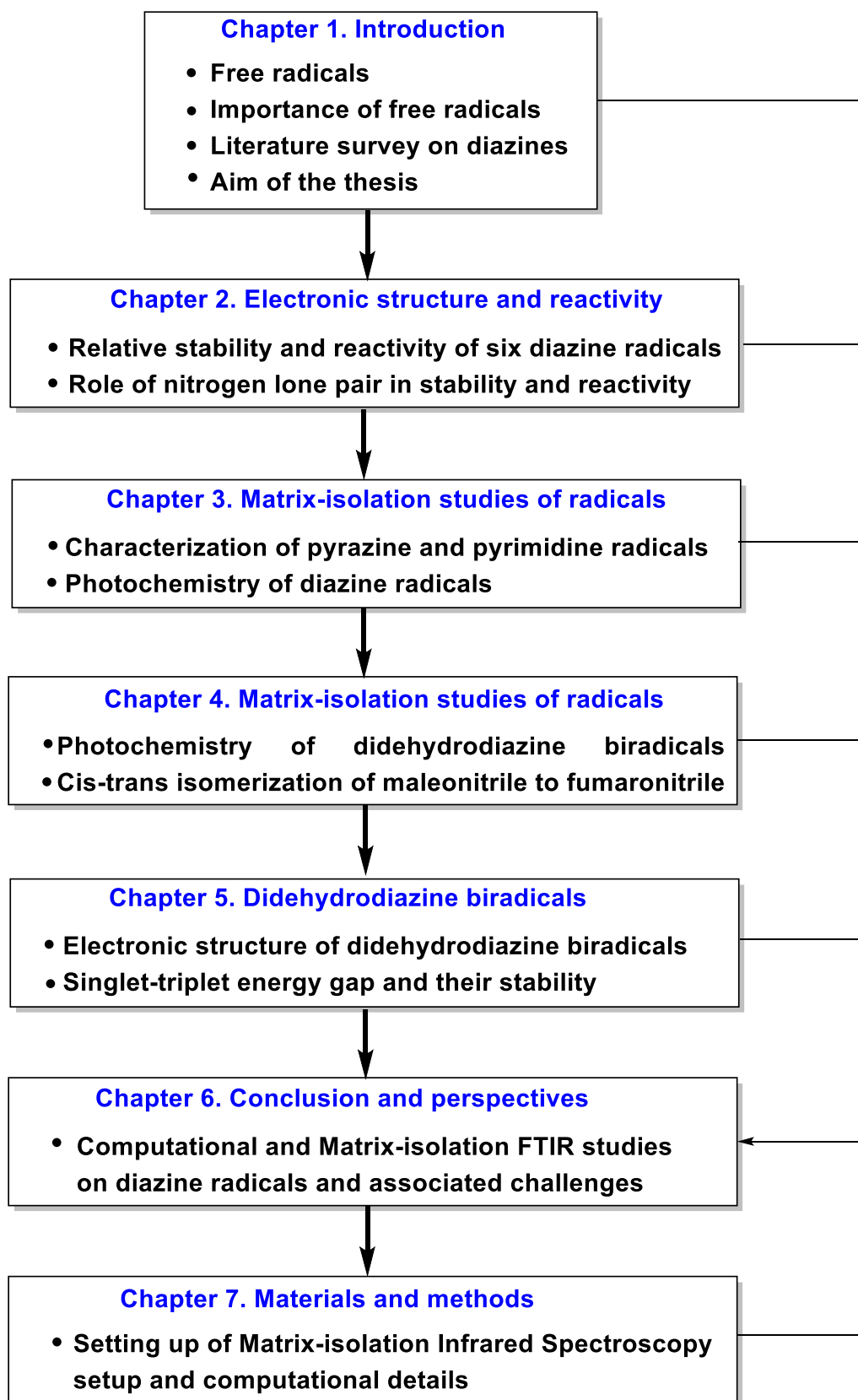
On the experimental side, setting up of our cryogenic matrix-isolation infrared spectroscopy facility from scratch has been partly occupied in the initial part, and the technique has been utilized for the generation and characterization of diazine radicals. In this regard, the matrix-isolation infrared spectroscopic experiments on 2-iodopyrazine, 2-iodopyrimidine, 3,6-diiodopyridazine, and 4,6-diiodopyrimidine in Ar and N_2 gases are discussed in the next part of the thesis. Particularly, photolysis method has been used for generating the selected radical species from their corresponding iodo-precursors. Through these investigations, 2-dehydropyrazine and 2-dehydropyrimidine radicals have been successfully characterized using infrared spectroscopy along with the help of computations. Various ring-opened and fragmented products have also been characterized.

In a similar way, 3,6-diiodopyridazine and 4,6-diiodopyrimidine have been used as the precursors to target (expected) 3,6-didehydropyridazine and 4,6-didehydropyrimidine biradicals, instead both of them led to ring-opened products. Based on the product analysis, various ring-opened products (diazine analogue of enediyne with a molecular formula $C_4H_2N_2$) have been observed and characterized for the first time under matrix isolation conditions, which includes maleonitrile and fumaronitrile. Furthermore, the isomerization mechanism associated with the conversion of maleonitrile to fumaronitrile under photochemical condition (from 3,6-diiodopyridazine as the precursor) has also been investigated using multireference methods by obtaining the minimum energy conical intersection.

In the last part, we explored the electronic structure of didehydrodiazine biradicals using multireference methods to obtain some insights on the stability of singlet and triplet states

as well as their singlet-triplet energy gaps. Didehydrodiazine biradicals form a very interesting 4c-6e interaction system in which two nitrogen lone pairs interact with two radical centres (unpaired electrons). We found out the nature of singlet biradicals as open-shell singlet and estimated the singlet-triplet energy gaps in didehydrodiazine biradical isomers. Also, the role of various possible interactions (radical-radical, lone pair-radical and lone pair-lone pair) in determining the S-T energy gaps.

The entire results and discussion on the diazine radicals and biradicals have been summarised in the conclusion part along with the perspectives. This is followed by a chapter on the materials and methods used for this thesis work, in which a brief discussion on the matrix isolation set up and the computational methods used are described.



Scheme 1.5 Organization of the thesis.

1.11 References

1. Muller, P. Glossary of Terms Used in Physical Organic Chemistry. *Pure & Appl. Chem.* **1994**, 66, 1077–1184.
2. Phaniendra, A.; Jestadi, B. D.; Periyasamy, L. Free Radicals: Properties, Sources, Targets, and Their Implication in Various Diseases. *Ind. J. Clin. Biochem.* **2015**, 30, 11–26.
3. Neta, P. Redox Properties of Free Radicals. *J. Chem. Educ.* **1981**, 58, 110–113.
4. (a) Gomberg, M. An Instance of Trivalent Carbon: Triphenylmethyl. *J. Am. Chem. Soc.* **1900**, 20, 757–771; (b) Tidwell, T. T. The History of Free Radical Chemistry. *Encyclopedia of radicals in chemistry, biology and materials*. John Wiley & Sons, Ltd. **2012**.
5. Hicks, R. G. What's New in Stable Radical Chemistry? *Org. Biomol. Chem.* **2007**, 5, 1321–1338.
6. Lu, D.; Wu, C.; Li, P. 3-center-5-electron Boryl Radicals with $\sigma^0\pi^1$ Ground State Electronic Structure. *Org. Lett.* **2014**, 16, 1486–1489.
7. (a) Rajca, A. Organic Diradicals and Polyradicals: From Spin Coupling to Magnetism? *Chem. Rev.* **1994**, 94, 871–893; (b) Krylov A. I. Triradicals. *J. Phys. Chem. A* **2005**, 109, 10638–10645.
8. (a) Veciana, J.; Rovira, C.; Crespo, M. I.; Armet, O.; Domingo, V. M.; Palacio, F. Stable Polyradicals with High-Spin Ground States. *J. Am. Chem. Soc.* **1991**, 113, 2552–2561; (b) Orms, N.; Rehn, D.; Dreuw, A.; Krylov, A. I. Characterizing Bonding Patterns in Diradicals and Triradicals by Density-Based Wave Function Analysis: A Uniform Approach. *J. Chem. Theory Comput.* **2018**, 14, 638–648.
9. Chen, Z. X.; Li, Y.; Huang, F. Persistent and Stable Organic Radicals: Design, Synthesis, and Applications. *Chem.* **2021**, 7, 288–322.
10. Muir, V. G.; Jason, A.; Burdick, J. A.; Chemically Modified Biopolymers for the Formation of Biomedical Hydrogels. *Chem. Rev.* **2020**, <https://dx.doi.org/10.1021/acs.chemrev.0c00923>.
11. Gligorovski, S.; Strekowski, R.; Barbati, S.; Vione, D. Environmental Implications of Hydroxyl Radicals ($\bullet\text{OH}$). *Chem. Rev.* **2015**, 115, 13051–13092.
12. Hayes, C. J.; Merle, J. K.; Hadad, C. M. The Chemistry of Reactive Radical Intermediates in Combustion and the Atmosphere. *Advances in physical Organic Chemistry* **2009**, 43, 79–134.
13. Zhang, M.; Ognier, S.; Touati, N.; Hauner, I.; Guyon, C.; Binet, L.; Tatouliau, M. A Plasma/Liquid Microreactor for Radical Reaction Chemistry: An Experimental and Numerical Investigation by EPR Spin Trapping. *Plasma Process Polym.* **2018**, 15, e1700188.
14. (a) Demarteau, J.; Debuigne, A.; Detrembleur, C. Organocobalt Complexes as Sources of Carbon-Centered Radicals for Organic and Polymer Chemistries. *Chem. Rev.* **2019**, 119, 6906–6955; (b) Chen, M.; Zhong, M.; Johnson, J. A. Light-controlled Radical Polymerization: Mechanisms, Methods, and Applications. *Chem. Rev.* **2016**, 116, 10167–10211.
15. Zard, S. Z. Radicals in Action: A Festival of Radical Transformations. *Org. Lett.* **2017**, 19, 1257–1269.
16. (a) Yan, M.; Lo, J. C.; Edwards, J. T.; Baran, P. S. Radicals: Reactive Intermediates with Translational Potential. *J. Am. Chem. Soc.* **2016**, 138, 12692–12714; (b) Schweitzer-Chaput, B.; Horwitz, M. A.; Beato, E. de Pedro.; Melchiorre, P. Photochemical Generation of Radicals from Alkyl Electrophiles Using a Nucleophilic Organic Catalyst. *Nature Chemistry* **2019**, 11, 129–135.
17. Bonjoch, J.; Diaba, F. Radical Reactions in Alkaloid Synthesis: A Perspective from Carbon Radical Precursors. *Eur. J. Org. Chem.* **2020**, 5070–5100.
18. Renaud, P.; Sibi, M. S. *Radicals in Organic Synthesis*; Eds.; WileyVCH Verlag GmbH: Weinheim, Germany, **2001**; Vols. 1 and 2 and references therein
19. Curran, D. P.; Porter, N. A.; Giese, B. *Stereochemistry of Radical Reactions: Concepts, Guidelines, and Synthetic Applications*. VCH: New York, **1996**; see also references therein
20. Romero, K. J.; Galliher, M. S.; Pratt, D. A.; Stephenson, C. R. J. Radicals in Natural Product Synthesis. *Chem. Soc. Rev.* **2018**, 47, 7851–7866.

21. (a) Orlando, J. J.; Tyndall, G. S. Laboratory Studies of Organic Peroxy Radical Chemistry: An Overview with Emphasis on Recent Issues of Atmospheric Significance. *Chem. Soc. Rev.* **2012**, *41*, 6294–6317; (b) Ehalt, D.H. Chemical Reactions in The Atmosphere. **1999**, 60–94 in Zellner, R. (ed.) *Global aspects of atmospheric chemistry*. Springer, New York.
22. (a) Riedel, K.; Lassey, K. Detergent of the Atmosphere. *Water & Atmosphere* **2008**, *16*, 1–2; (b) Lelieveld, J.; Dentener, F.J.; Peters, W.; Krol, M.C. On the role of Hydroxyl Radicals in the Self-cleansing Capacity of the Troposphere. *Atmospheric Chemistry and Physics* **2004**, *4*, 2337–2344; (c) Vaida, V. Atmospheric Radical Chemistry Revisited. *Science* **2016**, *353*, 650–651.
23. (a) Crounse, J. D.; Nielsen, L. B.; Jørgensen, S.; Kjaergaard, H. G.; Wennberg, P. O. Autoxidation of Organic Compounds in the Atmosphere. *J. Phys. Chem. Lett.* **2013**, *4*, 3513–3520; (b) Anglada, J. M.; Aplincourt, P.; Bofill, J. M.; Cremer, D. Atmospheric Formation of OH Radicals and H₂O₂ from Alkene Ozonolysis under Humid Conditions. *ChemPhysChem* **2002**, *2*, 215–221; (c) Molina, M. J.; Rowland, F. S. Stratospheric sink for chlorofluoromethanes: chlorine atom-catalyzed destruction of ozone. *Nature* **1974**, *249*, 810–812.
24. Bergendi, L.; Beneš, L.; Ďuračková, Z.; Ferencik, M. Chemistry, Physiology and Pathology of Free Radicals. *Life Sciences* **1999**, *65*, 1865–1874.
25. Southorn, P. A.; Garth, P. Free Radicals in Medicine: Chemical Nature and Biologic Reactions. *Mayo Clinic Proceedings* **1988**, *63*, 381–389.
26. (a) Meo, S. D.; Reed, T.T.; Venditti, P.; Victor, V. M. Role of ROS and RNS Sources in Physiological and Pathological Conditions. *Oxid Med Cell Longev.* **2016**, 1245049. (b) Ghosh, N.; Das, A.; Chaffee, S.; Roy, S.; Sen, C. K. Reactive Oxygen Species, Oxidative Damage and Cell Death. *Immunity and Inflammation in Health and Disease* **2018**, 45–55.
27. Auten, R. L.; Davis, J. M.; Oxygen Toxicity and Reactive Oxygen Species: The Devil is in the Details. *Pediatric Research* **2009**, *66*, 121–127.
28. (a) Lushchak, V. I. Free Radicals, Reactive Oxygen Species, Oxidative Stress and its Classification. *Chemico-Biological Interactions* **2014**, *224*, 164–175; (b) Prescott, C.; Bottle, S. E. Biological Relevance of Free Radicals and Nitroxides. *Cell Biochemistry and Biophysics* **2017**, *75*, 227–240.
29. (a) Lobo, V.; Patil, A.; Phatak, A.; Chandra, N. Free radicals, antioxidants and functional foods: Impact on human health. *Pharmacogn Rev.* **2010**, *4*, 118–126; (b) Bitzer-Quintero, O. K.; Dávalos-Marín, A. J.; Ortiz, G. G. Antioxidant activity of tryptophan in rats under experimental endotoxic shock. *Biomedicine & Pharmacotherapy* **2010**, *64*, 77–81.
30. McGuire, B. A. 2018 Census of Interstellar, Circumstellar, Extragalactic, Protoplanetary Disk, and Exoplanetary Molecules. *Astrophys. J. Suppl. Ser.* **2018**, *239*, 17–64.
31. Abplanalp, M. J.; Kaiser, R. I. On the Formation of Complex Organic Molecules in the Interstellar Medium: Untangling the Chemical Complexity of Carbon Monoxide–Hydrocarbon Containing Ice Analogues Exposed to Ionizing Radiation via a Combined Infrared and Reflection Time-of-Flight Analysis. *Phys. Chem. Chem. Phys.* **2019**, *21*, 16949–16980.
32. (a) Interstellar and Circumstellar Molecules. http://www.astrochymist.org/astrochymist_ism.html; (b) Parise, B.; Bergman, P.; Du, F. Detection of the hydroperoxyl radical HO₂ toward ρ Ophiuchi A - Additional constraints on the water chemical network. *A&A*, **2012**, *L11*, 541–544.
33. Balucani, N.; Skouteris, D.; Ceccarelli, C.; Codella, C.; Falcinelli, S.; Rosi, M. A Theoretical Investigation of the Reaction Between the Amidogen, NH, and the Ethyl, C₂H₅, Radicals: A Possible Gas-phase Formation Route of Interstellar and Planetary Ethanamine. *Mol. Astrophys.* **2018**, *13*, 30–37.
34. Mattioda, A. L.; Cruz-Diaz, G. A.; Ging, A.; Barnhardt, M.; Boersma, C.; Allamandola, L. J.; Schneider, T.; Vaughn, J.; Phillips, B.; Ricca, A. Formation of Complex Organic Molecules (Coms) from Polycyclic Aromatic Hydrocarbons (PAHs): Implications for ISM IR Emission Plateaus and Solar System Organics. *ACS Earth Space Chem.* **2020**, *4*, 2227–2245.
35. (a) Gupta, D.; Cheikh Sid Ely, S.; Cooke, I. R.; Guillaume, T.; Abdelkader Khedaoui, O.; Hearne, T. S.; Hays, B. M.; Sims, I. R. Low Temperature Kinetics of the Reaction between

- Methanol and the CN Radical. *J. Phys. Chem. A* **2019**, *123*, 9995–10003; (b) Cooke, I. R.; Gupta, D.; Messinger, J. P.; Sims, I. R. Benzonitrile as a Proxy for Benzene in the Cold ISM: Low Temperature Rate Coefficients for CN + C₆H₆. *Astrophys. J. Lett.* **2020**, *891*, L41.
36. Hudson, R. L.; Moore, M. H. Laboratory Studies of the Formation of Methanol and other Organic Molecules by Water + Carbon Monoxide Radiolysis: Relevance to Comets, Icy Satellites, And Interstellar Ices. *Icarus* **1999**, *140*, 451–461.
37. Chang, T.; Guo, Q.; Hao, H.; Wu, B.; Yang, Y. Formation of Radicals in Coal Pyrolysis Examined by Electron Spin Resonance. *AIP Advances* **2017**, *7*, 095303–095314.
38. Nakayama, A.; Kimata, H.; Marumoto, K.; Yamamoto, Y.; Hiroshi Yamagishi, H. Facile Light-Initiated Radical Generation from 4-Substituted Pyridine under Ambient Conditions. *Chem. Commun.* **2020**, *56*, 6937–6940.
39. Matsui, J. K.; Lang, S. B.; Heitz, D. R.; Molander, G. A. Photoredox-mediated Routes to Radicals: The Value of Catalytic Radical Generation in Synthetic Methods Development. *ACS Catal.* **2017**, *7*, 2563–2575; (b) Chen, J.-R.; Hu, X.-Q.; Lua, L.-Q.; Xiao, W.-J. Visible Light Photoredox-controlled Reactions of *N*-Radicals and Radical Ions. *Chem. Soc. Rev.*, **2016**, *45*, 2044–2056.
40. (a) Luo, P.-L.; Horng, E.-C. Simultaneous Determination of Transient Free Radicals and Reaction Kinetics by High-Resolution Time-Resolved Dual-Comb Spectroscopy. *Communications Chemistry* **2020**, *3*, 95–102; (b) Fleisher, A. J.; Bjork, B. J.; Bui, T. Q.; Cossel, K. C.; Okumura, M.; Ye, J. Mid-Infrared Time-Resolved Frequency Comb Spectroscopy of Transient Free Radicals. *J. Phys. Chem. Lett.* **2014**, *5*, 2241–2246.
41. (a) Orville-Thomas W.J. (1981) The History of Matrix Isolation Spectroscopy. In: Barnes A.J., Orville-Thomas W.J., Müller A., Gaufrès R. (eds) *Matrix Isolation Spectroscopy*. 76, Springer, Dordrecht; (b) Barnes A.J. (1994) Matrix Isolation Spectroscopy: Technique and Applications. In: Moortgat G.K., Barnes A.J., Le Bras G., Sodeau J.R. (eds) *Low-Temperature Chemistry of the Atmosphere*. 21, Springer, Berlin, Heidelberg.
42. Moore, T. A.; Okumura, M.; Seale, J. W.; Minton, T. K. UV Photolysis of ClOOCl. *J. Phys. Chem. A* **1999**, *103*, 1691–1695.
43. Neuhaus, P.; Grote, D.; Sander, W. Matrix-isolation, Spectroscopic Characterization, and Photoisomerization of *m*-Xylylene. *J. Am. Chem. Soc.* **2008**, *130*, 2993–3000.
44. Winkler, M.; Sander, W. Isolation of the Phenyl Cation in a Solid Argon Matrix. *Angew. Chem. Int. Ed.* **2000**, *39*, 2014–2016.
45. Clarke, R. H.; Nakagawa, K.; Isner, J. M. The Production of Short-Lived Free Radicals Accompanying Laser Photoablation of Cardiovascular Tissue. *Free Radicals Biol. & Med.* **1988**, *4*, 209–213.
46. Mardyukov, A. and Sander, W. (2012). Matrix Isolation of Radicals. In Encyclopedia of Radicals in Chemistry, Biology and Materials (eds C. Chatgililoglu and A. Studer).
47. Wentrup, C. Flash Vacuum Pyrolysis: Techniques and Reactions. *Angew. Chem. Int. Ed.* **2017**, *56*, 14808–14835.
48. Bucher, G.; Lal, M.; Rana, A.; Schmittel, M. Fragmentation of a Dioxolanyl Radical via Nonstatistical Reaction Dynamics: Characterization of the Vinyloxy Radical by ns Time-resolved Laser Flash Photolysis. *Phys. Chem. Chem. Phys.* **2018**, *20*, 19819–19828.
49. (a) Hoshino, M.; Konishi, R.; Seto, H.; Seki, H.; Sonoki, H.; Yokoyama, T.; Shimamori, H. Studies on Reactivity of Benzoyl and Benzoylperoxy Radicals Produced by Laser Flash Photolysis of Dibenzoyldiazene in Aerated Solutions. *Research on Chemical Intermediates* **2001**, *27*, 189–204; (b) Font-Sanchis, E.; Miranda, M. A.; Perez-Prieto, J.; Scaiano, J. C. Laser Flash Photolysis of [3,n]Paracyclophan-2-ones. Direct Observation and Chemical Behavior of 4,4'-(1,n-Alkanediyl)bisbenzyl Biradicals. *J. Org. Chem.* **2002**, *67*, 6131–6135.
50. (a) Reza, M. A.; Paul, A. C.; Reilly, N. J.; Liu, J. Laser-Induced Fluorescence and Dispersed Fluorescence Spectroscopy of Jet-Cooled Isopentoxy Radicals. *J. Phys. Chem. A* **2019**, *123*, 8441–8447; (b) Masumoto, I.; Washida, N.; Inomata, S.; Muraoka, A.; Yamashita, K. Laser-Induced Fluorescence of the CHFCHO Radical and Reaction of OH Radicals with Halogenated Ethylenes. *J. Chem. Phys.* **2019**, *150*, 174302–174309.

51. Dunkin, I. R. The matrix isolation technique and its application to organic chemistry. *Chem. Soc. Rev.* **1980**, 9, 1–23.
52. Andrews, L. Computational Spectroscopy: Methods, Experiments and Applications; Grunenberg, J., Ed.; Wiley-VCH: Weinheim, **2010**; pp 353–375.
53. (a) Radziszewski, J. G.; Hess, B. A. Jr.; Zahradnik, R. Infrared Spectrum of *o*-Benzynes: Experiment and Theory. *J. Am. Chem. Soc.* **1992**, 114, 52–57; (b) Winkler, M.; Cakir, B.; Sander, W. 3,5-Pyridyne – A Heterocyclic meta-benzynes derivative. *J. Am. Chem. Soc.* **2004**, 126, 6135 – 6149.
54. Chhantyal-Pun, R.; Roudjane, M.; Melnik, D. G.; Miller, T. A.; Liu, J. Jet-Cooled Laser-Induced Fluorescence Spectroscopy of Isopropoxy Radical: Vibronic Analysis of \tilde{B} - \tilde{X} and \tilde{B} - \tilde{A} Band Systems. *J. Phys. Chem. A* **2014**, 118, 11852–11870.
55. Sluggett, G. W.; McGarry, P. F.; Koptug, I. V.; Turro, N. J. Laser flash photolysis and time-resolved ESR study of phosphinoyl radical structure and reactivity. *J. Am. Chem. Soc.* **1996**, 118, 7367–7372.
56. Constantinides, C. P.; Koutentis, P. A. Stable N- and N/S-Rich Heterocyclic Radicals: Synthesis and Applications. *Adv. Heterocycl. Chem.* **2016**, 119, 173–207.
57. (a) Ehrenfreund, P.; Charnley, S. B. Organic Molecules in the Interstellar Medium, Comets, And Meteorites: A Voyage from Dark Clouds to The Early Earth. *Annu. Rev. Astron. Astrophys.* **2000**, 38, 427–483; (b) Kuan, Y.-J.; Charnley, S. B.; Huang, H.-C.; Kisiel, Z.; Ehrenfreund, P.; Tseng, W.-L.; Yan, C.-H. Searches for Interstellar Molecules of Potential Prebiotic Importance. *Adv. Space Res.* **2004**, 33, 31–39; (c) Materese, C. K.; Nuevo, M.; Bera, P. P.; Lee, T. J.; Sandford, S. Thymine and other prebiotic molecules produced from the ultraviolet photo-irradiation of pyrimidine in simple astrophysical ice analogs. *Astrobiology* **2013**, 13, 948–962; (d) Hendrix, J.; Bera, P. P.; Lee, T. J.; Head-Gordon, M. Cation, anion, and radical isomers of C₄H₄N: Computational characterization and implications for astrophysical and planetary environments. *J. Phys. Chem. A* **2020**, 124, 2001–2013.
58. Murata, T.; Asakura, N.; Ukai, S.; Ueda, A.; Kanzaki, Y.; Sato, K.; Takui, T.; Morita, Y. Intramolecular Magnetic Interaction of Spin-Delocalized Neutral Radicals through *m*-Phenylene Spacers. *ChemPlusChem* **2019**, 84, 680–685.
59. Baumann, M.; Baxendale, I. R. An overview of the synthetic routes to the best-selling drugs containing 6-membered heterocycles. *Beilstein J. Org. Chem.* **2013**, 9, 2265–2319.
60. Volochnyuk, D. M.; Grygorenko, O. O.; Gorlova, A. O. Fluorine-Containing Diazines in Medicinal Chemistry and Agrochemistry. *Fluorine in Heterocyclic Chemistry* **2014**, 2, 577–672.
61. Wilhelm, M. J.; Petersson, G. A.; Smith, J. M.; Behrendt, D.; Ma, J.; Letendre, L.; Dai, H.-L. UV Photolysis of Pyrazine and the Production of Hydrogen Isocyanide. *J. Phys. Chem. A* **2018**, 122, 9001–9013.
62. Vazquez, J.; Lopez Gonzalez, J. J.; Marquez, F.; Pongor, G.; Boggs, J. E. Experimental and Theoretical Analysis of the Vibrational Spectra and Theoretical Study of the Structures of 3,6-Dichloropyridazine and 3,4,5-Trichloropyridazine. *J. Phys. Chem. A* **2000**, 104, 2599–2612.
63. Caminati, W.; Moreschini, P.; Favero, P. G. The Hydrogen Bond between Water and Aromatic Bases of Biological Interest: Rotational Spectrum of Pyridazine-Water. *J. Phys. Chem. A* **1998**, 102, 8097–8100.
64. Kasende, O.; Zeegers-Huyskens, T. Infrared Study of Hydrogen-Bonded Complexes Involving Phenol Derivatives and Polyfunctional Heterocyclic Bases. 1. Pyridazine, Pyrimidine, and Pyrazine. *J. Phys. Chem.* **1984**, 88, 2132–2137.
65. Kiefer, J. H.; Zhang, Q.; Kern, R. D.; Yao, J.; Jursic, B. Pyrolyses of Aromatic Azines: Pyrazine, Pyrimidine, and Pyridine. *J. Phys. Chem. A* **1997**, 101, 7061–7073.
66. Zeldes, H.; Livingston, R. Paramagnetic Resonance Study of Liquids during Photolysis. XIV. Pyridine, Pyrazine, Pyrimidine, and Pyridazine. *J. Phys. Chem.* **1972**, 76, 1972–1979.
67. Jinguji, M.; Hosako, Y.; Obi, K. Hydrogen Atom Abstraction Reaction by Triplet Pyrazine at Low Temperature. *J. Phys. Chem.* **1979**, 83, 2551–2553.
68. Lee, J.; Li, F.; Bernstein, E. R. Spectroscopic Studies of Pyrazine in Cryogenic Solutions. *J. Phys. Chem.* **1983**, 87, 260–265.

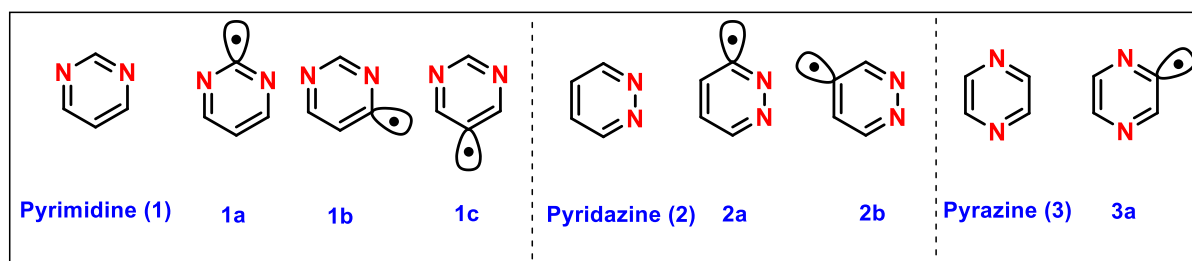
69. Chia, A. S-C.; Trimble, R. S., Jr. Acid-Base Properties of Some Pyrazines. *J. Phys. Chem.* **1961**, *65*, 863–866.
70. Zeng, J.; Hush, N. S.; Reimers, J. R. Solvent Effects on Molecular and Ionic Spectra. VIII. The $^1(n, \pi^*)$ Excited States of Pyridazine in Water. *J. Phys. Chem.* **1996**, *100*, 9561–9567.
71. Lahmani, F.; Ivanoff, N. Mercury Sensitization of the Isomerization of Diazines. *J. Phys. Chem.* **1972**, *76*, 2245–2248.
72. Breda, S.; Reva, I. D.; Lapinski, L.; Nowak, M. J.; Fausto, R. Infrared spectra of pyrazine, pyrimidine and pyridazine in solid argon. *J. Mol. Struct.* **2006**, *786*, 193–206.
73. Chatterjee, K.; Dopfer, O. Spectroscopic Identification of Fragment Ions of DNA/RNA Building Blocks: The Case of Pyrimidine. *Phys. Chem. Chem. Phys.* **2020**, *22*, 17275–17290.
74. Arpa, E. M.; Brister, M. M.; Hoehn, S. J.; Crespo-Hernández, C. E.; Corral, I. On the Origin of the Photostability of DNA and RNA Monomers: Excited State Relaxation Mechanism of the Pyrimidine Chromophore. *J. Phys. Chem. Lett.* **2020**, *11*, 5156–5161.
75. Samir, B.; Kalalian, C.; Roth, E.; Salghi, R.; Chakir, A. Gas-phase UV Absorption Spectra of Pyrazine, Pyrimidine and Pyridazine. *Chem. Phys. Lett.* **2020**, *751*, 137469–137474.
76. Ward, R. L. Electron Spin Resonance Studies of the Diazine Negative Ions. *J. Am. Chem. Soc.* **1962**, *84*, 332–334.
77. Knoth, I.; Neusser, H. J.; Schlag, E. W. Gas-Phase Two-Photon Spectroscopy of Polyazines. Pyrimidine. *J. Phys. Chem.* **1982**, *86*, 891–894.
78. Navarro, A.; Fernández-Gómez, M.; López-González, J. J.; Fernández-Liencres, M. P.; Martínez-Torres, E.; Tomkinson, J.; Kearley, G. J. Inelastic Neutron Scattering Spectrum and Quantum Mechanical Calculations on the Internal Vibrations of Pyrimidine. *J. Phys. Chem. A* **1999**, *103*, 5833–5840.
79. Wang, Z.-C.; Cole, C. A.; Demarais, N. J.; Snow, T. P.; Bierbaum, V. M. Reactions of Azine Anions with Nitrogen and Oxygen Atoms: Implications for Titan's Upper Atmosphere and Interstellar Chemistry. *J. Am. Chem. Soc.* **2015**, *137*, 10700–10709.
80. Choi, K.-W.; Ahn, D.-S.; Lee, J.-H.; Kim, S. K. Vibrational Spectroscopy of the Pyridazine Cation in the Ground State. *J. Phys. Chem. A* **2006**, *110*, 2634–2638.
81. Guin, M.; Patwari, G. N.; Karthikeyan, S.; Kim, K. S. Do *N*-heterocyclic Aromatic Rings Prefer π -stacking? *Phys. Chem. Chem. Phys.* **2011**, *13*, 5514–5525.
82. Pino, G. A.; Feraud, G.; Broquier, M.; Grégoire, G.; Soorkia, S.; Dedonder, C.; Jouvet, C. Non-radiative processes in protonated diazines, pyrimidine bases and an aromatic azine. *Phys. Chem. Chem. Phys.* **2016**, *18*, 20126–20134.
83. Kang, D. W.; Kim, H. L.; Kwon, C. H. Conformational Preference and Cationic Structure of 2-Methylpyrazine by VUV-MATI Spectroscopy and Natural Bond Orbital Analysis. *Phys. Chem. Chem. Phys.* **2019**, *21*, 9255–9264.
84. Nakamura, K. Emission Studies of Pyrazine in the Gas Phase. *J. Am. Chem. Soc.* **1971**, *93*, 3138–3140.
85. Taft, R. W.; Anvia, F.; Taagepera, M.; Catalan, J.; Elguero, J. Electrostatic Proximity Effects in the Relative Basicities and Acidities of Pyrazole, Imidazole, Pyridazine, and Pyrimidine. *J. Am. Chem. Soc.* **1986**, *108*, 3237–3239.
86. Verevkin, S. P.; Emel'yanenko, V. N.; Notario, R.; Roux, M. V.; Chickos, J. S.; Liebman, J. F. Rediscovering the wheel. Thermochemical analysis of energetics of the aromatic diazines. *J. Phys. Chem. Lett.* **2012**, *3*, 3454–3459.
87. Bent, D. V.; Hayon, E.; Moorthy, P. N. Chemistry of the triplet state of diazines in solution studied by laser spectroscopy. *J. Am. Chem. Soc.* **1975**, *97*, 5065–5071.
88. Wren, S. W.; Vogelhuber, K. M.; Garver, J. M.; Kato, S.; Sheps, L.; Bierbaum, V. M.; Lineberger, W. C. C-H Bond Strengths and Acidities in Aromatic Systems: Effects of Nitrogen Incorporation in Mono-, Di-, and Triazines. *J. Am. Chem. Soc.* **2012**, *134*, 6584–6595.
89. Lifshitz, A.; Suslensky, A.; Tamburu, C. Thermal Decomposition of 4-Methylpyrimidine. Experimental Results and Kinetic Modeling. *J. Phys. Chem. A* **2001**, *105*, 14, 3542–3554.
90. Ribeiro, F. d. A.; Almeida, G. C.; Wolff, W.; Boechat-Roberty, H. M.; Rocco, M. L. M. Fragmentation and Ion Desorption from Condensed Pyrimidine by Electron Impact:

- Implications for Cometary and Interstellar Heterocyclic Chemistry. *J. Phys. Chem. C* **2014**, *118*, 25978–25986.
91. Maclagan, R. G. A. R.; Gronert, S.; Meot-Ner, M. Protonated Polycyclic Aromatic Nitrogen Heterocyclics: Proton Affinities, Polarizabilities, and Atomic and Ring Charges of 1–5-Ring Ions. *J. Phys. Chem. A* **2015**, *119*, 127–139.
 92. Alkorta, I.; Elguero, J.; Del Bene, J. E. Azines as Electron-Pair Donors to CO₂ for N···C Tetrel Bonds. *J. Phys. Chem. A* **2017**, *121*, 8017–8025.
 93. Barckholtz, C.; Barckholtz, T. A.; Hadad, C. M. C-H and N-H Bond Dissociation Energies of Small Aromatic Hydrocarbons. *J. Am. Chem. Soc.* **1999**, *121*, 491–500.
 94. Fadden, M. J.; Hadad, C. M. Rearrangement Pathways of Aryl peroxy Radicals. I. The Azabenzenes. *J. Phys. Chem. A* **2000**, *104*, 6088–6094.
 95. Wang, W.; Hobza, P. Theoretical Study on the Complexes of Benzene with Isoelectronic Nitrogen-Containing Heterocycles. *ChemPhysChem* **2008**, *9*, 1003–1009.
 96. Hahn, S.; Stock, G. Efficient Calculation of Femtosecond Time-Resolved Photoelectron Spectra: Method and Application to the Ionization of Pyrazine. *Phys. Chem. Chem. Phys.* **2001**, *3*, 2331–2336.
 97. Shiozaki, T.; Woywod, C.; Werner, H.-J. Pyrazine Excited States Revisited Using the Extended Multi-State Complete Active Space Second-Order Perturbation Method. *Phys. Chem. Chem. Phys.* **2013**, *15*, 262–269.
 98. Mohan, N.; Suresh, C. H.; Kumar, A.; Gadre, S. R. Molecular Electrostatics for Probing Lone Pair– π Interactions. *Phys. Chem. Chem. Phys.* **2013**, *15*, 18401–18409.
 99. Sala, M.; Guerin, S.; Gatti, F. Quantum Dynamics of the Photostability of Pyrazine. *Phys. Chem. Chem. Phys.* **2015**, *17*, 29518–29530.
 100. Zierkiewicz, W.; Michalczyk, M.; Scheiner, S. Aerogen bonds formed between AeOF₂ (Ae = Kr, Xe) and diazines: comparisons between σ -hole and π -hole complexes. *Phys. Chem. Chem. Phys.* **2018**, *20*, 4676–4687.
 101. Wang, Y.; Wu, J. I.-C.; Li, Q.; Schleyer, P. v. R. Aromaticity and Relative Stabilities of Azines. *Org. Lett.* **2010**, *12*, 4824–4827.
 102. Adam, W.; Grimison, A.; Hoffmann, R. Hetaryne Intermediates. *J. Am. Chem. Soc.* **1969**, *91*, 2590–2599.
 103. Wiberg, K. B.; Nakaji, D.; Breneman, C. M. Azines. A Theoretical Study of Electron Delocalization. *J. Am. Chem. Soc.* **1989**, *111*, 4179–4190.
 104. Weber, P.; Reimers, J. R. Ab Initio and Density-Functional Calculations of the Vibrational Structure of the Singlet and Triplet Excited States of Pyrazine. *J. Phys. Chem. A* **1999**, *103*, 9830–9841.
 105. Ellenbogen, J. C.; Feller, D.; Davidson, E. R. Ab initio Calculation of the Properties and the Geometry of the Lowest Triplet State of Pyrazine. *J. Phys. Chem.* **1982**, *86*, 1583–1588.
 106. Cai, Z.-L.; Reimers, J. R. The Lowest Singlet (n, π^*) and (π, π^*) Excited States of the Hydrogen-Bonded Complex between Water and Pyrazine. *J. Phys. Chem. A* **2007**, *111*, 954–962.
 107. Howard, J. C.; Hammer, N. I.; Tschumper, G. S. Structures, Energetics and Vibrational Frequency Shifts of Hydrated Pyrimidine. *ChemPhysChem* **2011**, *12*, 3262–3273.
 108. Reimers, J. R.; Cai, Z.-L. Hydrogen Bonding and Reactivity of Water to Azines in their S₁ (n, π^*) Electronic Excited States in the Gas Phase and in Solution. *Phys. Chem. Chem. Phys.* **2012**, *14*, 8791–8802.
 109. Mennucci, B. Hydrogen Bond versus Polar Effects: An Ab Initio Analysis on $n\text{-}\pi^*$ Absorption Spectra and Nuclear Shielding of Diazines in Solution. *J. Am. Chem. Soc.* **2002**, *124*, 1506–1515.
 110. Chopra, N.; Chopra, G.; Kaur, D. Exploring the Role of Consecutive Addition of Nitrogen Atoms on Stability and Reactivity of Hydrogen-Bonded Azine–Water Complexes. *ACS Omega* **2019**, *4*, 8112–8121.
 111. Vogiatzis, K. D.; Mavrandonakis, A.; Klopper, W.; Froudakis, G. E. Ab initio Study of the Interactions between CO₂ and N-Containing Organic Heterocycles. *ChemPhysChem* **2009**, *10*, 374–383.

112. Su, M.-D. CASCSF Study on the Photochemical Transposition Reactions of Pyrazines. *J. Phys. Chem. A* **2006**, *110*, 9420–9428.
113. Scott, T.; Nieman, R.; Luxon, A.; Zhang, B.; Lischka, H.; Gagliardi, L.; Parish, C. A. A Multireference Ab Initio Study of the Diradical Isomers of Pyrazine. *J. Phys. Chem. A* **2019**, *123*, 2049–2057.
114. Chattopadhyay, S. Simplified Treatment of Electronic Structures of the Lowest Singlet and Triplet States of Didehydropyrazines. *J. Phys. Chem. A* **2019**, *123*, 5980–5994.

Chapter 2. Electronic Structure and Reactivity Studies of Dehydrodiazine Radicals

As previously discussed, the importance of dehydrodiazine radicals in various aspects, we explored the electronic structure of six isomeric diazine radicals. Introduction of radical centres in those diazines gains additional importance because they can provide three-centred-five-electrons (3c-5e) interactions that include the radical electron and the two nitrogen lone pairs. (Scheme 2.1) The involvement of five electrons and their multi-centric interactions are largely responsible for the electronic structural and stability aspects of these isomers; hence, studies on them gain value from the fundamental point of view.



Scheme 2.1 Three parent diazines (**1–3**) and their respective six dehydrodiazine radical isomers (**1a–c**, **2a–b**, **3a**).

Recently, we investigated the interaction between the nitrogen lone pair and the radical electron (2c-3e) in pyridyl radical isomers, where in spite of the presence of through bond interactions in all the three isomers, through space interactions are decisive in the relative stability order.^[1] Similarly, the interactions of the nitrogen lone pair in pyridine biradicals (3c-4e) have also been reported by various groups.^[2] In all those cases, the nitrogen lone pair is weakly interacting with a system that has already been stabilized through radical–radical (spin coupling) interactions. However, the relative position of the nitrogen is very important in influencing the singlet–triplet energy gap. Hoffmann has reported the presence of through bond coupling between the two nitrogen lone pairs (2c-4e) in pyrazine, where the symmetric combination of two lone pairs was well above their antisymmetric combination.^[3] If we extend such interactions to dehydrodiazine radicals, which possess two lone pairs and one radical electron (3c-5e), a few fundamental questions such as the following arise: (a) Among the lone pair–lone pair or radical–lone pair interactions, which one dominates in diazine radicals? (b) Does the interaction of two lone pairs with the radical centre happen cooperatively or through domination of one of them? (c) Is the through space interaction still decisive in diazine radicals too? (d) Finally, can such interactions be quantified? In this context, we have investigated six

isomeric dehydrodiazine radicals (**1a–c**, **2a–b** and **3a**), their relative stability and various possible factors influencing their stability such as role of heteroatom, nitrogen lone pairs, possibility of lone pair-radical interaction, mode of interaction, strength of various interaction using various quantum chemical methods and calculations.^[4]

2.1 First C-H bond dissociation energies of isomeric dehydrodiazines radicals

We estimated the first C-H bond dissociation energy from the respective diazines namely pyrimidine **1**, pyridazine **2** and pyrazine **3** which led to the corresponding radical isomers as shown in the figure 2.1. In diazines, six possible radical isomers exists in which three of them are dehydropyrimidines (**1a,1b** and **1c**), two dehydropyridazines (**2a** and **2b**) and one dehydro-pyrazine (**3a**). Bond dissociation energy (BDE) has been classified as the change in enthalpy/energy of a particular reaction. BDEs can be estimated by taking the difference of enthalpy/energy of product and reactants. Here we have estimated the BDEs the first C-H bond cleavage reactions in diazines (Figure 2.1). BDE values provide an insight about the thermodynamic stability of products, in this case radicals. A low BDE value implies a more stable product or in other words that the reaction is feasible in forward direction (or the ease of formation of radical species). We have estimated the BDEs (at 0 K) on different levels of theories like (U)B3LYP/cc-pVTZ, (U)M062X/cc-pVTZ and CBS-QB3. Indeed, all the levels of theory predict the same trend. Among these CBS-QB3 level of theory is known to be very accurate for the estimation of thermochemical data/values.^[5]

We have compared the relative stability of three dehydropyrimidines (**1a,1b** and **1c**) based on respective BDEs. Among dehydropyrimidines, we found the increasing order of BDEs as follows **1b** < **1a** < **1c**. Based on this trend we can conclude that **1b** is thermodynamically more stable followed by **1a** and **1c** among dehydropyrimidines. On the other hand, among dehydropyridazines, we found out that **2a** has less BDE value compared to **2b** which means **2a** is more thermodynamically stable compared to **2b**.

Based on the BDEs, we can also estimate the relative thermodynamic stability of all six dehydrodiazine radical isomers. In order to compare the relative stability, we found out the increasing order of BDE value trend as following **1b** < **3a** < **1a** < **2a** < **2b** < **1c**. Based on this trend we found out the relative thermodynamic stability order as the following **1b** > **3a** > **1a** > **2a** > **2b** > **1c**. (Figure 2.1) Based on this we found out that, 2-dehydropyrimidine **1b** is the most thermodynamically stable and 5-dehydropyrimidine **1c** is the least stable among all six dehydrodiazine radical isomers. At this point of discussion, we observed significant changes in bond dissociation energy of each C–H bond depending on the relative position with respect

to the two nitrogens. This clearly indicates the existence of interactions between the radical center and nitrogen lone pairs. However, the nature of interaction cannot be decided based on the BDE data alone.

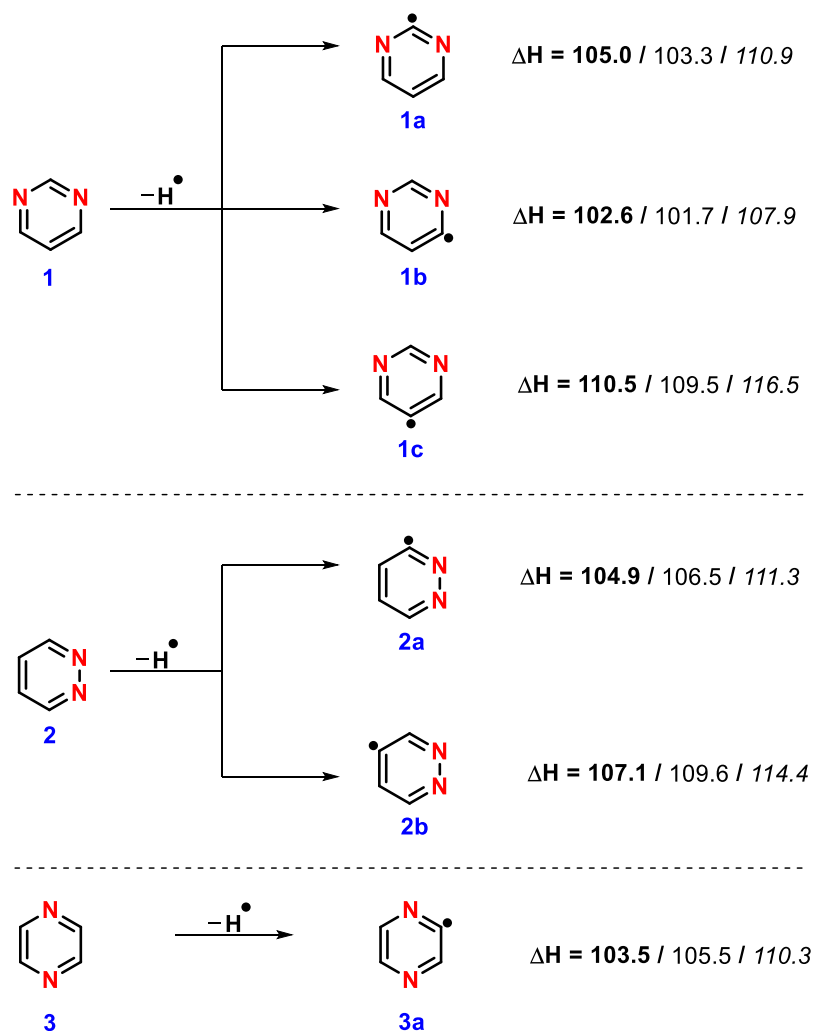


Figure 2.1 Bond dissociation energies (in kcal/mol at 0 K) corresponding to the first C–H bond of the isomeric diazine molecules (**1**, **2** and **3**) leading to the dehydrodiazine radicals (**1a–c**, **2a–b** and **3a**) at different levels of theory. Bold: (U)B3LYP/cc-pVTZ, Normal: (U)M06-2X/cc-pVTZ and Italics: CBS-QB3.

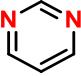
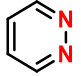
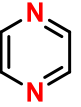
2.2 Relative thermodynamic stability of diazines and their isomeric radicals

In the previous section, BDE values help us in understanding the relative stability of all the six dehydrodiazine radical isomers. In this section, we have estimated the relative thermodynamic stability of all the diazines as well as their radical isomers based on comparison of their absolute zero-point corrected electronic energies. In this regard, we have estimated the

relative stability of diazines, pyrimidine **1**, pyridazine **2** and pyrazine **3** respectively at different levels of theory as well as different basis sets as mentioned in table 2.1.

Upon comparison of electronic energies, pyridazine was found to be the least stable and pyrimidine to be the most stable among these diazine molecules. Relative stability of these diazine molecules (pyrimidine, pyridazine and pyrazine) can be explained by the various possible interactions between nitrogen lone pairs. After getting the relative thermodynamic stability of pyrimidine, pyridazine and pyrazine, we estimated the relative thermodynamic stability of all the six dehydrodiazine radical isomers using electronic energies at various levels of theory.

Table 2.1 Relative electronic energies (zero point corrected) of all the diazines (**1**, **2** and **3**) at different levels of theory.

Level of theory	Relative energy (in kcal/mol at 0 K)		
			
	Pyrimidine 1	Pyridazine 2	Pyrazine 3
(U)B3LYP/6-311++G(d,p)	0.0	22.4	4.0
(U)B3LYP/cc-pVDZ	0.0	21.5	3.9
(U)B3LYP/aug-cc-pVDZ	0.0	21.6	3.8
(U)B3LYP/cc-pVTZ	0.0	21.9	4.0
(U)B3LYP/aug-cc-pVTZ	0.0	22.0	4.0
(U)B3LYP/cc-pVQZ	0.0	22.0	4.0
(U)B3LYP/aug-cc-pVQZ	0.0	21.9	4.0
(U)BLYP/cc-pVTZ	0.0	20.3	3.5
(U)M06-2X/cc-pVTZ	0.0	23.3	4.5
CBS-QB3	0.0	28.5	4.0
(U)CCSD(T)/cc-pVTZ/(U)B3LYP/cc-pVTZ	0.0	22.4	4.9
(U)CCSD(T)/cc-pVTZ/(U)M06-2X/cc-pVTZ	0.0	29.4	7.6

On closer inspection of absolute electronic energies of all the radical isomers, we found out that **1b** has the lowest absolute energy among all dehydrodiazine radicals. So, we estimated the relative energies of remaining isomers **1a**, **1c**, **2a**, **2b** and **3a** with respect to **1b** as mentioned in table 2.2.

The stability order of diazine radicals was obtained by comparison of the respective absolute energies of the individual isomers. The relative energies of radical isomers at different levels of theory and basis sets are also listed in table 2.2. In case of dehydropyrimidines, **1b** is found to be the most stable isomer followed by **1a** and **1c**. In a conventional point of view, nitrogen lone pairs interact with the electron deficient radical centre analogous to mesomeric effect that renders the stability. In this regard, the isomer **1a** is expected to be the most stable isomer, where the radical centre resides in between two nitrogen atoms. However, it turned out to be 1.7 to 3.1 kcal/mol higher than **1b**. At this point of discussion, this can be attributed to unequal contributions from the two competitive lone pair-lone pair (destabilizing) and lone pair-radical electron (stabilizing) interactions.

Table 2.2 Relative energies (zero point corrected) of dehydrodiazine radical isomers (**1a–c**, **2a–b** and **3a**) at different levels of theory.

Level of theory	Relative energy (in kcal/mol at 0 K)					
	Dehydropyrimidine radicals			Dehydropyridazine radicals		Dehydropyrazine radical
	1a	1b	1c	2a	2b	3a
(U)B3LYP/6-311++G(d,p)	2.5	0.0	7.8	24.7	26.8	4.9
(U)B3LYP/cc-pVDZ	2.2	0.0	7.8	23.9	25.8	4.8
(U)B3LYP/aug-cc-pVDZ	2.5	0.0	7.6	23.9	25.8	4.7
(U)B3LYP/cc-pVTZ	2.4	0.0	7.9	24.2	26.5	4.9
(U)B3LYP/aug-cc-pVTZ	2.5	0.0	7.9	24.3	26.5	4.9
(U)B3LYP/cc-pVQZ	2.4	0.0	8.0	24.3	26.6	4.9
(U)B3LYP/aug-cc-pVQZ	2.5	0.0	8.0	24.3	26.5	4.9
(U)BLYP/cc-pVTZ	3.1	0.0	7.6	22.7	23.2	4.0
(U)M06-2X/cc-pVTZ	1.7	0.0	8.0	25.6	28.7	5.9
CBS-QB3	3.0	0.0	8.6	25.4	28.5	6.0
(U)CCSD(T)/cc-pVTZ// (U)B3LYP/cc-pVTZ	1.9	0.0	7.4	26.3	29.4	6.5
(U)CCSD(T)/cc-pVTZ// (U)M06-2X/cc-pVTZ	2.0	0.0	6.6	26.4	29.4	7.6

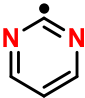
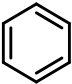
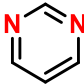
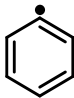
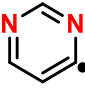

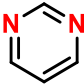
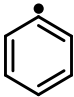
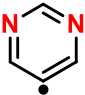

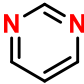
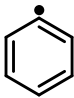
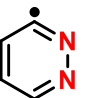

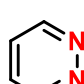

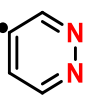
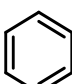
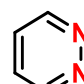
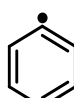
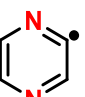

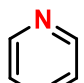
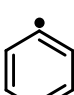
Among the dehydropyrimidine radicals, **1c** is the least stable in which both nitrogen atoms are *meta* to the radical centre, where both the interactions are relatively destabilizing. In the case of dehydropyridazine radicals, **2a** is found to be the most stable isomer. Here again

the stabilizing lone pair-radical electron interaction is more favourable only in the case **2a**, and so it is found to be more stable. Thus, the relative energy order in the above cases follows the **1b** < **1a** < **1c** and **2a** < **2b** trends. Based on the trend, it is evident that the stabilizing interaction between the radical electron and the lone pair is the decisive factor in determining the stability of various isomers. Hence, the relative position of nitrogen lone pairs and radical centre are vital in deciding the overall stability trend among the six isomeric dehydrodiazine radicals. The relative stability order among the six radicals at different levels of theory are consistent with (U)B3LYP/cc-pVTZ. This includes the single point energies at (U)CCSD(T)/cc-pVTZ level of theory either using the (U)B3LYP/cc-pVTZ or (U)M06-2X/cc-pVTZ optimized geometries as well.

2.3 Radical stabilization energy of isomeric dehydrodiazines radicals through isodesmic reaction

In the previous section, we compared the absolute energies of radical isomers relative to the most stable isomer. Generally radical stabilization energy (RSE) is an alternative way of measuring the stability of the radicals, in which a hypothetical isodesmic reaction between the radical and another reactant is considered in such a way that the bond breaking and bond-forming are of similar type.^[6] We have utilized benzene as the second reactant so that products comprise of the diazine and the phenyl radical. The enthalpy change (ΔH_{298}) accompanying such reactions will provide the RSEs. Since all the six radical isomers of dehydro-diazines are isoelectronic, the radical stabilization energy provides further clues on the interactions between the radical centre and the nitrogen atoms. The data for RSEs is listed in table 2.3 at (U)B3LYP/cc-pVTZ, (U)M06-2X/cc-pVTZ and CBS-QB3 levels of theory. More negative or less positive values of ΔH_{298} indicate a less stable radical isomer, whereas more positive or less negative values indicate a more stable radical isomer. Out of all six radical isomers, radical **1b** is found to be the most stable, in which the radical centre is at *ortho*- position to one nitrogen atom and *para*- to other nitrogen atom. Isomer **1c** is found to be the least stable among all six isomers, where the radical centre is at *meta*- position to both nitrogen atoms. All these evidences clearly indicated that the interaction between radical centre and lone pairs of electron plays a major role in determining the relative stability. Based on these radical stabilization energy values from isodesmic reactions at different levels of theory, we found out that order of stability for all the six radical isomers is in good agreement with the relative stability order obtained by comparing the absolute energies of the radicals in the previous section.

Table 2.3 Radical stabilization energies (RSEs in kcal/mol) of the isomeric dehydrodiazines radicals (**1a–c**, **2a–b** and **3a**) through isodesmic reactions at different levels of theory. Bold: (U)B3LYP/cc-pVTZ, Normal: (U)M06-2X/cc-pVTZ and Italics: CBS-QB3

Radicals	Reactant and products in the isodesmic reactions						ΔH_{298}	
1a		+		\longrightarrow		+		4.2 3.8 4.6
	1a				1			
1b		+		\longrightarrow		+		6.6 5.5 7.6
	1b				1			
1c		+		\longrightarrow		+		-1.3 -2.5 -1.1
	1c				1			
	<hr/>							
2a		+		\longrightarrow		+		4.2 3.1 4.1
	2a				2			
2b		+		\longrightarrow		+		2.0 0.04 1.0
	2b				2			
	<hr/>							
3a		+		\longrightarrow		+		5.7 4.1 5.1
	3a				3			

2.4 Geometrical parameters of diazines and their isomeric dehydrodiazines radicals

All the six dehydrodiazine radical isomers and their respective parent molecules (pyrimidine, pyrazine and pyridazine) have been optimized at (U)B3LYP/cc-pVTZ and (U)M06-2X/cc-pVTZ levels of theory and are shown in figure 2.2. Majority of the radical isomers are found to have a C_s structure, whereas **1a** and **1c** are optimized at C_{2v} structure.

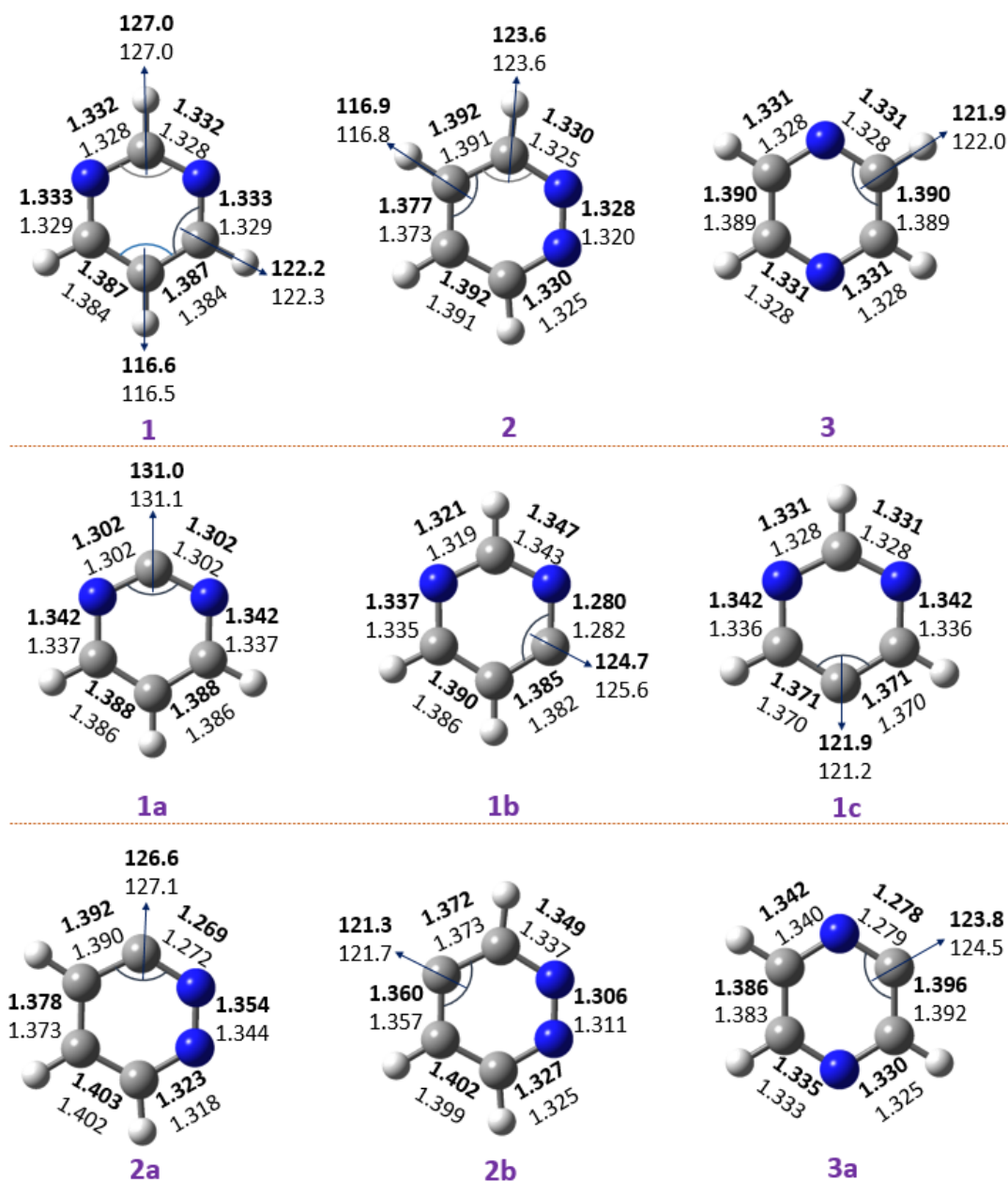


Figure 2.2 Optimized geometries of three parent diazines (**1–3**) and their respective six dehydrodiazine radical isomers (**1a–c**, **2a–b**, **3a**). The most important bond distances (in Å units) and the bond angles (in degrees) at the radical centres are mentioned. The indicated geometrical parameters in bold font correspond to (U)B3LYP/cc-pVTZ and those in normal font are estimated at the (U)M06-2X/cc-pVTZ levels of theory.

Based on the comparison of geometrical parameters, we found out that the internuclear distances between the radical centres and the adjacent atoms on either side have a contraction relative to the parent compound. Similarly, alternate bonds relative to the radical centres showed a marginal increase with respect to the parent compound. This general behaviour is consistent with our previous studies on the heterocyclic radicals. Apart from that, we also

observed a common trend in the bond angles at the radical centres, the value of which increased upon creation of radical centre in any one of the parent compounds. The extent of increase or decrease in the bond lengths and change in bond angles relative to their parent compound certainly depend on the relative position of the radical centre with respect to the nitrogen atoms.

2.5 Spin densities of isomeric dehydrodiazines radicals

Spin density is the difference of electron density of opposite spins in that particular molecule. The estimation of spin densities is found to be very useful in case of radicals particularly with heteroatom substitutions. As the spin density measures the extent of localization of unpaired electron (spin), it enables the understanding of interaction between the radical centre and the lone pair.^[7] Ideally open shell radical species should possess a total spin density value of one. If the spin density values are close to one means that radical is localized over that particular centre, whereas, deviation from one is considered as a parameter of delocalization of radical over the molecule that usually enhances the stability of the radical.

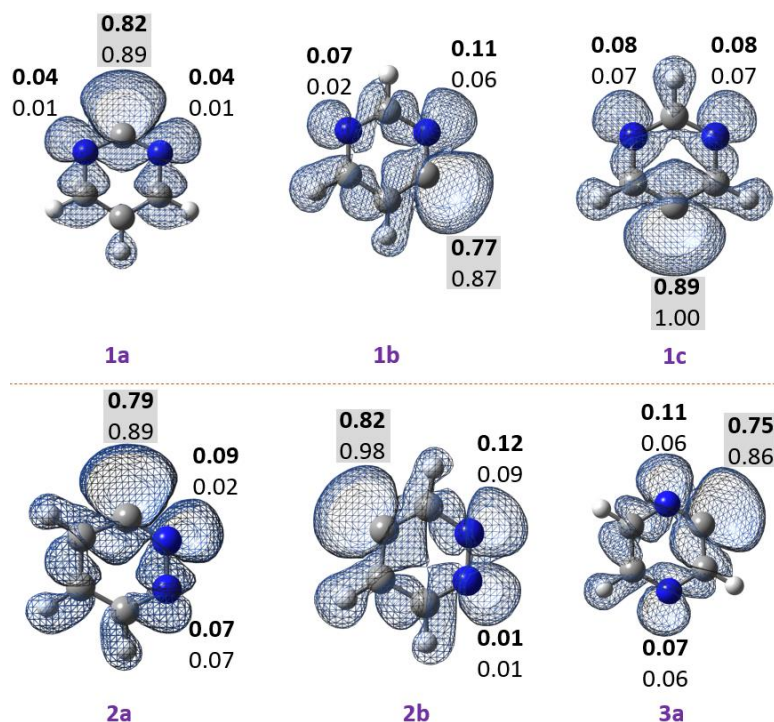


Figure 2.3 Mulliken spin densities of dehydropyrimidine (**1a–c**), pyridazine (**2a–b**) and pyrazine (**3a**) radicals. (Bold: (U)B3LYP/cc-pVTZ; Normal: (U)M06-2X/cc-pVTZ) Each radical isomer is rendered at an isovalue of 0.002.

Mulliken spin densities of all the six radical isomers have been calculated at the (U)B3LYP/cc-pVTZ and (U)M06-2X/cc-pVTZ levels of theory. The spin density values are listed in the figure 2.3. All the radicals are carbon-centred and have spin density values ranging between 0.75 to 0.89 at (U)B3LYP/cc-pVTZ level of theory. Besides in all the case, nitrogen

atoms also possess non-zero spin densities depending on proximity to the radical centre, which clearly indicates the presence of a stabilizing interaction between the radical centre and the lone pair of electrons. In general, larger values of spin densities indicate the more localization of radical at the particular centre, which is responsible for the high reactivity compared to other radical isomers.

2.6 Electrostatic potential and Mulliken charges of isomeric dehydrodiazines radicals

Similarly, the electrostatic potentials have also been derived for all the radicals.^[8] The electrostatic potential mapping of all the radicals showed an appearance of a weak negative potential close to the radical centres due to the involvement of interactions between nitrogen lone pairs and radical centres, and are mentioned in figure 2.4.

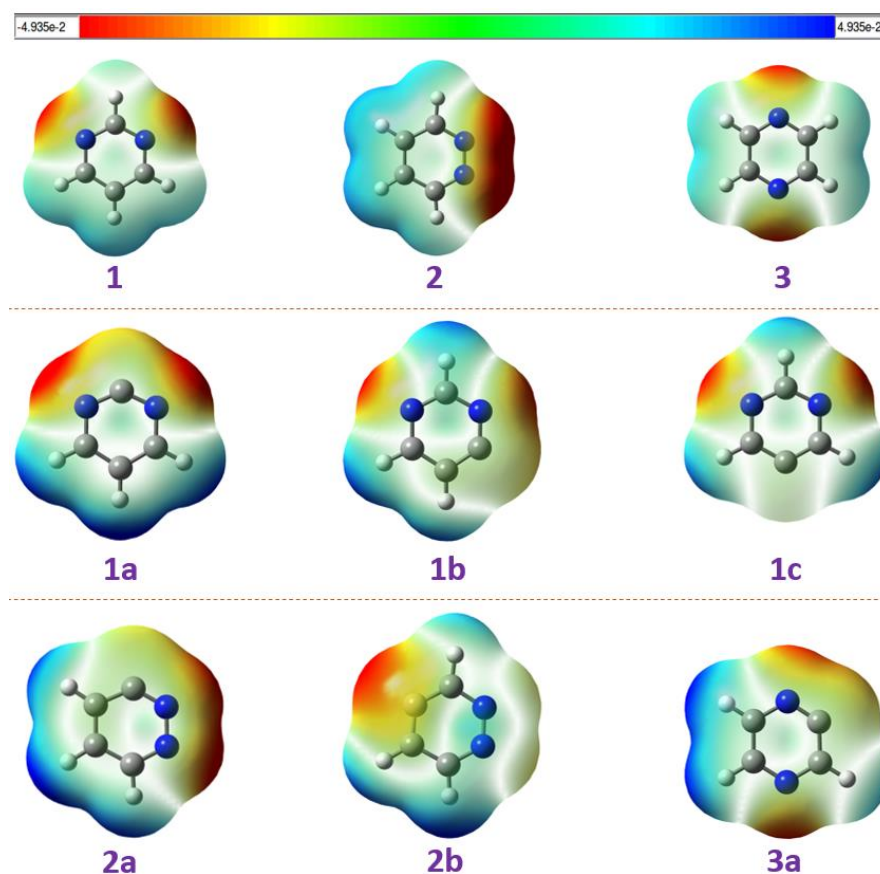


Figure 2.4 Electrostatic potential mapping of three parent diazines (**1–3**) and their respective six dehydrodiazine radical isomers (**1a–c**, **2a–b**, **3a**) at (U)B3LYP/cc-pVTZ level of theory.

Furthermore, we have considered the possibility of zwitterionic character in all the diazine radical isomers. In this regard, we have chosen the natural and Mulliken charges. (Figure 2.5) On comparison of the charges at the nitrogen centres with that of their respective

parent molecules, all the isomers except **1a** and **1c** showed a significant polarization of charges. This can be attributed to the unequal interactions of nitrogens with the radical centres.

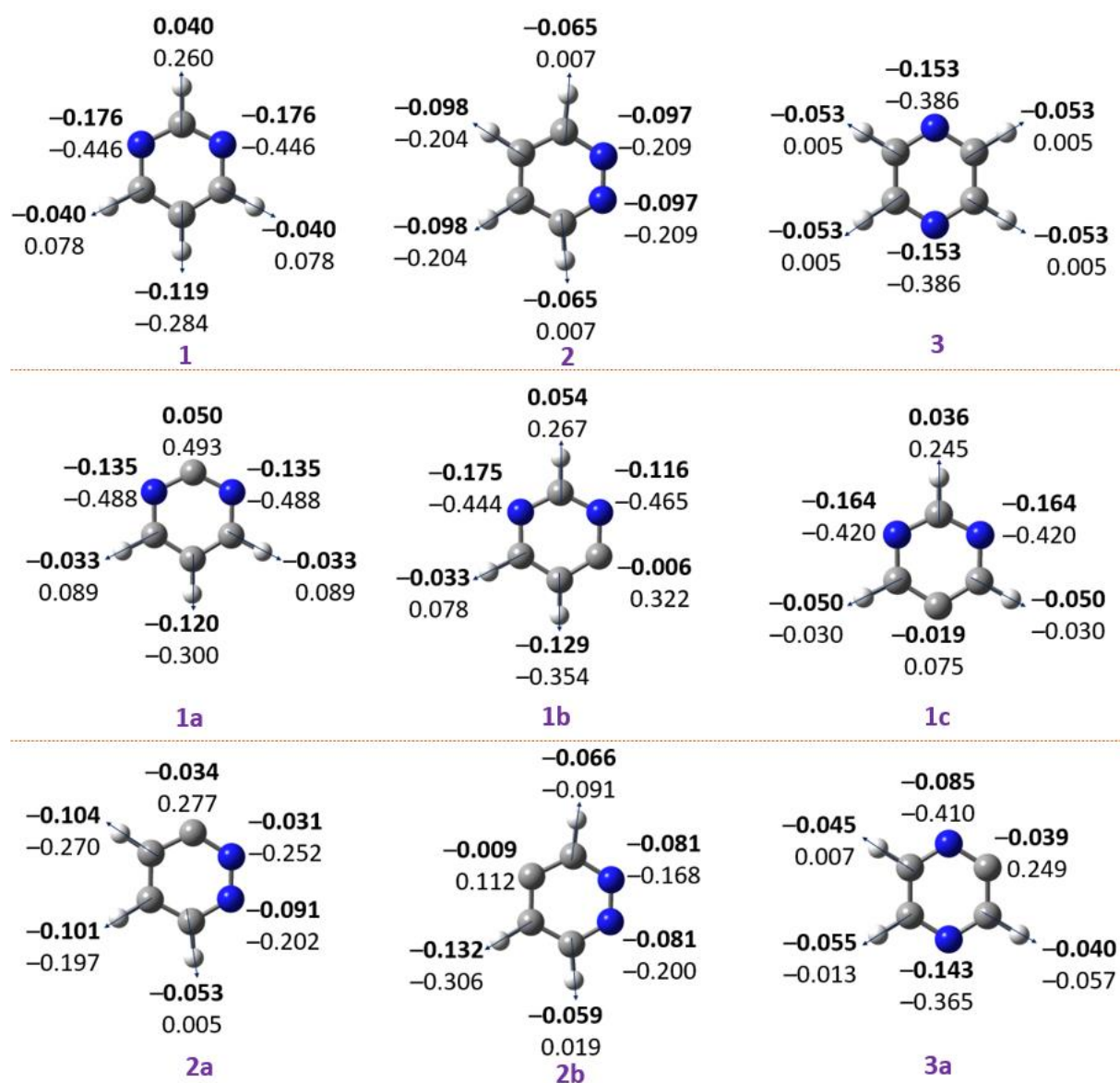


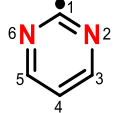

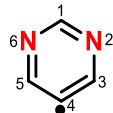
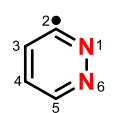
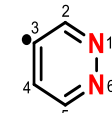
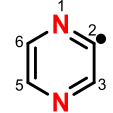
Figure 2.5 Natural and Mulliken charges of three parent diazines (**1–3**) and their respective six dehydrodiazine radical isomers (**1a–c**, **2a–b**, **3a**) at (U)B3LYP/cc-pVTZ level of theory. (Bold – Mulliken charges; Normal – Natural charges)

2.7 Natural bond orbital (NBO) analysis of isomeric dehydrodiazines radicals

In order to support the results so far, and also to obtain the quantitative terms in the interaction between the two lone pairs and radical centre, we have performed NBO analysis. The involvement of unrestricted formalism in such an analysis separates the interacting orbitals based on the spatial form as well as spin. On the basis of the Lewis structures, an independent

analysis of α - and β -spin is carried out and the resulting orbital interaction energies are based on second order perturbation approximation.^[9] We have performed the NBO calculations on all six radical isomers at (U)B3LYP/cc-pVTZ and (U)M06-2X/cc-pVTZ levels of theory as indicated in table 2.4. For dehydropyrimidine molecules the radical isomer **1a** is having C_{2v} structure and the radical centre is flanked between two nitrogen lone pairs. From the NBO data, we inferred the presence of a strong through space interaction between both the lone pairs and the radical centre in **1a** with an interaction energy of 10.1 kcal/mol. For all other radicals, we observed only one mode of through space interaction component between the radical centre and lone pair, when they are spatially at *ortho*- or *meta*- position to each other. However, there are several possibilities of through bond interactions. We have mentioned all possible through bond interaction components, which have significant interaction energies (>4.0 kcal/mol) between the lone pairs and the radical electron in table 2.4. Based on the results from NBO calculations, we found out that through space interaction between lone pair and radical centre was possible only when they are either *ortho* or *meta* to each other. The extent of TS interaction energy is maximal when the radical centre and lone pairs are *ortho* to each other. The strength of such interactions decreases upon moving to *meta* and the interaction was completely absent when they are *para* to each other. Similarly, we have also observed through bond interactions of lone pairs with radical centre. Through bond interaction component exists in almost all radicals and generally provides a stabilizing effect. The extent of the TB interaction energy between the nitrogen lone pair and the radical electron increases from *ortho* to *meta* to *para* in all the radical isomers. In case of C_s symmetric radical **1b**, the radical centre is *ortho* to one of the nitrogen atoms and *para* to the other nitrogen. Nitrogen lone pair which is *ortho* to radical has a TS interaction with the radical centre and exhibits an interaction energy of 17.2 kcal/mol. On the other hand, the nitrogen lone pair *para* to radical centre does not exert any TS interaction with the radical centre. Through bond interactions is the only mode of stabilizing interaction between the lone pair and the radical centre at *para* position. Similarly, dehydropyrimidine isomer **1c** possesses a C_{2v} symmetric structure, in which both the lone pairs reside at *meta* position with respect to the radical centre. In this case, the extent of TS interaction is observed to be 0.8 kcal/mol and such low values are attributed to the geometrical constraints. However, a significant amount of TB interactions stabilizes the radical centre. Based on BDE, RSE and

Table 2.4 The second order perturbation energies (in kcal/mol) from the natural bond orbital (NBO) analysis of dehydrodiazine radical isomers (**1a–c**, **2a–b** and **3a**). (Bold - (U)B3LYP/cc-pVTZ and normal-(U)M06-2X/cc-pVTZ) (atom numbering as per the gaussian output file)

1a 			1b 			1c 		
Donor	Acceptor	E	Donor	Acceptor	E	Donor	Acceptor	E
n(N2)	n*(C1)	10.1 12.5	n(N2)	n*(C3)	17.2 23.2	n(N2)	n*(C4)	0.8 1.1
n(N2)	$\pi^*_{(C1-N2)}$	0.7 0.4	n(N2)	$\pi^*_{(C1-N6)}$	5.6 6.5	n(N2)	$\pi^*_{(C1-N6)}$	5.6 6.7
n(N2)	$\pi^*_{(C1-N6)}$	4.1 4.9	n(N2)	$\pi^*_{(C3-C4)}$	3.1 3.8	n(N2)	$\pi^*_{(C3-C4)}$	5.5 6.2
n(N6)	n*(C1)	10.1 12.5	n(N2)	$\pi^*_{(N2-C3)}$	0.4 --	n(N6)	n*(C4)	0.8 1.1
n(N6)	$\pi^*_{(C1-N2)}$	4.1 4.9	n(N6)	n*(C3)	--	n(N6)	$\pi^*_{(C1-N2)}$	5.6 6.7
n(N6)	$\pi^*_{(C1-N6)}$	0.7 0.4	n(N6)	$\pi^*_{(C4-C5)}$	5.6 6.5	n(N6)	$\pi^*_{(C4-C5)}$	5.5 6.2
$\pi^*_{(C3-C4)}$	$\pi^*_{(C1-N2)}$	30.4 33.6	$\pi^*_{(C1-N6)}$	$\pi^*_{(N2-C3)}$	23.3 29.6	$\pi^*_{(C1-N2)}$	$\pi^*_{(C3-C4)}$	26.5 --
$\pi^*_{(C5-N6)}$	$\pi^*_{(C1-N2)}$	32.6 38.6	$\pi^*_{(C4-C5)}$	$\pi^*_{(N2-C3)}$	36.4 38.2	$\pi^*_{(C5-N6)}$	$\pi^*_{(C3-C4)}$	33.6 --
2a 			2b 			3a 		
n(N1)	n*(C2)	23.7 27.0	n(N1)	n*(C3)	0.7 1.0	n(N1)	n*(C2)	20.0 25.7
n(N1)	$\pi^*_{(C2-C3)}$	3.8 4.5	n(N1)	$\pi^*_{(C5-N6)}$	4.9 5.9	n(N1)	$\pi^*_{(C2-N1)}$	0.3 --
n(N1)	$\pi^*_{(C5-N6)}$	3.9 4.8	n(N1)	$\pi^*_{(C2-C3)}$	5.9 6.6	n(N1)	$\pi^*_{(C2-C3)}$	3.1 3.7
n(N6)	n*(C2)	0.6 0.7	n(N6)	$\pi^*_{(N1-C2)}$	1.5 7.2	n(N4)	n*(C2)	0.5 0.8
n(N6)	$\pi^*_{(C2-N1)}$	4.4 5.0	n(N6)	n*(C3)	--	n(N4)	$\pi^*_{(C5-C6)}$	5.0 5.8
n(N6)	$\pi^*_{(C5-N6)}$	0.7 --	n(N6)	$\pi^*_{(C4-C5)}$	5.9 6.9	n(N4)	$\pi^*_{(C2-C3)}$	6.4 7.2
$\pi^*_{(C3-C4)}$	$\pi^*_{(C2-N1)}$	29.2 30.8	$\pi^*_{(N1-C2)}$	$\pi^*_{(C3-C4)}$	27.0 35.6	$\pi^*_{(C5-C6)}$	$\pi^*_{(C2-N1)}$	28.6 33.3
$\pi^*_{(C5-N6)}$	$\pi^*_{(C2-N1)}$	15.6 21.7	$\pi^*_{(C5-N6)}$	$\pi^*_{(C3-C4)}$	22.9 30.5	$\pi^*_{(C3-N4)}$	$\pi^*_{(C2-N1)}$	34.6 40.8

relative energy data, we found out that radical **1b** is more stable than **1a** followed by **1c** among the three isomeric dehydro-pyrimidine radicals. The reason behind such trend is clarified quantitatively using the NBO analysis. In **1b** the radical centre is stabilized by TS and TB interactions from *ortho* and *para* lone pairs, respectively. Both contribute significantly to stabilize **1b** than **1a** and **1c**. In case of **1a**, both lone pairs are stabilizing the radical by TS interactions, however, with a lesser interaction energy. In case of **1c**, there is no significant TS interaction to stabilize the radical centre. Similar trends are also observed in the case of **2a**, **2b** and **3a** towards stability.

2.8 Molecular orbitals analysis of isomeric dehydrodiazines radicals

The geometrical parameters, NBO analysis and electrostatic potentials showed the presence of weak to strong interactions between the radical centre and the nitrogen lone pairs via through space and through bond in all the dehydrodiazine radical isomers. In order to understand further or confirm the nature of interaction between orbitals, we performed multireference calculations using complete active space self-consistent field (CASSCF) method. In these calculations, 9 orbitals have been chosen in the active space that include the six π -orbitals of the aromatic ring, two σ -orbitals corresponding to the lone pairs of nitrogen atoms and one σ -orbital corresponding to the radical centre. Correspondingly, we have included 11 electrons (6-aromatic, 2-lonepairs and one radical electron) in the active space for all the six radical isomers. The molecular orbitals corresponding to the complete active space are mentioned in figure 2.6 including the singly occupied molecular orbital, SOMO. In all the radical isomers, within the active space the low-lying orbitals are corresponding to the nitrogen lone pairs. Besides, the ground electronic states of the isomeric radicals have been derived from the SOMO, which was found to be either $^2A'$ or 2A_1 depending on their symmetry (C_s and C_{2v}). On comparison of the energetic ordering of the three molecular orbitals corresponding to nitrogen lone pairs and the radical electron, the interaction between them can be qualitatively identified. Particularly when the interacting orbitals are *ortho* (1,2-relation) to each other, TS interaction will be more dominant, whereas the *para* (1,4-relation) TB interactions will be preferred more. On the other hand, positioning of orbitals at *meta* (1,3-relation) leads to significant contributions of both the TS and TB interactions in a different proportion. According to Hoffmann's analysis on the consequences of TS and TB interactions on molecular orbitals, the former (TS) case can be understood when symmetric combination of the two interacting orbitals is low-lying compared to the antisymmetric combination. [3] For the

latter case (TB), the energetic ordering will be reversed in the two interacting orbitals, i.e., the antisymmetric combination will be well below the symmetric combination. In all the six radical isomers, the interaction of radical centre with each nitrogen lone pair is either by through space or through bond depending on the relative positions.

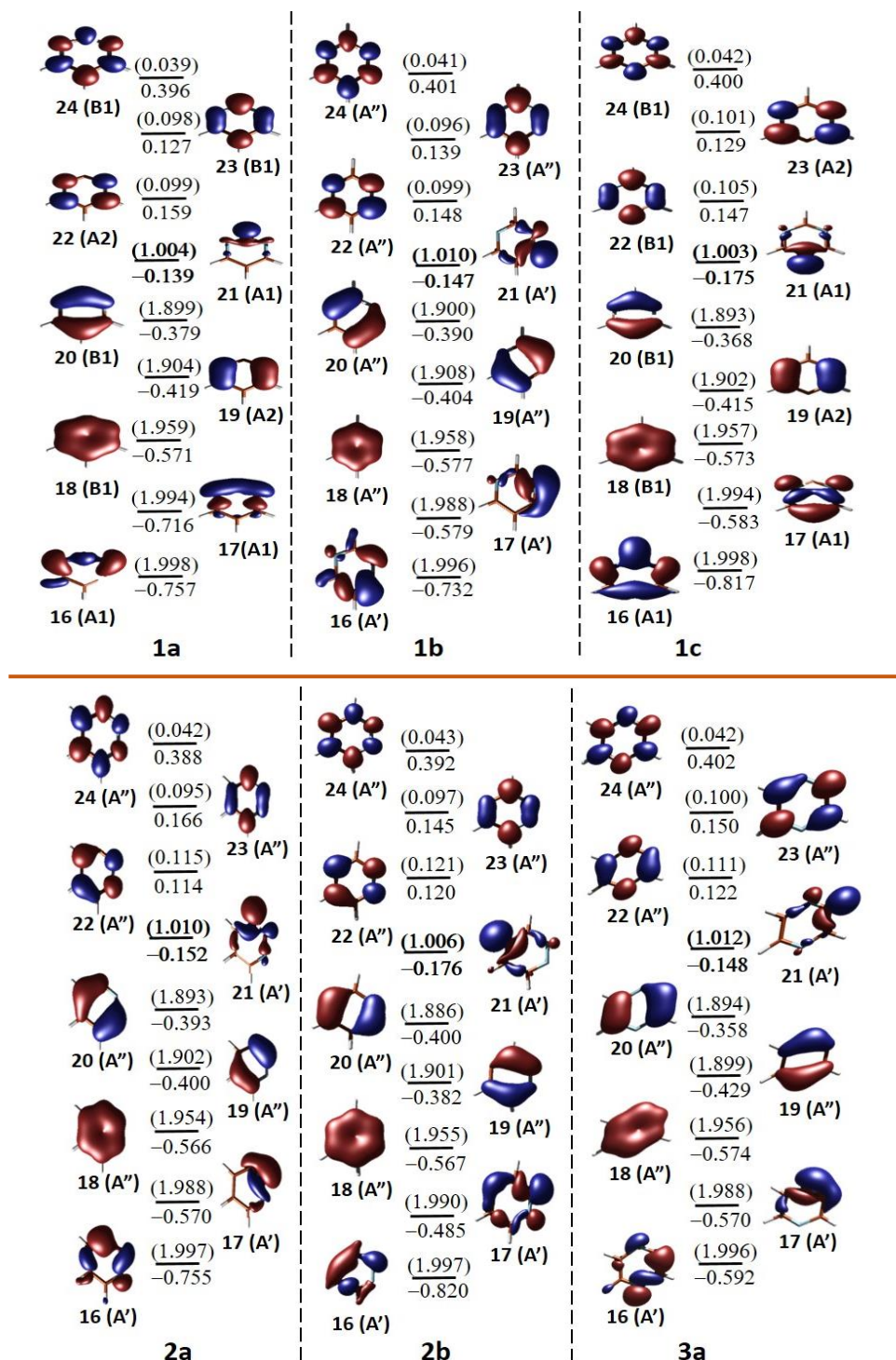


Figure 2.6 Molecular orbitals of six dehydrodiazine radical isomers (**1a–c**, **2a–b**, **3a**) using multiconfigurational CASSCF method at /cc-pVTZ level of theory.

Upon closer inspection, we observed that the molecular orbitals of all the isomeric radicals have TS interaction when one of the lone pairs and radical orbitals are *ortho* to each other. In such cases, the symmetric combination of lone pair is low lying relative to the anti-symmetric combination. Similarly, we have verified the existence of through bond interaction in all the radical isomers based on the ordering of molecular orbitals, where the antisymmetric combination is low lying compared to the symmetric combination. Thus, the multicentric interactions between the nitrogen lone pairs and the radical electrons are clearly understood from the results obtained from CASSCF calculations. Indeed, these results are in good agreement with the NBO results and afford evidences of through space and through bond interaction between lone pairs and radical centre.

2.9 Proton affinities of isomeric dehydrodiazines radicals

Through NBO analysis and MCSCF calculations, we have already confirmed that both nitrogens are interacting with the radical centre via through space and through bond interaction. At this juncture, evidences are required for understanding the relation between the relative position of nitrogen lone pairs and radical electron that can potentially lead to stronger or weaker interactions between them. In order to quantify the interaction between two lone pairs and radical centre, we have estimated the proton affinities (PA) at each nitrogen centre of all the six isomeric radical species.^[10a] (Figure 2.7) For comparison, the PA's of nitrogen atoms of the parent diazines have also been estimated. The PA values calculated at CBS-QB3 level of theory are quite similar to the experimentally reported the values for the corresponding parent molecules. Hence, the PA values at CBS-QB3 level of theory has been compared with (U)B3LYP/cc-pVTZ level of theory. Upon creating a radical centre, all the radical isomers showed a lower PA values relative to the nitrogens of the parent. Except **1a** and **1c**, which are having C_{2v} symmetry, due to lower symmetry all other isomers showed different PA values at both the nitrogen atoms. These once again clearly indicate the existence of interactions between the two lone pairs and the radical electron as well as their strength of it. Particularly, when the position of the nitrogen is adjacent to the radical centre (*ortho*) the drop in PA value relative to parent was maximum. This can be attributed to the unavailability of lone pair that is interacting through space with the radical electron. Upon changing the position either from *ortho* to *meta*, or *meta* to *para*, the values were found to change moderately. These changes in the PA values are consistent with the presence of through bond interactions between the radical centre and the nitrogen when they are *meta* or *para* to each other. Based on the estimation of proton affinities, it is apparent that the interaction between the lone pair and radical is strongest when

they are proximal and as the distance increases, it decreases. The only exception is in the case of **1a**, where the two nitrogen atoms sit adjacent to the radical centre on either side, in which the nitrogen has a drop of PA value of 4.7 kcal/mol relative to the parent. Interestingly, **2a** showed a higher PA value compared to **1a** at both nitrogen centres. Presumably, a negative intramolecular α -effect of adjacent nitrogen in **2a** (and also in **2b**) might be responsible for the increase in the proton affinity of **2a** relative to **1a**. In **2a** and **2b**, the lone pair-lone pair repulsive interaction is expected to dominate due to the *syn*-periplanar orientation.

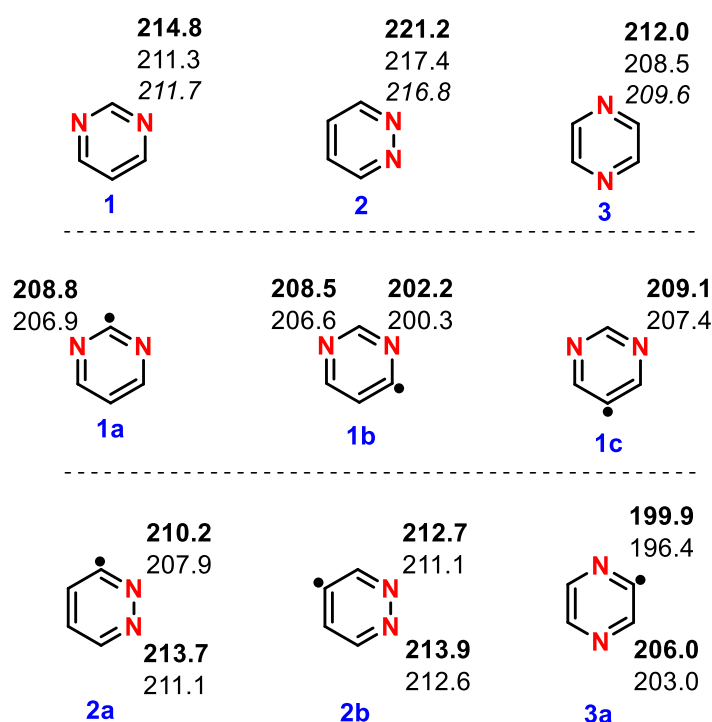


Figure 2.7 Proton affinities (in kcal/mol) of three parent diazines (**1–3**) and their respective six dehydrodiazine radical isomers (**1a–c**, **2a–b**, **3a**). The indicated PA values in bold font correspond to (U)B3LYP/cc-pVTZ, normal font correspond to CBS-QB3 levels of theory and those in italics (**1–3**) are the experimental values reported in literature.^[10b]

2.10 AIM analysis of isomeric dehydrodiazines radicals

Furthermore, the Bader's topological electron density mapping through AIM analysis was also performed to understand the interaction between the radical centres and the lone pair of nitrogens.^[11] We have obtained the bond critical and ring critical points through this analysis. Apart from that, we have estimated the charge density at the bond critical points that are mentioned in figure 2.8. Interestingly, the nitrogen atom(s) next to the radical centres show a substantial increase in electron density compared to their respective parent compounds, which

proves once again the existence of interaction between the radical electron and the nitrogen lone pairs. When there is no adjacent nitrogen on either side of the radical centre, there is a significant preference for interaction with carbon centres; however, those values are lower than that of interaction with nitrogen. The relative increase in the electron density along the bond critical points can be accounted for interactions between nitrogen lone pairs and radical centre.

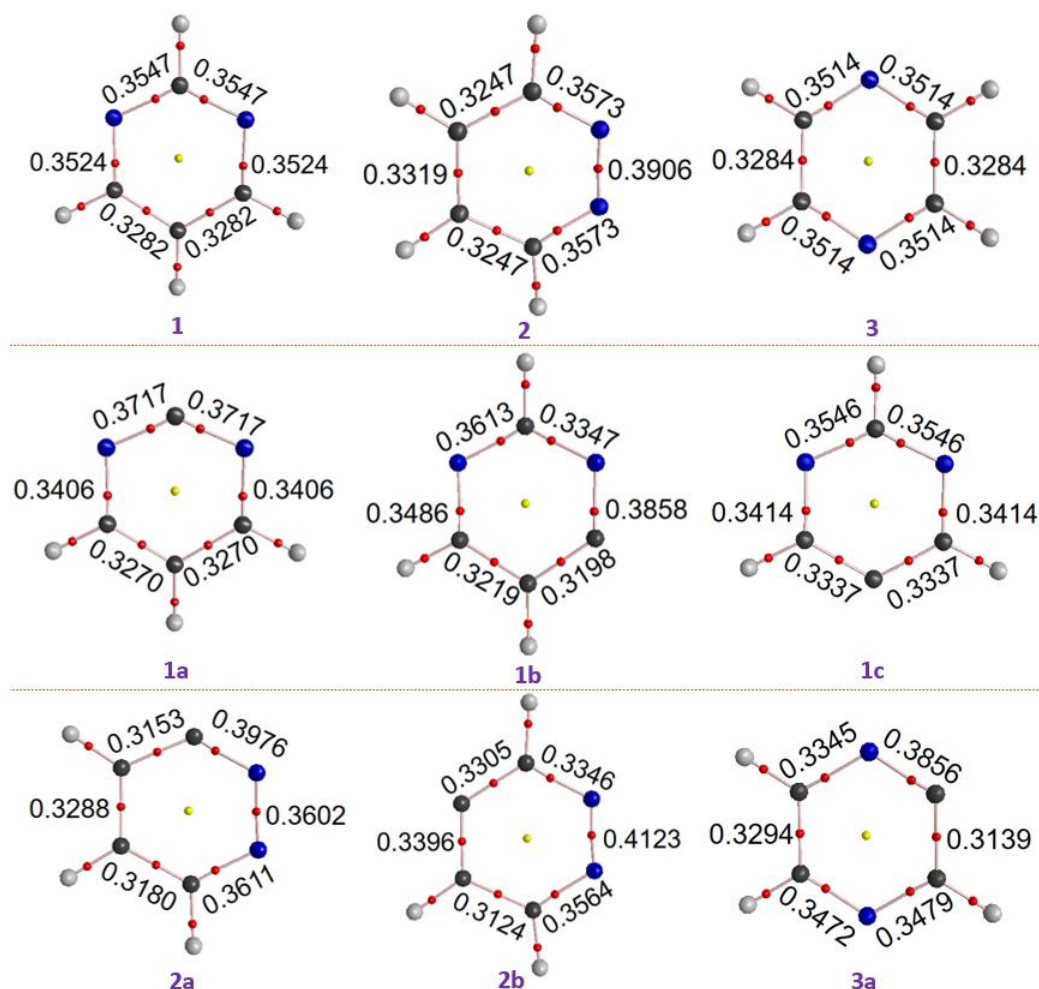


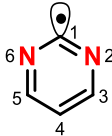
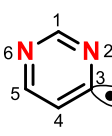
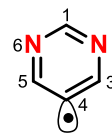
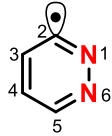
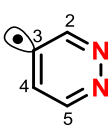
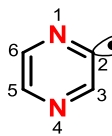
Figure 2.8 AIM analysis at (U)B3LYP/cc-pVTZ level of the three parent diazines (**1–3**) and their respective six dehydrodiazine radical isomers (**1a–c**, **2a–b**, **3a**) showing bond critical and ring critical points. The corresponding charge densities at each bond critical point are indicated.

2.11 Isotropic hyperfine coupling constants of isomeric dehydrodiazines radicals

Similarly, we have estimated the isotropic hyperfine coupling constant at the nitrogen atoms and radical centres in all the six isomeric diazine radical isomers.^[12] (Table 2.5) The results revealed a difference in the Fermi contact terms of both the nitrogen atoms in the case of non- C_{2v} symmetric isomers. On the other hand, **1a** and **1c** showed identical values of

hyperfine coupling constants. Furthermore, the nitrogen close to the radical centre showed a higher value. All these results clearly indicate the existence of disparity between the two nitrogens in interaction with the radical centre except in the case of **1a** and **1c**.

Table 2.5 Isotropic hyperfine coupling constant (in Gauss) of two ^{14}N atoms and ^{13}C radical centres for all the six isomeric dehydrodiazine radicals (**1a–c**, **2a–b**, **3a**) at (U)B3LYP/EPR-III level of theory.

 1a		 1b		 1c	
Atoms	Isotropic Fermi interactions	Atoms	Isotropic Fermi interactions	Atoms	Isotropic Fermi interactions
1 (^{13}C)	238.135	3 (^{13}C)	179.725	4 (^{13}C)	129.820
2 (^{14}N)	35.296	2 (^{14}N)	32.703	2 (^{14}N)	−0.389
6 (^{14}N)	35.296	6 (^{14}N)	0.230	6 (^{14}N)	−0.389
 2a		 2b		 3a	
2 (^{13}C)	193.960	3 (^{13}C)	119.912	2 (^{13}C)	174.936
1 (^{14}N)	42.660	1 (^{14}N)	0.394	1 (^{14}N)	33.928
6 (^{14}N)	7.942	6 (^{14}N)	9.009	4 (^{14}N)	−0.394

2.12 Summary of electronic structure of dehydro-diazines radicals

Through various quantum chemical computations, we have carried out detailed studies on the electronic structures of all the isomeric dehydrodiazines in order to understand the multicentric interactions between the two nitrogen lone pairs and radical electrons. Based on the relative stabilities of all isomeric dehydro-diazines, the dominating interactions among the 3c-5e configurations have been predicted. The electronic structure calculations revealed that the radical isomer **1b** was found to be the most stable followed by **1a** and **1c** among the three dehydropyrimidines. Using bond dissociation energies (BDEs) and radical stabilization energies (RSEs) through isodesmic reactions, we have obtained the stability order among the six diazine radicals: **1b** > **3a** > **1a** > **2a** > **2b** > **1c**. Spin densities of all these radicals showed

non-zero values at each nitrogen atom, clearly indicating the spin delocalization, possibly through the interaction between the radical centre and the nitrogen lone pair.

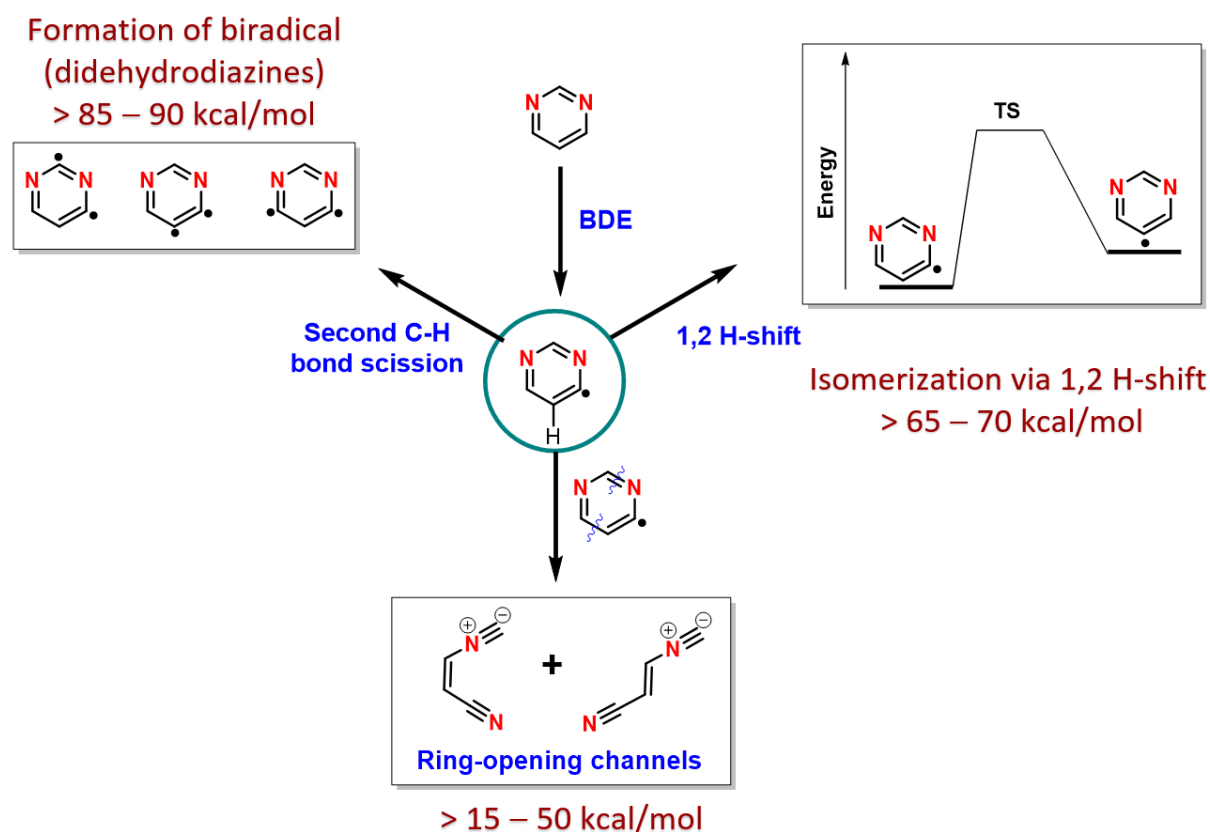
To envisage the reasons behind this stability order and to understand the mode of interactions, we have carried out natural bond orbital analysis. NBO analysis suggested that the stability of radical species is mainly determined by through bond and through space interactions. Among these two, through space interaction is the major factor that provides maximum stabilizing effect and is effective when the nitrogen lone pairs are at the *ortho* position to the radical centre. TS interaction completely vanishes when the lone pair and radical centre are *para* to each other. On the other hand, through bond interaction is more dominant when moving from *ortho* to *para* position. Based on that, the stability of isomer **1b**, in which one nitrogen lone pair is at the *ortho* position and the second one is at the *para* position with respect to the radical centre, can be attributed to the stabilizing influence of lone pairs on the radical centre by TS and TB interaction, respectively. On the other hand, radical isomer **1c** is the least stable among all the six isomers. In **1c**, both lone pairs are present at the *meta* position with respect to the radical and both TS and TB interactions are present but do not contribute significantly towards the stability of the radical. To gain further insights, multiconfigurational CASSCF calculations have been carried out that predicted that the singly occupied molecular orbitals in all the isomeric radicals are localized σ -orbitals. Qualitatively, MCSCF calculations also revealed the competitive nature of the TS and TB interactions. However, the dominant mode of interaction was clearly predicted in each individual isomer based on the energetic ordering of symmetric and antisymmetric combinations of the interacting orbitals corresponding to the radical electron and the nitrogen lone pair. This has also been illustrated through the estimation of proton affinity values of both nitrogens. The relative lowering of the values compared to their respective parent molecules provides information about the strength of the interaction between nitrogen and radical electron. Again, the AIM analysis and estimation of hyperfine coupling constants afforded conclusive evidence for the interactions between the nitrogen and radical centres. Thus, the relative position of the radical centre with respect to both the nitrogen lone pairs strongly influences the structural and stability aspects within the six dehydrodiazine radical isomers.

We have used B3LYP and M06-2X functional extensively in this work while exploring electronic structure and reactivity studies in chapter 2. Also, at every step we have compared the results obtained from these two functionals and they provided consistent results without a single exception when comparing energy ordering of diazines and their radical isomers. We have optimized these diazines using various DFT based functionals as well as perturbation

methods (MP2 and MP4) along with composite methods (CBS-QB3 and G4). We have extensively used B3LYP and M06-2X functionals throughout the thesis as these two functionals provide the spin contamination of 0.75 (that is standard value for molecules with one unpaired electron). On the other hand, other functionals lead to very high spin contamination (more than 1) for the optimization of these diazine molecules. Also, the computed vibrational spectra using these B3LYP and M06-2X functionals match very well with matrix-isolated spectrum within the range of few wavenumbers. In addition to that, plenty of literature reports including the large number of recent reports of using these functionals (B3LYP and M06-2X) in radical chemistry allows us to use them in our study.

2.13 Reactivity studies of isomeric dehydrodiazines radicals

After exploring the thermodynamic stability of dehydrodiazine radicals which are influenced by not only the stabilizing through space and through bond interactions between the individual lone pairs and the radical electron but also by the destabilizing and repulsive interaction between the two lone pairs of electrons. Although thermodynamic stability can be understood based on the qualitative and quantitative estimation of such interactions through electronic structure calculations, kinetic stability is equally important and a limiting factor towards applications. Furthermore, ring-opening of diazine radicals through unimolecular reactions can lead to several intermediates, ring-opened products, and fragmentation products that are quite valuable from astrochemical point of view considering the detection of several nitrogen-containing species in recent times.^[13] Understanding the kinetic stability of the diazine radicals will provide the nature and influence of 3c–5e interactions concerning reactivity. In this regard, we investigated the unimolecular reactivity pattern along with isomerization via 1,2-H shift in all the six isomeric radicals of diazines. (Scheme 2.2)



Scheme 2.2 Illustration of possible reaction channels in isomeric dehydrodiazine radicals (**1a–c**, **2a–b**, **3a**).

2.14 Isomerization through 1,2-H shift in isomeric dehydrodiazines radicals

A few of the dehydrodiazine radicals have hydrogens at vicinal position to the radical centres. As a result, the 1,2-H shifts can convert them into their corresponding radical isomers. Although a maximum of two adjacent hydrogen shifts are possible in each case, the presence and position of two nitrogen atoms restrict such possibilities. Due to this, all the diazine radicals can interconvert to one isomer only. For instance, the isomerization between **1b** and **1c** (in pyrimidine) or **2a** and **2b** (in pyridazine) is the only channel (Figures 2.9). In the case of pyrazine, the 1,2-H shift will be an isothermal process that can lead to the same isomer **3a**. Such a double-well symmetrical potential in the 1,2-H shift is also possible in the case of **2b** in the pyridazine radical isomer. In each case, the transition state is found to have the hydrogen atom occupying a position, which is symmetric relative to the origin (reactant radical) and the end position (product radical).

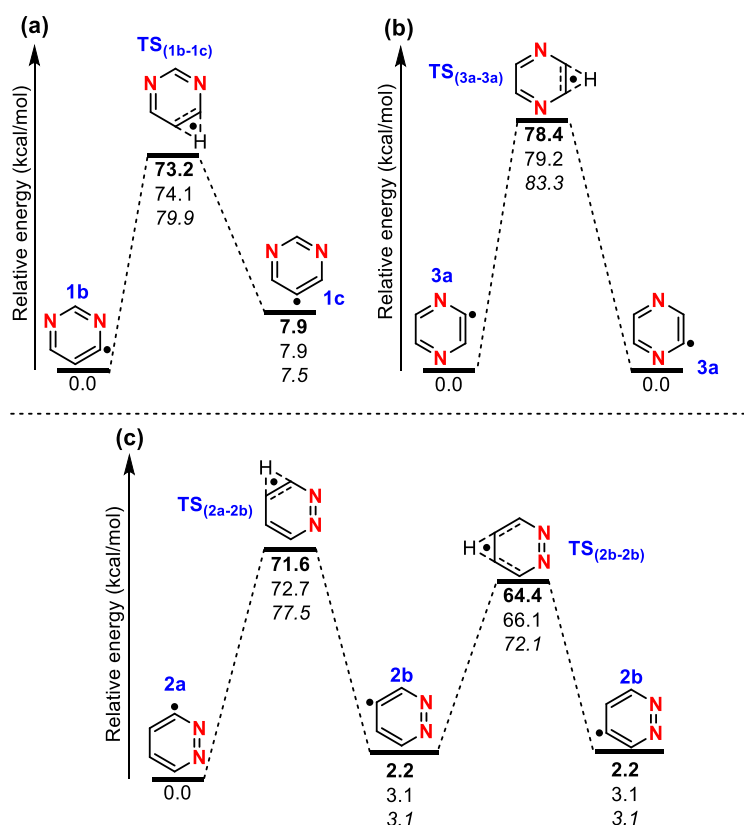


Figure 2.9 Isomerization through 1,2-H shift in isomeric (a) dehydropyrimidine (**1b** and **1c**), (b) dehydropyrazine (**3a**), and (c) dehydropyridazine (**2a** and **2b**) radicals at different levels of theory. Bold: (U)B3LYP/cc-pVTZ, normal: (U)M06-2X/cc-pVTZ, and italics: (U)CCSD(T)/cc-pVTZ/(U)B3LYP/cc-pVTZ

Besides that, the inspection of the barriers among all such isomerization reactions indicates a high barrier in the range between 64.4 and 78.4 kcal/mol. However, the barrier gets lowered in

1c and **1b** because the resulting radical product is stabilized by a through-space coupling between adjacent nitrogen and radical centre. This indicates that the thermodynamic stability of the radical is driving the isomerization reactions through 1,2-H shifts except in the isoenergetic transformations in **2b** and **3a**.

2.15 Unimolecular decomposition channels

All the six diazine radicals can in principle undergo reactions through ring-opening channels. These are important modes of reactivity that determine the kinetic stability order under unimolecular conditions due to involvement of relatively lower energy barriers. Based on our earlier work on the electronic structure studies including the first C–H bond dissociation energies (BDEs) of the diazines (pyrimidine **1**, pyridazine **2**, and pyrazine **3**), relative energies, and isodesmic reactions, we found out the role of through-space and through-bond interactions in determining the thermodynamic stability order. The analysis of geometrical parameters indeed revealed that the alternate bonds relative to the radical centres were found to be weakened (from the elongation of the bonds) in all the radicals. Such bonds are significant because these sites are prone to undergo ring-opening. Apart from that, the first C–H BDEs of dehydrodiazine radical isomers demand higher energy (>85 kcal/mol) to form didehydrodiazines (biradicals). The other possible mode of unimolecular reactivity, isomerization channel is restricted only to a limited number of diazine radicals, which makes the ring decomposition channel quite important. Remarkably, such ring-opening channels exhibited barriers in the range of 10–78 kcal/mol for all the six dehydro-diazines radical isomers. The complete unimolecular decomposition analysis at (U)B3LYP/cc-pVTZ and (U)M06-2X/cc-pVTZ levels of theory and single point energy at (U)CCSD(T)/cc-pVTZ level of theory are given in the respective figures. Intrinsic reaction coordinate (IRC) analysis has also been performed at the (U)B3LYP/cc-pVTZ level to verify the true transition states are part of the potential energy surfaces connecting the reactant and the product for the first ring-opening transition state.^[14]

2.15.1 Unimolecular decomposition channels of 2-dehydropyrimidine radical (**1a**)

In radical **1a**, the radical electron is located between the two nitrogen atoms. Due to the highly symmetric structure (C_{2v} point group), **1a** has only one possible channel for ring-opening. The foremost ring-opening happens through the cleavage of the N3–C4 bond via a transition state **TS_{1a-4}** with an estimated barrier of 44.3 kcal/mol at (U)B3LYP/cc-pVTZ level of theory (Figure 2.10, 2.11 and table 2.6). Such a highly endothermic step leads to the

formation of the product **4**, which can dissociate further either by a C–H bond cleavage or by a C–C bond cleavage. The expulsion of hydrogen leads to the ring-opened product, (Z)-2-propynylidene cyanamide **10** as the end product. On the other hand, the C–C bond cleavage leads to the fragmentation products acetylene **6** and a carbon-centered radical **5**, which is favored by 7.5 kcal/mol. Moreover, this channel is not only favored by a lower enthalpy factor (35.0 kcal/mol) but also has an entropic allowance (8.3 cal/K-mol) which is twice of the former step (4.2 cal/K-mol). The resulting radical **5** further isomerizes through a 1,2-H shift followed by C–N bond cleavage to yield HNC **8** and CN radical **9** as the end products.

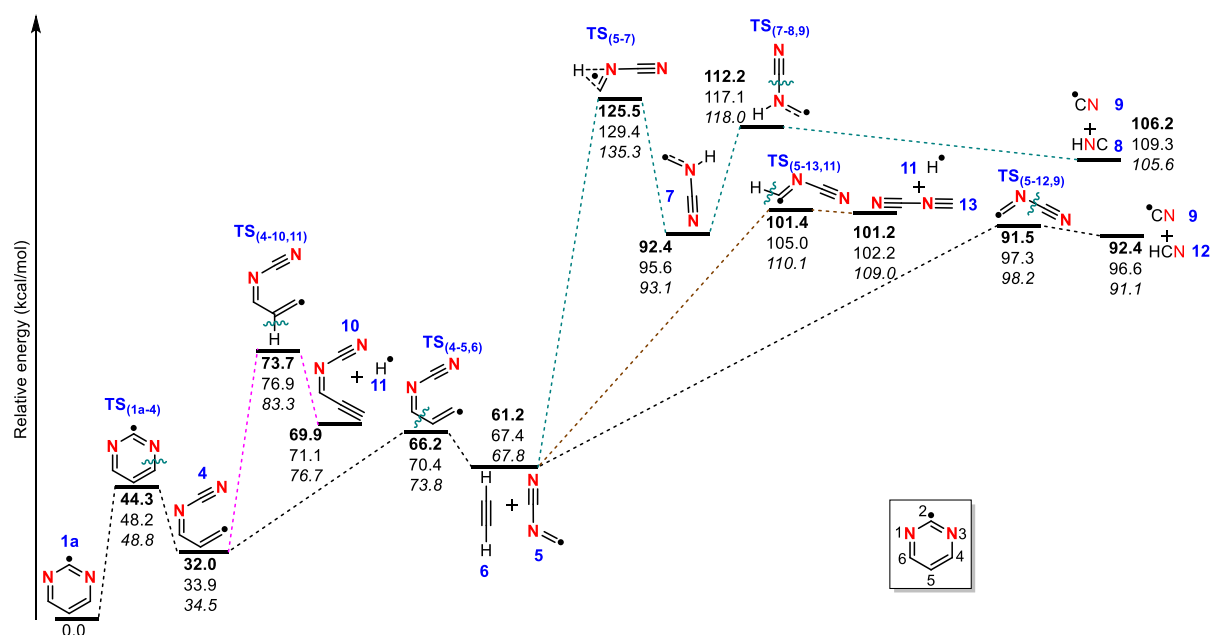


Figure 2.10 Unimolecular decomposition channels of 2-dehydropyrimidine (**1a**) radical. Bold: (U)B3LYP/cc-pVTZ, Normal: (U)M06-2X/cc-pVTZ and Italics: (U)CCSD(T)/cc-pVTZ// (U)B3LYP/cc-pVTZ

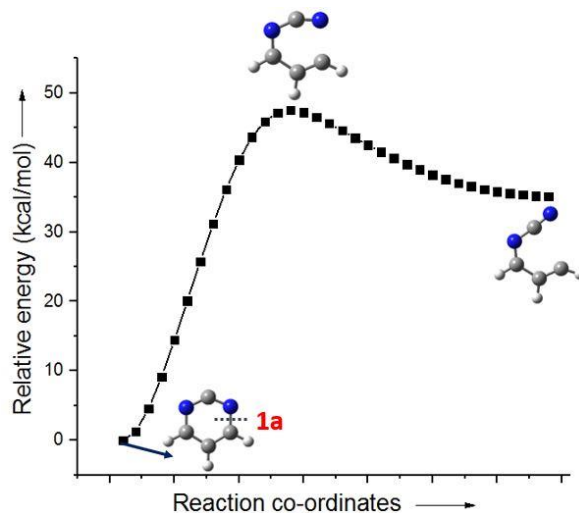


Figure 2.11 IRC analysis for 2-dehydropyrimidine (**1a**) radical unimolecular dissociation channels at (U)B3LYP/cc-pVTZ level of theory.

2.15.2 Unimolecular decomposition channels of 4-dehydropyrimidine radical (**1b**)

Radical isomer **1b** with a C_s symmetric structure can undergo ring-opening through two different channels, namely, C2–N3 and C5–C6 bond cleavages (Figures 2.12, 2.13 and table 2.6). A comparison of the relative barriers revealed the favourability of the bond cleavage through C2–N3 by a difference of 22.9 kcal/mol. Such a preference could be due to the stabilizing through-space interaction that exists between the radical centre and the nitrogen atom. Such ring-opening leads to an intermediate **14**. This species can exhibit another channel at a relatively high barrier (39.3 kcal/mol) through which it loses a hydrogen atom from the terminal carbon leading to the ring-opened species (*Z*)-3-isocyano-2-propenenitrile **17**. Alternatively, **14** can also undergo fragmentation with the loss of HCN involving a transition state **TS**_{14-15,12} with a barrier of 29.6 kcal/mol. The resulting β -cyanovinyl radical **15** loses a proton to form cyanoacetylene **16** as the end product with an estimated barrier of 40.4 kcal/mol.

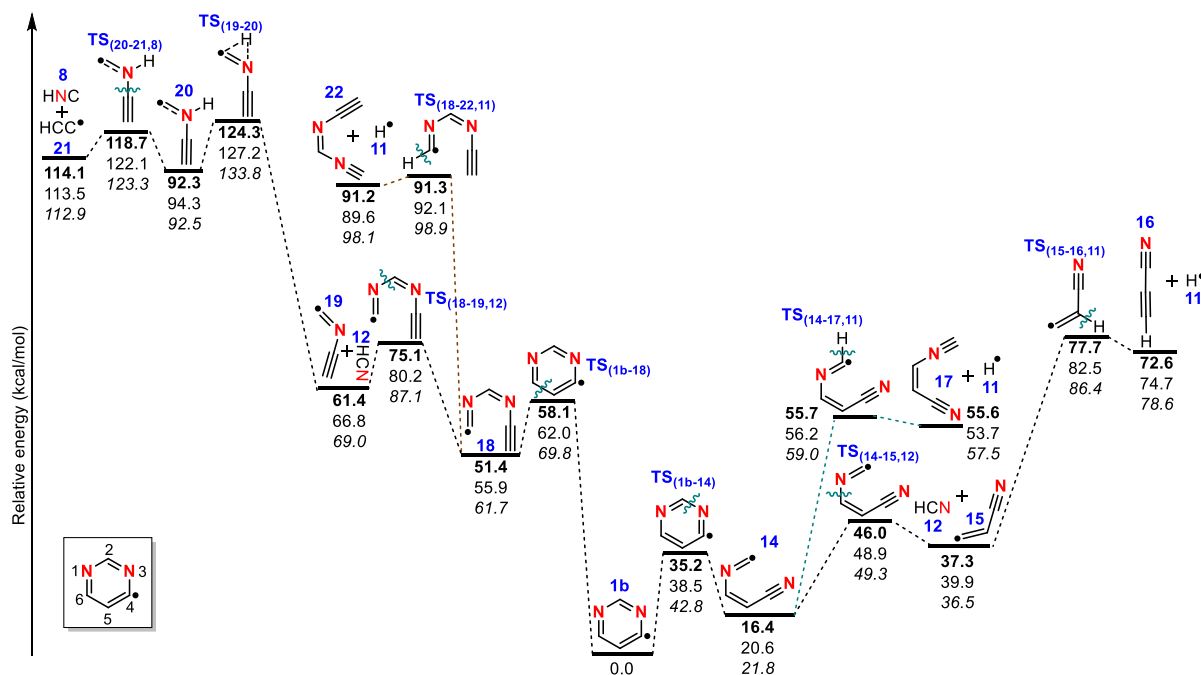


Figure 2.12 Unimolecular decomposition channels of 4-dehydropyrimidine (**1b**) radical. Bold: (U)B3LYP/cc-pVTZ, Normal: (U)M06-2X/cc-pVTZ and Italics: (U)CCSD(T)/cc-pVTZ/(U)B3LYP/cc-pVTZ

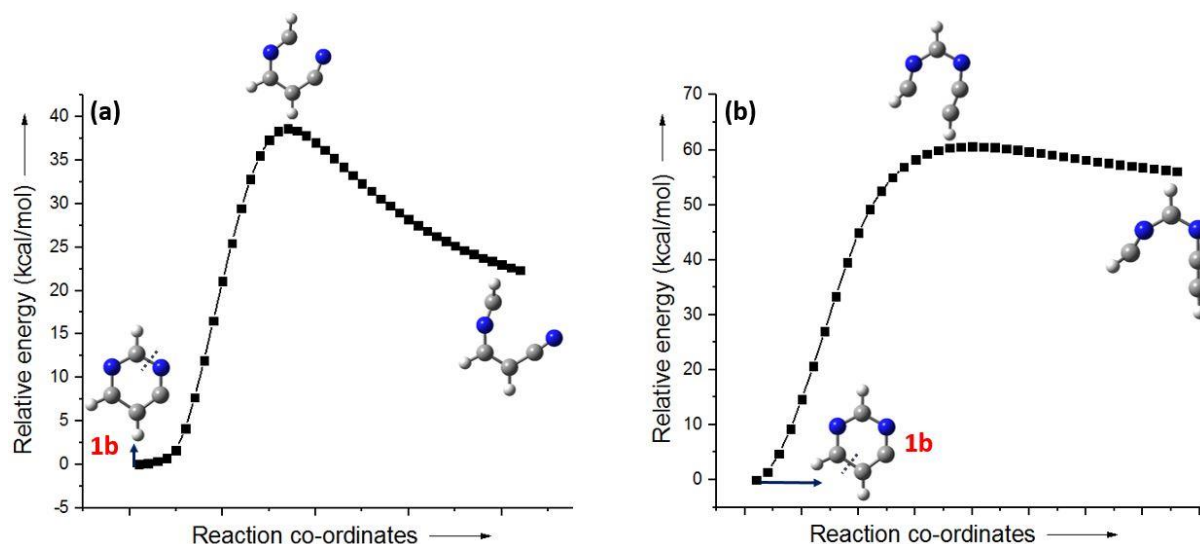


Figure 2.13 IRC analysis for 4-dehydropyrimidine (**1b**) radical unimolecular dissociation channels at (U)B3LYP/cc-pVTZ level of theory.

Alternatively, the ring-opening through the C5–C6 bond cleavage leads to product **18** through a late transition state **TS_{1b-18}** with an energy barrier of 58.1 kcal/mol. The resulting endothermic product **18** further undergoes fragmentation through a subsequent C–N bond cleavage to form HCN **12** and a radical **19** with a relatively low barrier of 23.7 kcal/mol. Indeed, the radical **19** behaves very similarly to the radical **5** in the case of **1a** and exhibits a 1,2-H shift followed by C–N bond cleavage to form HNC **8** and acetylenic radical HCC. **21**. The 1,2-H shift demands a huge barrier (62.9 kcal/mol), whereas the consecutive fragmentation step is essentially a low energy process with an estimated barrier of 26.4 kcal/mol. Based on ring-opening channels, the end decomposition products of 4-dehydropyrimidine **1b** were found to be cyanoacetylene **16**, HCN **12**, HNC **8**, and HCC. **21**.

2.15.3 Unimolecular decomposition channels of 5-dehydropyrimidine radical (**1c**)

Due to higher symmetry (C_{2v} point group), the radical isomer **1c** also undergoes ring-opening through the N3–C4 bond cleavage only (Figures 2.14, 2.15 and table 2.6). This leads to the preliminary intermediate **23** via a transition state **TS_{1c-23}** with an estimated barrier of 47.6 kcal/mol. The endothermic product **23** in the first step can further dissociate through a C–N bond cleavage resulting in the formation of HCN **12** and an imine radical **24** through a lower barrier of 16.0 kcal/mol. Else, **23** can lose a hydrogen atom to form a stable ring-opening product **10**. However, the ring-opening step requires 16.3 kcal/mol more energy than the fragmentation step. On the other hand, the fragmented intermediate **24** further leads to

cyanoacetylene **16** as the end product through the expulsion of a hydrogen atom, however with a larger barrier (30.6 kcal/mol).

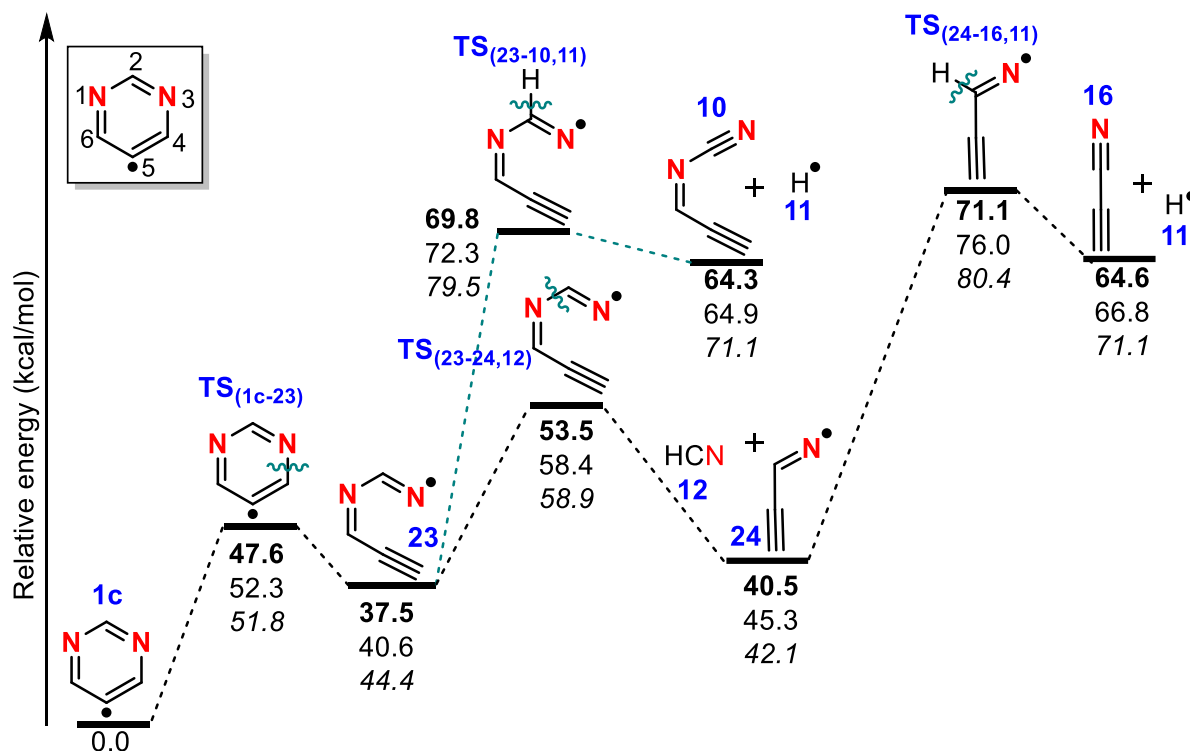


Figure 2.14 Unimolecular decomposition channels of 5-dehydropyrimidine (**1c**) radical. Bold: (U)B3LYP/cc-pVTZ, Normal: (U)M06-2X/cc-pVTZ and Italics: (U)CCSD(T)/cc-pVTZ/(U)B3LYP/cc-pVTZ

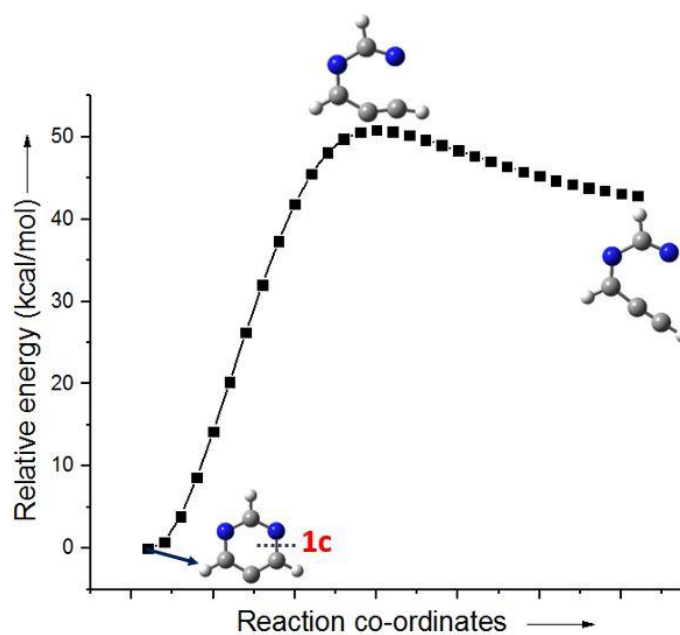


Figure 2.15 IRC analysis for 5-dehydropyrimidine (**1c**) radical unimolecular dissociation channels at (U)B3LYP/cc-pVTZ level of theory.

2.15.4 Unimolecular decomposition channels of 3-dehydropyridazine radical (2a)

The radical isomer **2a** has been optimized to a C_s symmetric structure as the energy minima on the potential energy surface. As a result, there are two possible ring-opening channels. These ring-opening channels happen through scission at either N1–N2 or C4–C5 bond (Figures 2.16, 2.17 and table 2.6). Indeed, the N1–N2 bond cleavage has been estimated to be the low energy channel with a preference of 66.4 kcal/mol over the C4–C5 bond breaking. Surprisingly, the possibility of loss of molecular nitrogen either in a concerted or step-wise channel did not happen. Once again, the through space interaction between the radical centre and the nitrogen at 2-position could be the driving force in this regard. Such an N–N bond cleavage in radical isomer **2a** leads to the intermediate **25** via **TS_{2a-25}** with an estimated barrier of 11.7 kcal/mol. Moreover, the reaction is exergonic, and so, this step is both thermodynamically as well as kinetically driven. The ring-opened intermediate **25** in principle can undergo two reaction channels, namely, a deprotonation pathway leading to the stable ring-opened maleonitrile **26**. Alternatively, the product **25** further dissociates to HCN **12** and an unstable vinyl nitrile radical **15**; both the channels were found to have nearly same barrier, which makes both the channels equally probable. The vinyl radical then undergoes a C–H bond breaking that leads to cyanoacetylene **16** and a hydrogen atom. Indeed, this step is very similar to the fragmentation of **14** in the case of **1b**. In an alternative channel for **2a**, the C4–C5 bond scission leads to a ring-contracted five-membered pyrazole radical **27** via a transition state **TS_{2a-27}** with an energy barrier of 78.1 kcal/mol.

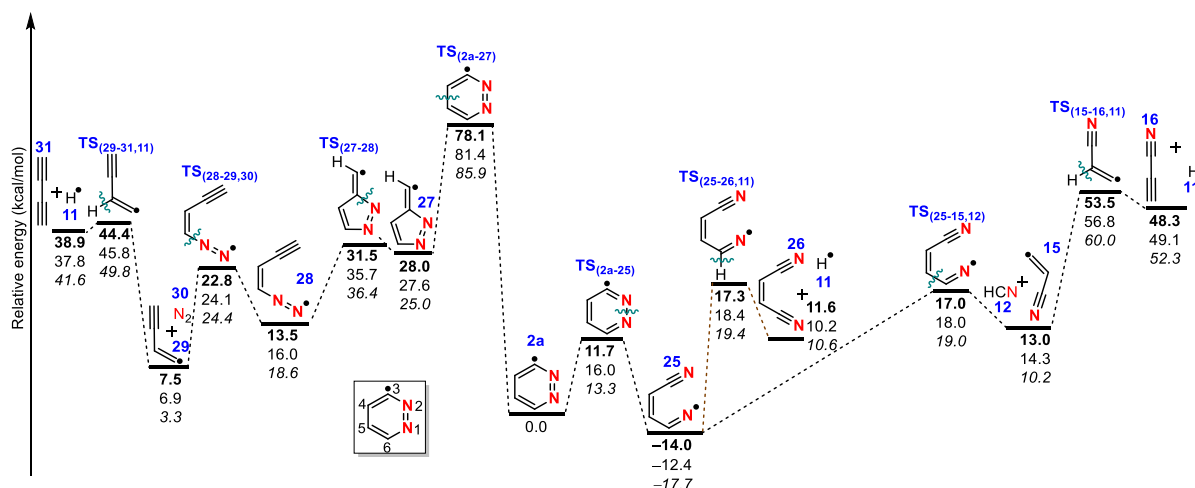


Figure 2.16 Unimolecular decomposition channels of 3-dehydropyridazine (**2a**) radical. Bold: (U)B3LYP/cc-pVTZ, Normal: (U)M06-2X/cc-pVTZ and Italics: (U)CCSD(T)/cc-pVTZ/(U)B3LYP/cc-pVTZ

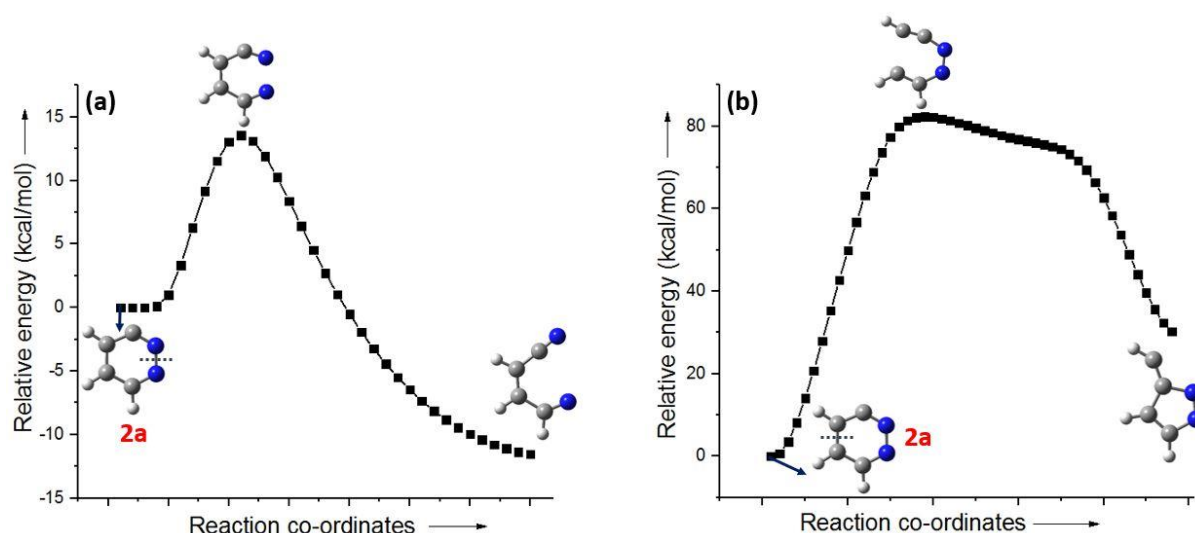


Figure 2.17 IRC analysis for 3-dehydropyridazine (**2a**) radical unimolecular dissociation channels at (U)B3LYP/cc-pVTZ level of theory.

Despite a very high barrier in the first step, this radical **27** further dissociates through a C–N bond scission to a ring-opened analogue **28** with an energy barrier of 3.5 kcal/mol. The loss of strain in the ring lowers the high positive enthalpy contribution and possibly drives the reaction forward. This is followed by the loss of molecular nitrogen, and so an increase in the entropy factor as well as a lower barrier of 9.3 kcal/mol makes this step more favourable (Table 2.6). The resulting radical **29** undergoes the loss of hydrogen to form butadiene **31** as the end product, however with a relatively higher barrier (36.9 kcal/mol).

2.15.5 Unimolecular decomposition channels of 4-dehydropyridazine radical (**2b**)

The other radical isomer of pyridazine **2b** also has a C_s symmetric structure on the ground state potential energy surface. Once again, the unsymmetrical environment on either side of the radical leads to two different ring-opening channels via, N2–C3 and C5–C6 bond cleavages (Figures 2.18, 2.19 and table 2.6). Similar to the previous cases, C–N bond scission channel is found to be more favourable compared with C–C bond scission by a difference of 27.3 kcal/mol. Ring-opening through the C–N bond scission leads to a radical intermediate **28** via **TS_{2b-28}** with an energy barrier of 28.4 kcal/mol. This radical intermediate further undergoes fragmentation with the loss of molecular nitrogen to another radical intermediate **29**, which leads to diacetylene as the end product through a C–H bond breaking. Except for the final step with a barrier of 36.8 kcal/mol, other steps were found to be lower than 30 kcal/mol that makes this channel more facile.

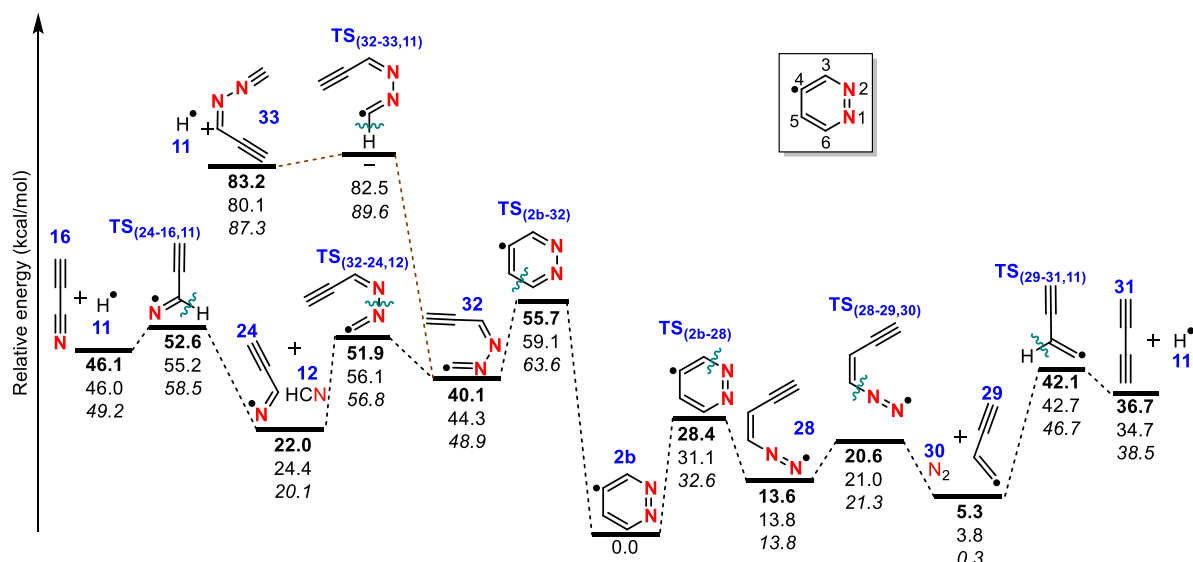


Figure 2.18 Unimolecular decomposition channels of 4-dehydropyridazine (**2b**) radical. Bold: (U)B3LYP/cc-pVTZ, Normal: (U)M06-2X/cc-pVTZ and Italics: (U)CCSD(T)/cc-pVTZ/(U)B3LYP/cc-pVTZ

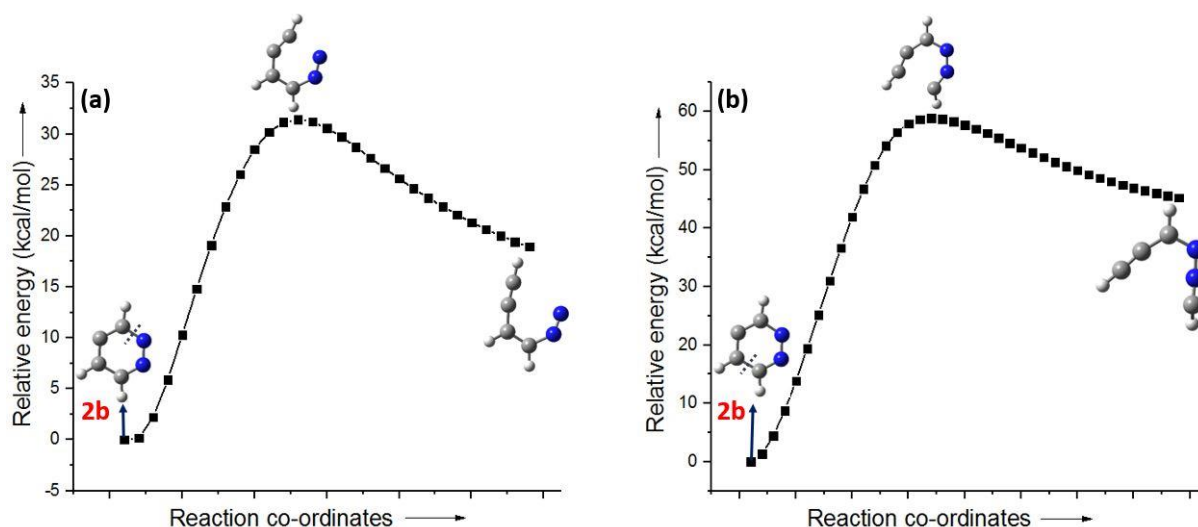


Figure 2.19 IRC analysis for 4-dehydropyridazine (**2b**) radical unimolecular dissociation channels at (U)B3LYP/cc-pVTZ level of theory.

On the other hand, the second ring-opening through C5–C6 bond cleavage leads to a radical intermediate **32** via **TS_{2b-32}** with an energy barrier of 55.7 kcal/mol. This radical intermediate **32** further dissociates to HCN and yet another imine radical intermediate **24**, which finally leads to cyanoacetylene **16** with the loss of hydrogen through a C–H bond scission from the molecule **24**. The direct formation of a ring-opening product **33** is also possible from **32** with the loss of a hydrogen atom, which demands 26.4 kcal/mol at (U)M06-2X/cc-pVTZ level of theory than that of the fragmentation channel.

2.15.6 Unimolecular decomposition channels of 2-dehydropyrazine radical (**3a**)

This radical isomer **3a** exists in C_s symmetry on the ground state potential energy surface, and due to the unsymmetrical nature on either side of the radical center, two different decomposition channels are possible (Figures 2.20, 2.21 and table 2.6). Interestingly, both the ring-opening channels involve C–N bond cleavage as the preliminary step. However, the ring-opening involving the nitrogen adjacent to the radical center (N1–C6) is found to be the lower energy channel relative to the other pathway (involving C3–N4 bond breaking) by 7.7 kcal/mol. Ring-opening through the N1–C6 bond cleavage involves the transition state **TS_{3a-34}** that leads to a radical intermediate **34** with an energy barrier of 44.6 kcal/mol. This radical intermediate **34** dissociates further through the loss of acetylene **6** with a late transition state **TS_{34-35,6}**. This endothermic step is followed by a C–H bond breaking leading to cyanogen NCCN **36**. In an alternate pathway, the ring-opening channel occurs through the C3–N4 bond cleavage leading to a radical intermediate **38** via **TS_{3a-38}** with an energy barrier of 52.3 kcal/mol. Interestingly, both the channels also involve the ring-opening products formation through the first ring-opened intermediates **34** and **38** through the loss of a hydrogen atom and lead to the same product **37**. Although the formation of **34** is more facile compared with the formation of **38**, the above-mentioned ring-opening step requires a higher barrier for the former than the latter. The corresponding barriers for **34** and **38** to lose hydrogen forming **37** are 40.0 and 33.5 kcal/mol, respectively.

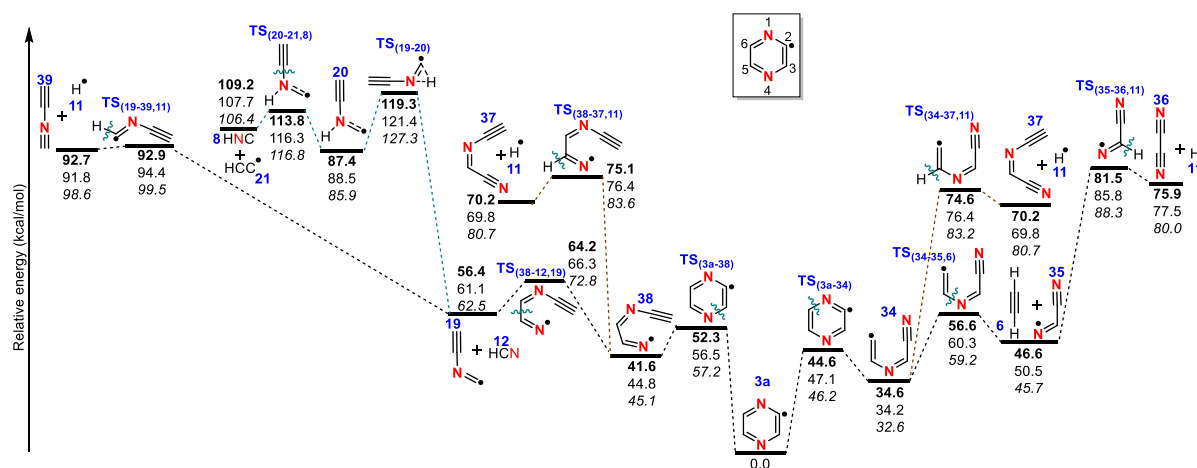


Figure 2.20 Unimolecular decomposition channels of 2-dehydropyrazine (**3a**) radical. Bold: (U)B3LYP/cc-pVTZ, Normal: (U)M06-2X/cc-pVTZ and Italics: (U)CCSD(T)/cc-pVTZ/(U)B3LYP/cc-pVTZ

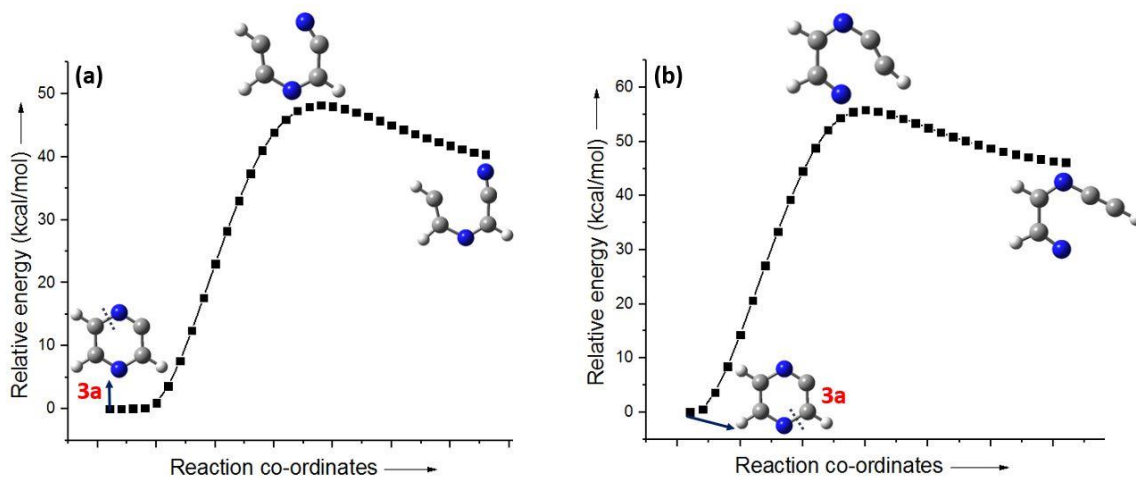


Figure 2.21 IRC analysis for 2-dehydropyrazine (**3a**) radical unimolecular dissociation channels at (U)B3LYP/cc-pVTZ level of theory.

Similar to the previous channel, this radical intermediate **38** also undergoes fragmentation with the loss of HCN to form a radical imine **19**, which further undergoes a 1,2-H shift to form **20** before dissociating into HNC and HCC. radical **21**. Except in the isomerization between **19** and **20** through a 1,2-H shift, the rest of the steps were found to be endothermic. Also, barriers were lower than the first step indicating initial ring-opening as the rate-determining step.

2.16 Overall reactivity patterns in diazine radicals

Through our previous investigations on electronic structure studies, the six dehydrodiazines exhibited a thermodynamic stability order as follows: **1c** < **2b** < **2a** < **1a** < **3a** < **1b**. Primarily, the 3c–5e interactions (the combined effect of interaction between nitrogen lone pairs in stabilizing the radical centers and the destabilizing interactions between the nitrogen lone pairs) played a significant role in this regard. However, by considering the lowest energy barriers for each one of the radical isomers under unimolecular reactivity conditions, the order completely changed. The resulting kinetic stability order of the diazine radicals is **2a** < **2b** < **1b** < **1a** < **3a** < **1c**. Dehydro-pyridazines (**2a** and **2b**) are kinetically the least stable, whereas dehydro-pyrimidine and dehydro-pyrazine isomers are more stable among these dehydrodiazines. The dominating lone pair–lone pair (repulsive) interaction over the lone pair–radical interaction (stabilizing) is responsible for lower kinetic stability in the former. On the other hand, dehydro-pyrimidine and dehydro-pyrazine have a stabilizing lone pair–radical interaction.

Table 2.6: Free energy, enthalpy and entropy of activation (ΔG^\ddagger , ΔH^\ddagger and ΔS^\ddagger) at 298 K for all the reaction steps in the unimolecular dissociation channels. (Bold: (U)B3LYP/cc-pVTZ; normal: (U)M06-2X/cc-pVTZ)

Reactant	TS	ΔG^\ddagger (kcal/mol)	ΔH^\ddagger (kcal/mol)	ΔS^\ddagger (cal/K-mol)	Reactant	TS	ΔG^\ddagger (kcal/mol)	ΔH^\ddagger (kcal/mol)	ΔS^\ddagger (cal/K-mol)
1a	TS _{1a-4}	43.5	44.8	4.5	2a	TS _{2a-25}	11.5	11.8	1.3
		47.4	48.7	4.5			15.7	16.2	1.6
4	TS _{4-5,6}	32.5	35.0	8.3	25	TS _{2a-27}	77.5	78.7	4.3
		35.7	37.2	5.1			80.9	82.0	3.8
5	TS _{4-10,11}	40.9	42.1	4.2	28	TS _{25-15,12}	30.0	31.5	5.1
		42.3	43.5	3.9			29.9	30.9	3.5
7	TS ₅₋₇	64.0	64.5	1.9	29	TS _{25-26,11}	31.0	31.6	2.0
		61.6	62.4	2.5			30.6	31.1	1.9
1b	TS _{5-12,9}	28.9	30.9	6.6	32	TS _{28-29,30}	8.5	9.6	3.7
		28.7	30.5	6.2			7.6	8.4	2.6
14	TS _{5-13,11}	39.3	40.8	5.2	2b	TS _{29-31,11}	36.8	37.2	1.2
		37.1	38.2	3.5			38.9	39.2	1.0
15	TS _{7-8,9}	18.6	20.3	5.8	3a	TS _{2b-28}	27.5	29.1	5.2
		20.5	22.0	5.1			30.6	31.7	3.7
18	TS _{1b-14}	34.9	35.6	2.5	34	TS _{2b-32}	55.0	56.4	4.8
		38.2	39.0	2.5			58.6	59.8	3.8
19	TS _{1b-18}	57.6	58.6	3.5	35	TS _{32-24,12}	11.1	12.0	2.8
		61.6	62.6	3.4			11.2	12.1	3.0
20	TS _{14-15,12}	29.0	29.9	3.3	38	TS _{32-33,11}	—	—	—
		28.0	28.7	2.4			37.1	38.8	5.7
27	TS _{14-17,11}	37.6	40.1	8.4	23	TS _{3a-34}	44.0	45.2	3.8
		34.7	36.2	5.0			46.5	47.6	3.6
24	TS _{15-16,11}	40.4	40.8	1.4	38	TS _{3a-38}	51.9	52.9	3.1
		42.5	42.9	1.1			56.1	57.0	2.9
1c	TS _{18-19,12}	23.2	24.0	2.7	34	TS _{34-35,6}	20.7	22.5	6.1
		24.1	24.5	1.3			25.2	26.5	4.6
22	TS _{18-22,11}	38.1	40.7	8.8	35	TS _{34-37,11}	39.8	40.3	1.7
		35.4	36.8	4.6			42.0	42.4	1.2
25	TS ₁₉₋₂₀	62.6	63.1	1.5	38	TS _{35-36,11}	34.9	35.2	0.9
		60.0	60.5	1.7			35.3	35.5	0.7
26	TS _{19-39,11}	35.6	37.0	4.8	38	TS _{38-19,12}	21.3	23.2	6.5
		32.9	33.8	3.1			22.3	24.0	5.7
28	TS _{20-21,8}	25.1	27.0	6.5	23	TS _{38-37,11}	32.9	33.8	2.8
		26.7	28.4	5.7			31.4	31.8	1.5
29	TS _{1c-23}	46.7	48.1	4.8	23	TS _{23-24,12}	15.3	16.3	3.6
		51.4	52.8	4.6			17.4	18.1	2.4
30	TS ₂₇₋₂₈	3.3	3.6	1.1	24	TS _{23-10,11}	32.2	32.6	1.1
		7.9	8.3	1.3			31.7	31.8	0.2
31	TS _{24-16,11}	30.6	30.8	0.6			30.8	31.0	0.5

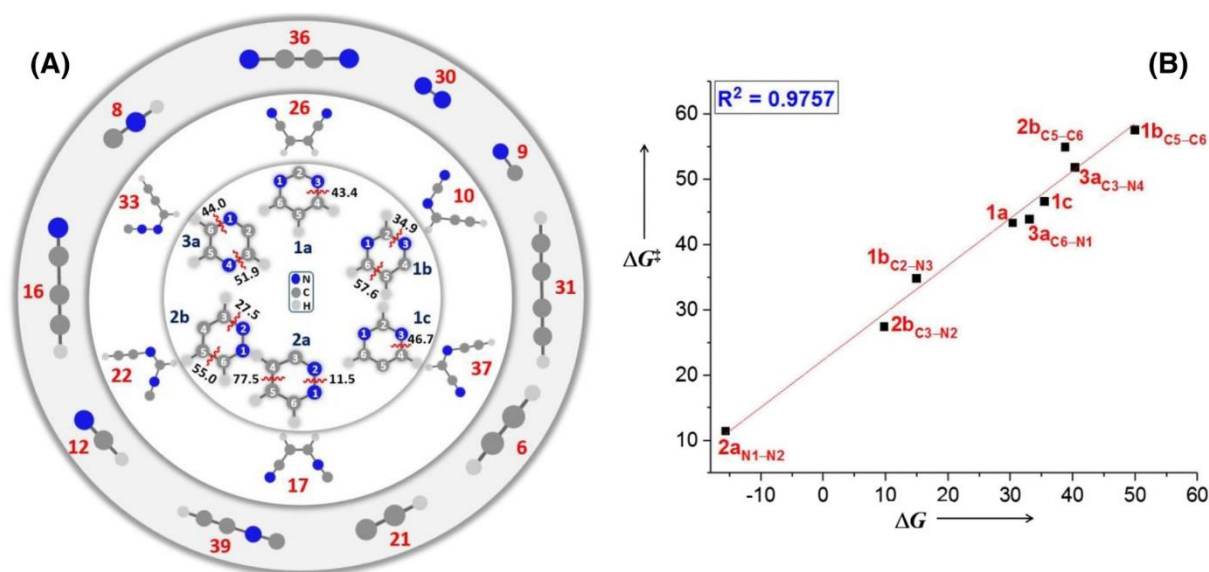


Figure 2.22 (a) Summary of the unimolecular ring decomposition and fragmentation channels of six isomeric dehydro-diazine radicals (the free energy changes corresponding to the first ring-opening steps are given in kcal/mol); the stable ring-opening products having a molecular formula C₄N₂H₂, the products after the loss of one hydrogen atom from those radicals are indicated in the second circle; the end products through fragmentation step are depicted in the third circle). (b) Linear correlation depicting the relation between free energy barrier for the first ring-opening step and the corresponding free energy of the ring-opening product relative to each radical.

Also, we observed a concerted transition state for N₂ loss from dehydropyridazine radicals (**2a** and **2b**). However, these transition states were only located at HF/STO-3G level of theory. Every attempt for optimizing these transition states at (U)B3LYP and (U)M06-2X levels was unsuccessful.

Interestingly, the ring-opening step leading to the cyano products exhibits lower barriers than acetylenic products. In other words, all the diazine radicals prefer ring decomposition step through a C–N bond breaking rather than a C–C bond breaking. To gain additional insights, we compared the free energy changes accompanying the ring-opening step with the free energy of activation, which showed an excellent linear correlation, except for the C4–C5 bond cleavage step in **2a** (Figure 2.22B). This confirms that the ring-opening step has a strong thermodynamic driving force.

Although energetically expensive in all the diazine radicals, a subsequent C–H bond breaking from the first ring decomposition step leads to six ring-opening products **10**, **17**, **22**, **26**, **33**, and **37**. Such products are stable isomers of a molecular formula C₄N₂H₂ and are diaza-analogs of enediyne, and so aza-Bergman cyclization of such molecules is very interesting.

Furthermore, the end products in the unimolecular dissociation channels of dehydro-diazine radical isomers are small molecular fragments, such as, CN radical, HCN, HCCH, HNC, HCC radical, HCCCN, HCCCCH, N₂, and NCCN, which are part of the interstellar medium (ISM).^[13]

2.17 Summary of reactivity studies of isomeric dehydrodiazines radicals

Through this investigation, we have explored the reactivity of dehydro-diazine radical isomers through isomerization (1,2-H shift), ring-opening, and fragmentation channels under unimolecular reactivity conditions. Because the isomerization channels have high barriers (64.4–78.4 kcal/mol) and only a restricted number of isomers can undergo such reactions, their kinetic stability is mainly controlled by the unimolecular decomposition channels (11.7–78.1 kcal/mol). The ring-opening can happen either by a C–C, C–N, or N–N bond cleavage, particularly at those bonds residing alternately to the radical center. Indeed, the ring-opening through the C–C bond cleavages was found to be energetically expensive compared with the C–N bond breaking. Primarily, the interaction between the radical center and the nitrogen lone pair adjacent to it dictates this selectivity. On the basis of the unimolecular dissociation channels, we obtained the kinetic stability order of the six dehydro-diazines radicals as **2a** < **2b** < **1b** < **1a** < **3a** < **1c**, which has a strong thermodynamic driving force.^[15] Overall, the 3c–5e interaction imparts the selectivity in the ring-opening, whereas the ring-opened radical intermediate influences the kinetic stability in diazine radicals.

2.18 References

1. Sah, C.; Jacob, L.; Saraswat, M.; Venkataramani, S. Does a Nitrogen Lone Pair Lead to Two Centered–Three Electron (2c–3e) Interactions in Pyridyl Radical Isomers? *J. Phys. Chem. A* **2017**, *121*, 3781–3791.
2. (a) Hoffner, J.; Schottelius, M. J.; Feichtinger, D.; Chen, P. Chemistry of the 2,5-Didehydropyridine Biradical: Computational, Kinetic, and Trapping Studies toward Drug Design. *J. Am. Chem. Soc.* **1998**, *120*, 376–385; (b) Rau, N. J.; Wenthold, P. G. Experimental Investigation of the Absolute Enthalpies of Formation of 2,3-, 2,4-, and 3,4-Pyridynes. *J. Phys. Chem. A* **2011**, *115*, 10353–10362; (c) Nam, H. H.; G. E. Leroi, G. E.; J. F. Harris, J. F. Didehydropyridines (Pyridynes): An ab Initio Study. *J. Phys. Chem.* **1991**, *95*, 6514–6519; (d) Liu, R.; Tate, D. R.; Clark, J. A.; Moody, P. R.; Van Buren, A. S.; Krauser, J. A. Density Functional Theory Study of Molecular Structures and Vibrational Spectra of 3,4- and 2,3-Pyridyne. *J. Phys. Chem.* **1996**, *100*, 3430–3434; (e) Kraka, E.; Cremer, D. The para-Didehydropyridine, *para*-Didehydropyridinium, and Related Biradicals: A Contribution to the Chemistry of Eneidyne Antitumor Drugs. *J. Comput. Chem.* **2001**, *22*, 216–229; (f) Winkler, M.; Cakir, B.; Sander, W. 3, 5-Pyridyne – A Heterocyclic *meta*-Benzyne Derivative. *J. Am. Chem. Soc.* **2004**, *126*, 6135–6149.
3. Hoffmann, R. Interaction of Orbitals Through Space and Through Bonds. *Acc. Chem. Res.* **1971**, *4*, 1–9.
4. Saraswat, M.; Venkataramani, S. Through Bond and Through Space Interactions in Dehydro-Diazine Radicals: A Case Study of 3c-5e Interactions. *Phys. Chem. Chem. Phys.* **2018**, *20*, 4386–4395.
5. Somers, K. P.; Simmie, J. M. Benchmarking Compound Methods (CBS-QB3, CBS-APNO, G3, G4, W1BD) against the Active Thermochemical Tables: Formation Enthalpies of Radicals. *J. Phys. Chem. A* **2015**, *119*, 8922–8933.
6. Ponomarev, D. A.; Takhistov, V. V. What are Isodesmic Reactions? *J. Chem. Educ.* **1997**, *74*, 201–203.
7. Glaser, R.; Choy, G. S. – C. Spin Polarization versus Spin Delocalization. Topological Electron and Spin Density Analysis of the Rotational Automerization of Allyl Radical Including Electron Correlation Effects. *J. Phys. Chem.* **1994**, *98*, 11379–11393.
8. Mohan, N.; Suresh, C. H.; Kumar, A.; Gadre, S. R. Molecular electrostatics for probing lone pair– π interactions. *Phys. Chem. Chem. Phys.* **2013**, *15*, 18401–18409.
9. Foster, J. P.; Weinhold, F. Natural Hybrid Orbitals. *J. Am. Chem. Soc.* **1980**, *102*, 7211–7218.
10. (a) Kolboe, S. Proton Affinity Calculations with High Level Methods. *J. Chem. Theory Comput.* **2014**, *10*, 3123–3128; (b) Hunter, E. P. L.; Lias, S. G. Evaluated Gas Phase Basicities and Proton Affinities of Molecules: An Update. *J. Phys. Chem. Ref. Data.* **1998**, *27*, 413–656.
11. Bader, R. F. W. A Quantum Theory of Molecular Structure and its Applications. *Chem. Rev.* **1991**, *91*, 893–928.
12. Barone, V. Electronic, Vibrational and Environmental Effects on the Hyperfine Coupling Constants of Nitroside Radicals. H₂NO as a Case Study. *Chem. Phys. Lett.* **1996**, *262*, 201–206.
13. McGuire, B. A. 2018 Census of Interstellar, Circumstellar, Extragalactic, Protoplanetary Disk, and Exoplanetary Molecules. *Astrophys. J. Suppl. Ser.* **2018**, *239*, 17–64.
14. Fukui, K. The path of Chemical Reactions – the IRC Approach. *Acc. Chem. Res.* **1981**, *14*, 363–368.
15. Saraswat, M.; Venkataramani, S. Thermal unimolecular reactivity pathways in dehydro-diazines radicals. *J Phys Org Chem.* **2021**; *34*: e4152.

Chapter 3. Matrix-Isolation FTIR Spectroscopic Studies of 2-iodopyrazine and 2-iodopyrimidine

3.1 Introduction:

After the computational exploration of the electronic structure, thermodynamic stability, and thermal reactivity aspects of all isomeric dehydrodiazine radicals, we shifted our attention towards experimental characterization and studies of these radicals. In this regard, we attempted the matrix isolation infrared spectroscopic investigations under cryogenic conditions to characterize a few selected radicals among them. The aim of such experiments is to generate and characterize dehydrodiazine radicals, and also to explore the photochemistry of dehydrodiazine radicals under the matrix-isolation condition. Also, our earlier reactivity studies of dehydrodiazine radicals provided insights on the possible ring-opened and fragmentation products under thermal conditions.^[1] Under matrix isolation experimental conditions, the photochemistry of dehydrodiazine radicals can possibly lead to some or all ring-opening and fragmentation products, however, through the excited states. In recent times, *N*-heterocycles have gained a lot of importance in the spectroscopic characterization due to their relevance in prebiotic chemistry.^[2] Also, *N*-containing species play a crucial role as potential precursors of amino acids and nucleobases of DNA and RNA.^[3] As discussed in the reactivity studies, some of the ring-fragmented products obtained from the dehydrodiazine radicals have relevance in astrochemical perspectives and interstellar medium as they have been detected in various regions of the space.^[4] Furthermore, the mode of ring-opening and ring-fragmented products provide preliminary clues in the photochemistry of dehydrodiazine radicals, however, mechanistic aspects are quite interesting and equally challenging to investigate. So far, only prototypical heterocyclic radicals such as pyridyl and didehydropyridine biradicals have been investigated through matrix isolation technique.^[5] To the best of our knowledge, there is no literature available on the generation and direct characterization of dehydrodiazine radicals using the available spectroscopic methods. Addition of one more nitrogen atom into the six membered aromatic ring such as pyridine, makes it more nitrogen rich, which makes it fascinating to study using the matrix isolation technique. Of all the possible isomers of diazine radicals, pyrimidine-based 2-dehydropyrimidine **1a**, and pyrazine-based 2-dehydropyrazine **3a** radicals have been considered in this investigation. Generally, iodo precursors are known for their well-documented photochemistry, and so the matrix isolation experiments including their generation, characterization and their photochemistry using relevant iodo precursors have been carried out.^[5a,6]

3.2 Matrix isolation FTIR spectroscopic study of 2-dehydropyrazine radical (3a)

We attempted to generate and characterize 2-dehydropyrazine radical **3a** under matrix isolation condition using 2-iodopyrazine molecule (**46**) as a precursor. The experiments, results based on the photochemistry of the 2-iodopyrazine have been described as follows:

3.3 Deposition of 2-iodopyrazine (46)

2-Iodopyrazine (**46**) precursor has been purchased from Sigma Aldrich and used for all the matrix experiments without any further purification. 2-Iodopyrazine (**46**) exists in liquid form at room temperature and has a significantly high vapor pressure. An aliquot of sample has been deposited under high vacuum at $-10\text{ }^{\circ}\text{C}$ to $-5\text{ }^{\circ}\text{C}$. The precursor has been deposited for 45 min along with Ar gas at a flow rate of 5 sccm using a digital mass flow controller, following which, an IR spectrum has been recorded at 4 K. (Figure A5 in appendix) The matrix isolated IR spectral features indicate prominent features at 1106.5, 1450.0, 1510.0, 1004.5, 1037.5 and 1371.5 cm^{-1} . Upon comparison of the matrix isolated spectrum with the computed spectrum at B3LYP/DGTZVP level of theory, we observed that the precursor 2-iodopyrazine (**46**) has indeed been deposited over the cold KBr window without any signs of decomposition during deposition process.

3.4 Photochemistry of 2-iodopyrazine (46)

After the successful deposition of 2-iodopyrazine (**46**), the matrix isolated precursor in solid argon at 4 K has been subjected to irradiation at 284 nm UV-light for inducing photochemistry. The choice of wavelength has been decided based on the solution phase UV-Vis spectrum of 2-iodopyrazine (**46**) in acetonitrile, which exhibited an absorbance feature at 284 nm. The photochemistry has been followed by using the infrared spectroscopy. After 15 min of irradiation, the resulting IR spectrum has shown a decrease in signal intensities due to the precursor 2-iodopyrazine with the appearance of new features at 933.0, 1483.5, and 1347.5 cm^{-1} . Whereas prolonged irradiation (120 min) led to maximum changes in the spectral features. The inspection of difference spectrum between irradiated (at 284 nm) and the deposited spectrum noticeably provide all the spectral changes due to photochemistry. (Figure 3.1a) Obviously, the irradiation at 284 nm led to the consumption of precursor 2-iodopyrazine (**46**) along with the formation of new photoproduct(s). In order to identify the newly formed species, we further irradiated the matrix containing the photoproducts at different wavelengths of light.

Upon irradiation at longer wavelength at 350 nm, we observed that the intensity of the peaks corresponding to the precursor 2-iodopyrazine (**46**) increased (Figure 3.1b) with the simultaneous decrease of majority of the new signals that were observed after irradiation at 284 nm. Indeed, a few of the newly formed signals started growing at 350 nm irradiation, which indicated the presence of more than one photoproduct. In an independent control experiment, irradiation was started at 350 nm after deposition, which did not lead to any changes in the spectral features indicating no photochemistry. Based on this data, in particular, the wavelength selective bleaching (at 284 nm) and the formation (at 350 nm) of precursor we inferred the involvement of a radical species. Since light induced homolytic cleavage of C-I bond is well-documented^[5a,6], the irradiation at 284 nm presumably led to the formation of 2-dehydropyrazine radical (**3a**), whereas upon irradiation at 350 nm, the recombination of the radical with iodine atom is plausible, which can lead to the re-formation of the precursor. (Figure 3.1a and 3.1b)

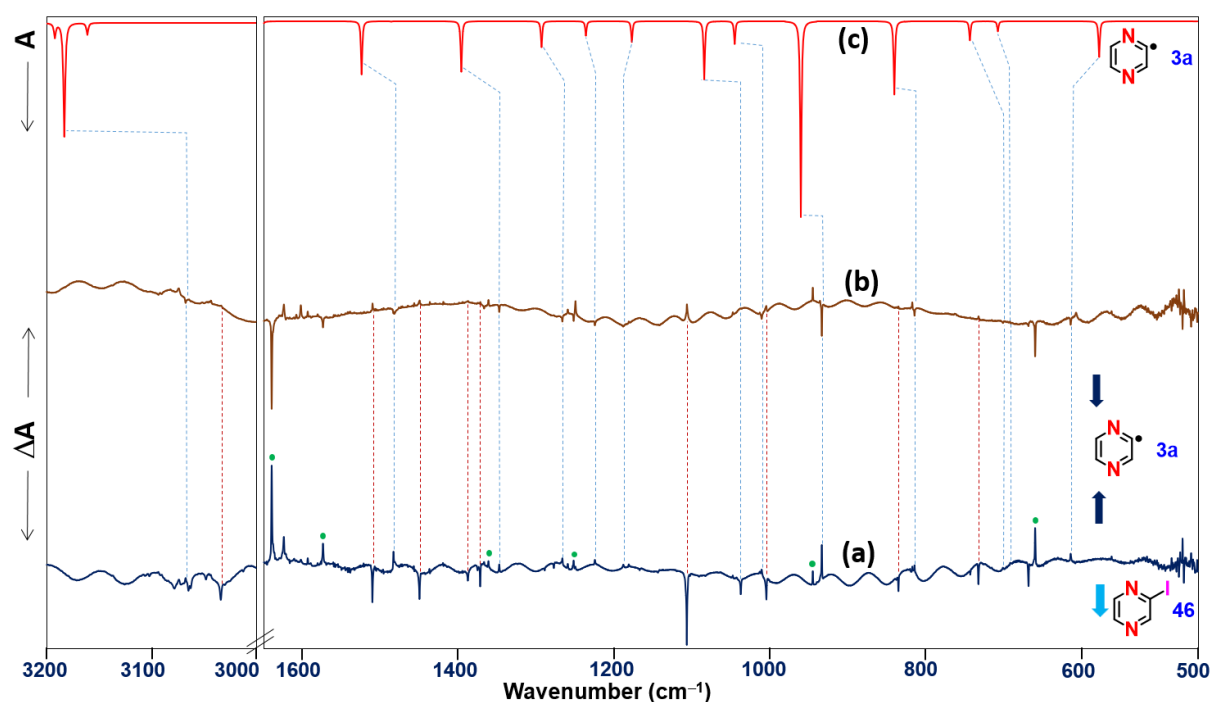


Figure 3.1. IR spectrum of 2-dehydropyrazine radical (**3a**) (Ar, 4K). (a) Difference spectrum after 284 nm irradiation and the deposition spectrum of **46**; the bands pointing upward are forming upon irradiation at 284 nm and those pointing downward are due to the precursor **46** (green dots = unassigned) (b) difference spectrum: the bands pointing upward formed upon irradiation at 350 nm and those pointing downward decreased upon irradiation at 350 nm on a matrix containing photoproducts of **46** due to 284 nm irradiation; (c) computed harmonic vibrational spectrum of 2-dehydropyrazine radical (**3a**) ((U)B3LYP/cc-pVTZ level of theory, unscaled).

Table 3.1 Computed harmonic vibrational frequencies ((U)B3LYP/cc-pVTZ) and experimental IR spectroscopic data (Ar and N₂ matrices, 4 K) of 2-dehydropyrazine radical (**3a**).

Mode	Symmetry	Computed		Experimental (Ar, 4 K)		Experimental (N ₂ , 4 K)	
		$\nu_{\text{calcd.}}$ (cm ⁻¹)	I_{rel}	ν (cm ⁻¹)	I_{rel}	ν (cm ⁻¹)	I_{rel}
1	A''	365.6	16 (8.4)	—	—	—	—
2	A''	436.3	17 (9.0)	—	—	—	—
3	A'	577.4	18 (9.6)	613.5	20	612.0	23
4	A'	707.6	5 (2.8)	691.5	< 1	691.5	< 1
5	A''	743.6	10 (5.2)	700.5	11	700.5	13
6	A''	840.8	37 (19.7)	814.0	23	816.0	21
7	A''	951.6	0 (0.0)	—	—	—	—
8	A'	960.6	100 (52.7)	933.5	100	935.0	100
9	A''	988.0	0 (0.0)	—	—	—	—
10	A'	1045.7	12 (6.1)	1010.5	14	1012.5	13
11	A'	1084.0	30 (15.7)	1037.5	26	1037.5	31
12	A'	1177.8	11 (5.6)	1188.0	11	1190.0	10
13	A'	1236.7	7 (3.9)	1224.5	14	1221.5	17
14	A'	1293.4	13 (7.0)	1266.5	13	1268.5	11
15	A'	1396.5	26 (13.6)	1347.5	25	1349.5	24
16	A'	1486.4	0 (0.1)	—	—	—	—
17	A'	1524.9	27 (14.3)	1483.5	41	1480.0	50
18	A'	1653.2	13 (6.9)	1589.0	< 5	1591.0	< 5
19	A'	3161.5	6 (3.0)	3044	< 3	3062	< 5
20	A'	3183.9	53 (28.0)	3074	32	3096	47
21	A'	3192.4	7 (3.5)	3085	< 5	3100	< 5

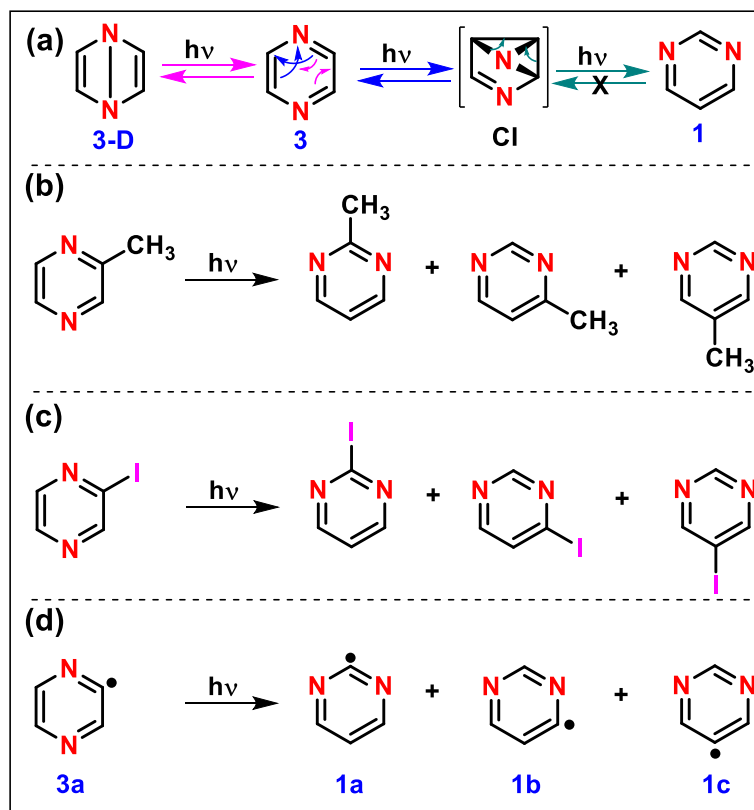
In this regard, the experiments have been repeated for consistency as well as to understand the wavelength dependent interconversion between the potential 2-dehydropyrazine radical (**3a**) and the precursor 2-iodopyrazine (**46**) at 284 and 350 nm, respectively. In order to confirm the spectral assignment for **3a**, the IR signals have been compared with the vibrational data computed at (U)B3LYP/cc-pVTZ level of theory. The unscaled computed spectral signature showed excellent agreement with the observed spectral data within the spectral shifts under matrix-isolation conditions, which unambiguously confirmed the 2-dehydropyrazine radical **3a** (Table 3.1). Indeed, the same behaviour has also been observed in the case of photochemistry in nitrogen matrix at identical conditions. Only a

slight variation in the spectral shifts due to the change in the host has been observed, which is well-known in literature.^[7]

Apart from 2-dehydropyrazine radical (**3a**), we have also observed a few additional signals upon irradiation at 284 nm. These signals include 1639.5, 1575.5, 945.5 and 659.0 cm⁻¹. We found out that these unassigned signals were also underwent bleaching upon irradiation at 350 nm, with the simultaneous formation of a few new signals that were growing along with the precursor 2-iodopyrazine (**46**) signals. Along with the precursor, a few ring-opening products started to appear that have been understood based on the signals in the region corresponding to N≡C/C≡N/C≡C stretching (2200 to 2050 cm⁻¹). Since the source for formation of the precursor has been ascertained to the radical (**3a**), the other set of signals behaving similar to the radical signals could be responsible for the ring-opening products. In order to understand these species, we have performed additional matrix photochemistry experiments at different wavelengths, which have been discussed in the next section along with the photochemistry of 2-dehydropyrazine radical (**3a**).

Also, the presence of additional signals along with radicals could be due to the possible isomerization products along with few ring-opening and fragmented products as mentioned previously. Rui Fausto and co-workers studied the matrix isolated IR spectrum of pyrimidine, pyrazine and pyridazine and observed a photochemical conversion of pyrazine into pyrimidine upon irradiation through a nitrogen transposition.^[8] (Scheme 3.1a) An involvement of conical intersection (CI) has been proposed in such conversion under photochemical conditions. Subsequently, Ming-der Su explored the photochemical mechanistic aspects of transposition reaction in the isomerization of pyrazine to pyrimidine computationally, and compared it with a similar reaction in methyl pyrazine and established the CIs and also their possible access through 254 nm irradiation conditions.^[9] (Scheme 3.1b) Assuming similar channels involving conical intersections, we considered the possibilities of transposition or isomerization products of both precursor **3** and radical **3a** in our experiments as mentioned in scheme 3.1c,d. In this regard, we compared our experimental data corresponding unassigned signals with the computed vibrational spectra of all possible isomerization products based on which, we ruled out the isomerization products of precursor **3** such as 2-, 4- and 5-iodopyrimidines and dehydropyrimidines. (Figure A6 in appendix) Along a similar line, it is quite unlikely to obtain the corresponding radical isomers **1a-c** as indicated in the scheme 3.1. On the other hand, the further photochemistry of the **3** and **3a** led to a lot of ring-opening products. In order to understand the common products including the fragmentation products (*vide infra*), to analyse

the ring-opening pathways, and also to obtain deeper insights, we have chosen the precursor 2-iodopyrimidine (Section 3.6). More importantly, the purpose of this precursor was to generate and characterize the 2-dehydropyrazine radical (**3a**).

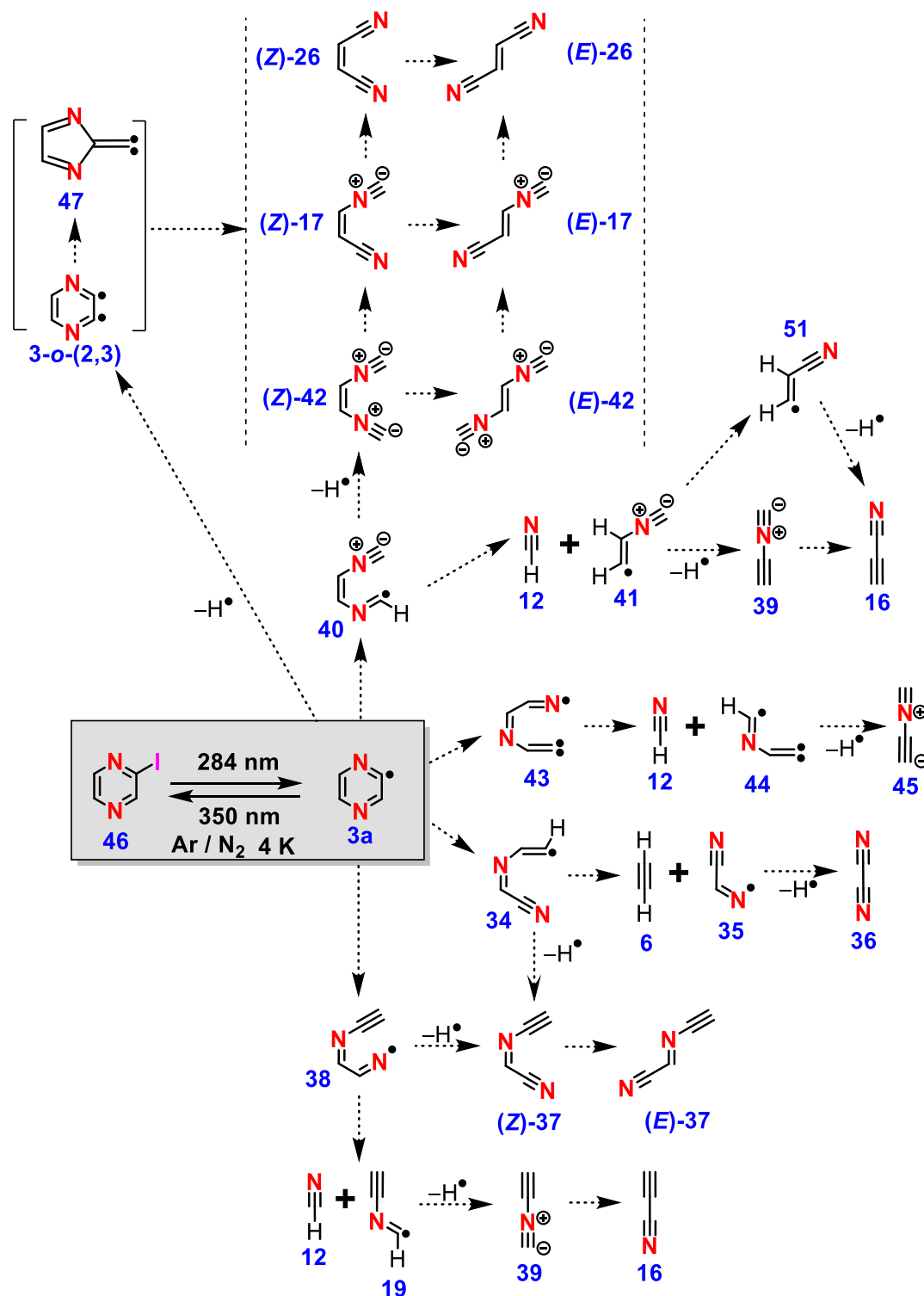


Scheme 3.1 Isomerization under photochemical condition: (a) transposition of pyrazine into pyrimidine reported by Rui Fausto and co-workers (ref 8); (b) isomerization of methyl pyrazine to methyl pyrimidines explored by Ming-der Su (ref 9); possible photoisomerization of (c) 2-iodopyrazine into iodopyrimidines; and (d) 2-dehydropyrazine radical into dehydropyrimidines radicals.

3.5 Photochemistry of 2-dehydropyrazine radical (**3a**), ring-opening and fragmentation

After confirming the generation and characterization of the target 2-dehydropyrazine radical (**3a**) at 284 nm, we further irradiated the matrix containing the photoproducts with shorter wavelength of light at 254 nm. Upon irradiation at 254 nm, we observed that the intensity of peaks corresponding to the precursor 2-iodopyrazine (**46**) and 2-dehydropyrazine radical (**3a**) decreased and several new sets of signals started appearing. Upon prolonged irradiation at 254 nm, the signals corresponding to the precursor 2-iodopyrazine (**46**) and pyrazine radical (**3a**) disappeared completely. The simultaneous formation of new

photoproduct(s) with prominent signatures in the region of $\text{C}\equiv\text{C-H}$, $\text{C}\equiv\text{N}$, $\text{C}\equiv\text{C}$ stretchings, and $\text{H-C}\equiv\text{C-H}$ (*Z* and *E*-isomeric) torsional bending modes indicated the ring-opening and fragmentation type products under such irradiation conditions. Various pathways for the ring scission and the possible ring-opening and photo-fragmented products originating from 2-dehydropyrazine radical (**3a**) have been depicted in the scheme 3.2.



Scheme 3.2 Possible ring-opening channels in 2-dehydropyrazine radical (**3a**).

Considering the challenges involved in the identification of such ring-opening and fragmentation species, the experiments have been repeated by varying the duration of irradiation and sequence of the wavelengths of irradiation. As a preliminary step, we have identified and assigned a few signals corresponding to the ring-fragmented products in Ar and N₂ matrix under prolonged irradiation conditions at 254 nm based on the available literature. The major photo-fragmentation products include HCCCN (**16**)^[10] (3315, 2267, 667, 504 cm⁻¹), HCCNC (**39**)^[10] (3328, 2033 cm⁻¹), CN radical (**9**)^[11] (2044 cm⁻¹) and HCN (**12**)^[10] (3297, 727 cm⁻¹) in Ar matrix, which have been readily identified based on the literature data.

In addition, we also observed a set of very intense signals in the region 2050-2200 cm⁻¹ upon irradiation at 254 nm, which may belong to the ring-opening products containing isonitrile and nitrile groups that may have formed from 2-dehydropyrazine radical (**3a**). Indeed, some of them appeared at lower intensities at 284 nm under prolonged irradiation conditions. As mentioned in scheme 1, the photochemistry of 2-dehydropyrazine radical (**3a**) may lead to various ring-opened radical species of formula C₄H₃N₂. They may further undergo a loss of hydrogen (as H radical/atom) to form isomeric ring-opening products (C₄H₂N₂) or fragmentation step under photochemical conditions. In order to analyse the spectral data and identify various photoproducts, we have closely inspected the computed vibrational spectra of several possible isonitrile (-N≡C) containing molecules (listed in scheme 1) due to their strong signature. In this regard, a comparison of the growth rates of various experimental signals, their frequencies, intensities and also the splitting pattern of the signals, if any, have been carefully compared. In addition, the signals appeared around 1000 to 600 cm⁻¹ have also been considered towards the assignment of such isonitriles. This region was particularly chosen because the (*Z*)- and (*E*)- isomeric H-C=C-H moieties can be differentiated based on their characteristic signals. Due to the fact that identification of several new photoproducts is difficult with a single precursor, the photochemistry of other Iodo-diazine precursors has been considered as an alternative strategy, which in principle, can lead to some of common photoproducts. In this regard, we have also performed matrix isolation spectroscopic experiments under photochemical conditions using 2-iodopyrimidine (**48**) as a precursor, which is described in preceding section before the analysis of the ring-opening products. The possible transposition of nitrogen under photochemical conditions is one of the reasons for the choice of 2-iodopyrimidine (**48**) as a precursor.

3.6 Matrix isolation FTIR spectroscopic study of 2-dehydropyrimidine radical (**1a**)

We attempted to generate and characterize 2-dehydropyrimidine radical **1a** under matrix isolation condition using 2-iodopyrimidine molecule (**48**) as a precursor. The experimental results based on the photochemistry of the 2-iodopyrimidine are described as follows:

3.7 Deposition of 2-iodopyrimidine (**48**)

2-Iodopyrimidine (**48**) has been synthesized from the commercially available 2-chloropyrimidine (**49**) using the standard literature procedure.^[12] 2-Iodopyrimidine (**48**) sample has been deposited at -10 to 0 °C under the high vacuum for 120 min with Ar gas at a flow rate of 5 sccm. Matrix-isolated infrared spectrum of 2-iodopyrimidine (**48**) at 4 K exhibited prominent features at 1142.0, 1552.5, 1548.5, 1380.5, and 1374.0 cm^{-1} . (Figure A7 in appendix) The comparison of the IR spectrum of 2-iodopyrimidine (**48**) with the computed vibrational spectrum at B3LYP/DGTZVP level of theory showed excellent agreement with majority of the signals within the usual shifts due to matrix. Due to the presence of a small amount of the 2-chloropyrimidine (**49**) as an impurity, the deposition spectrum exhibited additional signals at 1390.0, 1557.0, 1565.0, and 1174.5 cm^{-1} . These signals have been confirmed by a separate matrix isolation experiment using 2-chloropyrimidine (**49**) and computed infrared spectrum of it at B3LYP/DGTZVP level of theory. (Figure A8 in appendix)

3.8 Photochemistry of 2-iodopyrimidine (**48**)

After the successful deposition of 2-iodopyrimidine (**48**), the matrix isolated precursor has been subjected to irradiation at 254nm UV-light towards generating the target 2-dehydropyrimidine radical (**1a**). After 4 min of irradiation, the recorded IR spectra revealed the decrease in the signal intensities due to the precursor 2-iodopyrimidine (**48**) with the appearance of new signals. The prolonged irradiation conditions at the same wavelength led to many new signals that were similar to the ones that we observed in the case of photochemistry of 2-iodopyrazine (**46**). Now the question is whether the 2-dehydropyrimidine (**1a**) radical has been formed under this condition or not. In order to answer this, and also to characterize the signals due to the radical **1a**, if at all formed, further experiments under matrix isolation condition have been carried out using different wavelengths of light like in the case of 2-iodopyrazine (**46**). (Figure 3.2)

In this regard, the matrix containing the preliminary photoproducts (occurred at shorter irradiation times) obtained at 254 nm has been subjected to irradiation at 365 nm wavelength for 45 min. Under these conditions, we observed spectral changes as increase in the intensity of the signals corresponding to precursor 2-iodopyrimidine (**48**) (Figure 3.2b) that was accompanied by a decrease in the intensity of newly formed signals at 254 nm. Based on the similarity to the photochemistry in 2-iodopyrazine (**46**), those signals formed at 254 nm and subsequently bleached at 365 nm have been considered belonging to a single species. Also, the wavelength selective disappearance and formation of the precursor envisaged that the most likely species can be 2-dehydropyrimidine radical (**1a**). Once again, the photochemical cleavage of C-I bond (at 254 nm) and recombination of the radical with iodine atom (at 365 nm) could be responsible for this behaviour. (Figure 3.2a and 3.2b) Furthermore, this set of irradiation sequences has been repeatedly performed for consistency, and to gain the information on wavelength dependent photo equilibrium between 2-dehydropyrimidine radical (**1a**) and its precursor 2-iodopyrimidine (**48**) using lights of wavelength 254 and 365 nm, respectively.

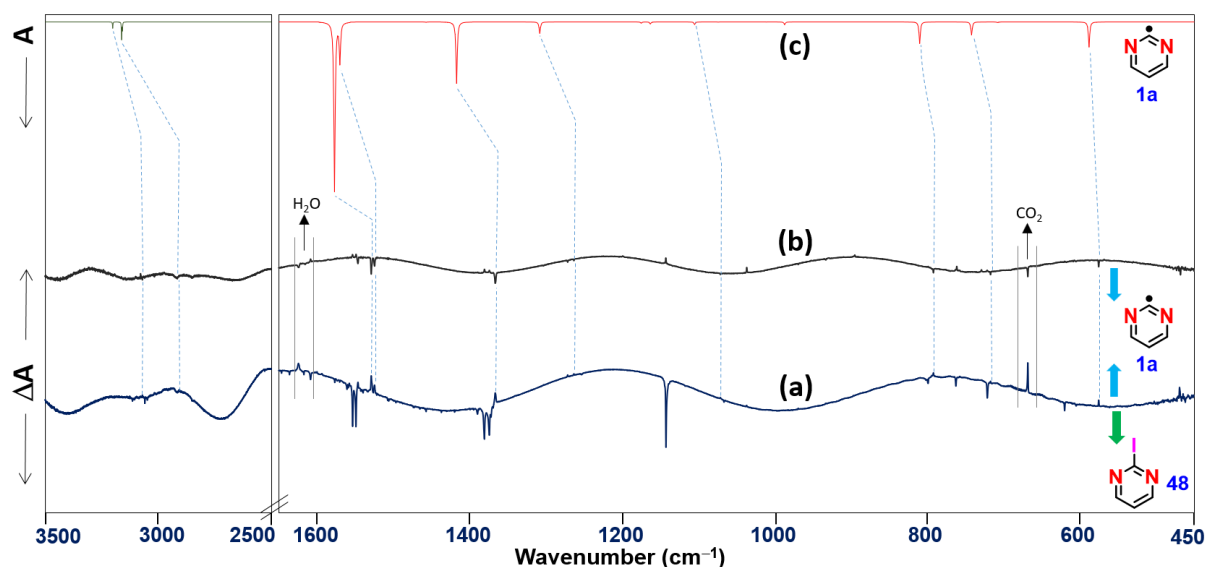


Figure 3.2 Matrix-isolated IR spectrum of 2-iodopyrimidine (**48**) (Ar, 4K). (a) The difference spectrum after 254 nm irradiation (for 4 min) and the deposition spectrum; the bands pointing upward formed upon irradiation at 254 nm and those pointing downward are due to the precursor **48**. (b) Difference spectrum: the bands pointing upward are forming and those pointing downward are decreasing upon irradiation at 365 nm at a matrix containing photoproducts of **48** due to 254 nm irradiation; (c) Computed harmonic vibrational spectrum of 2-dehydropyrimidine radical (**1a**) (B3LYP/cc-pVTZ level of theory, unscaled).

Table 3.2 Computed harmonic vibrational frequencies ((U)B3LYP/cc-pVTZ) and experimental IR spectroscopic data (Ar and N₂ matrices, 4 K) of 2-dehydropyrimidine radical (**1a**).

Mode	Symmetry	Computed		Experimental (Ar, 4 K)		Experimental (N ₂ , 4 K)	
		$\nu_{\text{calcd.}}$ (cm ⁻¹)	I_{rel}	ν (cm ⁻¹)	I_{rel}	ν (cm ⁻¹)	$I_{\text{rel.}}$
1	B ₁	382.1	0 (0.1)	—	—	—	—
2	A ₂	385.4	0 (0.0)	—	—	—	—
3	B ₂	588.5	15 (24.7)	575.0	31	576.0	10
4	A ₁	708.3	0 (0.6)	—	—	—	—
5	B ₁	742.6	8 (12.8)	716.5	13	718.0	9
6	B ₁	810.0	13 (21.2)	791.5	10	793.5	11
7	A ₁	987.3	2 (2.8)	—	—	—	—
8	A ₂	1001.1	0 (0.0)	—	—	—	—
9	B ₁	1011.6	0 (0.0)	—	—	—	—
10	A ₁	1074.0	0 (0.1)	—	—	—	—
11	B ₂	1105.5	2 (2.6)	—	—	—	—
12	A ₁	1163.6	1 (2.0)	—	—	—	—
13	B ₂	1175.5	1 (1.2)	—	—	—	—
14	B ₂	1308.7	7 (11.3)	1263.0	< 4	1262.5	< 5
15	A ₁	1417.7	36 (60.2)	1366.0	67	1363.0	34
16	B ₂	1457.8	0 (0.4)	—	—	—	—
17	A ₁	1570.5	24 (38.8)	1524.5	43	1520.5	47
18	B ₂	1577.7	100 (165.4)	1528.5	100	1530.0	100
19	A ₁	3159.9	5 (8.0)	2849.0	< 5	—	—
20	B ₂	3163.6	10 (17.3)	2911.5	9	2908.5	< 5
21	A ₁	3202.7	4 (6.3)	3069.5	< 5	3071.5	< 5

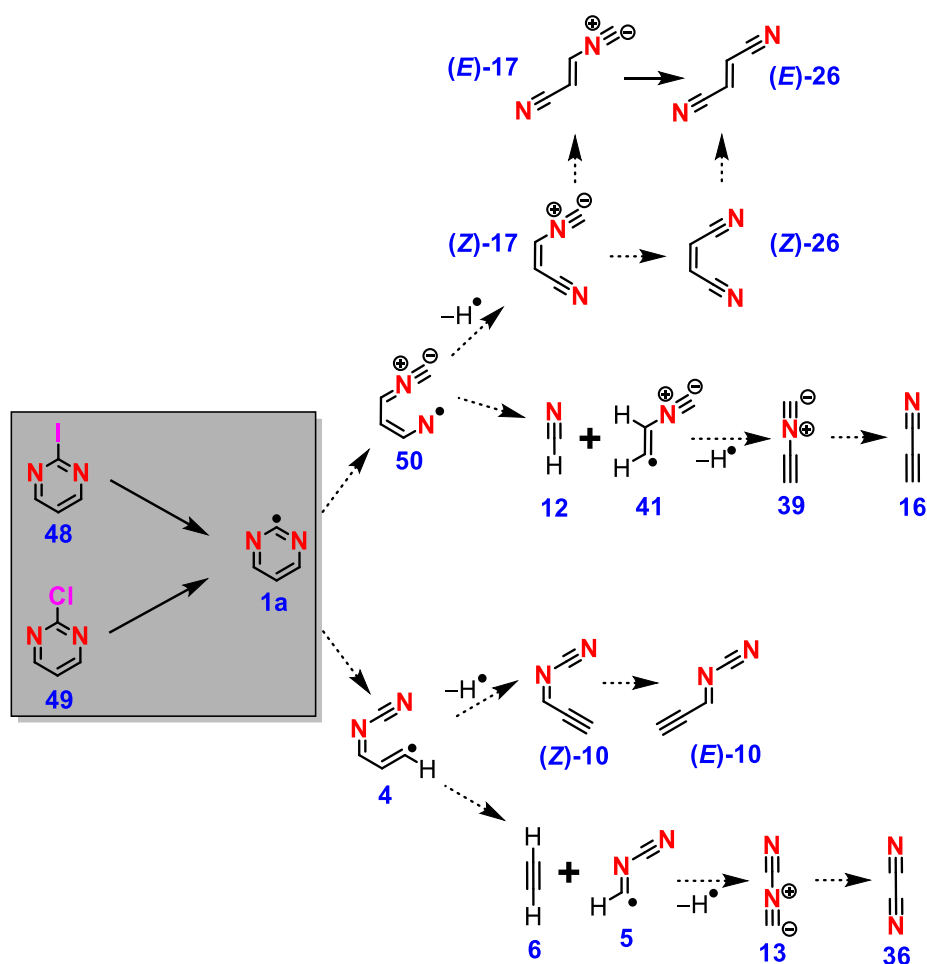
In order to confirm the signals corresponding to the 2-dehydropyrimidine radical (**1a**), computed vibrational spectrum at (U)B3LYP/cc-pVTZ level of theory has been considered, which showed a good agreement within the experimental shift. The complete assignment of the infrared spectral data due to the radical **1a** is listed in table 3.2.

Since the deposition of 2-iodopyrimidine (**48**) contained a small amount of 2-chloropyrimidine (**49**), we have performed separate experiments to rule out the photoproducts due to 2-chloropyrimidine (**49**) from the assigned signals of 2-dehydropyrimidine radical (**1a**). The irradiation at 254 nm on the matrix isolated 2-chloropyrimidine (**49**) led to the same set of new signals as in the case of **48**, however exhibited a slow photochemistry with lower yields. This can be attributed to the greater bond strengths of C-Cl over C-I under photochemical conditions. These new sets of signals exactly matched the signals assigned for 2-

dehydropyrimidine radical (**1a**). This demonstrates that no deviation in the photochemical channels has been observed despite the presence of the 2-chloropyrimidine (**49**) as an impurity.

3.9 Photochemistry of 2-dehydropyrimidine radical (**1a**), ring-opening and fragmentation

After generating and characterizing the 2-dehydropyrimidine radical (**1a**), we have subjected the matrix isolated pyrimidine radical (**1a**) to prolonged irradiation condition at 254 nm and monitored the spectral changes. Similar to the experiment on 2-iodopyrazine (**46**), we have observed various sets of signals upon irradiation at 254 nm. Interestingly, some common spectral features (signals) have been observed in the IR spectrum containing the photoproducts due to 2-iodopyrimidine (**48**) and 2-iodopyrazine (**46**) indicating common products. In this regard, we considered various possibilities of the ring-opening or ring-fragmented channels and photoproducts originating from 2-dehydropyrimidine radical (**1a**) as mentioned in scheme 3.3. Due to higher symmetry (C_{2v}) of 2-dehydropyrimidine radical (**1a**) lesser number of channels are expected for ring-opening and fragmentation pathways in comparison to the C_s symmetric 2-dehydropyrazine radical (**3a**).



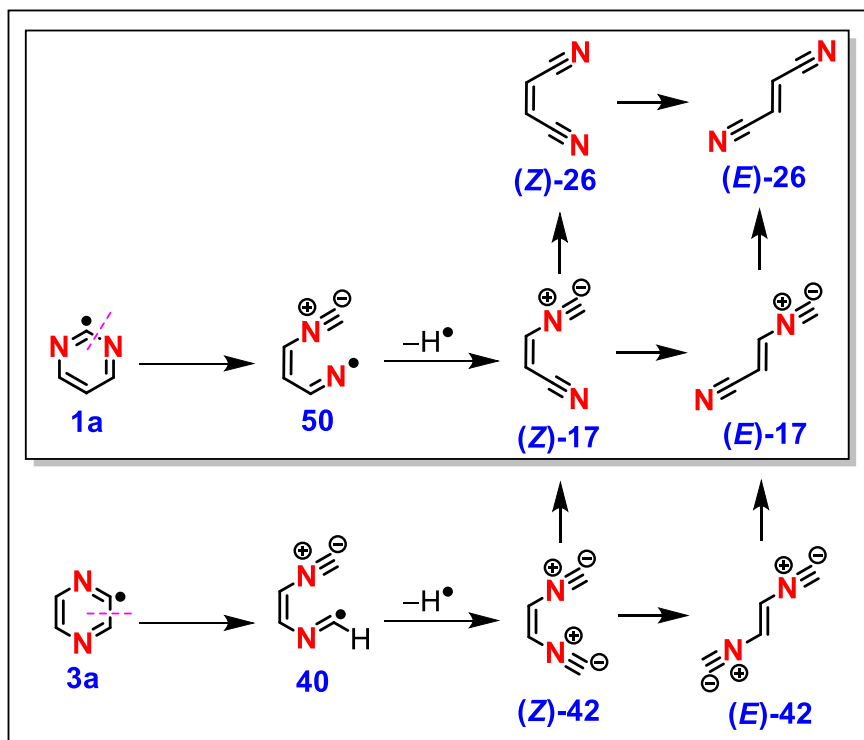
Scheme 3.3 Possible ring-opening channels in 2-dehydropyrimidine radical (**1a**).

Likewise, in the case of pyrazine radical **3a**, we have identified some of the ring-fragmented small molecules such as HCCCN (**16**),^[10] HCCNC (**39**)^[10] and HCN (**12**)^[10] with the help of the available literature data upon prolonged irradiation at 254 nm. In order to understand, analyse, and characterize the several possible ring-opening products, we have compared the data obtained from the photochemistry of both 2-dehydropyrazine radical (**3a**) and 2-dehydropyrimidine radical (**1a**). The proceeding section will describe the details of such analysis in elucidation of the photoproducts obtained based on the experimental evidences and computational data.

3.10 Analysis of ring-opening species (Z)/(E)-**17**, (Z)/(E)-**26** and (Z)/(E)-**42** (diazine analogues of enediyne with molecular formula C₄H₂N₂)

As indicated before, irradiation at a shorter wavelength ($\lambda = 254$ nm) led to the observation of a very intense set of signals in the region of 2050-2200 cm⁻¹, which can be assigned to the potential photoproducts containing nitrile (less intense) and isonitrile (more intense) functional group containing species. Based on the possibilities of ring-opening modes, 2-dehydropyrazine radical (**3a**) and 2-dehydropyrimidine radical (**1a**) can be expected to yield products such as (Z)/(E)-**17**, (Z)/(E)-**26** and (Z)/(E)-**42** following a C-H bond scission step. The loss of proton can happen before the ring-opening step or proceed after the ring-scission. Under former condition, didehydrodiazines are the potential products. Due to dominant through space and through bond interactions between lone pairs and radical electrons, all such didehydrodiazines are expected to be singlet ground state structures. Indeed, such species can possibly be formed due to the abstraction of the hydrogen of the radical species by iodine atom, which is present within the matrix cage at the end of C-I bond cleavage under photochemical step.^[13] However, we did not observe any signal that can be unambiguously assigned to the didehydrodiazine biradical. Besides that, the 2-dehydropyrimidine radical (**1a**) may have lower probability to form the didehydropyrimidine as the radical centre is flanked by the two nitrogen atoms, and the hydrogen abstraction is less likely. Due to the fact that the C-H bond scission is more facile, the ring-opened products can lead to the species such as (Z)/(E)-**17**, (Z)/(E)-**26** and (Z)/(E)-**42**. (Scheme 3.4). Considering the various possible ring-opening modes, we observed that only (Z)/(E)-**17**, (Z)/(E)-**26** ring-opening products are probable products from 2-dehydropyrimidine radical (**1a**) as described in scheme3.3. Since several signals appeared in that region and also the availability of a greater number of ring cleavage possibilities,

presumably, all these ring-opening products (*Z*)/(*E*)–**17**, (*Z*)/(*E*)–**26** and (*Z*)/(*E*)–**42** are formed in the case of 2-dehydropyrazine radical (**3a**) as described in scheme 3.4.

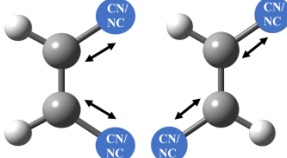
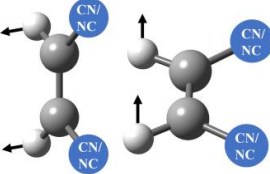
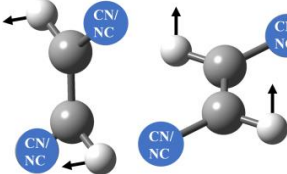
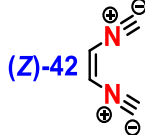
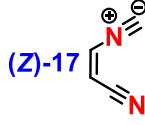
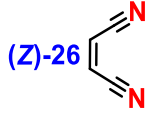
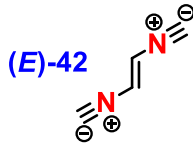
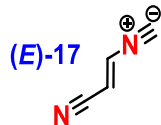
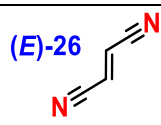


Scheme 3.4 Possible common ring-opening products of 2-dehydropyrazine radical (**3a**) and 2-dehydropyrimidine radical (**1a**).

As described before, (*Z*)–**42** can be formed either via C–H bond scission from the radical intermediate (**40**) or through ring-opening of the elusive 2,3-didehydropyrazine intermediate (**47**), an *o*-benzyne analogue. Ring-opening species (*Z*)–**42**, can further undergo either a *cis-trans* (*Z-E*) or isonitrile ($-N\equiv C$) – nitrile ($-C\equiv N$) isomerization. The *cis-trans* (*Z-E*) isomerization of *Z*–**42** can lead to *E*–**42** at 365 nm irradiation, whereas the formation of (*Z*)–**17** (via $-N\equiv C$ to $-C\equiv N$ isomerization) happens at 254 nm irradiation. Similarly, (*Z*)–**17** can undergo both isomerization pathways to form (*E*)–**17** and (*Z*)–**26**. Among these, the ring opening species (*Z*)–**26** (maleonitrile) has only the possibility of *cis-trans* (*Z-E*) isomerization to form (*E*)–**26** (fumaronitrile) as the reverse $-C\equiv N$ to $-N\equiv C$ isomerization is unfavourable. Irradiation at 365 nm can induce the *cis-trans* (*Z-E*) isomerization, and irradiation at 254 nm leads to isonitrile ($-N\equiv C$) – nitrile ($-C\equiv N$) isomerization. Based on the experimental data on the photochemistry of 2-dehydropyrazine radical (**3a**) and 2-dehydropyrimidine radical (**1a**), and the computed vibrational spectra including the sequence of the appearance of the products, their signal positions, intensities, sequence of appearance, etc., all the ring-opening products

(*Z*)/(*E*)-**17**, (*Z*)/(*E*)-**26** and (*Z*)/(*E*)-**42** have been fully characterized. (figure 3.3, table 3.3 and table A2, A3, A4 in appendix). In addition, we have characterized (*Z*)-**26** (maleonitrile) and (*E*)-**26** (fumaronitrile) separately from an independent precursor, 3,6-diiodopyridazine, which is part of the next chapter. The next section will provide the details of the evidences, based on which the assignments for the ring-opening and the fragmentation products, as well as the possible sequence and fate of those species have been described in detail.

Table 3.3 Characteristic vibrational normal modes of ring-opening products (*Z*)/(*E*)-**17**, (*Z*)/(*E*)-**26** and (*Z*)/(*E*)-**42** and their intensities.

Species	Characteristic Vibrational modes		
	2150 – 2400 cm ⁻¹	700 – 800 cm ⁻¹	900 – 1000 cm ⁻¹
	NC and CN stretching	HCCH bending	HCCH bending
	 Z-(CN/NC) + E-(CN/NC)	 Z-(CN/NC)	 E-(CN/NC)
 (Z)-42	Very strong	Medium	Absent
 (Z)-17	Very strong	Medium	Absent
 (Z)-26	Very weak	Medium	Absent
 (E)-42	Very strong	Absent	Medium
 (E)-17	Very strong	Absent	Medium
 (E)-26	Very weak	Absent	Medium

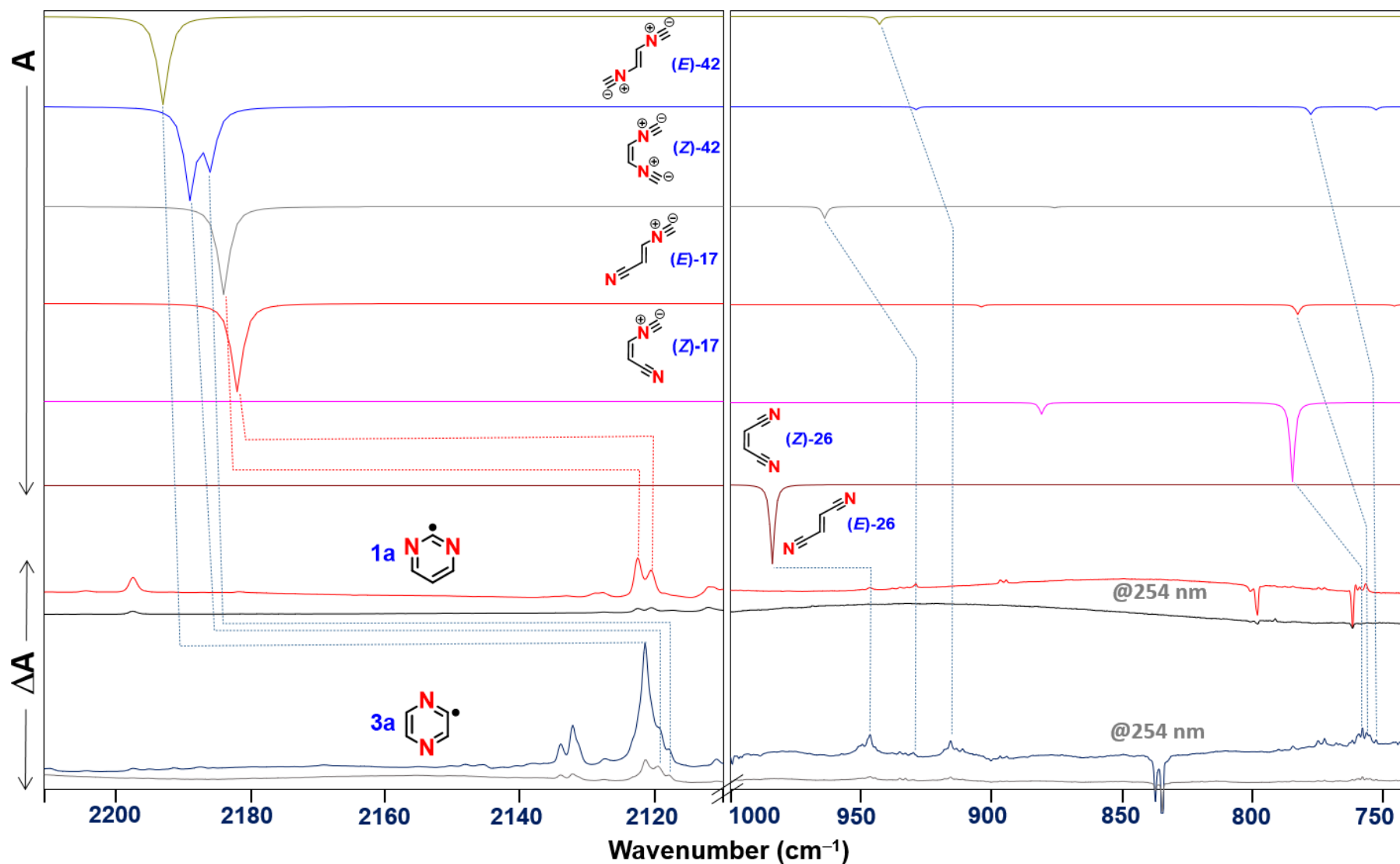
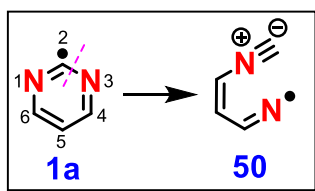


Figure 3.3 Ring-opening species (Z)/(E)-17, (Z)/(E)-26 and (Z)/(E)-42 from 2-dehydropyrazine radical (3a) and 2-dehydropyrimidine radical (1a).

3.11 Ring-opened and ring-fragmented products and radical intermediates from 2-dehydropyrimidine (1a)

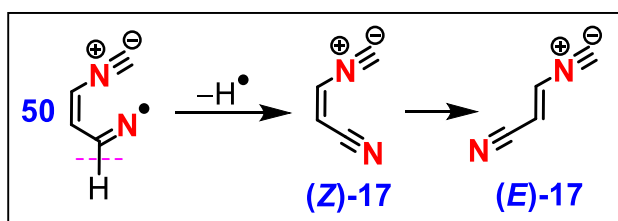
3.11.1 Ring-opening through C2-N3 bond cleavage



Scheme 3.5 Formation of first ring-opened radical intermediate **50** from 2-dehydropyrimidine radical (**1a**).

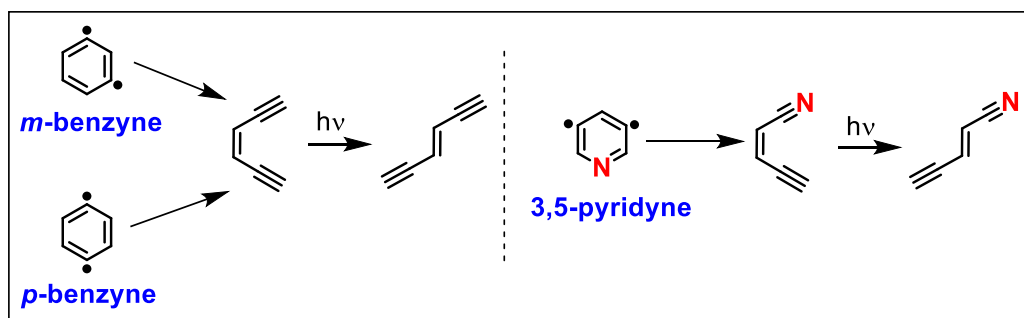
After isolating and characterizing the 2-dehydropyrimidine radical (**1a**), we further explored its photochemistry by irradiating at 254 nm. For analysis, the growth pattern of various signals, specifically other than those of 2-dehydropyrimidine radical (**1a**) have been considered. The most intense signal at 2111.0 cm^{-1} and another signal at 1585.5 cm^{-1} have been tentatively assigned to the first ring-opening *N*-centred radical (**50**) in comparison with the computed vibrational spectrum. Since hydrogen abstraction by the iodine atom is less probable (because of the two nitrogens adjacent to the radical center), ring-opening without the loss of hydrogen could be responsible for the formation of the radical **50**. Due to the fact that the isonitrile group should be part of the molecule, we considered the C-N bond as a potential bond to break. Since this radical species started appearing only after a certain time of irradiation at 254 nm, we assume that the 2-dehydropyrimidine radical (**1a**) as the source. Further upon prolonged irradiation, all the signals corresponding to this radical completely disappeared indicating intermediate nature of this species. All the observed signals corresponding to this ring-opening radical intermediate (**50**) along with computed vibrational frequencies have been listed in table A8 in appendix.

3.11.2 Formation of ring-opened products (*Z*)/(*E*)-17



Scheme 3.6 Formation of ring-opened products (*Z*)/(*E*)-**17** from of ring-opening radical intermediate **50**.

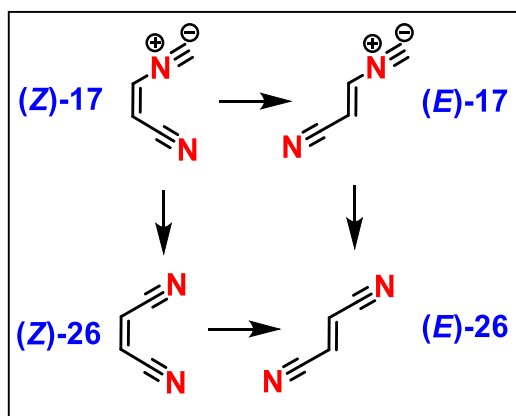
These ring-opened products (*Z*)/(*E*)-**17** have been observed upon irradiating 2-dehydropyrimidine radical (**1a**) for prolonged time at 254 nm. This molecule (*Z*)-**17** can be formed via the loss of H atom from the ring-opened radical intermediate (**50**) under photochemical condition. This ring-opened molecule (*Z*)-**17** has intense absorption due to the presence of isonitrile ($\text{-N}\equiv\text{C}$) group in the $2200\text{--}2100\text{ cm}^{-1}$ region and other characteristic features due to the torsional motion of HC-CH in *Z*-form (around $700\text{--}800\text{ cm}^{-1}$). Based on the broadness and additional signals in the isonitrile region, and the torsional motion of HC-CH in *E*-form (around $900\text{--}1000\text{ cm}^{-1}$), we inferred the presence of *trans* isomer (*E*)-**17**. The observed IR signals at 2121.0 cm^{-1} , and 759.0 cm^{-1} have been assigned to the (*Z*)-**17**, whereas, the peaks at 2122.5 cm^{-1} and 929.0 cm^{-1} have been assigned to the (*E*)-**17** based on the comparison with computed vibrational spectra at B3LYP/cc-pVTZ level of theory. Interestingly, we observed the conversion of *Z*-isomer into the *E*-isomer upon irradiation at 254 and 365 nm, which not only corroborates with the literature reports on benzyne and pyridine chemistry (Scheme 3.7) under photochemical conditions but it is also useful in assigning the signals due to the two species. [5b,14]



Scheme 3.7 *Cis-trans* (*Z-E*) isomerization in ring-opened products obtained from *m*-benzyne, *p*-benzyne and 3,5-pyridyne.

Besides that, we have observed the isonitrile ($\text{-N}\equiv\text{C}$) to nitrile ($\text{-C}\equiv\text{N}$) isomerization at 254 nm along with *Z-E* conversion. However, at 365 nm irradiation only *Z-E* isomerisation has been observed. Additional evidences for the assignment of these two species have been obtained from the experiment with 2-iodopyrazine, where these two ring-opened products (*Z*)/(*E*)-**17** are equally probable. Finally, the complete assignment of all the observed signals corresponding to the ring-opening products (*Z*)/(*E*)-**17** have been confirmed using the computed vibrational frequencies at B3LYP/cc-pVTZ level of theory as listed in table A2 in appendix.

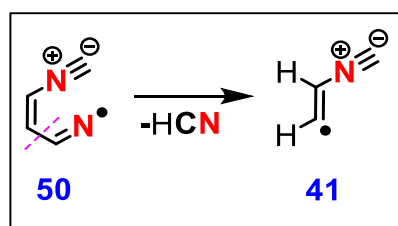
3.11.3 Formation of ring-opened products (Z)/(E)-26



Scheme 3.8 *Cis-trans* (Z-E) isomerization in (Z)/(E)-26 and (Z)/(E)-17 obtained from 2-dehydropyrimidine radical (1a) upon irradiation at 254 nm.

Another pair of ring-opened products maleonitrile (Z)-26 and fumaronitrile (E)-26 have also been observed in the photochemistry of 2-dehydropyrimidine radical (1a), which are one of the stable pairs of compounds of molecular formula $C_4H_2N_2$. These two ring-opened products (Z)/(E)-26 formed only at the later stage of irradiation at 254 nm from the previously mentioned species (Z)/(E)-17 by isonitrile ($-N\equiv C$) to nitrile ($-C\equiv N$) isomerization. The observed IR peaks assigned to maleonitrile are 760.0, 870.0, 1011.5, and 3066.5 cm^{-1} , and the signals 945.5, and 3087.5 cm^{-1} are assigned to fumaronitrile. These two ring-opened products maleonitrile (Z)-26 and fumaronitrile (E)-26 are stable under matrix-isolation conditions and do not undergo any further fragmentation. Further, the assignments for maleonitrile (Z)-26 and fumaronitrile (E)-26 have been confirmed in other experiments using the precursor, 2-iodopyrazine (46), and 3,6-diiodopyridazine (52). All observed signals corresponding to these ring-opened products (Z)/(E)-26 along with the computed vibrational frequencies at B3LYP/cc-pVTZ level of theory have been listed in table A3 in appendix.

3.11.4 Formation of fragmentation product 41



Scheme 3.9 Formation of ring-opened radical intermediate 41 from 50 via HCN elimination.

The first ring-opened radical intermediate (**50**) from 2-dehydropyrimidine radical **1a**, also led to yet another radical intermediate **41**, through a fragmentation step with the elimination of HCN **12**. Indeed, we observed the growth of signals due to HCN (3297, 727 cm^{-1})^[10] and a signal at 2129 cm^{-1} , which have been tentatively assigned to **41** with the help of computed vibrational spectrum at (U)B3LYP/cc-pVTZ level of theory, under prolonged irradiation at 254 nm. (Figure 3.4) During this condition, we observed the disappearance of **50**. Earlier we provided evidences for the formation of the ring-opened products (*Z*)/(*E*)-**17** indicating that **50** undergoes two parallel pathways through the C-H scission (to form (*Z*)/(*E*)-**17**) and fragmentation to form HCN and **41**. Further, the radical intermediate (**41**) is susceptible to C-H scission forming the fragmented products, which can be understood from the continuous decrease in the intensity of the signal at 2129.0 cm^{-1} upon continued irradiation at 254 nm. All the observed signals corresponding to this ring-opened radical intermediate (**41**) along with the computed vibrational frequencies have been listed in table A10 in appendix.

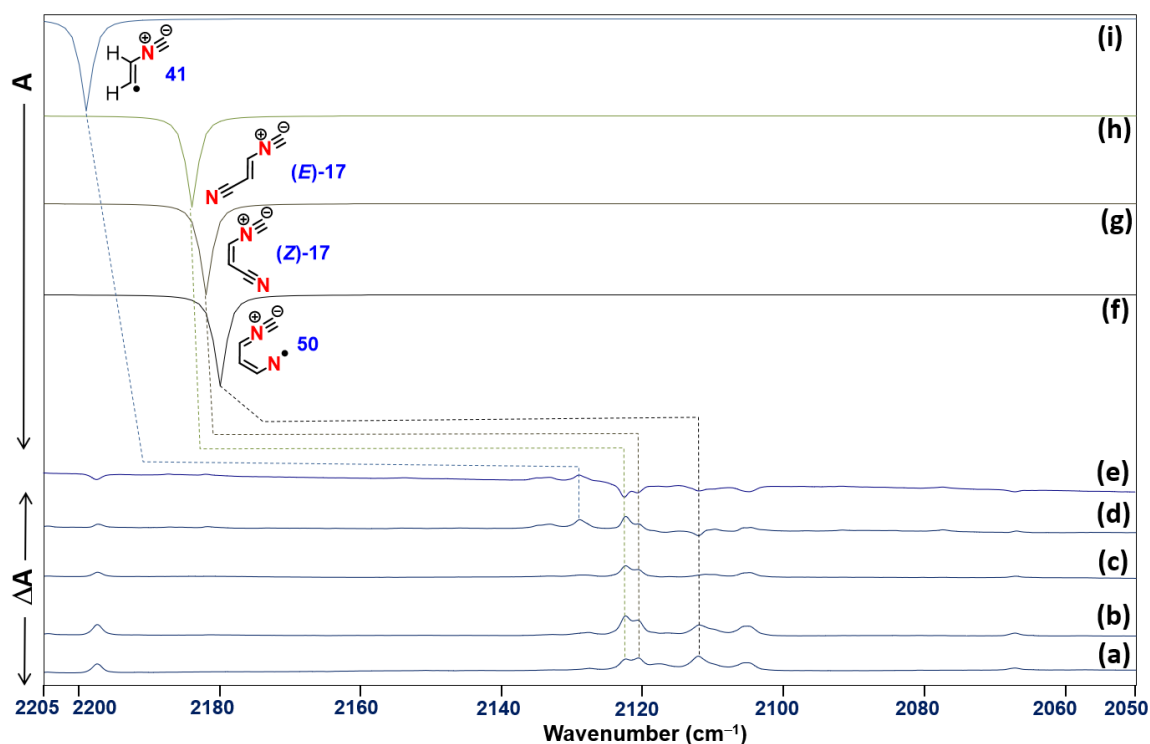
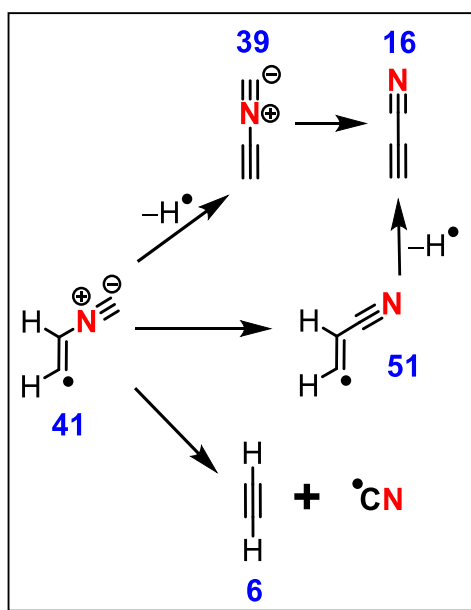


Figure 3.4 Photochemistry of 2-dehydropyrimidine radical (**1a**) (Ar, 4 K). (a) Difference spectrum after 254 nm irradiation (for 5 min); (b) the difference spectrum after 254 nm irradiation (for 10 min); (c) the difference spectrum after 254 nm irradiation (for 15 min); (d) the difference spectrum after 254 nm irradiation (for 25 min); (e) the difference spectrum after 254 nm irradiation (for 90 min); Computed vibrational spectrum (B3LYP/cc-pVTZ level of theory, unscaled) of (f) ring-opened intermediate (**50**), (g) ring-opened product (*Z*)-**17**, (h) ring-opened product (*E*)-**17**, and (i) ring-opened intermediate (**41**).

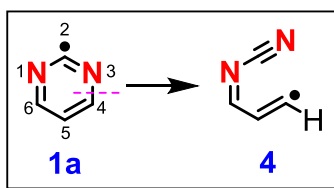
3.11.5 Isomerization and fragmentation products of **41**

Scheme 3.10 Formation of ring-fragmented small molecules HCCNC, HCCCN, HCCH and CN radical from the ring-opened radical intermediate **41**.

As mentioned before, the radical intermediate **41** can undergo fragmentation reaction to form various stable and small molecules either via the H-atom loss or via-acetylene formation. We have observed the stable HCCNC (**39**) (3328, 2033 cm^{-1}) HCCCN (**16**) (3315, 2269, 2076, 667 cm^{-1}) HCCH (**6**) (3289, 737 cm^{-1}) and CN (**9**) radical (2044.5 cm^{-1}) as ring-fragmented products, whose origin has been ascertained to the radical intermediate **41**. The peaks corresponding to HCCNC (**39**) have been assigned as 3328 cm^{-1} , 2033 cm^{-1} , and these peaks match very well with the available literature values. Further, the HCCNC (**39**) undergoes isomerization to HCCCN (**16**) via isonitrile ($-\text{N}\equiv\text{C}$) to nitrile ($-\text{C}\equiv\text{N}$) isomerization process at 254 nm. We have assigned the peaks at 3315, 2269 and 2076 cm^{-1} to HCCCN (**16**), which are available in the literature.^[10] Along with these species, we observed the presence of CN radical with the characteristic signal at 2044.5 cm^{-1} . We also observed the formation of acetylene as the ring-fragmented product upon prolonged irradiation of 2-dehydropyrimidine (**1a**) at 254 nm. Besides that, we have also observed the characteristic signals corresponding to acetylene and HNC as HNC- C_2H_2 complex at 3448.0 cm^{-1} , which is in good agreement with the reported value.^[10] Upon prolonged irradiation, we also observed the ring-fragmented products that originate from radical intermediate **41**. This radical intermediate (**41**) can also undergo isomerization to another ring-opened radical intermediate (**51**) via isonitrile ($-\text{N}\equiv\text{C}$) to nitrile ($-\text{C}\equiv\text{N}$) isomerization process at 254 nm, which can further lead to stable small molecule

HCCCN (**16**) via H-atom loss. We observed two signals at 663.5 and 716.5 cm^{-1} that have been tentatively assigned to the radical intermediate **51**.

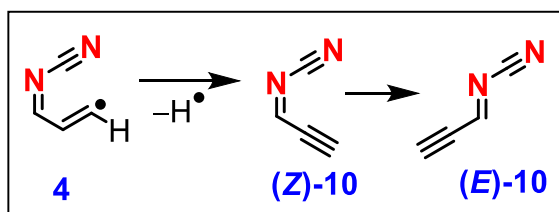
3.11.6 Ring-opening through C4-N3 bond cleavage



Scheme 3.11 Formation of second ring-opened radical intermediate **4** from 2-dehydropyrimidine radical (**1a**).

2-Dehydropyrimidine radical (**1a**) can undergo ring-opening through different bond cleavages under photochemical conditions as well. For instance, a bond scission at N3-C4 can potentially lead to the radical intermediate **4**. Apart from the ring-opened radical intermediate (**50**), we also observed a set of signals at 1573.0, 1612.0, and 2182.0 cm^{-1} with the most intense and characteristic signal in the region of 1550-1700 cm^{-1} (imine region), based on which this can be assigned to the ring-opened radical intermediate (**4**). Upon further irradiation, such signals exhibited disappearance, which provided further evidence that they belong to the same species. Also, these observed signals showed a good agreement with the computed vibrational frequencies of the ring-opened radical intermediate (**4**), which have been listed in the table A8 in appendix.

3.11.7 Formation of ring-opening products (Z)/(E)-**10**



Scheme 3.12 Formation of ring-opening products (Z)/(E)-**10** from of ring-opened radical intermediate **4**.

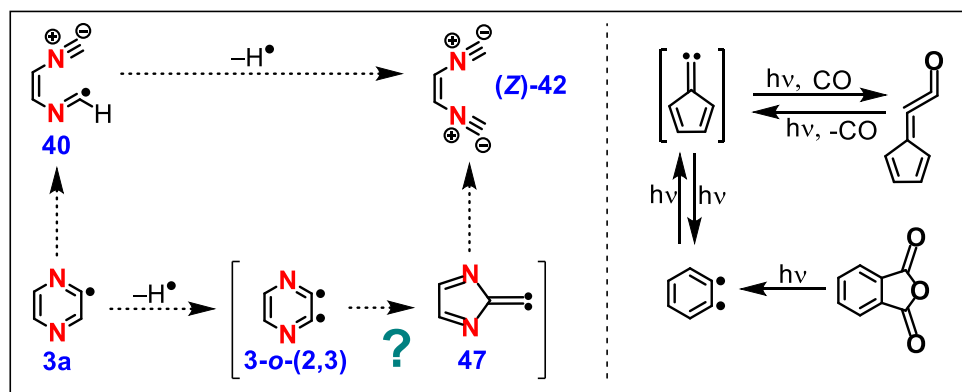
As indicated previously, the ring-opened radical intermediate (**4**) with the radical centre at terminal carbon exhibited a decrease in intensity upon irradiation at 254 nm. Since the radical can potentially lead to ring-opened (Z)/(E)-**10** products through the loss of H-atom, we tentatively assigned the signals that were growing in the region 1550-1700 cm^{-1} to the ring-opened species (Z)/(E)-**10**. The most intense and characteristic signal at 1593.5 cm^{-1} and the peak at 2197.0 cm^{-1} have been assigned to (Z)-**10** based on the computed vibrational spectrum at B3LYP/cc-pVTZ level of theory. As we observed the Z/E-isomerisation upon irradiation at

254 nm, we observed the signals corresponding to (*E*)-**10** upon prolonged irradiation. The most intense and characteristic signal of (*E*)-**10** assigned to 1599.5 cm^{-1} including the overlapping signal of (*Z*)/(*E*)-**10** at 2197.0 cm^{-1} . In addition, we observed characteristic signals in acetylenic region for (*Z*)/(*E*)-**10**. Signal at 3318.0 cm^{-1} is assigned for (*Z*)-**10** and the signal at 3319.5 cm^{-1} has been assigned for (*E*)-**10** based on the sequence of their appearance. (Figure 3.5 e, f and g) All the observed signals corresponding to these ring-opened products (*Z*)/(*E*)-**10** along with computed vibrational frequencies have been listed in table A6 in appendix.

3.12 Ring-opening and ring-fragmented products and radical intermediates from 2-dehydropyrazine radical (3a)

3.12.1 Didehydropyrazine vs diazafulvenediyl carbene analogue

As described before, irradiation of 2-iodopyrazine at 284 nm led to the 2-dehydropyrazine radical (**3a**), which has been understood from the behaviour at 365 nm irradiation. Since the computed vibrational spectrum of **3a** at (U)B3LYP/cc-pVTZ level of theory has agreement only with a certain number of signals, the remaining signals may belong to one or more species.



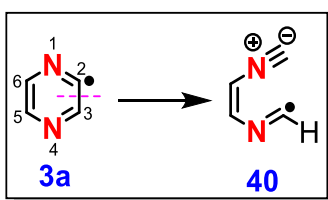
Scheme 3.13 Formation of ring-opening products (*Z*)/(*E*)-**42** from 2-dehydropyrazine radical (**3a**).

The unassigned signals include the most intense signal at 1639.5 cm^{-1} . We considered various possible radical species from the 2-dehydropyrazine radical (**3a**) as mentioned in scheme 1. These include the isomeric iodopyrimidines (based on the possible photochemical isomerization of pyrazine to pyrimidine)^[8] 2,3-didehydropyrazine (possible hydrogen abstraction by the iodine atom), and 2H-imidazol-2-ylidenyl carbene **47** (based on the isomerization of didehydropyrazine), etc. The carbene has been considered based on the possible ring contraction step associated with *o*-benzyne under photochemical step, which consequently

react to form a ketene due to reaction with CO within the cage, if phthalic anhydride is the precursor.^[15] Indeed, the fulvenediyl carbene has not been characterized yet.^[16]

However, none of the species other than **47** exhibit a signal that can be accounted for the observed signal at 1639.5 cm^{-1} , and so the new set of signals have been tentatively assigned to the species (**47**). Moreover, the most intense signal due to the corresponding didehydropyrazine **3-o-(2,3)** is expected to exhibit its breathing normal mode around 450 cm^{-1} (420.5 cm^{-1} at CCSD(T)/TZ2P), however, no such signal has been observed under our experimental conditions, based on which we ruled this species out. Presumably, the ring contraction step proceeded the hydrogen abstraction step that could be responsible for the formation of **47**. An additional evidence has been observed based on the ring-opening step at 350 nm leading to (*Z*)-**42** (*vide infra*), under which condition the radical **3a** underwent recombination with the iodine atom. Indeed, the species **47** is expected to be a singlet carbene as the adiabatic energy difference between the singlet and triplet state is 41.9 kcal/mol . Besides that, the computed vibrational spectrum of singlet carbene (**47**) at B3LYP/cc-pVTZ level of theory exhibited the most intense signal around 1672.2 cm^{-1} . To gain further insights, we have also calculated the vibrational spectrum of singlet carbene (**47**) at the gold standard method CCSD(T)/TZ2P level of theory, where the most intense signal was estimated to be 1694.2 cm^{-1} . (Table A7 in appendix) These observations helped us in tentatively assigning the signals corresponding to the carbene intermediate (**47**).

3.12.2 Ring-opening through C2-C3 bond cleavage

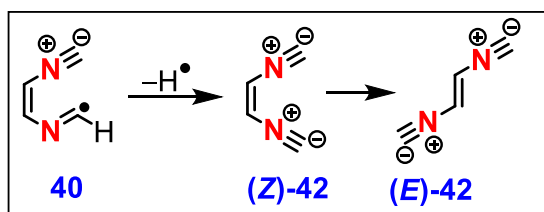


Scheme 3.14 Formation of first ring-opened radical intermediate **40** from 2-dehydropyrazine radical (**3a**).

During the prolonged irradiation of the matrix containing 2-dehydropyrazine radical (**3a**) at 284 nm , we have observed a few other signals along with those due to pyrazine radical (**3a**). One of the intense signals at 945.0 cm^{-1} has been assigned to the ring-opening radical intermediate (**40**). This radical intermediate has the most intense and characteristic signal at 985.5 cm^{-1} in computed vibrational spectrum at B3LYP/cc-pVTZ level of theory and the rest of the signals are relatively lower in intensity. Upon irradiating the matrix containing photoproducts at shorter wavelength (254 nm), we observed that those signals corresponding

to the ring-opened radical intermediate (**40**) started disappearing due to further fragmentation of the radical intermediate (**40**) via H-abstraction of C-N bond cleavage and get completely diminished at the later stage of irradiation. All the observed signals corresponding to this ring-opened radical intermediate (**40**) along with computed vibrational frequencies have been listed in table A9 in appendix.

3.12.3 Formation of ring-opening products (*Z*)/(*E*)–**42**

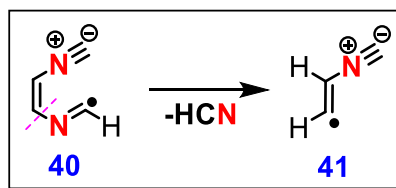


Scheme 3.15 Formation of ring-opened products (*Z*)/(*E*)–**42** from the ring-opened radical intermediate **40**.

We have observed a few very intense signals in the region of 2200-2100 cm^{-1} upon prolonged irradiation at 284 nm. These signals appeared rapidly upon irradiation at shorter wavelength (254 nm). We observed that signals corresponding to the radical intermediate (**40**) were disappearing and the signals in the isonitrile region (2200-2100 cm^{-1}) were appearing. These new sets of signals were assigned to the ring-opened products (*Z*)/(*E*)–**42**. At the initial stage of 254 nm irradiation, we observed three tiny signals next to each other and upon prolonged irradiation the two signals were merged with the most intense third signal as described in figure 3.3. We have closely looked at the computed vibrational spectrum of (*Z*)–**42** and (*E*)–**42** at B3LYP/cc-pVTZ level of theory and found out that (*Z*)–**42** isomer exhibits a split signal corresponding to two $\text{-N}\equiv\text{C}$ stretching modes (symmetric and anti-symmetric combinations), whereas, (*E*)–**42** has a single signal corresponding to the $\text{-N}\equiv\text{C}$ stretching. Based on these computed spectra, we have assigned the signals of (*Z*)/(*E*)–**42**. Out of three tiny signals at a very early stage of irradiation, two of them (red shifted ones) have been assigned to (*Z*)–**42** and the remaining signal has been assigned to (*E*)–**42**. As the irradiation at 254 nm continued, the signals corresponding to (*E*)–**42** grew due to the *Z*-*E* isomerization at 254 nm. In addition to that, (*Z*)–**42** and (*E*)–**42** isomers have a characteristic signal in the ranges of 700-800 cm^{-1} and 900-1000 cm^{-1} , respectively. We have observed these two signals upon prolonged irradiation as they have lower intensity compared to the $\text{-N}\equiv\text{C}$ stretching. Signal at 756 cm^{-1} has been assigned to the (*Z*)–**42** isomer, and the signal at 915 cm^{-1} has been assigned to the (*E*)–**42** ring-opening product. Upon continued irradiation at 254 nm, these ring-opened

products (Z)/(E)-**42** have been converted into the (Z)/(E)-**17** and (Z)/(E)-**26** with the Z-E isomerization as well as by isonitrile ($-\text{N}\equiv\text{C}$) to nitrile ($-\text{C}\equiv\text{N}$) isomerization. Description of ring-opening products (Z)/(E)-**17** and (Z)/(E)-**26** has been mentioned in the ring-opening of 2-dehydropyrimidine radical (**1a**). All the observed signals corresponding to these ring-opened products (Z)/(E)-**42** along with computed vibrational frequencies have been listed in table A4 in appendix.

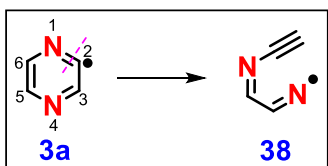
3.12.4 Formation of ring-opening radical intermediate **41**



Scheme 3.16 Formation of ring-opened radical intermediate **41** from **40** via HCN elimination.

The first ring-opening radical intermediate (**40**) led to the ring-opening product (Z)/(E)-**42** via the loss of H-atom as we discussed in the last section. This radical can also lead to other fragments such as of the radical (**41**) via HCN (**12**) removal. The radical species (**41**) was also observed in the photochemistry of 2-dehydropyrimidine (**1a**). All the signals corresponding to species (**41**) have been described previously. Also, all the observed signals corresponding to this ring-opened radical intermediate (**41**) along with computed vibrational frequencies have been listed in table A10 in appendix.

3.12.5 Ring-opening through N1-C2 bond cleavage

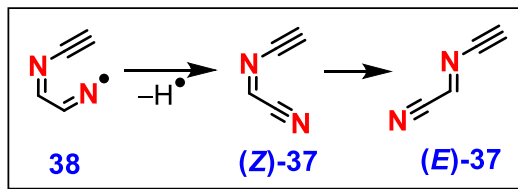


Scheme 3.17 Formation of second ring-opened radical intermediate **38** from 2-dehydropyrazine radical (**3a**).

The C_s symmetric 2-dehydropyrazine radical (**3a**) can lead to various ring-opening channels. Apart from the ring-opened radical species **40**, we have observed a new set of signals along with the presence of various ring-opening products and radical intermediates during the prolonged irradiation of the matrix containing 2-dehydropyrazine radical (**3a**) at 254 nm. Radical intermediate **38** can be formed via C-N bond cleavage from 2-dehydropyrazine radical (**3a**). We observed the set of signals (3318.0, 775.5, 674.0, 1198.5 cm^{-1}) upon irradiation at 254 nm. These signals have been tentatively assigned to the radical intermediate **38**, which has the most intense and characteristic signals in the acetylic region along with a few other signals.

This ring-opening radical intermediate **38** can further dissociate and form stable ring-opening products. All the observed signals corresponding to this ring-opened radical intermediate (**38**) along with computed vibrational frequencies have been listed in table A9 in appendix.

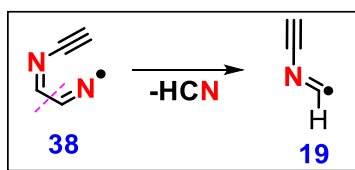
3.12.6 Formation of ring-opening products (*Z*)/(*E*)–**37**



Scheme 3.18 Formation of ring-opened products (*Z*)/(*E*)–**37** from the ring-opened radical intermediate **38**.

Upon prolonged irradiation at 254 nm, we observed a set of signals (at 3320.0 and 3312.0 cm^{-1}) in the acetylenic C-H stretching region 3250 – 3350 cm^{-1} along with the previously identified ring-fragmented products such as HCCNC (**39**) and HCCCN (**16**). Ring-opening nitrogen centred radical intermediate **38** can lead to the stable ring-opened species (*Z*)/(*E*)–**37** upon continuous irradiation at 254 nm via H-atom loss. Computationally the vibrational spectra of (*Z*)–**37** and (*E*)–**37** exhibit the most intense signals at 3473.1 cm^{-1} and 3472.3 cm^{-1} , respectively, followed by the second most intense signals at 553.7 cm^{-1} and 695.1 cm^{-1} for (*Z*)–**37** and (*E*)–**37**, respectively at B3LYP/cc-pVTZ level of theory. (Figure 3.5a-c) We assigned the characteristic signals at 3320.0 and 504.5 cm^{-1} for (*Z*)–**37** and 3312.0 and 623.5 cm^{-1} for (*E*)–**37**. Also, all the observed signals corresponding to the ring-opened products (*Z*)/(*E*)–**37** along with computed vibrational frequencies have been listed in table A5 in appendix.

3.12.7 Formation of radical intermediate **19**



Scheme 3.19 Formation of ring-opened radical intermediate **19** from **38** via HCN elimination.

The ring-opened radical intermediate **38** can also dissociate further via HCN formation upon prolonged irradiation at 254 nm. We observed a new set of signals (1060.5, 674.5, 505.0 and 3312.x cm^{-1}) upon continuous irradiation at 254 nm. (Figure 3.5 a, d) These new set of signals have been assigned to the radical intermediate **19**, which can also subsequently form more stable small molecules HCCNC (**39**) and HCCCN (**16**) that have been identified. Interestingly, this radical intermediate **19** can also form the stable small molecule HCNCC **45**

via H-atom loss from the acetylenic position having the most intense and characteristic signal at 2102.0 cm^{-1} as reported in literature, which we have seen in our experiments too and assigned to HCNCC **45**.

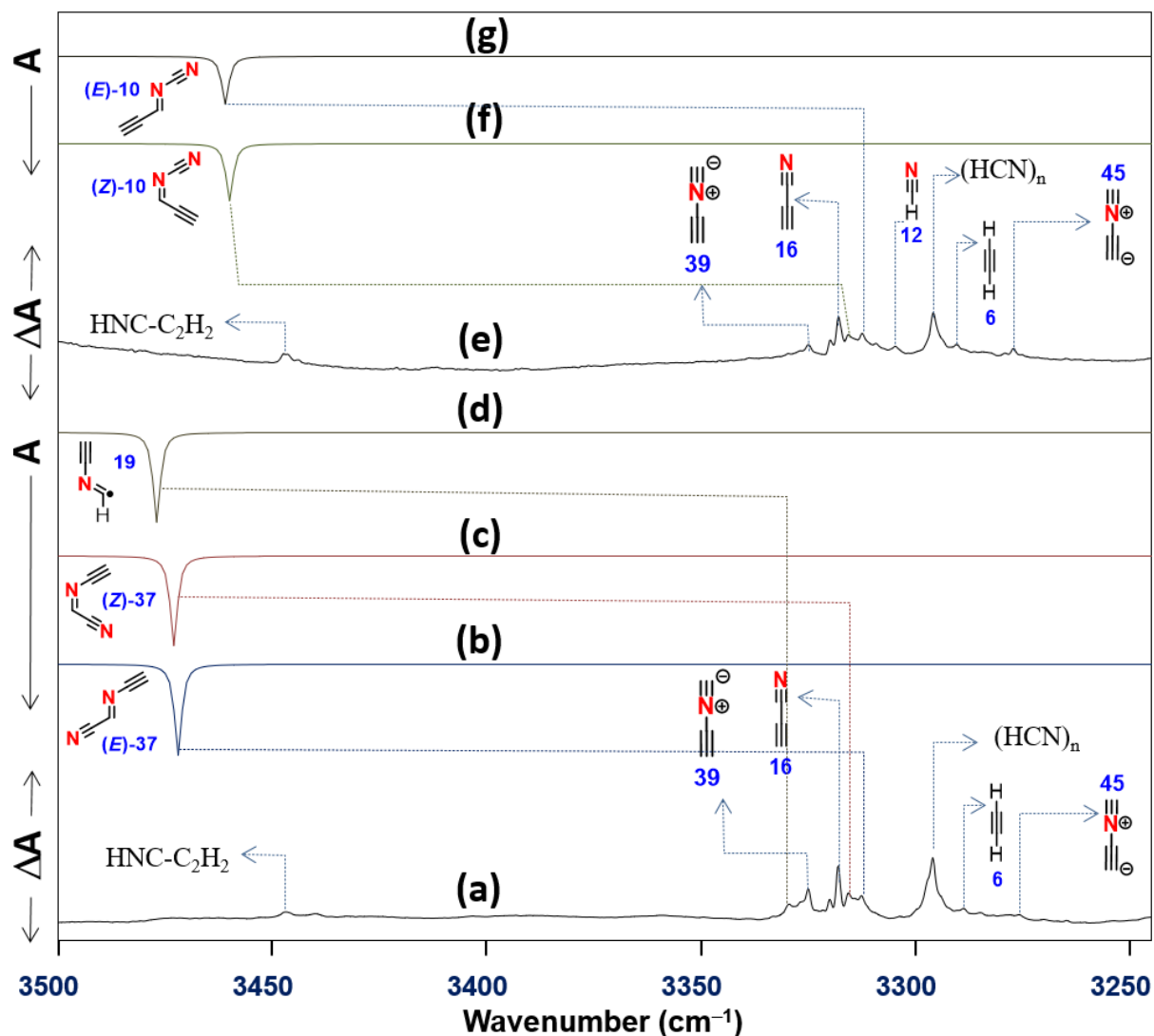
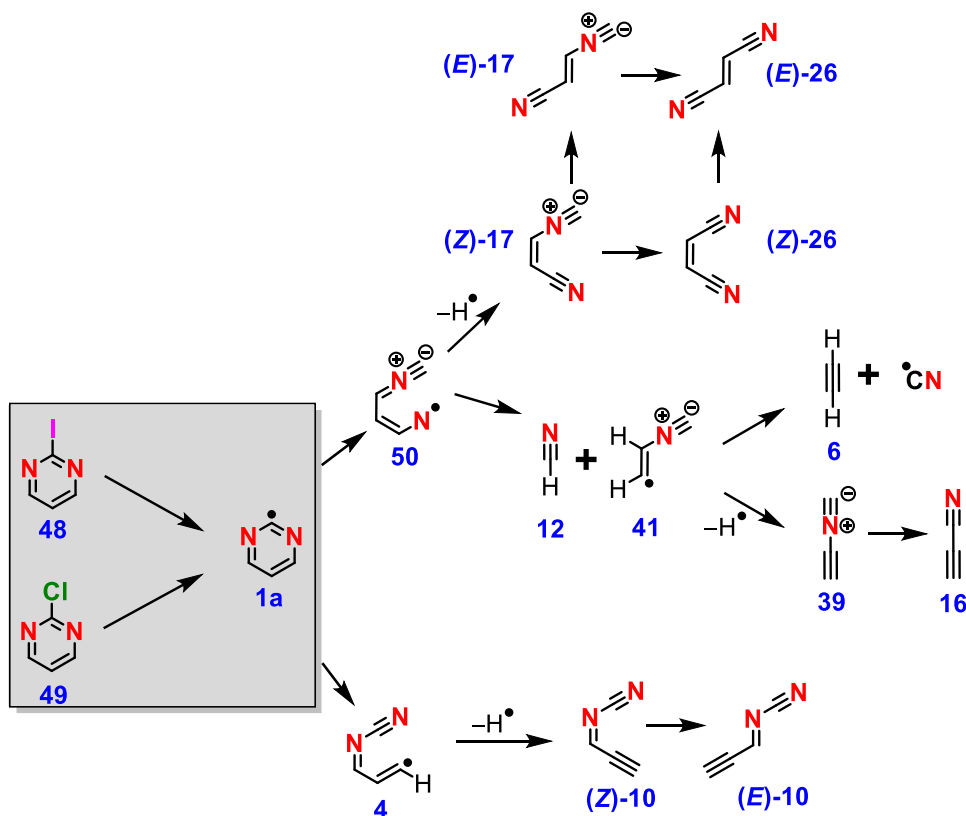


Figure 3.5. Photochemistry of 2-dehydropyrimidine radical (**1a**) and 2-dehydropyrazine radical (**3a**). (acetylenic C-H stretching region, Ar, 4 K) (a) Difference spectrum after 254 nm irradiation (for 5 min) of 2-dehydropyrazine radical (**3a**); Computed vibrational spectrum (B3LYP/cc-pVTZ level of theory, unscaled) of (b) ring-opening product (*E*)-**37**, (c) ring opening product (*Z*)-**37**, and (d) ring opening radical intermediate **19**. (e) Difference spectrum after 254 nm irradiation (for 15 min) of 2-dehydropyrimidine radical (**1a**); Computed vibrational spectrum (B3LYP/cc-pVTZ level of theory, unscaled) of (f) ring-opening product (*Z*)-**10**, and (g) ring opening product (*E*)-**10**.

3.13 Summary of photochemistry of 2-dehydropyrimidine (1a)

Through this investigation, we have successfully generated the 2-dehydropyrimidine radical (**1a**) from its iodo- and chloro-precursors in argon matrix at 4 K. Based on the behaviour at 350 nm irradiation condition and in comparison, with the computations, majority of the signals due to the target **1a** have been unambiguously assigned. Further two important ring-opened radical intermediates **4** and **50** and the formation of a subsequent isomeric species with molecular formula $C_4H_2N_2$ through the loss of hydrogen atom have been confirmed and all of them have been characterized. Apart from that, many fragmentation products have also been characterized under prolonged irradiation conditions at 254 nm. The complete photochemistry of **48** has been described in the scheme 3.20.



Scheme 3.20 Observed photochemistry and ring-opened channels in 2-dehydropyrimidine radical (**1a**).

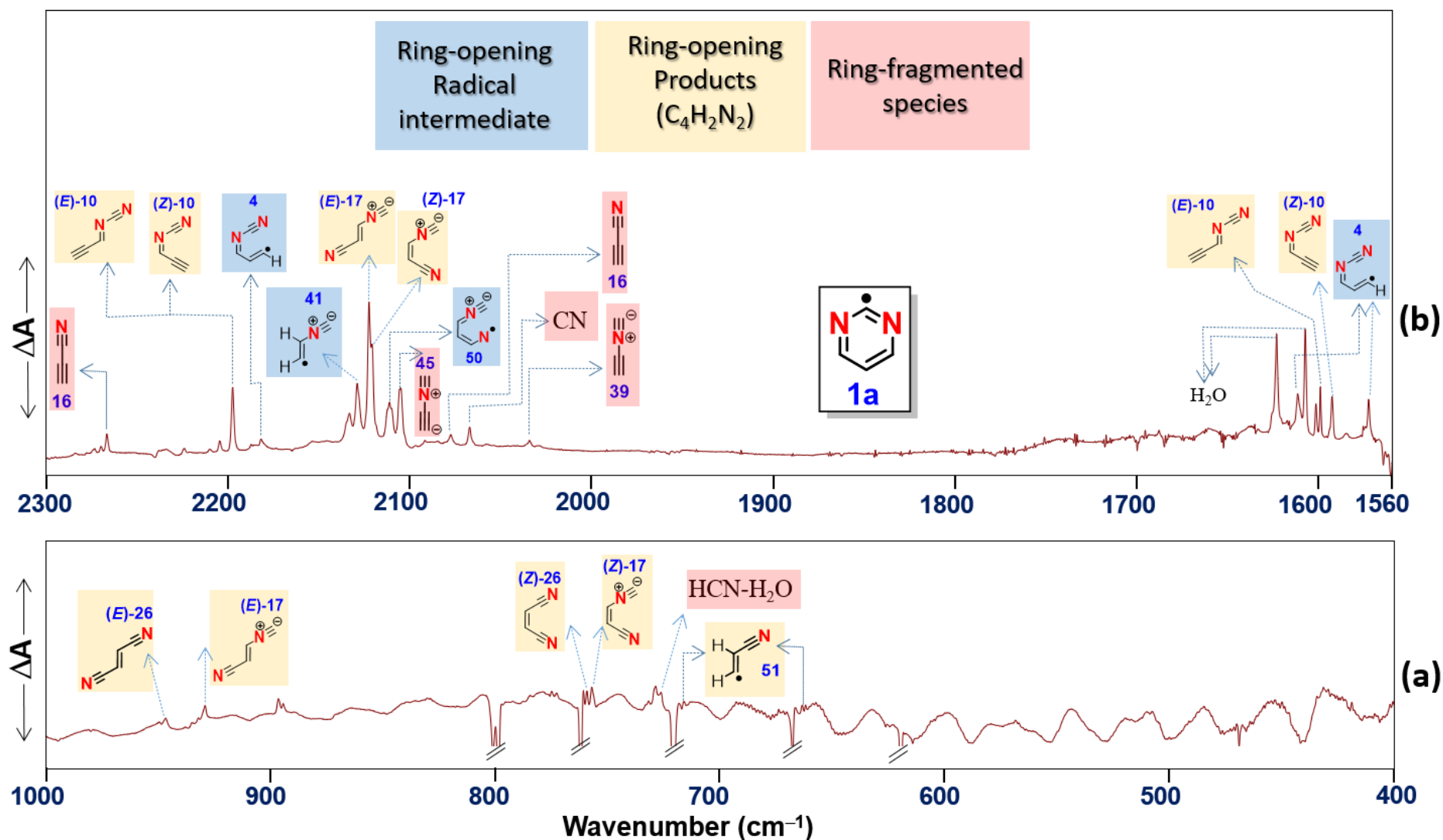
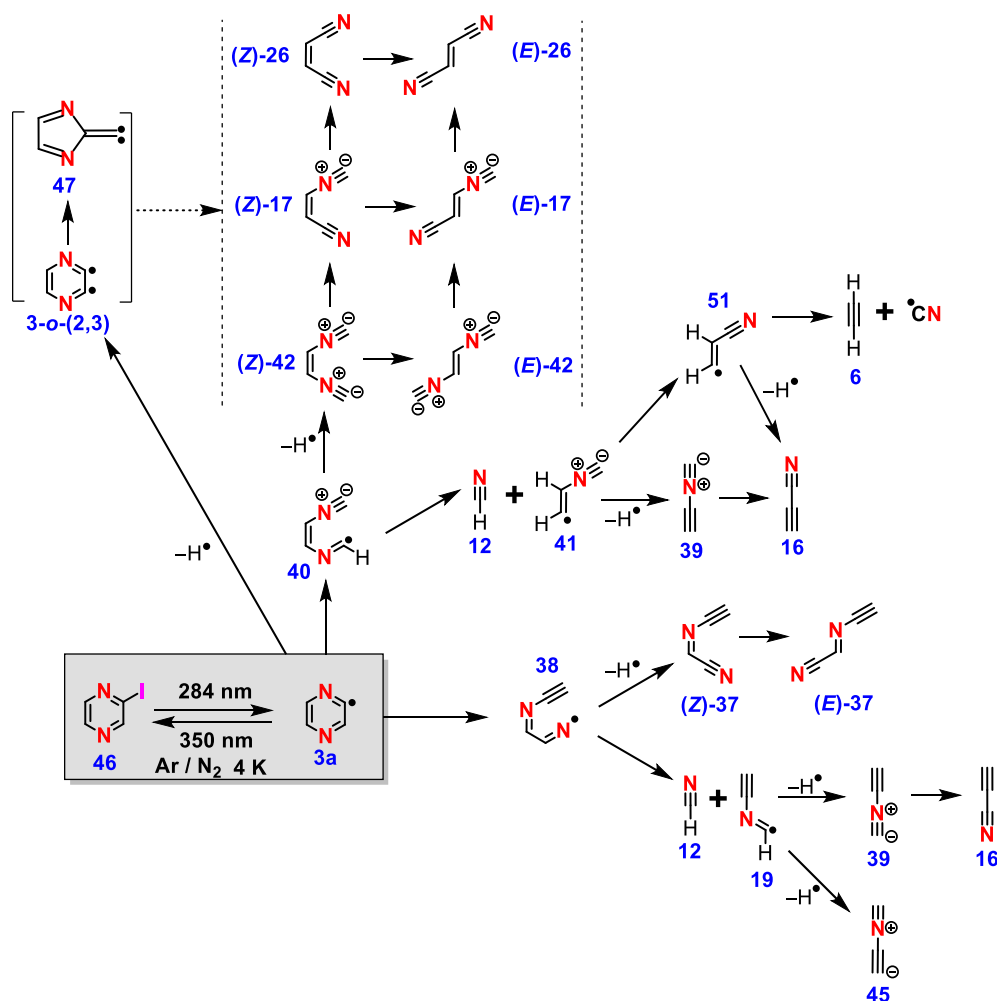


Figure 3.6 Observed photochemistry, ring-opened and ring-fragmented products, and intermediates from of 2-dehydropyrimidine radical (**1a**) at 254 nm irradiation in the region (a) 400-1000 cm^{-1} ; (b) 1560-2300 cm^{-1} .

3.14 Summary of photochemistry of 2-iodopyrazine

In a similar way as in the case of 2-iodopyrimidine, we have successfully generated and characterized the 2-dehydropyrazine radical **3a** from the 2-iodopyrazine precursor upon irradiation at 284 nm. This dehydro-pyrazine radical **3a** along with iodine atom showed a wavelength dependent reversibility with its precursor 2-iodopyrazine upon irradiation at 365 nm and 284 nm. Further, irradiation at 254 nm led to the photochemistry of dehydropyrazine radical that produced photo-fragmented products. Some of the photo-fragmented products are HCCCN, HCCNC and HCN complex. Some of the peaks corresponding to the photo products are unassigned. Furthermore, a few different ring-opened radicals out of the pyrazine radical and the formation of a subsequent isomeric species with $C_4H_2N_2$ molecular formula through the loss of hydrogen atom have also been observed. Almost all of them have been characterized with the data collected from the photochemistry of 2-iodopyrimidine and computational vibrational spectra. The complete photochemistry of **46** has been depicted in the scheme 3.21.



Scheme 3.21 Observed photochemistry and ring-opening channels in 2-dehydropyrazine radical (**3a**).

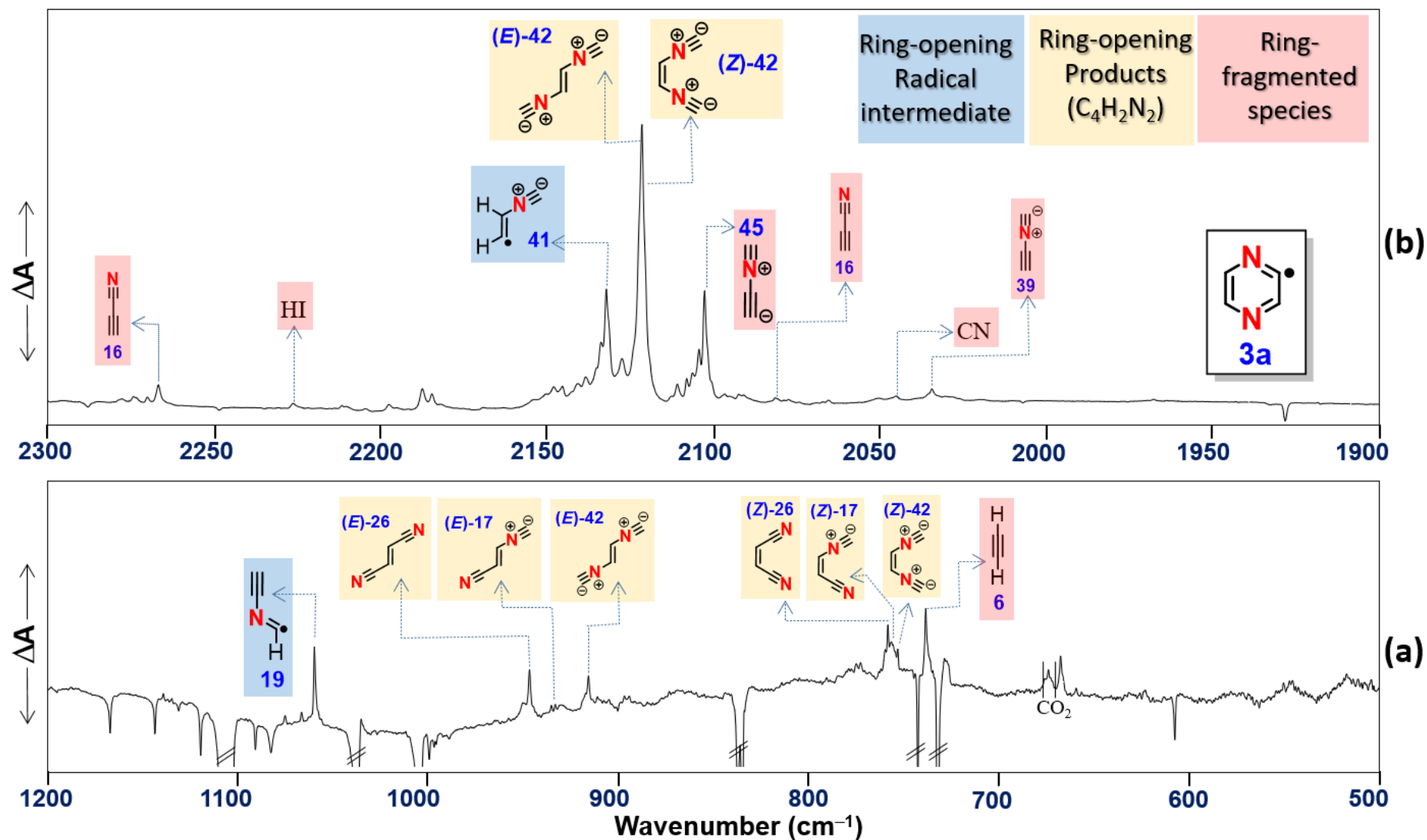


Figure 3.7 Observed photochemistry, ring-opened and ring-fragmented products, and intermediates from of 2-dehydropyrazine radical (**3a**) at 254 nm irradiation in the region (a) 500-1200 cm⁻¹; (b) 1900-2300 cm⁻¹.

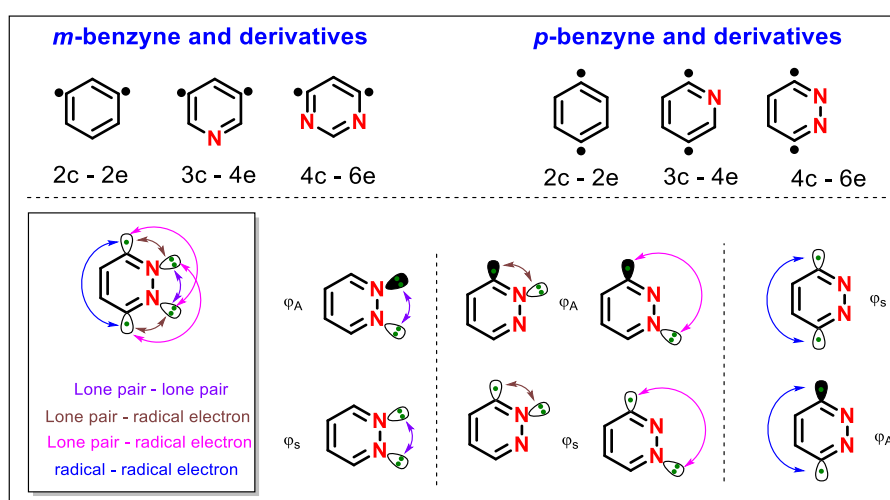
3.15 References:

1. Saraswat, M.; Venkataramani, S. Thermal unimolecular reactivity pathways in dehydrodiazines radicals. *J Phys Org Chem.* **2021**; 34: e4152.
2. Peeters, Z.; Botta, O.; Charnley, S. B.; Kisiel, Z.; Kuan, Y.-J.; Ehrenfreund, P. Formation and photostability of N-heterocycles in space. *A&A* **2005**, 433, 583–590.
3. Oba, Y.; Takano, Y.; Naraoka, H.; Watanabe, N.; Kouchi, A. Nucleobase synthesis in interstellar ices. *Nature Comm.* **2019**, 10, 4413–4420.
4. McGuire, B. A. 2018 Census of Interstellar, Circumstellar, Extragalactic, Protoplanetary Disk, and Exoplanetary Molecules. *Astrophys. J. Suppl. Ser.* **2018**, 239, 17–64.
5. (a) Korte, A.; Mardyukov, A.; Sander, W. Pyridyl- and pyridylperoxy radicals – A matrix isolation study. *Austr. J. Chem.* **2014**, 67, 1324–1329; (b) Winkler, M.; Cakir, B.; Sander, W. 3,5-Pyridyne – A Heterocyclic meta-benzyne derivative. *J. Am. Chem. Soc.* **2004**, 126, 6135 – 6149; (c) Berry, R. S.; Kramer, J. M. 3,4-Pyridyne and its dimer. *J. Am. Chem. Soc.* **1971**, 93, 1303 – 1304.
6. Haupa, K. A.; Chen, K.-P.; Li, Y.-K.; Lee, Y.-P. Infrared spectra of (Z)- and (E)-C₂H₃C(CH₃)I radicals produced upon photodissociation of (Z)- and (E)-(CH₂I)HCC(CH₃)I in solid para-hydrogen. *J. Phys. Chem. A* **2020**, 124, 5887–5895.
7. Dunkin, I. R. Matrix-Isolation Techniques: A Practical Approach. Oxford Press: New York. **1998**.
8. (a) Lahmani, F.; Ivanoff, N. Mercury Sensitization of the Isomerization of Diazines. *J. Phys. Chem.* **1972**, 76, 2245–2248; (b) Breda, S.; Reva, I. D.; Lapinski, L.; Nowak, M. J.; Fausto, R. Infrared spectra of pyrazine, pyrimidine and pyridazine in solid argon. *J. Mol. Struct.* **2006**, 786, 193–206.
9. Su, M.-D. CASCFS Study on the Photochemical Transposition Reactions of Pyrazines. *J. Phys. Chem. A* **2006**, 110, 9420–9428.
10. Touni, A.; Couturier-Tamburelli, I.; Chiavassa, T.; Pietri, N. Photolysis of astrophysically relevant acrylonitrile: A matrix experimental study. *J. Phys. Chem. A* **2014**, 118, 2453–2462.
11. Gong, Y.; Andrews, L.; Liebov, B. K.; Fang, Z.; Garner III, E. B.; Dixon, D. A. Reactions of laser-ablated U atoms with (CN)₂: infrared spectra and electronic structure calculations of UNC, U(NC)₂, and U(NC)₄ in solid argon. *Chem. Commun.* **2015**, 51, 3899–3902.
12. Wang, H.-L.; Katon, J.; Balan, C.; Bannon, A. W.; Bernard, C.; Doherty, E. M.; Dominguez, C.; Gavva, N. R.; Gore, V.; Ma, V.; Nishimura, N.; Surapaneni, S.; Tang, P.; Tamir, R.; Thiel, O.; Treanor, J. J. S.; Norman, M. H. Novel Vanilloid Receptor-1 Antagonists: 3. The identification of a second-generation clinical candidate with improved physicochemical and pharmacokinetic properties. *J. Med. Chem.* **2007**, 50, 3528–3539.
13. Venkataramani, S.; Winkler, M.; Sander W. 1,2,3-Tridehydrobenzene. *Angew. Chem. Int. Ed.* **2005**, 44, 6306–6311.
14. (a) Sander, W.; Exner, M.; Winkler, M.; Balster, A.; Hjerpe, A.; Kraka, E.; Cremer, D. Vibrational Spectrum of m-Benzyne: A Matrix Isolation and Computational Study. *J. Am. Chem. Soc.* **2002**, 124, 13072–13079.; (b) Sander W. m-Benzyne and p-Benzyne. *Acc. Chem. Res.* **1999**, 32, 669–676.
15. Radziszewski, J. G.; Hess, B. A., Jr.; Zahradnik, R. Infrared Spectrum of o-Benzyne: Experiment and Theory. *J. Am. Chem. Soc.* **1992**, 114, 52–57.
16. Winkler, M. The Fulvenediyls and Related Biradicals: Molecular and Electronic Structure. *J. Phys. Chem. A* **2005**, 109, 1240–1246.

Chapter 4. Matrix-Isolation FTIR Spectroscopic Studies of 3,6-diiodopyridazine and 4,6-diiodopyrimidine

Generation and characterization of heterocyclic biradicals is both interesting and also very complex due to the presence of various possible interactions such as radical-radical, radical-lone pair and lone pair-lone pair interactions, which influence their stability as well as their reactivity.^[1] Simplest aromatic biradicals (*ortho*-, *meta*- and *para*-benzynes) have been generated and characterized in which radical-radical interaction dictates the reactivity.^[2] Introducing one heteroatom (nitrogen) in benzyne increases the complexity as well as the possibility of forming a wide range of photo- and thermal-products from didehydropyridynes (pyridine analogues of benzyne).^[3] Additional nitrogen (by replacing a second CH) in pyridynes results in isomeric biradicals of diazines (didehydrodiazines). We have chosen the 3,6-didehydropyridazine and 4,6-didehydropyrimidine biradicals as our experimental target as they represent diazine analogues of *para*- and *meta*-benzyne, respectively.

Although the targets 3,6-didehydropyridazine and 4,6-didehydropyrimidine biradicals are structurally simple but the complexity that arises due to various interactions and reactivity pattern that makes them intriguing biradicals. The major interactions include, (i) lone pair–lone pair interaction (comparable to the pyridazine), (ii) radical–lone pair interactions (similar to the 3-dehydropyridazine radical) and, (iii) spin-spin interactions (analogous to the *p*-benzyne). Overall, reactivity and stability aspects of these biradicals are strongly influenced by the combination of all the above-mentioned interactions (Scheme 4.1). Such a complex interplay of four centered- six-electrons (4c-6e-) interactions can render multiconfigurational character.



Scheme 4.1 The *meta*- and *para*-benzyne and their pyridine and diazine analogues with various possible orbital interactions.

We have considered 3,6-diiodopyridazine and 4,6-diiodopyrimidine as potential precursors, owing to the photolabile C-I bonds as discussed in the previous chapter. Photochemical experiments have been performed under matrix-isolation conditions at cryogenic temperature (4 K).

4.1 Deposition of 3,6-diiodopyridazine (52)

The sample 3,6-diiodopyridazine (purchased from Sigma Aldrich, 97% purity white to beige color in crystals or flakes form) is used without any further purification and is sublimed at 170 °C-180 °C. A sample of 3,6-diiodopyridazine has been deposited for 120 minutes along with excess amount of argon to form a matrix at 4 K. The matrix-isolated precursor showed prominent and sharp infrared features at 1374.0 and 1098.5 cm^{-1} , along with few weak signals around 1020.0 and 822.0 cm^{-1} . Upon comparison of the matrix-isolated spectrum with the computed spectrum at B3LYP/DGTZVP level of theory, we observed that the precursor 3,6-diiodopyridazine (52) has indeed been deposited over the cold KBr window without any signs of decomposition during the deposition process. (Figure A9 in appendix)

4.2 Photochemistry of 3,6-diiodopyridazine (52)

After the characterization, the matrix containing the precursor 3,6-diiodopyridazine (52) has been irradiated at 254 nm, and the photochemistry is followed by infrared spectroscopy (Figure 4.1). Due to the irradiation, the signals corresponding to the precursor have shown a decrease in intensity, whereas few new peaks at 760.0, 870.0, 1011.5, and 3066.5 cm^{-1} have shown an increase in intensity. After 12 minutes irradiation, we have observed only these features, whereas when the duration of irradiation was extended, additional signals at 945.5, and 3087.5 cm^{-1} appeared. Incidentally, the peak at 1011.5 cm^{-1} has also exhibited a slight increase indicating that this feature is common in both the sets of signals. By inspecting these two sets, the sequence of their growth and the characteristic features at 760.0 and 945.5 cm^{-1} , we have tentatively assigned them as maleonitrile (Z)-26, and fumaronitrile (E)-26, respectively. The tentative assignments have been further confirmed by comparing the experimental data with the computed spectral data at B3LYP/cc-pVTZ level of theory for both the species and shows an excellent agreement within experimental shifts. (Figure 4.1 and Table A3 in appendix) Also, the assignment for maleonitrile (Z)-26 and fumaronitrile (E)-26 signals have been confirmed with the photochemical data obtained in the 2-iodopyrazine (46) and 2-iodopyrimidine (48).

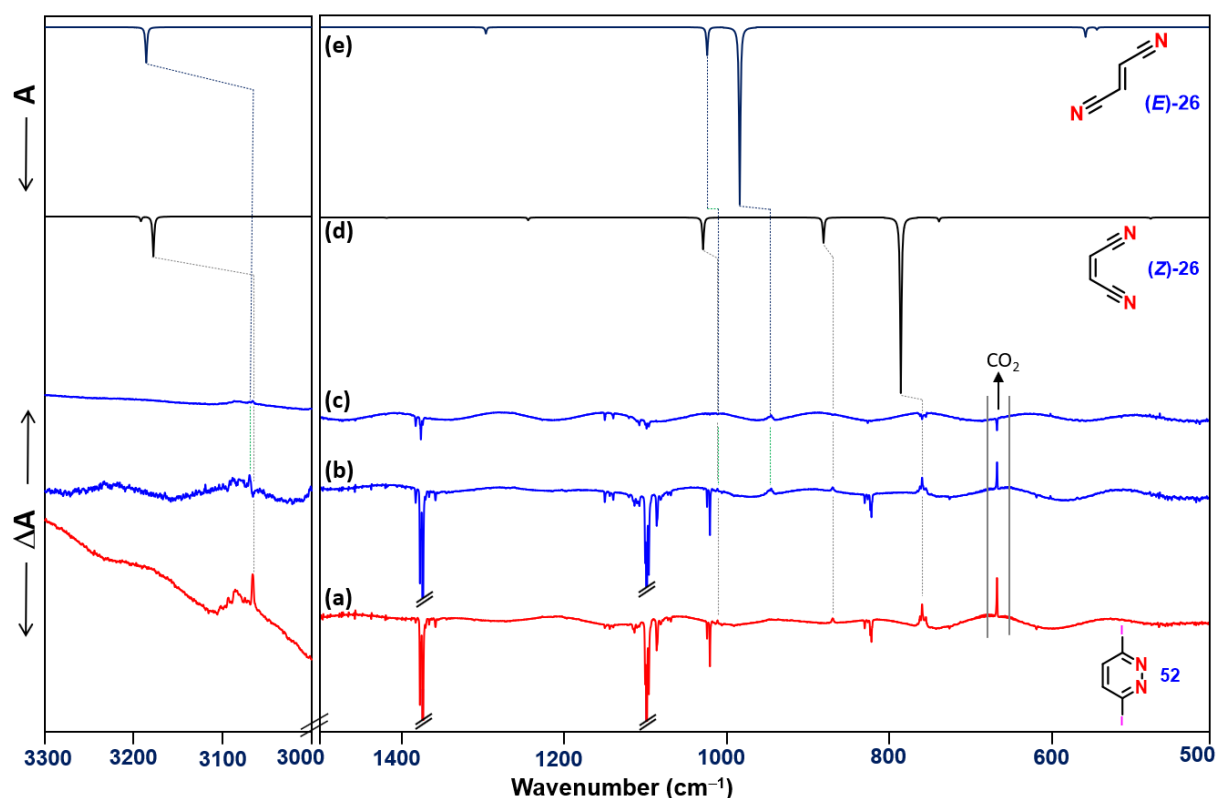
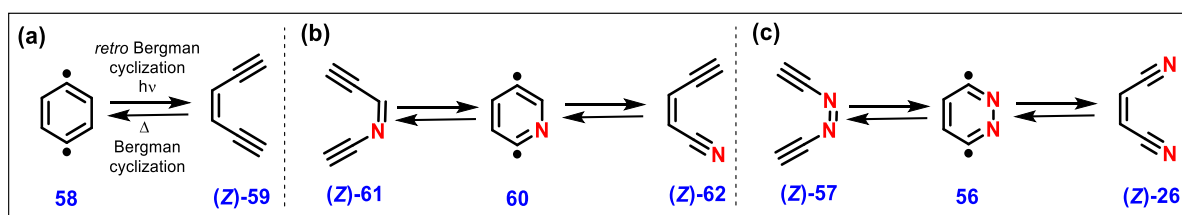


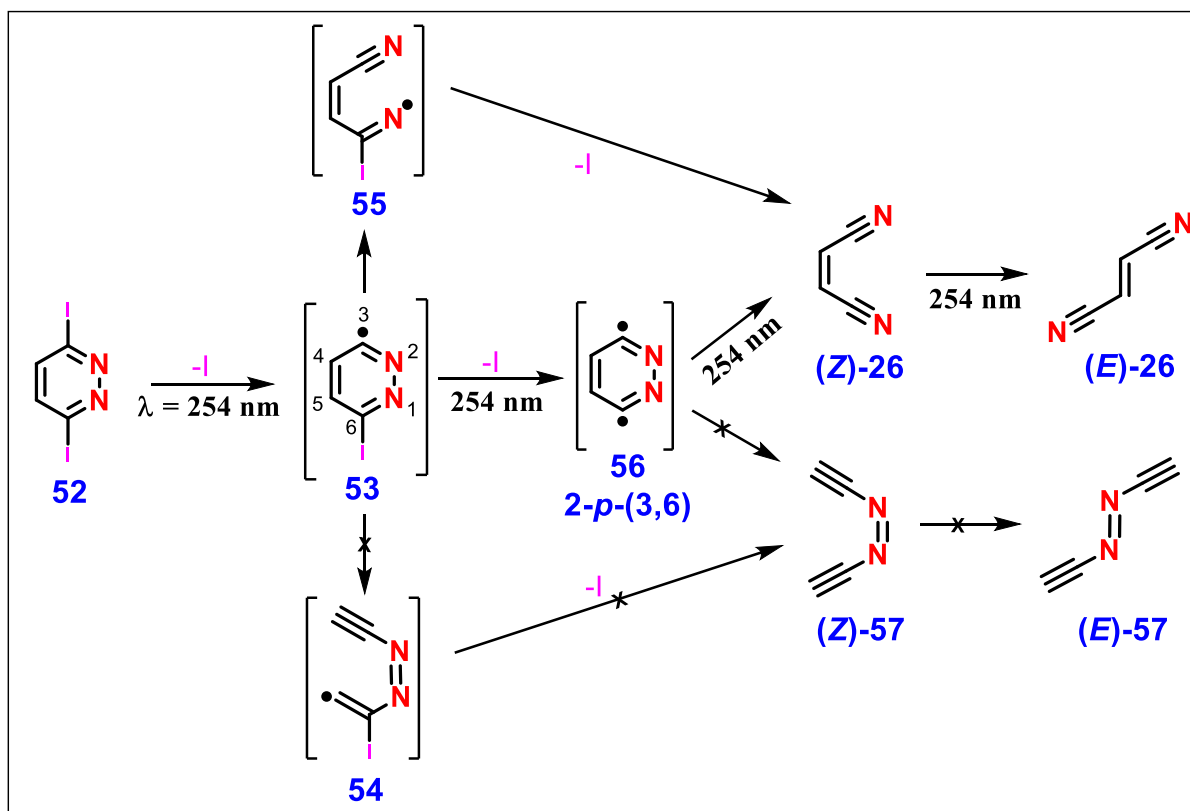
Figure 4.1 FTIR spectral data (as region-wise splits) on the photochemistry of 3,6-diiodopyridazine **52** in an argon matrix at 4 K. (a) Difference spectrum after 12 min irradiation at 254 nm on the matrix isolated **52**. (Bands pointing downwards belong to the precursor **52**, and those pointing upwards belong to the ring opening product (*Z*)-**26**.) (b) Difference spectrum after 32 min irradiation at 254 nm on the matrix isolated **52**. (Bands pointing downwards belong to the precursor **52**, and those pointing upwards belong to the ring opening products (*Z*)-**26** and (*E*)-**26**.) (c) Difference spectrum indicating the photochemical isomerization of (*Z*)-**26** into (*E*)-**26** by 254 nm irradiation. (d) Computed spectrum of (*Z*)-**26**. (B3LYP/cc-pVTZ level of theory, unscaled); (e) Computed spectrum of (*E*)-**26**. (B3LYP/cc-pVTZ level of theory, unscaled); The figure here does not show the spectral range between 1500 – 3000 cm^{-1} as no significant signal, except from the CO/CO₂ impurity, was seen in this region for this set of experiments.

Based on the experimental observation of (*Z*)-**26** under photochemical conditions, we inferred the plausible intermediacy of 3,6-didehydropyridazine biradical **56**. However, we have not observed any signal that can be accounted for the biradical **56** other than those corresponding to (*Z*)-**26** and (*E*)-**26**. The same experiment has also been performed in nitrogen matrix. Indeed, a similar set of signals corresponding to (*Z*)-**26** and (*E*)-**26** have been observed in this case as well. Since, two symmetric C-I bonds are present in the precursor, a step-wise cleavage of the precursor can lead to a monoradical **53**, whereas the simultaneous breaking

generates the target biradical **56**. However, both of them have not been observed under the given experimental conditions. Indeed, the retro-Bergman cyclization of the biradical **56** can open in two possible ways, via (i) N1-N2 bond cleavage to the (Z)-**26**, and (ii) C4-C5 bond cleavage leading to the azo-derivative (Z)-**57**. Since the observed products are (Z)-**26** and (E)-**26**, the ring might have opened by N1-N2 bond breaking (Scheme 4.2). Apparently, the formation of (E)-**26** happened only at the later stage of irradiation confirming the (Z)-**26** as its origin. The combined photochemistry of the 3,6-diiodopyridazine **52** is indicated in scheme 4.3.



Scheme 4.2 Bergman cyclization and retro-Bergman cyclization in (a) *para*-Benzyne^[4]; (b) 2,5- didehydropyridine^[4]; (c) 3,6-didehydropyridazine



Scheme 4.3 Photochemistry of 3,6-diiodopyridazine **52**

4.3 Computational analysis and mechanistic aspects

Since the photochemistry experiments in argon and nitrogen matrices did not provide direct evidence for the desired biradical, we shifted our focus towards the computational aspects of 3,6-didehydropyridazine **56**. In this regard, we attempted the electronic structure calculations related to the geometry and stability of **56**. In addition, mechanistic studies have also been carried out to obtain the reason for the absence of biradical **56** by photolysis of the precursor 3,6-diiodopyridazine **52**. Various levels of theory were adopted for optimizing the singlet state 3,6-didehydropyridazine **56**, however, we could not locate the structure corresponding to an energy minima. All our attempts in optimizing the singlet state biradical led only to a ring-opened structure, an acyclic species (*Z*)-**26** through N-N bond cleavage. Indeed, previous attempts towards optimizing the 3,6-didehydropyridazine **56** in its singlet ground state also failed that led only to ring-opened structure.^[4] The same trend was observed even at the multireference CASSCF calculations. On the other hand, the triplet state structure could be optimized to a stable minimum at DFT and CASSCF levels of theory.

In order to understand the stability aspects of the biradical **56**, we have performed molecular orbital analysis in comparison with the parent pyridazine **2** and 3-dehydropyridazine **2a** (Figure 4.2). In this regard, the multireference CASSCF calculations have been performed for pyridazine **2**, 3-dehydropyridazine **2a**, and 3,6-didehydropyridazine **56** in their singlet and triplet states. The MOs and their occupancies have been analysed and helped in obtaining insights into various interactions in biradical **56**. Also, such analysis has been utilized in the identification of through space (TS) and through bond (TB) interactions, which can render stability. Previously, Gleiter et al. have investigated the lone pair–lone pair interactions in diazines and pointed out that dominating TS and TB interactions led to a wider separation of the two lone pair orbitals.^[5] Due to the spatial proximity of lone pairs and maximum influence of such interactions, the splitting between the orbitals in pyridazine has been experimentally determined to be high (2.0 eV).

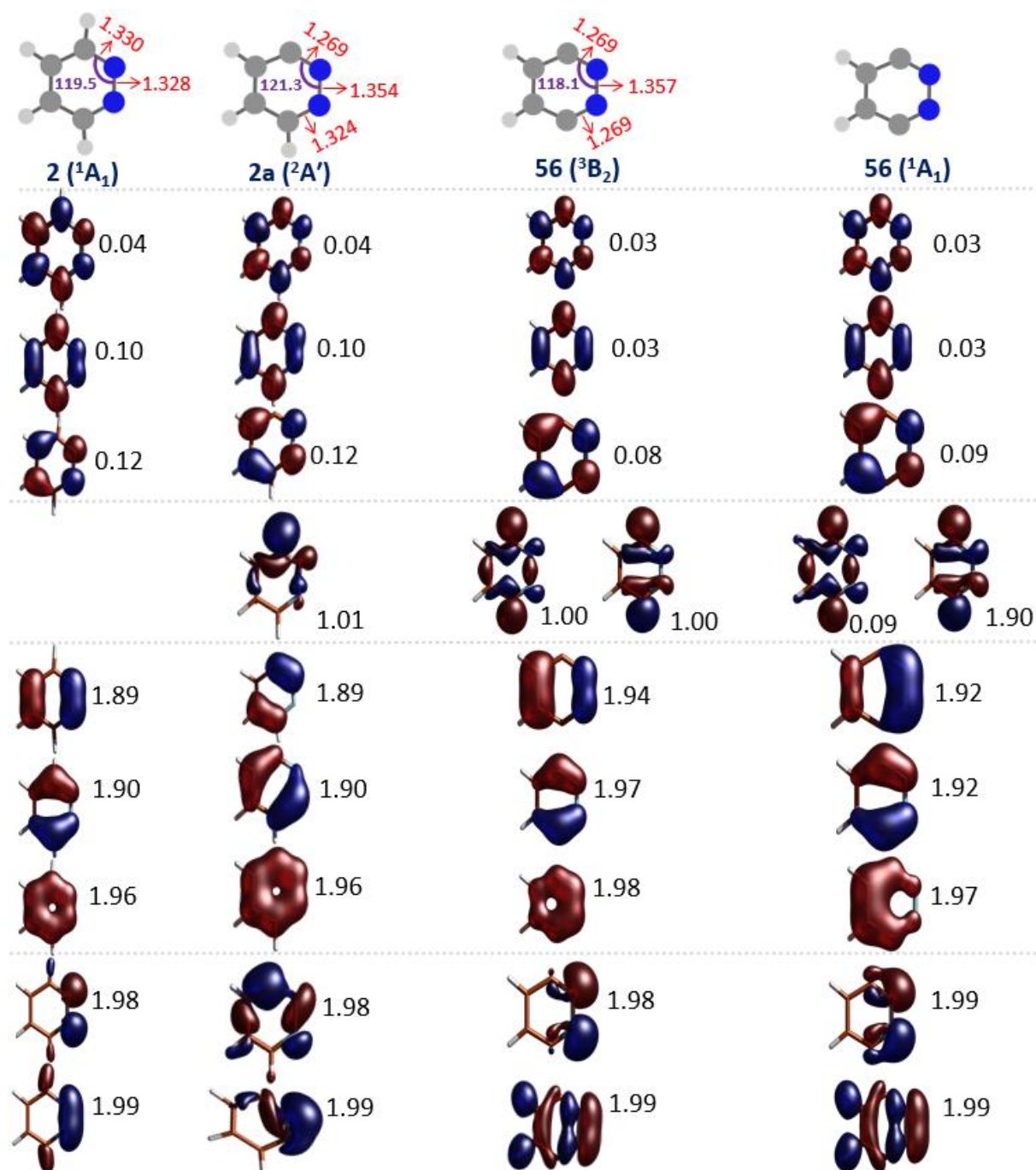


Figure 4.2 Optimized geometries (B3LYP/cc-pVTZ level of theory; selected bond distances (in Å) in red, and bond angles (in degrees) in purple are indicated), and molecular orbitals (CASSCF/cc-pVDZ level of theory for pyridazine **2**, 3-dehydropyridazine radical **2a**, triplet and singlet 3,6-didehydropyridazine **56** with an active space (10,8), (11,9), (12,10) and (12,10), respectively. (All the MOs have been rendered at an isovalue of 0.05, and the corresponding orbital occupancies are indicated; For the singlet state of **56**, optimized geometry from the triplet state has been utilized.)

On the other hand, creation of a radical centre adjacent to one of the nitrogen atoms in **2**, the TS interaction between the radical and the nitrogen (**2a**) electrons dominates.^[6] This has been confirmed based on the lowering of proton affinity relative to the parent, and the ordering of orbitals corresponding to symmetric and antisymmetric combinations of radical and adjacent lone pair. Now, on the addition of yet another radical centre in **2a** results in the biradical **56** which can be stabilized only in a triplet state. Indeed, the 3B_2 -**56** has degenerate SOMOs that correspond to the biradical orbitals with bonding and anti-bonding combinations. Counterintuitively, a stable biradical **56** at a singlet state demands one of the orbitals (an antisymmetric combination of the radical orbitals) to be a low-lying (HOMO). In such scenario, the involvement of antisymmetric combination of nitrogen lone pairs in the HOMO orbital could be the driving force behind the destabilization of the singlet state.

For understanding the selectivity in the ring-opening channels, optimized geometries of both the products (*Z*)-**26**, and (*Z*)-**57** have been compared (Figure 4.3). The interatomic distance between the two nitrogen atoms in (*Z*)-**57** is found to be 1.268 Å, which is shorter than that of pyridazine **2** (1.328 Å), or the dehydropyridazine radical **2a** (1.354 Å). The prevailing lone pair–lone pair repulsion is a plausible reason for the non-formation of (*Z*)-**57** through the C-C ring-opening channel. Furthermore, the HOMO-LUMO gaps in both the ring-opening products also corroborate with this assumption.

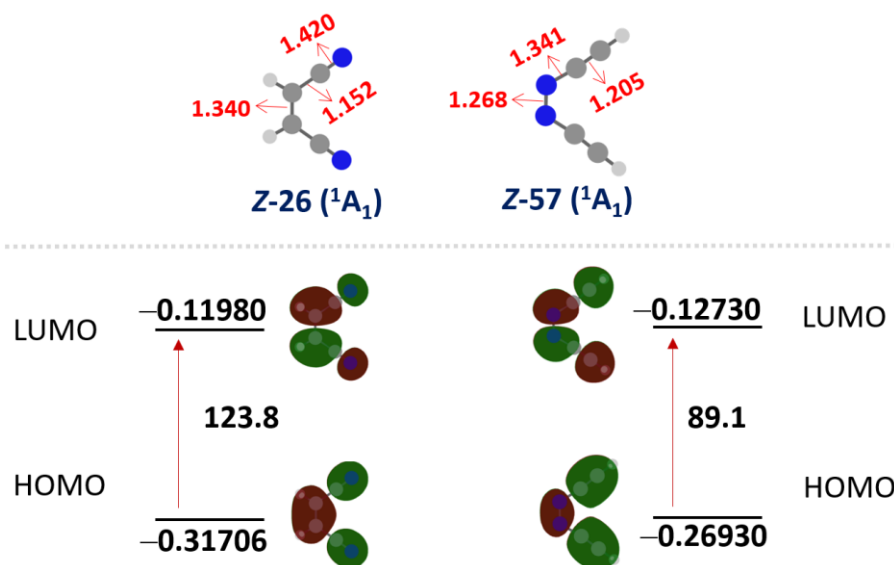


Figure 4.3 Optimized geometries (selected bond distances (in Å) and molecular orbitals at B3LYP/cc-pVTZ level of theory; for maleonitrile (*Z*)-**26** and *Z*-diethynyldiazene (*Z*)-**57**.

For understanding the potential energy surfaces of biradical **56**, the thermal ring-opening channels have also been considered, and the intrinsic reaction coordinate (IRC) analysis corresponding to both the ring-opening products have been carried out (Figure 4.4a). Transition state corresponding to the C-C bond breaking has been located on the PES using QST2 method. Further, IRC analysis has been performed to locate the full PES for reactant and the product geometries. Both the TS and IRC analysis have been performed at B3LYP/cc-pVTZ, M06-2X/cc-pVTZ, and CASSCF(6,5)/cc-pVDZ levels of theory. On the computed IRC path, we observed that TS corresponding to C-C bond cleavage led to the product (Z)-**57** in the forward direction. On the other hand, IRC path in the reverse direction originating from the same TS led to the ring-opening product (Z)-**26**, instead of locating the 3,6-didehydropyridazine **56** as a minimum (Figure 4.4a). The inspection of the geometries involved in the reaction pathway reveals the increasing N-N distance along the down-hill path leading to the thermodynamically more stable ring-opened product (Z)-**26**. Presumably, this is responsible for the failure of optimizing the energy minima of the biradical **56**. On the other hand, the ring-opening product (Z)-**57** is energetically high-lying that is connected by a transition state. Thus, the ring-opening towards (Z)-**26** is controlled by both the thermodynamic as well as kinetic factor.

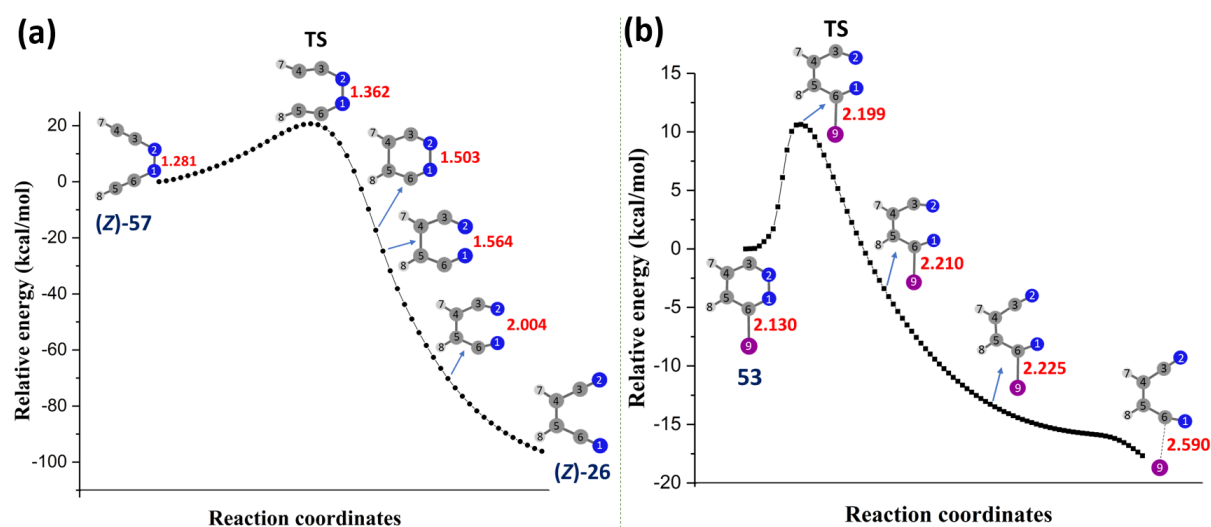


Figure 4.4 Potential energy surfaces involving: (a) the biradical **56** and the two possible ring-opening products (Z)-**57**, and (Z)-**26** (B3LYP/cc-pVTZ level of theory); (b) the possible ring opening channel of the monoradical **53** (B3LYP/DGTZVP level of theory).

In yet another possibility, the 3-dehydro-5-iodopyridazine monoradical **53** can directly lead to the ring-opening before the formation of the biradical **56**. In this regard, we also considered the thermal ring-opening channels arising from **53** (Figure 4.4b). Due to the

presence of iodine, we characterized this channel at B3LYP/DGTZVP level of theory. Here, we estimated the first C-I bond dissociation energy of the diiodopyridazine **52**, which is found to be 61.1 kcal/mol. Typically the second C-H BDEs in benzene are found to be lower than the first BDEs due to the TS or TB stabilizing interaction between the two radical electrons in the *ortho*-, *meta*-, and *para*-benzynes.^[7] Hence, the second C-I bond dissociation energy is also expected to be lower, however, the failure of optimizing the biradical **56** means, such estimation is impossible in this case. On the other hand, attempts have been made to obtain the barriers for the thermal ring-opening channels of the monoradical **53** as well. Surprisingly, the ring-opening of **53** happened only through the N-N bond cleavage with an estimated barrier of 10.6 kcal/mol, whereas the transition state corresponding to the C-C bond cleavage could not be located. Similar to the previous case, the ring-opened radical **55** has also been part of a downhill potential energy surface and so led to simultaneous ring-opening as well as the expulsion of iodine to form (Z)-**26** (Figure 4.4b). Based on this barrier, we concluded that the direct ring-opening of monoradical **53** to form (Z)-**26** is quite unlikely under matrix isolation conditions. This also indicates that the photochemical step is necessary, which can lead to the cleavage of another C-I bond along with the ring-opening step.

To shed further light in to the failure in trapping the biradical **56**, we also inspected the thermal ring-opening steps in the cases of *p*-benzyne **58** and 2,5-pyridyne **60** (Figure 4.5). The estimated barriers for ring-opening in *para*-benzyne is found to be in the range 4.1 to 8.7 kcal/mol at different levels of theory, which are consistent with earlier reports.^[8] However, upon introduction of a nitrogen atom, the symmetry of the biradical reduces that leads to two different channels with different barriers. Particularly, the C-C bond breaking is almost 20 times higher in barrier compared to the C-N bond cleavage. Indeed, the C-N bond cleavage channel is found to be susceptible at different levels of theory. At the (U)B3LYP level, we observed a favourable ring-opening with an estimated barrier of 1.0 kcal/mol, however upon changing to the M06-2X, CCSD(T) levels, it showed a barrierless step, which is very similar to 3,6-didehydropyridazine **56**. In this context, the role of nitrogen is very critical for the ring-opening and additional nitrogen makes the ring-opening even more facile. Indeed, the inspection of activation parameters associated with both channels in 2,5-pyridyne **60** revealed a substantial positive enthalpy factor (22.1 kcal/mol) and a small entropy factor (1.5 cal/K.mol), which makes it energetically unfavorable towards the C-C bond cleavage. (Table 4.1). Whereas, a small barrier with 1.0 kcal/mol and 0.1 cal/K.mol corresponding to enthalpy and entropy factors, respectively drive this reaction towards the C-N bond cleavage, leading to

a thermodynamically more stable product (*Z*)-**62**. With the additional nitrogen, the barrier can shrink even further and hence, in the case of **56**, the reaction behaves very similarly towards the N-N bond breaking.

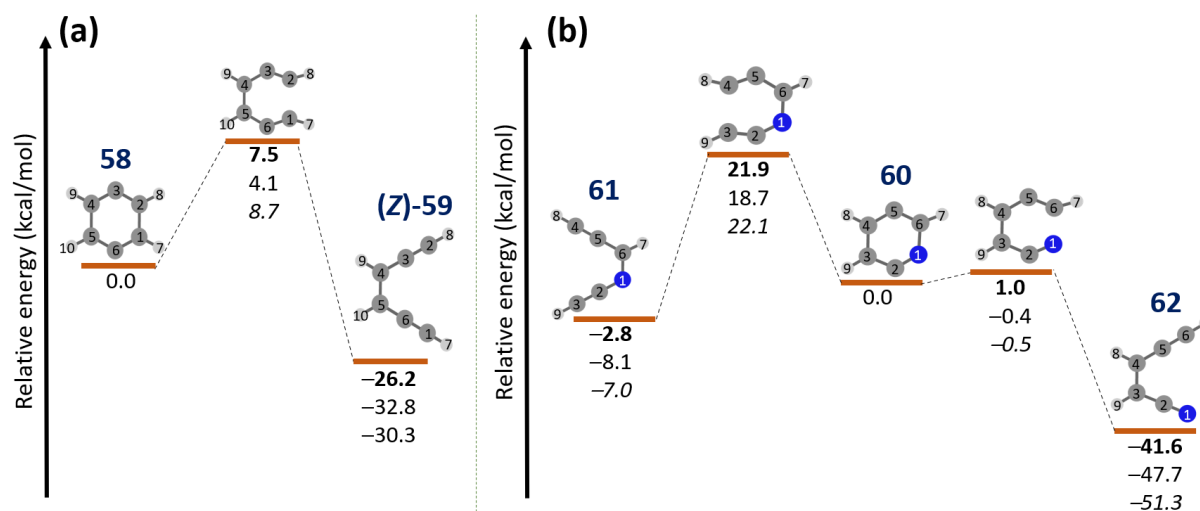


Figure 4.5 Energy profiles of (a) *p*-benzyne **58**, and (b) the biradical **60** connecting to the two possible ring-opening products (*Z*)-**61** and (*Z*)-**62** (The energy values relative to the biradicals are indicated. Bold: B3LYP/cc-pVTZ, Normal: M06-2X/cc-pVTZ and Italics: CCSD(T)/cc-pVTZ// B3LYP/cc-pVTZ)

Table 4.1 Change in thermodynamic parameters of thermal ring-opening channels in 2,5-didehydropyridine (**60**) and *p*-benzyne (**58**) at (U)B3LYP/cc-pVTZ (bold) and (U)M06-2X/cc-pVTZ (normal) levels of theory.

Species	ΔH^\ddagger (kcal/mol)	ΔG^\ddagger (kcal/mol)	ΔS^\ddagger (cal/K-mol)
TS_{60-Z-62}	1.0 0.5	1.0 0.3	0.1 -0.7
Z-62	-40.7 -46.8	-43.0 -49.0	7.8 7.1
TS_{60-Z-61}	22.1 18.8	21.6 18.6	1.5 0.7
Z-61	-1.7 -7.2	-4.1 -9.4	8.2 7.2
TS_{58-Z-59}	7.6 3.9	7.0 4.4	1.9 -1.5
Z-59	-25.3 -32.2	-27.9 -33.7	8.6 4.7

4.4 Photoisomerization of (Z)-26 to (E)-26

During the continuous irradiation at 254 nm, we observed that maleonitrile (Z)-26 is getting converted to a more stable isomer fumaronitrile (E)-26 through photochemical channels. A few experimental reports are already existing on the light induced *cis-trans* isomerization in matrix conditions.^[9] Although, the photoisomerization between anionic maleonitrile to its isomer has been investigated as a barrierless pathway, the exact mechanism for the photoisomerization of the neutral analogue has not been explored yet.^[10] Therefore, computational investigation would be interesting to explore the photochemical pathways of this system. In this regard, we have performed the SA-CASSCF calculations for understanding the photochemical conversion of (Z)-26 to (E)-26.

The vertical excitation energy calculation is performed by using EOM-CCSD method with cc-pVDZ basis set. The MP2/cc-pVDZ optimized ground state geometry was used for this calculation. The excitation energies and oscillator strengths for valence singlet excited states S_1 to S_2 are shown in table 4.2. The first excited state can be assigned as π - π^* type transition. Its oscillator strength is found to be 0.401, which supports this assignment. From natural orbital analysis, it can be further confirmed that S_1 transition originates from π -type orbital (delocalized over C=N perpendicular to the molecular plane) to π -type orbital, which is a localized anti-bonding π -orbital with dominant contributions from C and N atoms. The calculated excitation energy is found to be 6.429 eV, which lies in deep UV range. The second excited state can also be assigned as a π - π^* type transition. Its oscillator strength is found to be 0.00. From natural orbital analysis, it can further be confirmed that S_2 transition originates from π -type orbital (delocalized over C=N in the molecular plane) to the π -type orbital, which is a localized anti-bonding π -orbital with dominant contributions from C and N atoms. The transition between two orthogonal π -orbitals result in net oscillator strength to be zero. The calculated excitation energy is found to be 6.652 eV, which again lies in deep UV range. We have also calculated transition energies with SA3-CAS(50,6e)/cc-pVDZ method. The value of transition energy is found to be 7.23 eV and 7.88 eV, respectively.

Table 4.2 The vertical excitation energies of maleonitrile and fumaronitrile .

State	Maleonitrile (Z)-26			Fumaronitrile (E)-26		
	Nature of transition	Excitation energy ^a (eV)	Oscillator Strength ^b	Nature of transition	Excitation energy ^a (eV)	Oscillator Strength ^b
S ₁	π - π^*	6.429 (7.232)	0.401	π - π^*	6.549 (6.950)	0.541
S ₂	π - π^*	6.652 (7.881)	0.000	π - π^*	6.803 (7.490)	0.000

^aThe vertical excitation energies at EOM-CCSD level of theory with cc-pVDZ level of theory (normal) and SA3-CAS(5o,6e)/cc-pVDZ level of theory (in the parentheses) are indicated;

^bOscillator strength (f) at EOM-CCSD/cc-pVDZ level of theory.

In order to establish the *cis-trans* photoisomerization pathways in (Z)-26, geometry optimization has been performed for all the key species and intermediates involved in ground and excited state potential energy surfaces. The minimum energy structure corresponding to the conical intersection has been optimized at the CASSCF/cc-pVDZ level of theory. Additionally, we also found a transition state on the S₁ surface, which leads to the S₁/S₀-MECI. All the key parameters of the optimized geometries have been given in Figure 4.6 and Table 4.3. The optimized ground state geometry of maleonitrile (Z)-26 has a planar C_{2v} structure. The key features of S₀ structure at CASSCF/cc-pVDZ level are as follows: the central C=C (C3-C4) bond distance is 1.298 Å, the two C-C bond distances (C2-C3 and C4-C5) are 1.467 and 1.451 Å and two C≡N bond distances (N1-C2 and N6-C5) are 1.190 and 1.129 Å, respectively.

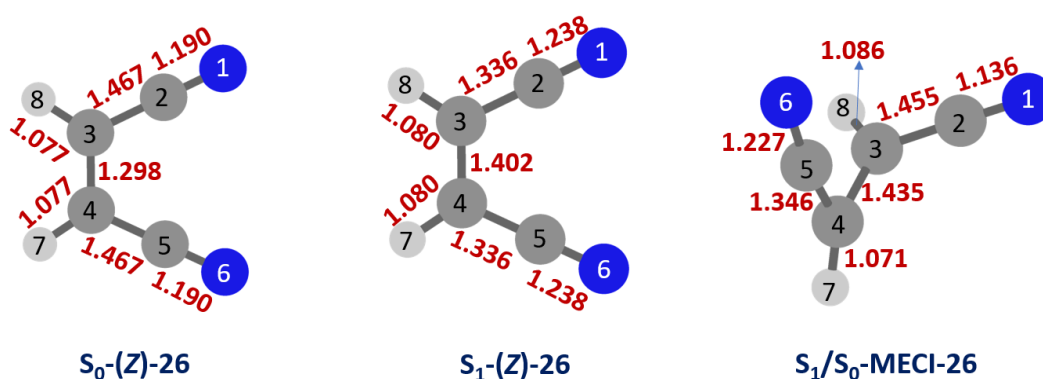


Figure 4.6 CASSCF(6,5)/cc-pVDZ geometries (in Å) for the S₀-(Z)-26, S₁-(Z)-26 and S₁/S₀-MECI-(Z)-26.

Table 4.3 Bond angles and dihedral angles (in deg) corresponding to the S_0 , S_1 , and S_1/S_0 -MECI geometries of (Z)-**26** from the CASSCF(6,5)/cc-pVDZ level of theory.

Bond Angles						
Species	N1C2C3	C2C3C4	C3C4C5	C4C5N6	C4C3H8	C3C4H7
S_0 -(Z)- 26	172.76	125.86	124.24	177.10	118.58	120.42
S_1 -(Z)- 26	178.64	125.02	122.11	178.27	120.93	119.38
S_1/S_0 -MECI	177.70	122.25	75.34	173.15	123.55	142.37

Dihedral angles					
Species	N1C2C3C4	C2C3C4C5	C3C4C5N6	C5C4C3H8	C2C3C4H7
S_0 -(Z)- 26	180.00	0.00	180.00	180.00	180.00
S_1 -(Z)- 26	180.00	0.00	0.00	180.00	180.00
S_1/S_0 -MECI	112.29	99.70	173.8	90.43	82.86

The first excited state geometry S_1 -(Z)-**26** also has a planar structure with a C_s symmetry. The major difference between the S_0 and S_1 state structures are the following: (a) the central C=C (C3-C4) bond elongated by 0.104 Å; (b) the two C-C bond distances shortened by 0.131 Å (C2-C3), and 0.036 Å (C4-C5), respectively; (c) the two C≡N bond distances are elongated by 0.119 Å (C2-N1), and 0.009 Å (C5-N6), respectively. Elongation of C=C bond and C≡N bonds are in agreement with π - π^* nature of the S_1 state, which weakens the bond strength due to the excitation of an electron to an anti-bonding π^* orbital. On the other hand, the contraction of C2-C3 and C4-C5 bonds indicates a partial double bond character at the S_1 state.

Through geometry optimization, a MECI structure on S_1/S_0 seam has been located. It is primarily a non-planar twisted geometry. The optimized geometry corresponding to the S_1/S_0 -MECI-(Z)-**26** revealed a torsional change involving C=C (C3-C4) bond. By comparing MECI and S_1 state structures, it is found that the main deformation is an out-of-plane motion involving the dihedral angles, N1C2C3C4, C2C3C4C5 and C2C3C4H7. More importantly, to attain the MECI optimized structure along the S_1 surface, the bending at C4C5N6, the planar deformation along C2C3C4C5, and also the elongations in C3-C4 and C≡N (C5-N6) bonds are required to undergo changes. Indeed, these results are quite similar to the reports on the *cis-trans* isomerization of acrylonitrile, crotonitrile and methylacrylonitrile by Schuurman and co-

workers.^[11] In this regard, we also attempted to locate a transition state along the S_1 surface connecting to the MECI geometry but it was unsuccessful.

The MECI is further characterized by g-, h-vectors and topographical parameters. The g-, and h- are defined as gradient difference (g) and derivative coupling (h) vectors. In this regard, we have visualized these vectors, and are depicted in figure 4.7. The g-vector is primarily a bond-alteration coordinate and h-vector is twisting motion about C=C (C3-C4) bond. Geometry changes along the g-vector led to the more stable (*E*)-**26** isomer, whereas, the h-vector led to the (*Z*)-**26** isomer originating from the MECI. Using these g- and h-vectors, the surfaces along S_0 and S_1 have been generated around the MECI (Figure 4.7b). The plots of branching space PESs clearly show that the MECI is vertically oriented CI, suggesting an efficient non-adiabatic population transfer through this CI.

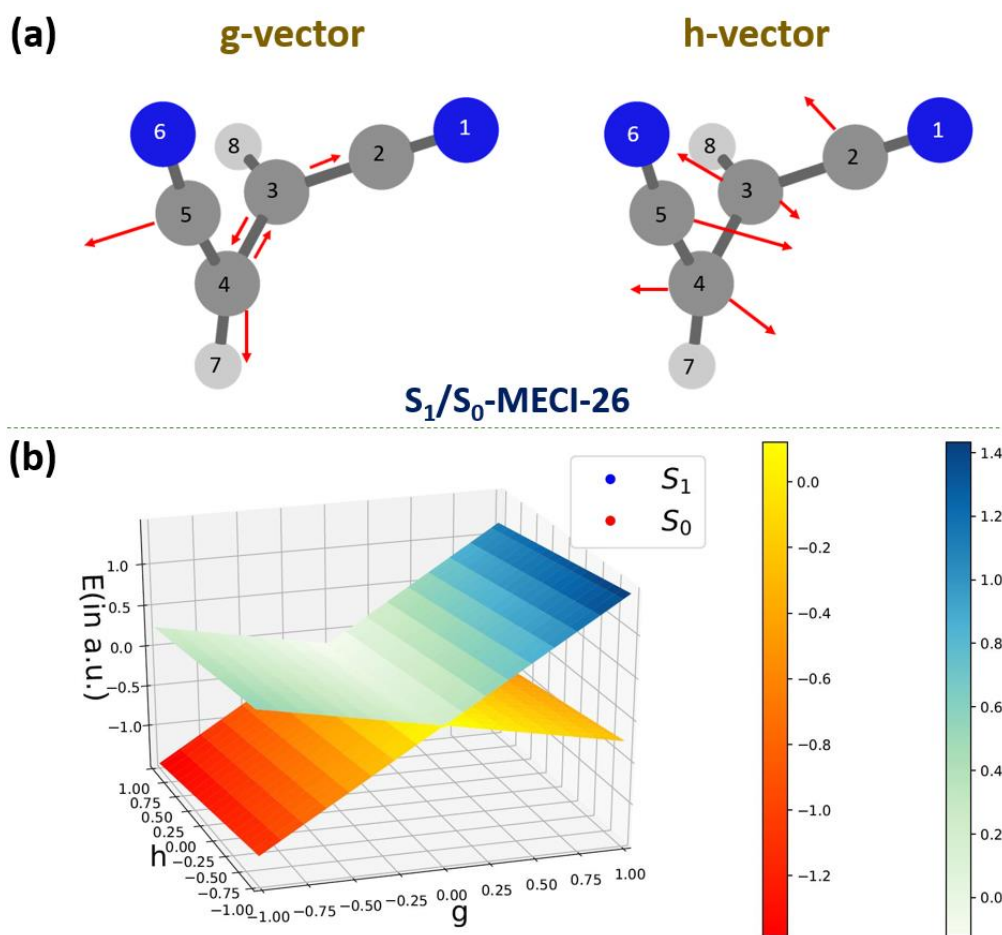


Figure 4.7 (a) The gradient difference (g) and derivative coupling (h) vectors of S_1/S_0 -MECI- (*Z*)-**26**, those lift the degeneracy around the minimum energy conical intersection (MECI), were computed with CASSCF(6,5)/cc-pVDZ level of theory; (b) Generated S_1 and S_0 surface along the g and h-vector.

After optimizing the key species involved in the surfaces S_0 , and S_1 , the reaction path for *cis-trans* isomerization have been rendered by calculation of linear interpolated coordinate. After looking carefully at these structures, the reaction coordinate can be approximated as H8C3C4H7 dihedral angle. To do so, a single point energy calculation has been performed by varying the same dihedral angle. Based on a 1D-potential energy cut, the photo-relaxation mechanism can easily be deduced. Firstly, the molecule relaxes from Franck-Condon (FC) structure to a minimum energy structure on S_1 electronic state without any barrier. (Figure 4.8) At the MECI, the ground state and the first singlet excited state surfaces turned out to be degenerate, which is responsible for the molecules to enable rotation along the dihedral H8C3C4H7, and relax back to the S_0 state either as (*E*)-**26** (product) or (*Z*)-**26** (reactant).

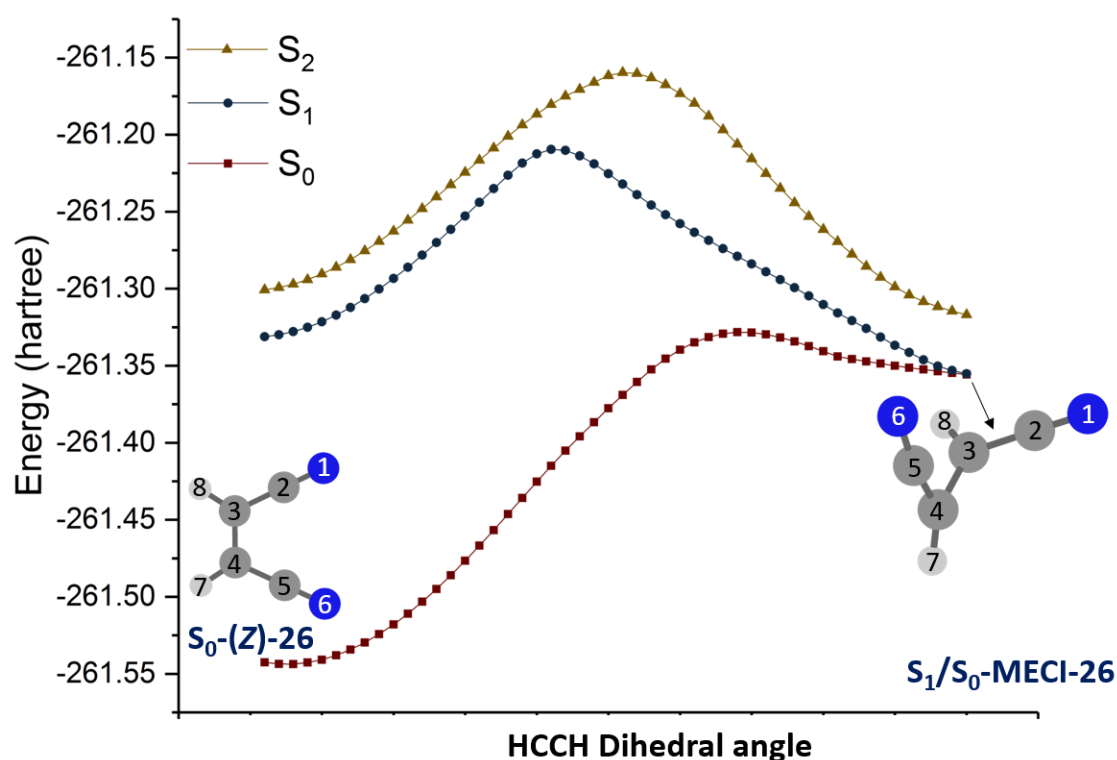


Figure 4.8 Potential energy curves along the isomerization of (*Z*)-**26** into (*E*)-**26** at CASSCF(6,5)/cc-pVDZ level of theory.

The relative energies of all key structures with respect to FC structure are shown in the Figure 4.9, where the structures have been placed on the x-axis in a decreasing order of energy of their S_1 state. After initial relaxation, an in-plane deformation involving the elongation of C=C (C3-C4) and C≡N bonds takes FC structure to S_1 minima that lowers the energy of S_1 state by 0.70 eV. Twisting around C=C bond and bending motions convert the S_1 state planar

to MECI structure, where the energy gap vanishes. Therefore, static calculations confirm the experimental observation. Upon irradiation of light, (*Z*)-**26** relaxes to the ground state of (*E*)-**26** through radiation-less transition by accessing MECI, which provide efficient funnel for photo-relaxation.

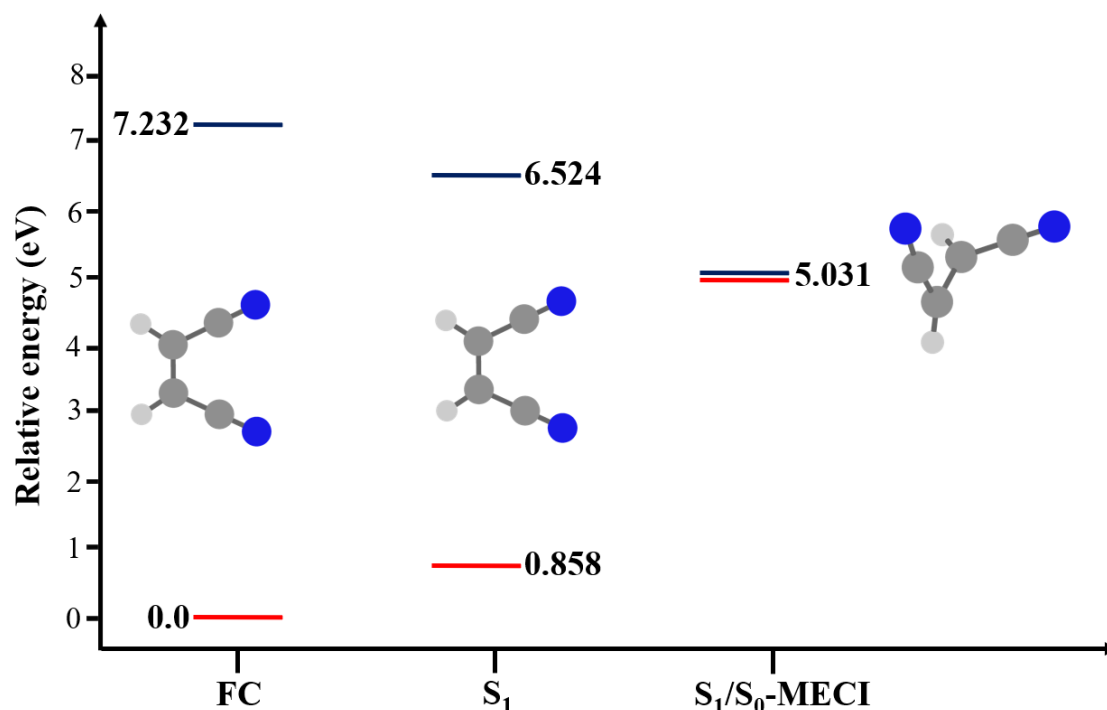


Figure 4.9 Relative energies of S_0 and S_1 states with respect to FC structures towards the MECI geometry.

4.5 Summary of photochemistry of 3,6-diiodopyridazine:

Through these investigations, we attempted at the direct observation of the biradical 3,6-didehydropyridazine **56** using matrix isolation infrared spectroscopy. However, due to the thermodynamic instability, we were unable to trap this traceless *p*-benzyne analogue. DFT and *ab initio* calculations involving multireference predicted the biradical to be a stationary point in the downhill pathway of the potential energy surface leading to the ring-opened product maleonitrile (*Z*)-**26**. Using the MO analysis, and the reaction mechanistic studies, the reasons for the instability and the barrierless ring-opening have been ascertained. Alternative pathways like the formation of direct ring-opening from the monoradical **53** has been ruled out based on the computations. Furthermore, the interesting *cis-trans* isomerization between maleonitrile to fumaronitrile has been monitored by experiments. The involvement of the S_1 state isomerization through a MECI has been computationally confirmed.

4.6 Deposition of 4,6-diiodopyrimidine (**63**)

The precursor 4,6-diiodopyrimidine (**63**) has been synthesized from the commercially available 4,6-dichloropyrimidine using the standard literature procedure.^[12] 4,6-Diiodopyrimidine (**63**) precursor has been deposited at 50 °C under high vacuum for 60 min with Ar gas kept at a flow rate of 5 sccm. Matrix-isolated infrared spectrum of 4,6-diiodopyrimidine (**63**) at 4 K exhibited prominent features at 1510.0, 1498.5, 1425.5, 1400.5, 1260.0, 1074.5 and 719.0 cm⁻¹. (Figure A10 in appendix) The comparison of the IR spectrum of 4,6-diiodopyrimidine (**63**) with the computed vibrational spectrum at B3LYP/DGTZVP level of theory showed excellent agreement with majority of the signals within usual shifts due to matrix.

4.7 Photochemistry of 4,6-diiodopyrimidine (**63**)

After the characterization, the matrix containing the precursor 4,6-diiodopyrimidine (**63**) has been subjected to irradiation at 254 nm, and the photochemistry is followed by infrared spectroscopy (Figure 4.10). Due to the irradiation, the signals corresponding to the precursor show a decrease, whereas a few new peaks at 1599.5, 1593.5, 2091.0, 2120.5, 3310.0 and 3313.5 cm⁻¹ show a growth. Upon extended irradiation time, additional signals at 2045.5, 2269.0 and 3315.0 cm⁻¹ have started appearing. By inspecting these two sets of signals, the sequence of their growth and the characteristic features in isonitrile (-N≡C) stretching (2200-2100 cm⁻¹), imine (-C=N-) stretching (1550-1650 cm⁻¹) and acetylenic C-H stretching (3250-3350 cm⁻¹) regions, we have tentatively assigned them as a part of ring-opening products (*Z*)-**66**, and (*E*)-**66**, respectively, which presumably originated through an 4,6-didehydropyrimidine biradical (**65**) intermediate. The tentative assignments have been further confirmed by comparing the experimental data with the computed spectral data at the B3LYP/cc-pVTZ level of theory for both the species and have shown an excellent agreement within their experimental shifts (Figure 4.10 and Table A11 in appendix). However, we have not observed any signals corresponding to 4,6-didehydropyrimidine biradical (**65**) in our experiment based on the computationally predicted IR signals (B3LYP/cc-pVTZ: 1486.4, 886.5, 1195.2, and 621.8 cm⁻¹ ¹CCSD(T)/TZ2P: 1501.2, 928.6, 832.6 and 1329.6 cm⁻¹) estimated in the singlet ground state. In addition to the ring-opening products (*Z*)-**66** and (*E*)-**66**, we observed the signals corresponding to ring-fragmented products HCN, CN radical and cyanoacetylene HCCCN. All the observed signals corresponding to these ring opening products (*Z*)/(*E*)-**66** along with computed vibrational frequencies have been listed in table A11 in appendix. Also, the

computed vibrational frequencies of 4,6-didehydropyrimidine biradical (**65**) at B3LYP/cc-pVTZ and CCSD(T)/TZ2P level of theory are mentioned in table A12 in appendix.

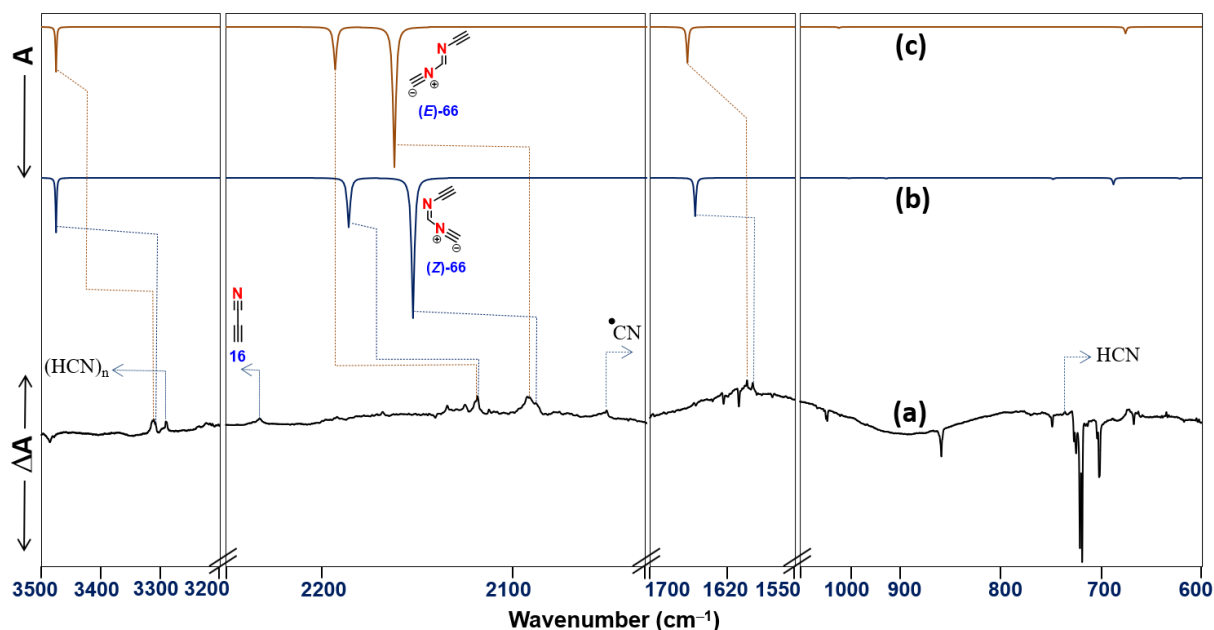
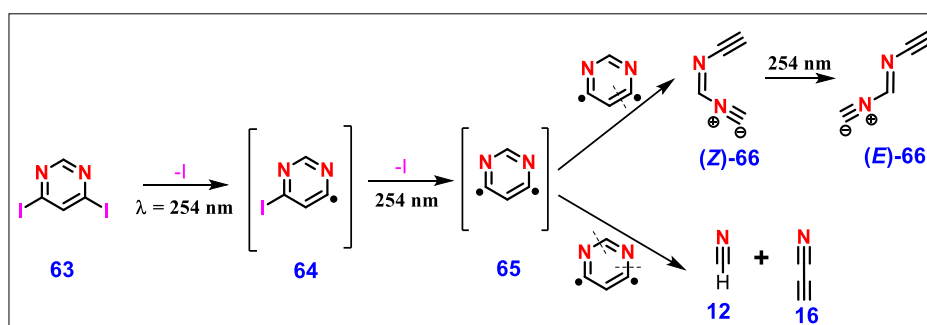


Figure 4.10 FTIR spectral data (as region-wise splits) on the photochemistry of 4,6-diiodopyrimidine **63** in an argon matrix at 4 K. (a) Difference spectrum after 40 min irradiation at 254 nm on the matrix isolated **63**. (Bands pointing downwards belong to the precursor **63**, and those pointing upwards belong to the ring-opening product (*Z*)-**66** and (*E*)-**66** and ring-fragmented products); (b) Computed spectrum of (*Z*)-**66**. (B3LYP/cc-pVTZ level of theory, unscaled); (c) Computed spectrum of (*E*)-**66**. (B3LYP/cc-pVTZ level of theory, unscaled).

4.8 Summary of photochemistry of 4,6-diiodopyrimidine (**63**)

We attempted to characterize 4,6-didehydropyrimidine biradical (**65**) from the 4,6-diiodopyrimidine **63** precursor using photolysis method. We could not isolate or characterize the targeted biradical under photochemical condition and ended up with the ring-opening products ((*Z*)-**66** and (*E*)-**66**) and ring-fragmented products HCN, HCCCN and CN radical as mentioned in scheme 4.4.



Scheme 4.4 Photochemistry of 4,6-diiodopyrimidine **63**

4.9 References

1. (a) Scott, T.; Nieman, R.; Luxon, A.; Zhang, B.; Lischka, H.; Gagliardi, L.; Parish, C. A. A Multireference ab initio Study of the Diradical Isomers of pyrazine. *J. Phys. Chem. A* **2019**, *123*, 2049–2057; (b) Chattopadhyay, S. Simplified Treatment of Electronic Structures of the Lowest Singlet and Triplet States of Didehydropyrazines. *J. Phys. Chem. A* **2019**, *123*, 5980–5994.
2. (a) Wenk, H. H.; Winkler, M.; Sander, W. One Century of Aryne Chemistry. *Angew. Chem., Int. Ed.* **2003**, *42*, 502–528; (b) Sander, W. *m*-Benzyne and *p*-benzyne. *Acc. Chem. Res.* **1999**, *32*, 669–676; (c) Wenthold, P. G.; Paulino, J. A.; Squires, R. R. The absolute heats of formation of *o*- *m*- and *p*-benzyne. *J. Am. Chem. Soc.* **1991**, *113*, 7414–7415; (d) Wenk, H. H.; Winkler, M.; Sander, W. One Century of Aryne Chemistry. *Angew. Chem., Int. Ed.* **2003**, *42*, 502–528.
3. (a) Nam, H. H.; Leroi, G. E.; Harrison, J. F. Didehydropyridines (pyridynes): an ab initio study. *J. Phys. Chem.* **1991**, *95*, 6514–6519; (b) Cramer, C. J. Bergman, Aza-Bergman, and Protonated Aza-Bergman Cyclizations and Intermediate 2,5-Arynes: Chemistry and Challenges to Computation. *J. Am. Chem. Soc.* **1998**, *120*, 6261–6269.
4. Cioslowski, J.; Szarecka, A.; Moncrieff, D. Energetics, electronic structures and geometries of didehydroazines. *Mol. Phys.* **2003**, *101*, 839–858.
5. Gleiter, R.; Heilbronner, E.; Hornung, V. Lone Pair Interaction in Pyridazine, Pyrimidine, and Pyrazine. *Angew. Chem. Intl. Ed.* **1970**, *9*, 901–902.
6. Saraswat, M.; Venkataramani, S. Through Bond and Through Space Interactions in Dehydro-Diazine Radicals: A Case Study of 3c-5e Interactions. *Phys. Chem. Chem. Phys.* **2018**, *20*, 4386–4395.
7. Karton, A.; Kaminker, I.; Martin, J. M. L. Economical post CCSD(T) computational thermochemistry protocol and applications to some aromatic compounds. *J. Phys. Chem. A* **2009**, *113*, 7610–7620.
8. Luxon, A. R.; Orms, N.; Kanters, R.; Krylov, A. I.; Parish, C. A. An ab Initio Exploration of the Bergman Cyclization. *J. Phys. Chem. A* **2018**, *122*, 1, 420–430.
9. (a) Marquardt, R.; Balster, A.; Sander, W.; Kraka, E.; Cremer, D.; Radziszewski, J. G. *p*-Benzyne. *Angew. Chem., Int. Ed. Engl.* **1998**, *37*, 955–958; (b) Winkler, M.; Cakir, B.; Sander, W. 3,5-Pyridyne – A Heterocyclic meta-benzyne derivative. *J. Am. Chem. Soc.* **2004**, *126*, 6135–6149.
10. Klaiman, S.; Cederbaum, L. S. Barrierless Single-Electron- Induced Cis-Trans Isomerization. *Angew. Chem., Int. Ed.* **2015**, *54*, 10470–10473.
11. MacDonell, R. J.; Schalk, O.; Geng, T.; Thomas, R. D.; Feifel, R.; Hansson, T.; Schuurman, M. S. Excited state dynamics of acrylonitrile: substituent effects at conical intersections interrogated via time-resolved photoelectron spectroscopy and ab initio simulation. *J. Chem. Phys.* **2016**, *145*, 114306–114316.
12. Wang, H.-L.; Katon, J.; Balan, C.; Bannon, A. W.; Bernard, C.; Doherty, E. M.; Dominguez, C.; Gavva, N. R.; Gore, V.; Ma, V.; Nishimura, N.; Surapaneni, S.; Tang, P.; Tamir, R.; Thiel, O.; Treanor, J. J. S.; Norman, M. H. Novel Vanilloid Receptor-1 Antagonists: 3. The identification of a second-generation clinical candidate with improved physicochemical and pharmacokinetic properties. *J. Med. Chem.* **2007**, *50*, 3528–3539.

Chapter 5. Electronic Structure of Didehydrodiazine biradicals

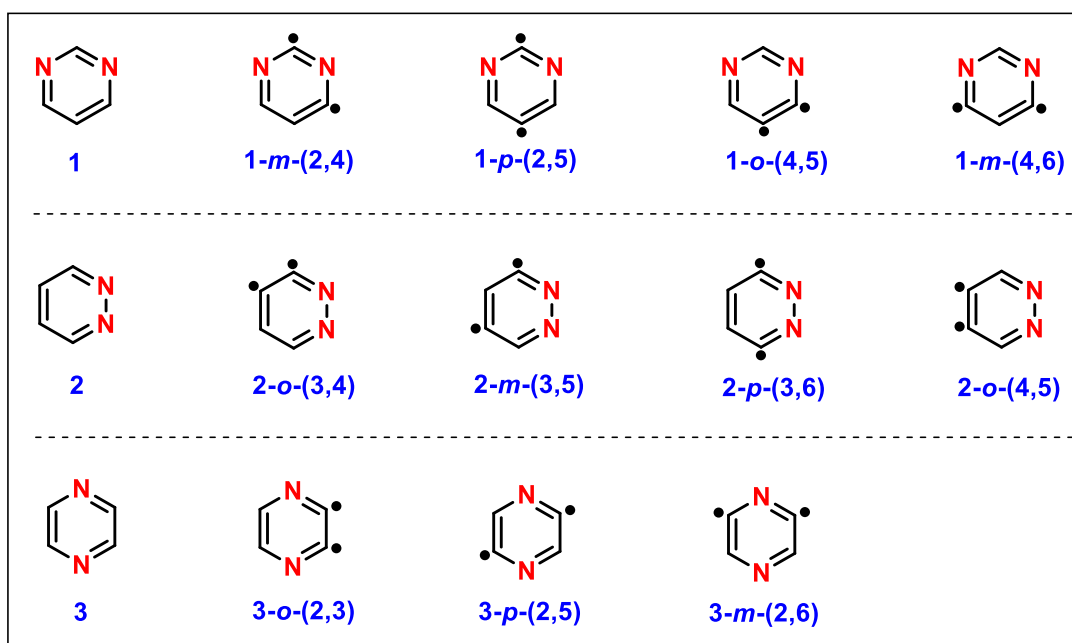
5.1 Introduction

In the earlier chapter, we described our attempts to generate and characterize dehydrodiazine biradicals (**56** and **65**) from the precursors 3,6-diiodopyridazine **52** and 4,6-diiodopyrimidine **63**. We could not detect or characterize those target biradicals, instead only ring-opening products were observed. Although these ring-opened products are expected to be formed from the biradical intermediates, presumably the stability of the biradicals did not allow detection under matrix-isolation conditions. As discussed before, the 3,6-didehydropyridazine biradical **56** is found to be unstable (or non-existent) in singlet state and directly undergoes a barrierless ring-opening to form maleonitrile. However, this biradical is stable in its triplet state. Also, during the investigations on radicals, 2-dehydropyrazine **3a** and 2-dehydropyrimidine radicals **1a**, one of the potential pathways under photochemical consideration is the loss of the hydrogen atom in forming biradicals prior to the ring-opening products formation. These instances motivate us to investigate the electronic structure of didehydrodiazine biradicals and their stability in singlet and triplet states. Understanding of these didehydrodiazine species will give additional insights in the chemistry of diazines, and mechanistic information of ring-opening species. Since they are analogous to benzyne and pyridyne type reactive intermediates, the 4-centered-6-electrons (4c-6e) interactions (between radical-radical, radical-lone pair and lone pair-lone pair) can provide clue to the thermodynamic and kinetic stability of such biradicals.

In this regard, we have explored the electronic structures of pyrimidine biradicals (didehydropyrimidines) and pyridazine biradicals (didehydropyridazines) with the help of DFT and multireference methods. Recently, multireference *ab initio* studies of pyrazine biradicals (didehydropyrazines) have been reported, however there is no report available for pyrimidine and pyridazine biradicals except the estimation of standard enthalpies of formation.^[1-3] Also, the adiabatic and vertical energy gaps between low lying singlet and triplet states have been computed through multireference calculations. In addition to that, optimized geometries, unpaired electron density, active space molecular orbitals, and AIM analysis have been performed for didehydropyrimidine and didehydropyridazine biradicals.

5.2 Didehydrodiazine biradicals and nomenclature used:

There are four possible biradicals derived from pyrimidine [2,4-didehydropyrimidine **1-m-(2,4)**, 2,5-didehydropyrimidine **1-p-(2,5)**, 4,5-didehydropyrimidine **1-o-(4,5)**, and 4,6-didehydropyrimidine **1-m-(4,6)**], and four biradicals from pyridazine [3,4-didehydropyridazine **2-o-(3,4)**, 3,5-didehydropyridazine **2-m-(3,5)**, 3,6-didehydropyridazine **2-p-(3,6)**, and 4,5-didehydropyridazine **2-o-(4,5)**], and three possible biradicals from pyrazine [2,3-didehydropyrazine **3-o-(2,3)**, 2,5-didehydropyrazine **3-p-(2,5)** and 2,6-didehydropyrazine **3-m-(2,6)**]. (Scheme 5.1) The low-lying singlet, triplet state geometries and the singlet-triplet energy gaps have been estimated for the various biradical isomers derived from didehydropyrimidine and pyridazines.



Scheme 5.1 Diazines (pyrimidine **1**, pyridazine **2** and pyrazine **3**), and their possible biradicals.

Multireference CASSCF method has been used for characterizing the singlet and triplet states and also the energy gaps between them. In order to choose the active space for CASSCF calculations, initially, restricted open shell Hartree-Fock (ROHF) calculations have been performed with cc-pVTZ basis set for all the eight biradicals of pyrimidine and pyridazine. Using these ROHF calculations, the molecular orbitals and their irreducible representations have been identified towards constructing the active space for CASSCF calculations. MCSCF calculations were performed for each biradical with cc-pVTZ basis set.

5.3 Active space for CASSCF calculations

All the eight biradicals (didehydropyrimidines and didehydropyridazines) have been optimized at the following point groups: C_s for 2,4-didehydropyrimidine **1-m-(2,4)**, 4,5-didehydropyrimidine **1-o-(4,5)**, 3,4-didehydropyridazine **2-o-(3,4)**, 3,5-didehydropyridazine **2-m-(3,5)** and C_{2v} for 2,5-didehydropyrimidine **1-p-(2,5)**, 4,6-didehydropyrimidine **1-m-(4,6)**, 3,6-didehydropyridazine **2-p-(3,6)**, 4,5-didehydropyridazine **2-o-(4,5)**. The complete active space (CAS) for multireference calculations have been constructed from 12 electrons and 10 orbitals for all biradicals. This active space consists of six π -orbitals of aromatic ring (3 fully occupied π - and 3 virtual π^*), the two orbitals corresponding to in-phase and out-of-phase combination of nitrogen lone pairs and two orbitals corresponding to the unpaired electrons (biradicals).

5.4 Singlet-Triplet energy gaps through vertical and adiabatic energies gaps:

We have performed the multireference CASSCF calculations with cc-pVTZ basis set using the active space of 12 electrons and 10 orbitals. We optimized both singlet and triplet states for these pyrimidines and pyridazine based biradicals. Surprisingly, we observed the ring-opening fragments of 2,4-didehydropyrimidine **1-m-(2,4)** and 3,6-didehydropyridazine **2-p-(3,6)** biradicals during the geometry optimization (energy minimization) in their respective singlet states. However, these two biradicals are stable in their triplet states. All the optimized geometries are mentioned in the next section. (Figure 5.3, 5.4 and 5.5) For each didehydropyrimidine and didehydropyridazine biradical, we have estimated the vertical and adiabatic energy gaps and compared them with that of didehydropyrazines reported recently.^[1,2]

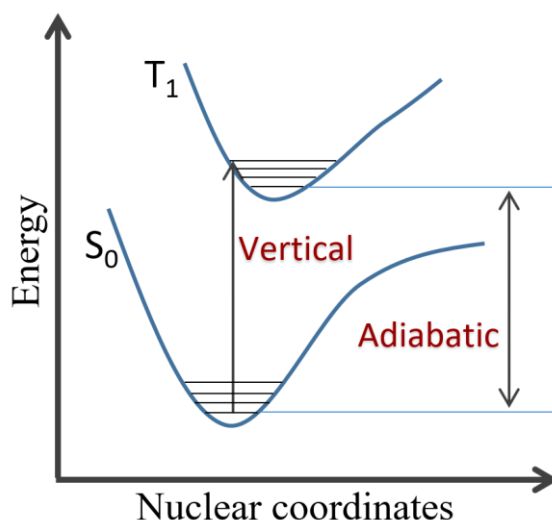


Figure 5.1 Representation of Vertical and Adiabatic energies gap.

5.4.1 Vertical energy gaps:

Vertical energy gaps have been estimated for didehydropyrimidine and didehydropyridazine biradicals where both singlet and triplet states are stable. These gaps have been estimated from the electronic energy differences of singlet and triplet states. In this regard, we have considered the energy of singlet (optimized geometry) and triplet (without optimization, triplet state energy at the singlet state geometry). (Figure 5.1) This energy gap is known as vertical energy gap between two different states. Vertical energy gaps have been mentioned in table 5.1. Since all the didehydrodiazines biradical isomers are isoelectronic, we have compared their vertical energy gaps. As we have discussed in chapter 2, the stability and reactivity of dehydrodiazine radical isomers depend on the interaction between nitrogen lone pairs and unpaired electrons. Similarly, in didehydrodiazines, the vertical energy gaps also depend on the interaction between two nitrogen lone pairs and the two unpaired electrons. For didehydrodiazines biradicals, the interaction between radical-radical, lone pair-radical and lone pair-lone pair is expected to play a major role in determining the ground state as well as the S-T energy gaps. We observed that, 4,5-didehydropyridazine **2-o-(4,5)** biradical has the highest S-T vertical energy gap of 85.6 kcal/mol, which implies that singlet state is highly stabilized compared to triplet state and exists as the ground state. The very high S-T energy gap in 4,5-didehydropyridazine **2-o-(4,5)** biradical could be due to the effective/strong radical-radical interaction as it is the only biradical without the presence of an adjacent (*ortho*-) nitrogen atom to radical centre. As we already discussed, the nature and mode of interaction between radical centre and nitrogen lone pairs, the strong TS interaction has been observed at the *ortho* position with respect to nitrogen lone pair which diminishes with increasing distance.^[4,5] In all other isomers, at least one of the nitrogen atoms is present at the adjacent (*ortho*) position, which exhibits S-T energy gaps in the range of 14.9–47.5 kcal/mol due to the presence of TS interaction. This relatively low S-T energy gap in other diazine biradicals (upon comparison with 4,5-didehydropyridazine **2-o-(4,5)** biradical, 85.6 kcal/mol) can be attributed to the effective lone pair-radical interaction. Based on these vertical S-T energy gaps, we observed a significant role of nitrogen lone pairs in determining the biradical ground state as well as in their S-T energy gaps. Similarly, in didehydropyrazine biradicals, **3-o-(2,3)** has a high S-T vertical energy gap due to strong interaction between two adjacent radical centre and these values for didehydropyrazine biradicals have been taken from the references [1, and 2].

5.4.2 Adiabatic energy gaps:

Similarly, we have investigated the adiabatic energy gap between singlet and triplet states. Adiabatic energy gap is the difference in the energy of singlet (optimized geometry) and triplet (optimized geometry) states. Adiabatic energy gap is always less compared to the vertical excitation energy as we use the optimized triplet state energy here, instead of the triplet state energy at singlet geometry. (Figure 5.1) We have observed a trend in the S-T adiabatic energy gap similar to the vertical energy gap. In this case too, 4,5-didehydropyridazine **2-o-(4,5)** biradical has the highest S-T adiabatic energy gap (69.9 kcal/mol) and others are relatively low in the range of 4.1–26.3 kcal/mol. (Figure 5.2 and table 5.1)

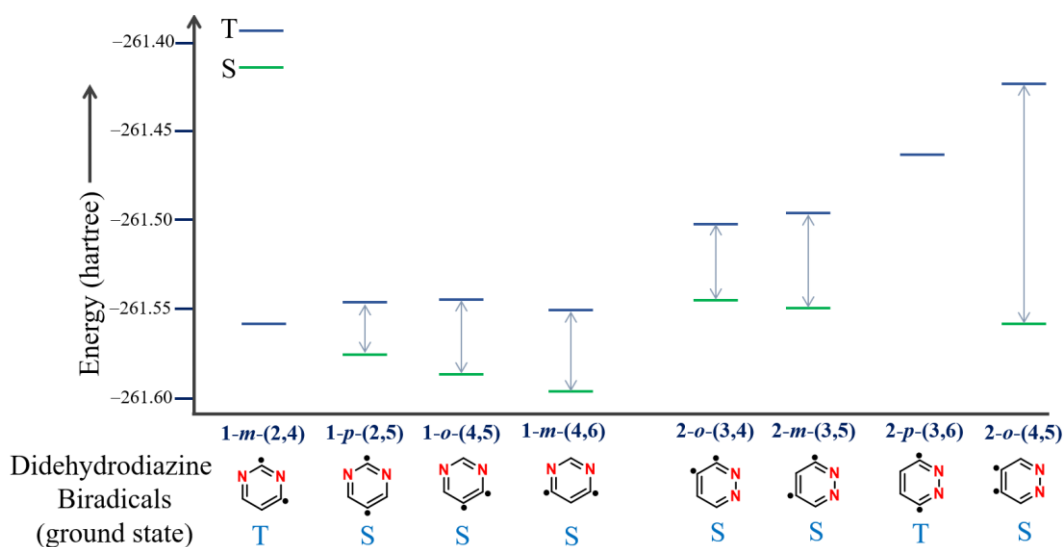
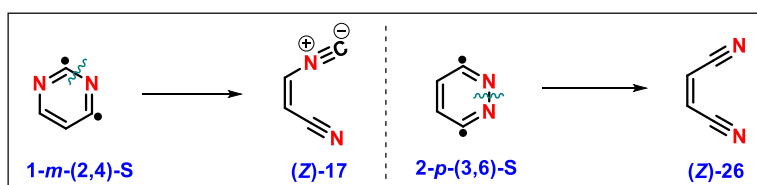


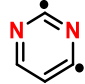
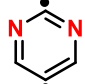
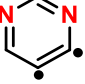
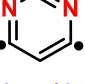
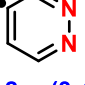
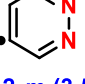
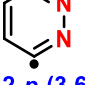
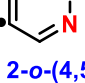
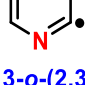
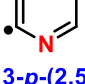
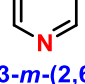
Figure 5.2 Energy profiles of optimized geometries in singlet and triplet state corresponding to didehydropyrimidine and didehydropyridazine biradicals at CASSCF (12,10)/cc-pVTZ level of theory along with their ground state multiplicity mentioned in bottom line.

During the geometry optimization of didehydropyrimidine and didehydropyridazine biradicals in their singlet and triplet states, we found out that two of biradicals **1-m-(2,4)** and **2-p-(3,6)** (one each in pyrimidine and pyridazine) are unstable in their singlet states and lead to more stable ring-opening isomers as mentioned in scheme 5.2. Due to the absence of singlet states in these biradicals (**1-m-(2,4)** and **2-p-(3,6)**), vertical and adiabatic energy gaps could not be estimated.



Scheme 5.2 Ring-opening of 2,4-didehydropyrimidine **1-m-(2,4)** and 3,6-didehydropyridazine **2-p-(3,6)** biradicals in their singlet state.

Table 5.1 Vertical and adiabatic energy gaps of didehydrodiazines biradicals (in kcal/mol) at CASSCF(12,10)/cc-pVTZ level of theory.

Didehydrodiazine biradicals	Vertical Energy gaps	Adiabatic Energy gaps
 1- <i>m</i> -(2,4)	—	—
 1- <i>p</i> -(2,5)	18.6	10.4
 1- <i>o</i> -(4,5)	14.9	4.1
 1- <i>m</i> -(4,6)	27.9	22.0
 2- <i>o</i> -(3,4)	47.5	26.3
 2- <i>m</i> -(3,5)	28.5	13.0
 2- <i>p</i> -(3,6)	—	—
 2- <i>o</i> -(4,5)	85.6	69.9
 3- <i>o</i> -(2,3)	25.3 ^a	8.9 ^a
 3- <i>p</i> -(2,5)	18.2 ^a	11.6 ^a
 3- <i>m</i> -(2,6)	12.3 ^a	1.9 ^a

^adata from the literature references [1, and 2]

Based on the vertical and adiabatic S-T energy gaps, we have observed a significant role of nitrogen lone pairs in determining the biradical ground state as well as their S-T energy gaps. Both singlet and triplet states are influenced with the various possible interactions between nitrogen lone pairs and radical centres (mainly through space TS interaction). The interaction of nitrogen lone pairs in singlet states implies the nature of singlet states, which is open-shell singlet and rules out the possibility of closed-shell singlet in which no interaction is possible between nitrogen lone pairs and radical centres. Further, we confirmed the open-shell nature of the singlet state in the molecular orbital analysis.

5.5 Geometrical parameters of dehydropyrimidines and dehydropyridazines biradicals

All the didehydropyrimidine and pyridazine biradical isomers and their respective parent molecules (pyrimidine **1** and pyridazine **2**) have been optimized to their minimum energy geometries at (U)B3LYP/cc-pVTZ and (U)M06-2X/cc-pVTZ levels of theory and are shown in figure 5.3, 5.4 and 5.5. We have compared the changes in geometrical parameters (bond lengths and bond angles) upon creating biradicals from their respective parent molecules at above mentioned levels of theories. Also, we have mentioned the geometrical parameters at CASSCF level of theory for all possible biradicals with the active space of 12 electrons and 10 orbitals. Majority of the biradical isomers are found to have C_s and C_{2v} structures. Based on the comparison of geometrical parameters, we found out that the internuclear distances between the radical centres and the adjacent atoms in either side have a contraction/same relative to the parent compound in their singlet and triplet states with few exceptions. This exception only exists in singlet states where the two radical centres are adjacent (*ortho*-) to each other for example, **1-o-(4,5)-S** and **2-o-(3,4)-S**. In these two singlets, the internuclear distance has been increased in one of the sides of the radical centre. This can be understood from the *ortho*-benzyne type bonding situation between the two radical centers and the resulting distorted hexagon geometry in their singlet states. Apart from that, the alternate bonds relative to the radical centres showed a marginal increase with respect to the parent compound except in a case of **2-o-(3,4)-T**. This general behaviour of internuclear distances is consistent with our previous studies on the dehydropyrimidines (**1a-c**) and dehydropyridazines (**2a-b**) radicals described in chapter 2. In addition to that, we have also inspected the changes in bond angles at the radical centres in all the singlet and triplet biradicals. We observed a general trend on the bond angles at the radical centres, the value of which increased relative to the corresponding parent diazine. However, exceptions have been observed in those same above mentioned biradicals **1-o-(4,5)-S** and **2-o-(3,4)-S**, where the bond angles at the radical centers

have been decreased due to the distorted geometry in their singlet states. The reason for the distorted hexagon geometry could be the presence of nitrogen lone pairs adjacent to the radical centres. The extent of increase or decrease in the bond lengths and change in bond angles relative to their parent compound certainly depend on the relative position of the radical centre and the nitrogen atoms at which nitrogen lone pairs can participate in the interaction. Also, we have observed the changes in internuclear distances between the radical centres when they are *ortho*-, *meta*- and *para*- to each other in their singlet and triplet states. These changes help us in identifying the role of nitrogen atoms and the interaction of its lone pair with the radical centres.

All the geometrical parameters have been mentioned for the didehydropyrimidine biradicals in figure 5.3 and, for the didehydropyridazine biradicals in figure 5.4 at (U)B3LYP/cc-pVTZ, (U)M06-2X/cc-pVTZ and CASSCF/cc-pVTZ level of theory. We could not locate the minimum energy geometry for the **1-*m*-(2,4)** and **2-*p*-(3,6)** in their singlet states. These two biradicals are not stable over the PES in their singlet states and led to the ring opening structures upon geometry optimization. However, their geometrical parameters in the triplet states have been mentioned separately in figure 5.5.

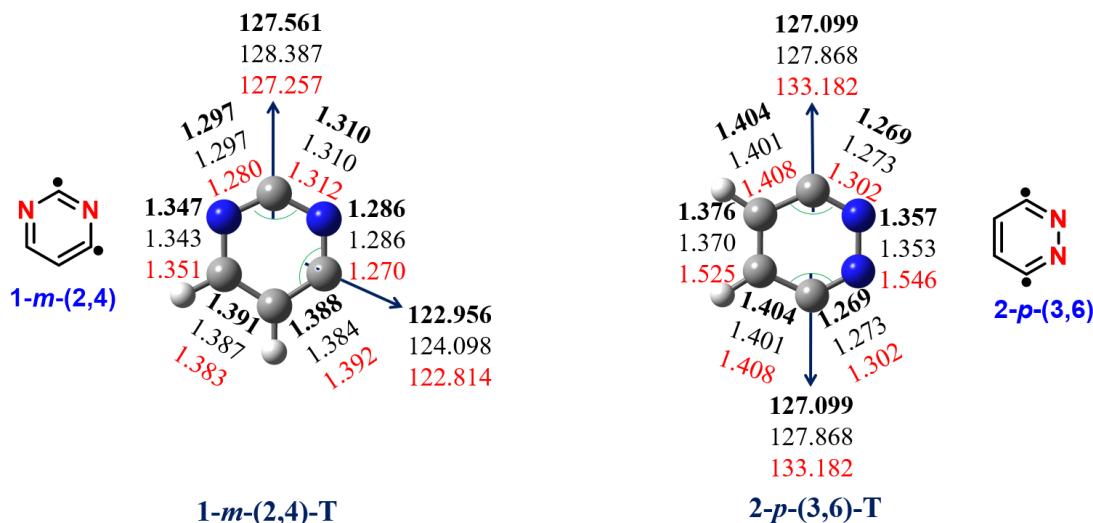


Figure 5.3 Optimized geometries of the triplet states of 2,4-didehydropyrimidine biradical **1-*m*-(2,4)** and 3,6-didehydropyridazine biradical **2-*p*-(3,6)**. The most important bond distances (in Å units) and the bond angles (in degrees) at the radical centres are mentioned. The indicated geometrical parameters in bold font correspond to (U)B3LYP/cc-pVTZ and those in normal font are estimated at the (U)M06-2X/cc-pVTZ levels of theory. Parameters in red correspond to CASSCF/cc-pVTZ level of theory.

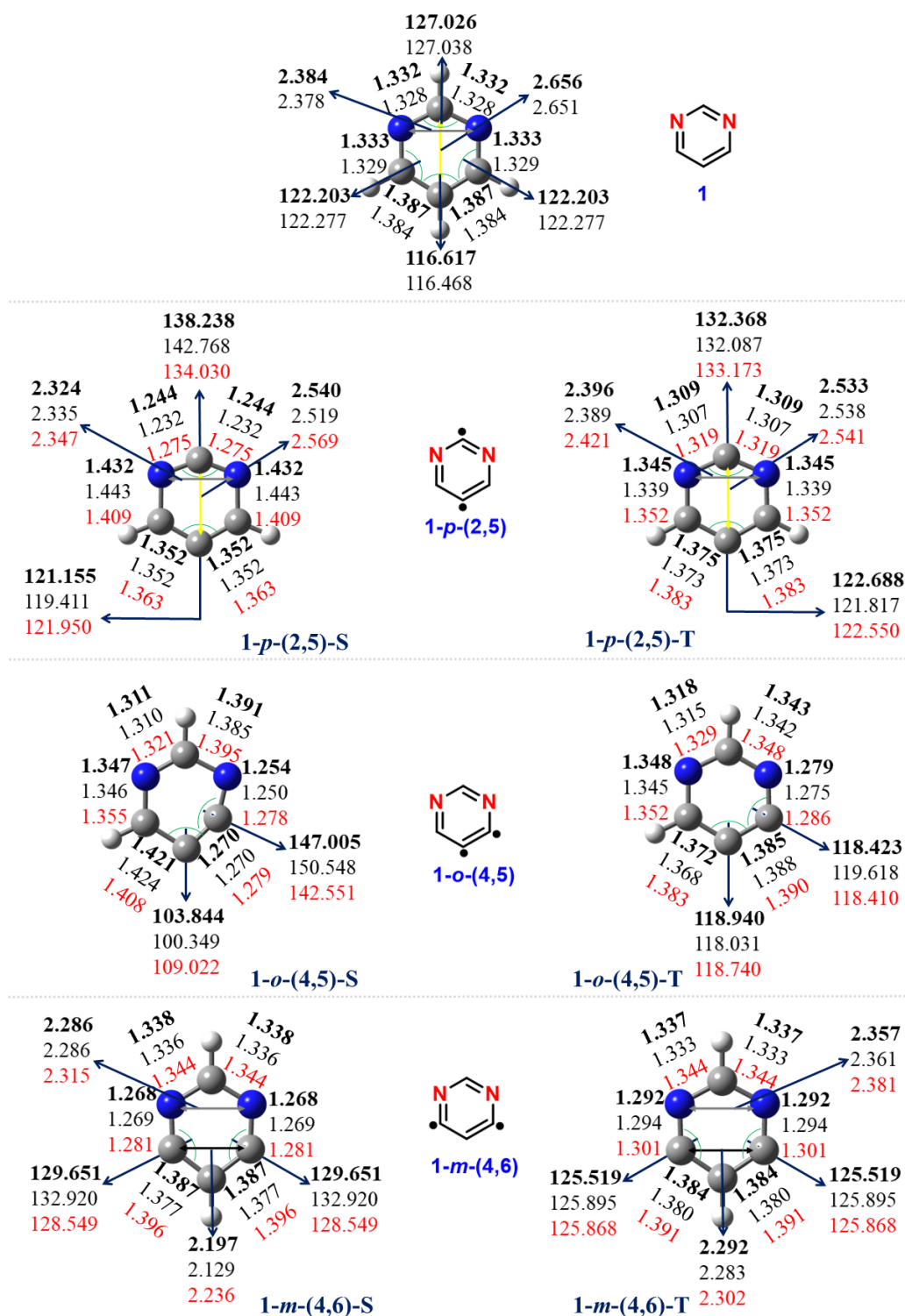


Figure 5.4 Optimized geometries of the didehydropyrimidine biradical isomers and its parent compound pyrimidine. The most important bond distances (in Å units) and the bond angles (in degrees) at the radical centres are mentioned. The indicated geometrical parameters in bold font correspond to (U)B3LYP/cc-pVTZ and those in normal font are estimated at the (U)M06-2X/cc-pVTZ levels of theory. Parameters in red correspond to CASSCF/cc-pVTZ level of theory.

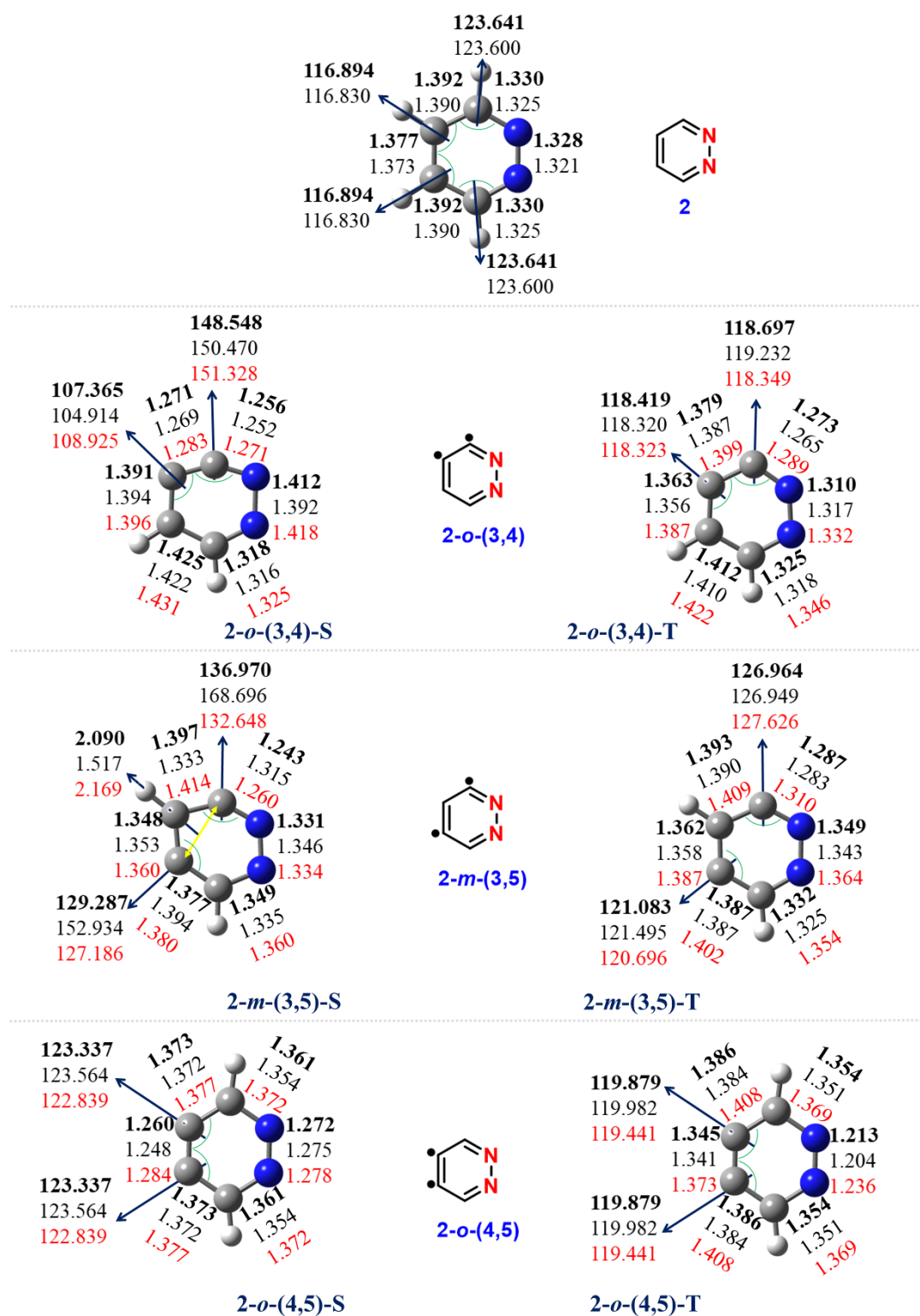


Figure 5.5 Optimized geometries of the didehydropyridazine biradical isomers and its parent compound pyridazine. The most important bond distances (in Å units) and the bond angles (in degrees) at the radical centres are mentioned. The indicated geometrical parameters in bold font correspond to (U)B3LYP/cc-pVTZ and those in normal font are estimated at the (U)M06-2X/cc-pVTZ levels of theory. Parameters in red correspond to CASSCF/cc-pVTZ level of theory.

5.6 Molecular orbitals analysis of didehydrodiazines

Further, we have closely inspected the molecular orbitals from the multireference calculations, where 10 orbitals and 12 electrons have been used as the active space. This includes the six-benzene type π -orbitals (3 π -occupied and π^* -virtual), two nitrogen lone pairs and two orbitals corresponding to unpaired electrons for each case. We have listed all the active space molecular orbitals of singlet and triplet states for didehydropyrimidine and didehydropyridazine biradicals at CASSCF (12,10)/cc-pVTZ level of theory. We have separated the molecular orbitals as follows: lone pair orbitals, occupied π -orbitals, radical orbitals (unpaired electron) and π^* -virtual orbitals and mentioned their orbital occupancies for all the didehydropyrimidine and didehydropyridazine biradicals in their singlet and triplet states. Molecular orbitals corresponding to only triplet states have been mentioned for 2,4-didehydropyrimidine **1-m-(2,4)** and 3,6-didehydropyridazine **2-p-(3,6)** biradicals as these two biradicals are not stable in their singlet states. Upon inspection at the orbital occupancies for all the active space orbitals, we found out that those corresponding to radical orbitals are in the range of 0.59–0.73 which confirmed the open-shell nature of all these biradicals in their singlet states. Also, the multireference nature has been further confirmed from the significant orbital occupancies at all the virtual orbitals as well as the deviation in the occupancy of completely filled orbitals from two. Furthermore, we have analyzed the interaction between radical-radical and nitrogen lone pair with radicals (unpaired electrons). Insights for radical-radical interactions can be visualized from the orbitals corresponding to the two formerly unpaired electrons containing orbitals. Upon inspecting those orbitals, we observed the lowering of the symmetric combination of two radical orbitals relative to the corresponding antisymmetric combination, which confirmed the existence of through space interaction between these two radical orbitals. Particularly, this situation persists only when the two radical orbitals are present at *ortho*- and *meta*- to each other. In other words, two radical orbitals are interacting with each other through space when they are *ortho*- and *meta*- to each other. This through space interaction can be visualized from the molecular orbitals of 2,4-didehydropyrimidine **1-m-(2,4)**, 4,5-didehydropyrimidine **1-o-(4,5)**, 4,6-didehydropyrimidine **1-m-(4,6)**, 3,4-didehydropyridazine **2-o-(3,4)**, 3,5-didehydropyridazine **2-m-(3,5)**, 4,5-didehydropyridazine **2-o-(4,5)** biradicals in their singlet and triplet states where two unpaired electrons are *ortho*- and *meta*- to each other.

On the other hand, the remaining biradicals where two radicals are present *para*- to each other, we observed an opposite trend in the order of radical orbitals i.e their antisymmetric

combination is lower in energy compared to that of symmetric combination. This is the characteristic of through bond interaction. In other words, two radical orbitals are interacting with each other through bond when they are situated at *para*- to each other. This through bond phenomena between two radicals have been observed in 2,5-didehydropyrimidine **1-*p*-(2,5)**, and 3,6-didehydropyridazine **2-*p*-(3,6)** biradicals. Similarly, this through space and through bond interaction can easily be visualized between nitrogen lone pairs and radical orbitals by inspecting the molecular orbitals corresponding to the two nitrogen lone pairs.

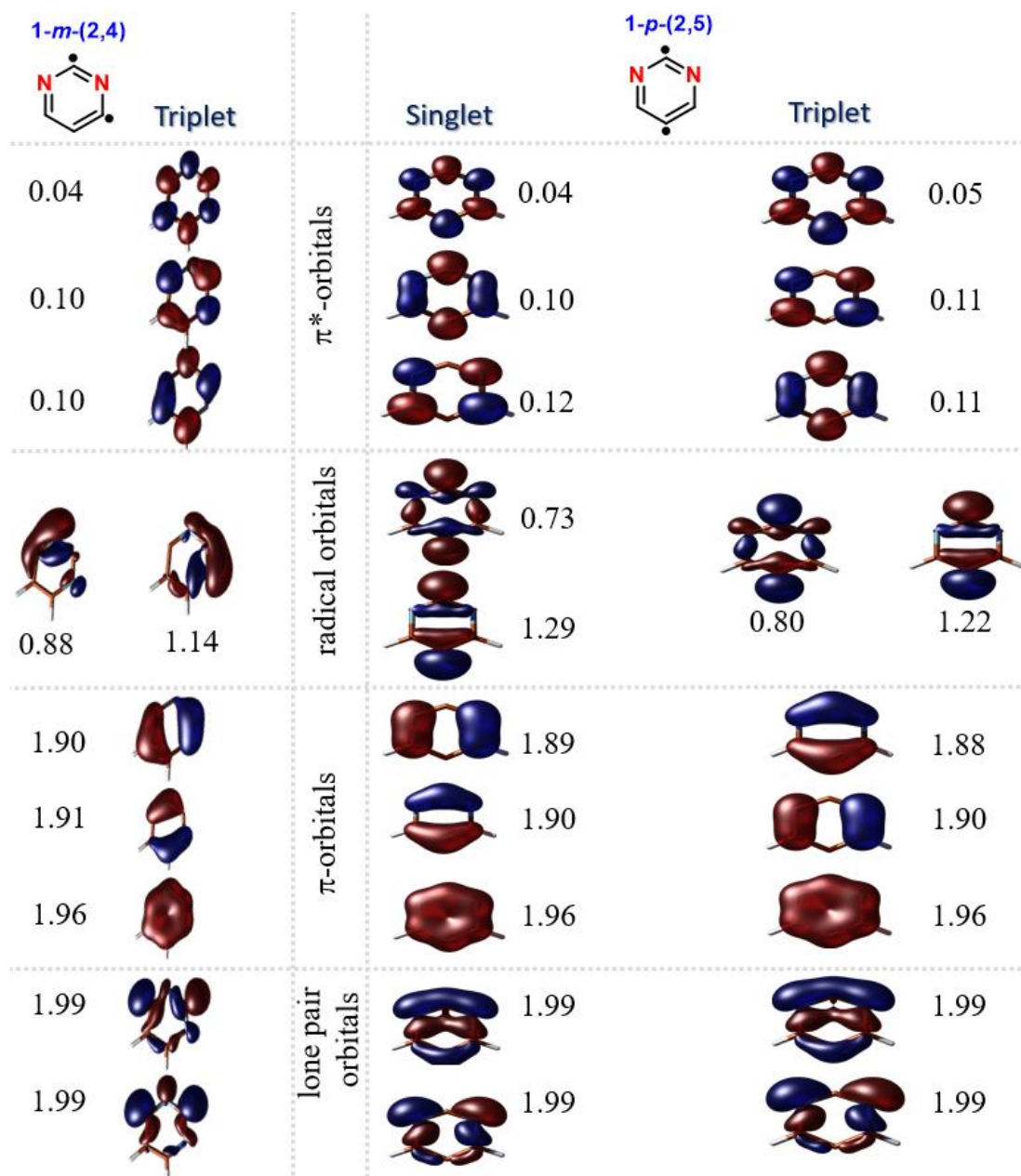


Figure 5.6 Molecular orbitals corresponding to the active space (12 electron, 10 orbitals) of the didehydropyrimidine biradical isomers (**1-*m*-(2,4)** triplet state and **1-*p*-(2,5)** in singlet and triplet state) using multiconfigurational CASSCF/cc-pVTZ level of theory. Molecular orbitals have been rendered using MOLDEN software package at an isovalue of 0.05.

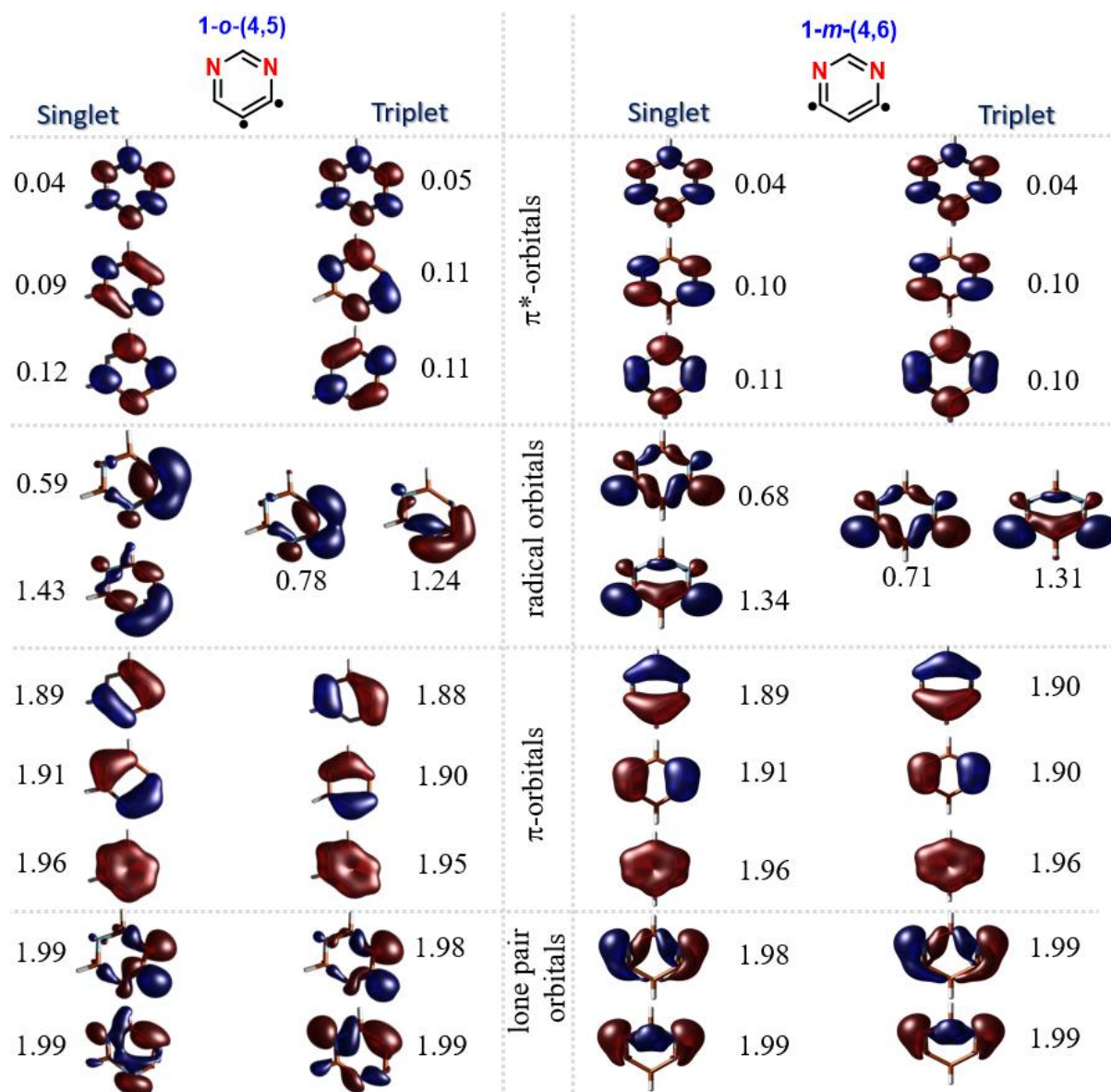


Figure 5.7 Molecular orbitals corresponding to the active space (12 electron, 10 orbitals) of the didehydropyrimidine biradical (**1-o-(4,5)** and **1-m-(4,6)** in singlet and triplet state) isomers using multiconfigurational CASSCF/cc-pVTZ level of theory. Molecular orbitals have been rendered using MOLDEN software package at an isovalue of 0.05.

This through space interaction is very strong when two interacting orbitals are adjacent (*ortho*-) to each other and diminishes as the distance is increased from *ortho*- to *meta*- to *para*. Highest S-T energy gap in 4,5-didehydropyridazine **2-o-(4,5)** biradical can be easily understood by considering such orbital interactions. In 4,5-didehydropyridazine **2-o-(4,5)** biradical, two unpaired electrons are strongly interacting to each other through space interactions with very less perturbation from the nitrogen lone pairs as they are situated at the *meta*- position to radicals.

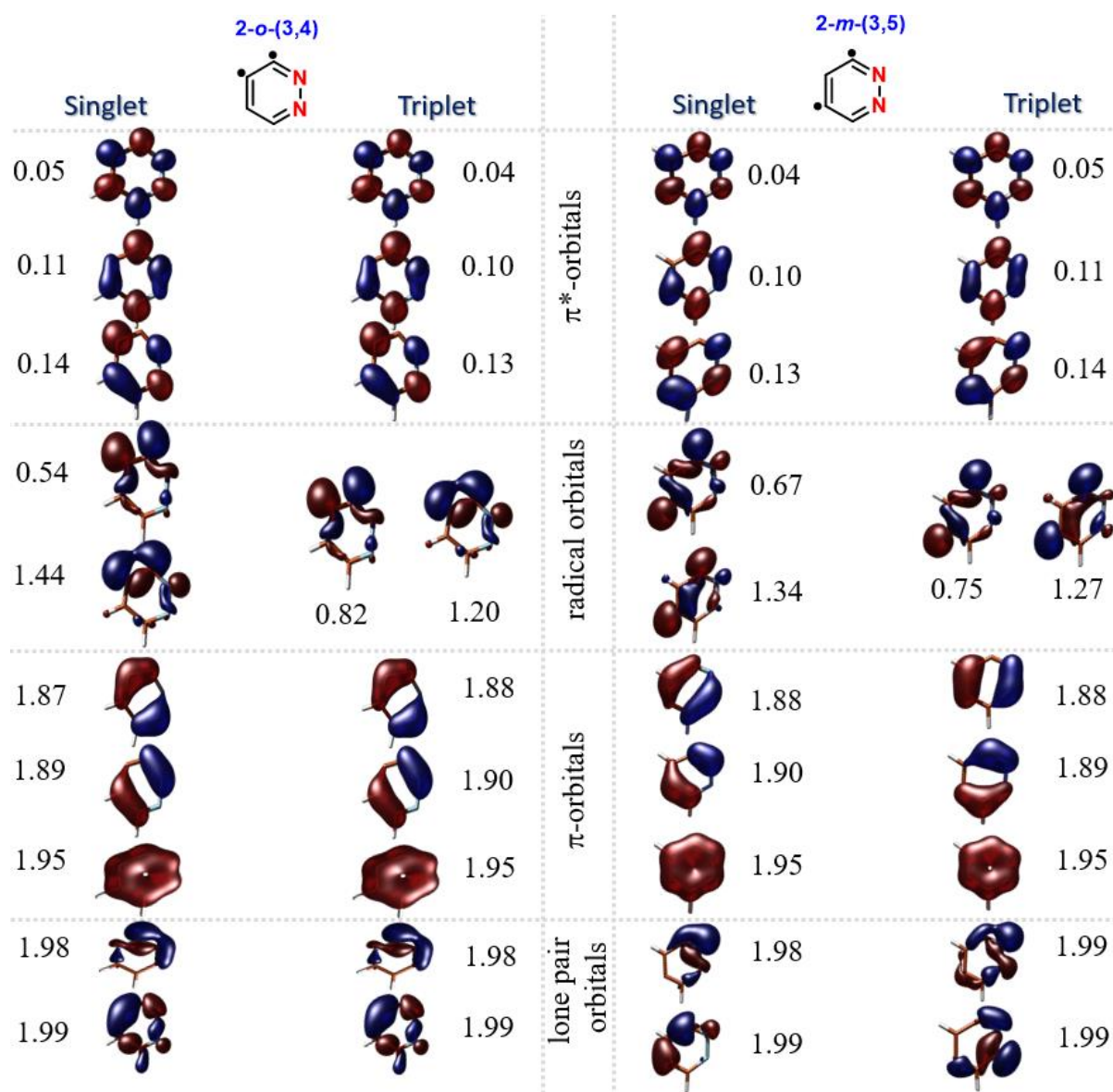


Figure 5.8 Molecular orbitals corresponding to the active space (12 electron, 10 orbitals) of the didehydropyridazine biradical isomers (**2-o-(3,4)** and **2-m-(3,5)** in singlet and triplet state) using multiconfigurational CASSCF/cc-pVTZ level of theory. Molecular orbitals have been rendered using MOLDEN software package at an isovalue of 0.05.

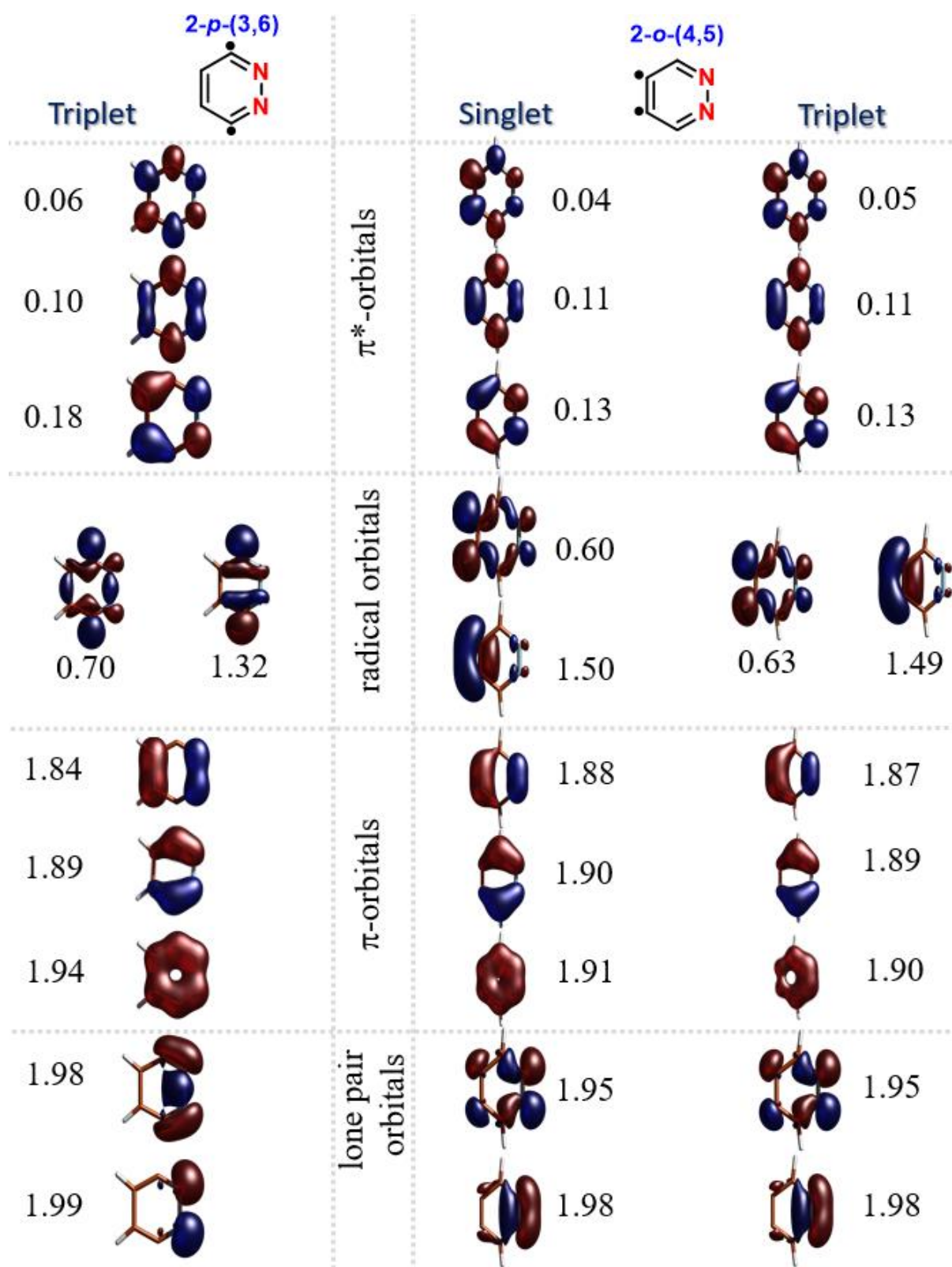


Figure 5.9 Molecular orbitals corresponding to the active space (12 electron, 10 orbitals) of the didehydropyridazine diradical isomers (2-*p*-(3,6) triplet state and 2-*o*-(4,5) in singlet and triplet state) using multiconfigurational CASSCF/cc-pVTZ level of theory. Molecular orbitals have been rendered using MOLDEN software package at an isovalue of 0.05.

5.7 Spin densities of triplet didehydrodiazines

We have estimated the spin density of all the didehydropyrimidine and didehydropyridazine biradicals in their triplet states using the density function theory. Spin density values at the radical centres provide the insights of localization and delocalization of unpaired electron density in the molecule as well as the indirect information about the presence of interaction with heteroatom upon delocalization of spin density. We have closely observed the values of spin densities of unpaired electrons and mentioned in figure 5.10. We found that unpaired spin is not completely localized over the radical centres as the value is deviating from one. However, some part of this unpaired electron density is delocalized over the ring (and over the nitrogen atoms) and can be visualised from the significant values of spin density at the nitrogen atoms, which further confirm the interaction of nitrogen lone pairs with unpaired electrons with possible mode of interactions.

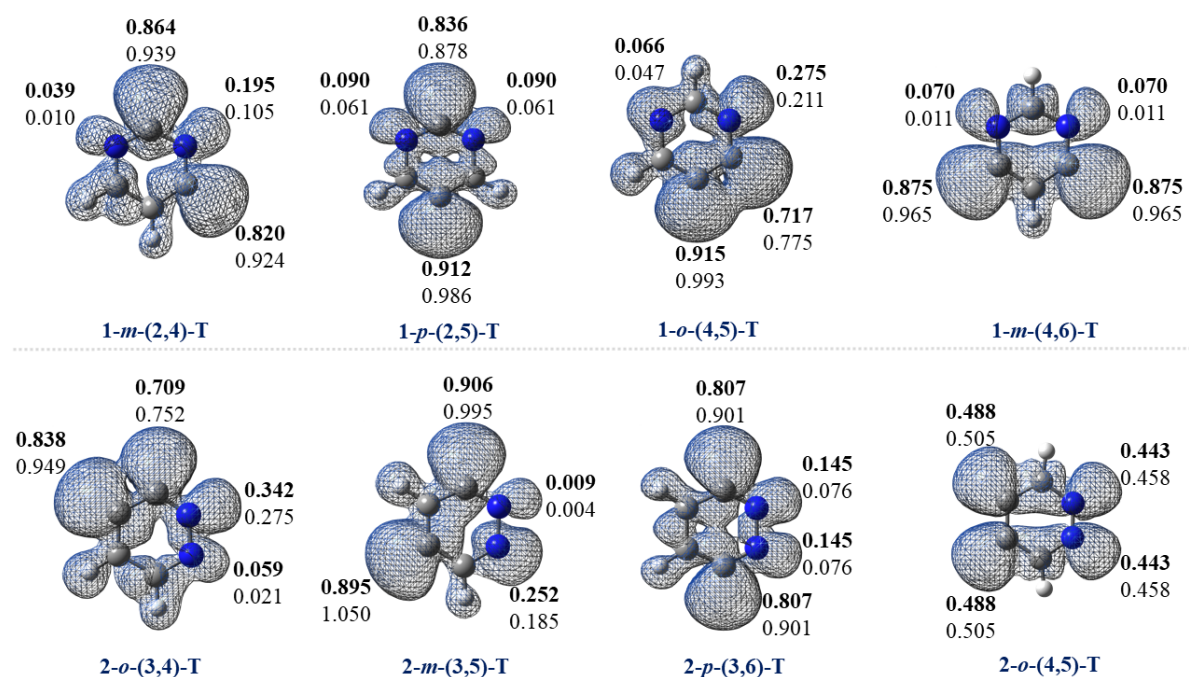


Figure 5.10 Spin densities of didehydropyrimidine and didehydropyridazine biradicals in their triplet state at (U)B3LYP/cc-pVTZ (bold); and (U)M06-2X/cc-pVTZ (normal) levels of theory.

5.8 Atoms-in-molecules analysis:

In order to further confirm the role of nitrogen lone pairs and the insights about their interaction in determining the electronic structures of didehydrodiazines biradicals, we have done the AIM analysis and for all parent diazines (pyrimidine **1**, pyridazine **2** and pyrazine **3**) and their biradicals and listed in figure 5.11, 5.12 and 5.13. We have investigated and analyzed

the charge densities at all the bond critical points for all the above-mentioned molecules. AIM analysis has been performed at (U)B3LYP/cc-pVTZ level of theory.

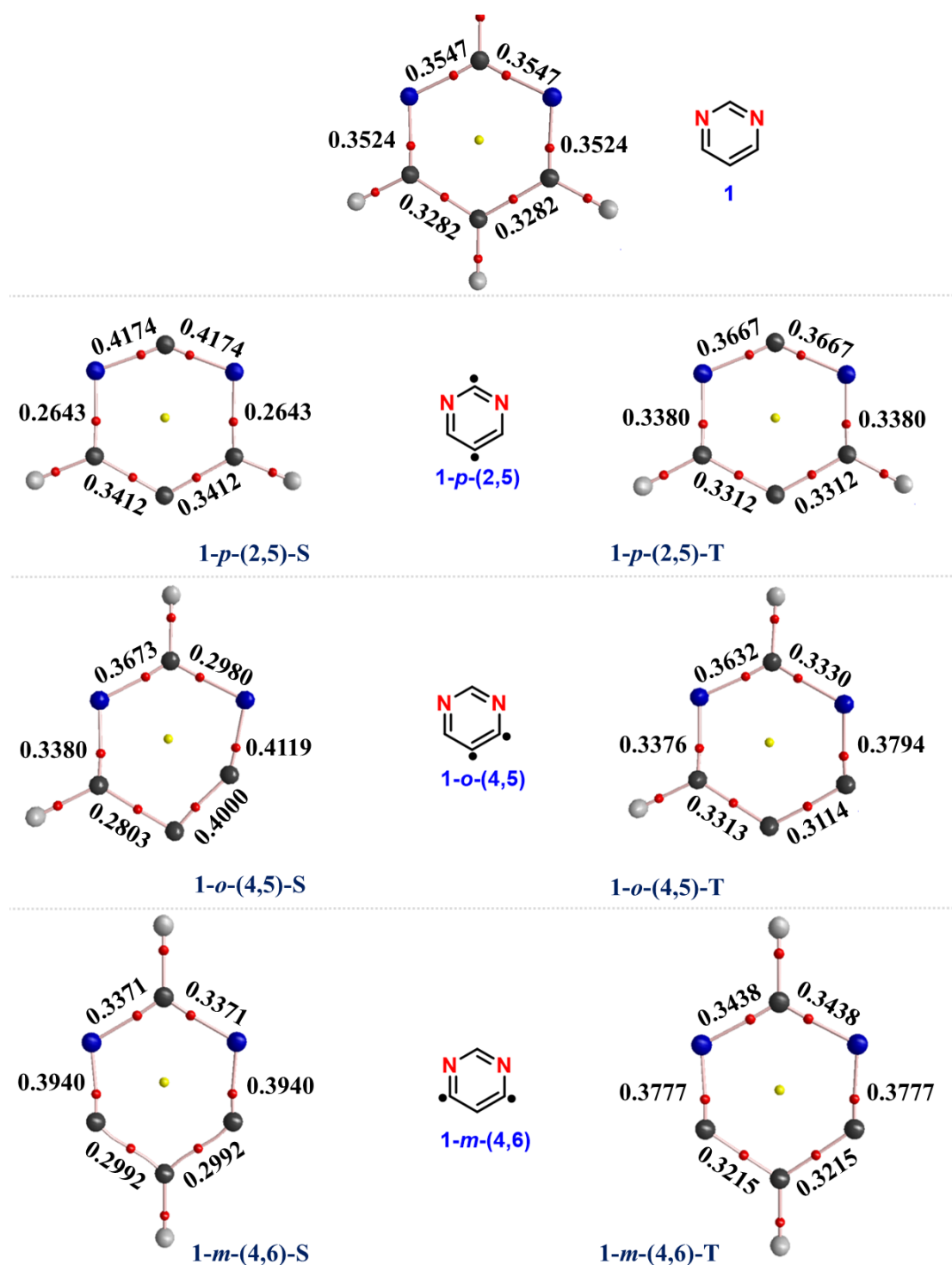


Figure 5.11 AIM analysis of the pyrimidine and didehydropyrimidine biradical isomers with bond critical and ring critical points. The corresponding charge/electron densities of each bond critical point are indicated at (U)B3LYP/cc-pVTZ level of theory.

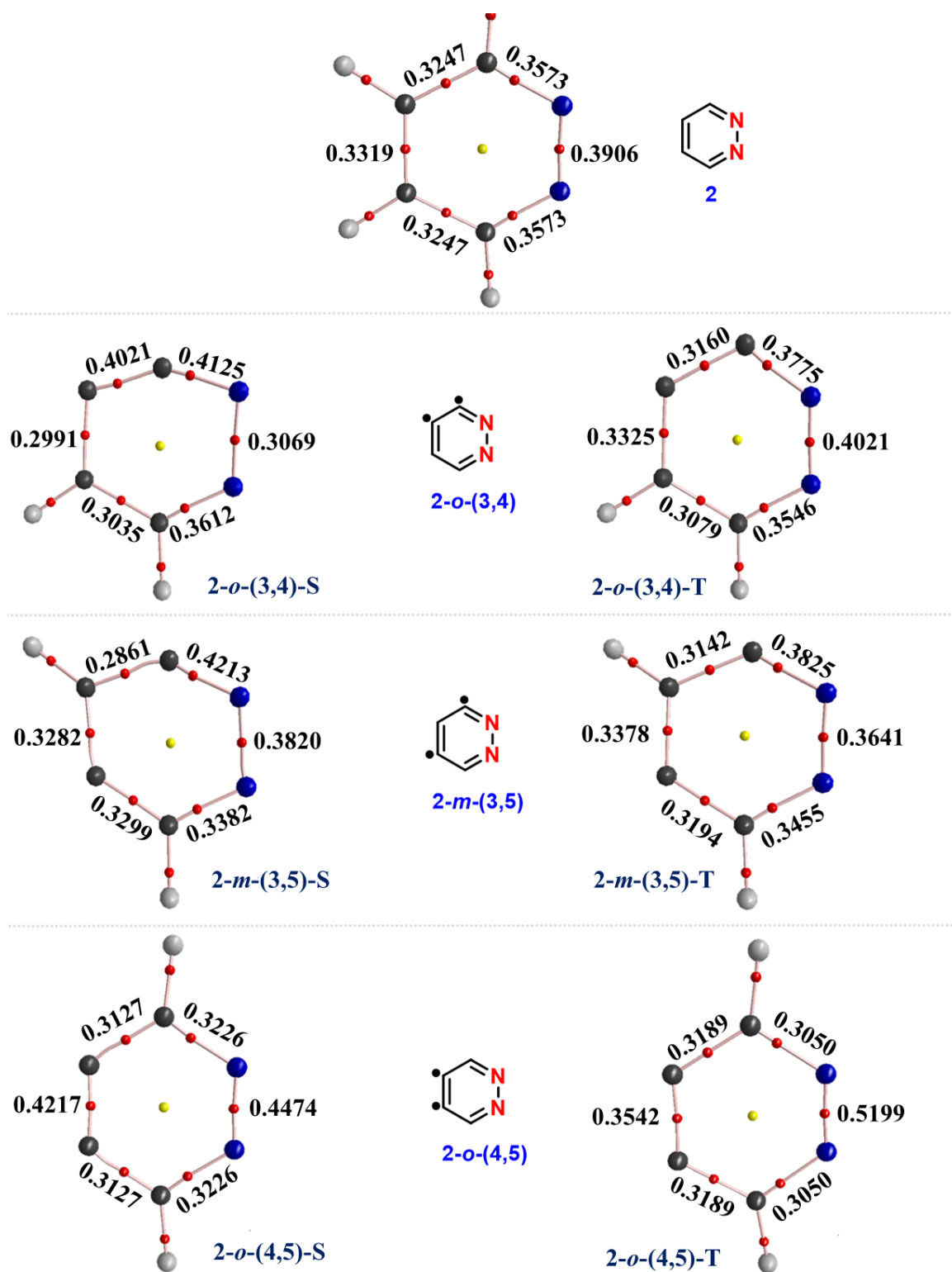


Figure 5.12 AIM analysis of the pyridazine and didehydropyridazine biradical isomers with bond critical and ring critical points. The corresponding charge/electron densities of each bond critical point are indicated at (U)B3LYP/cc-pVTZ level of theory.

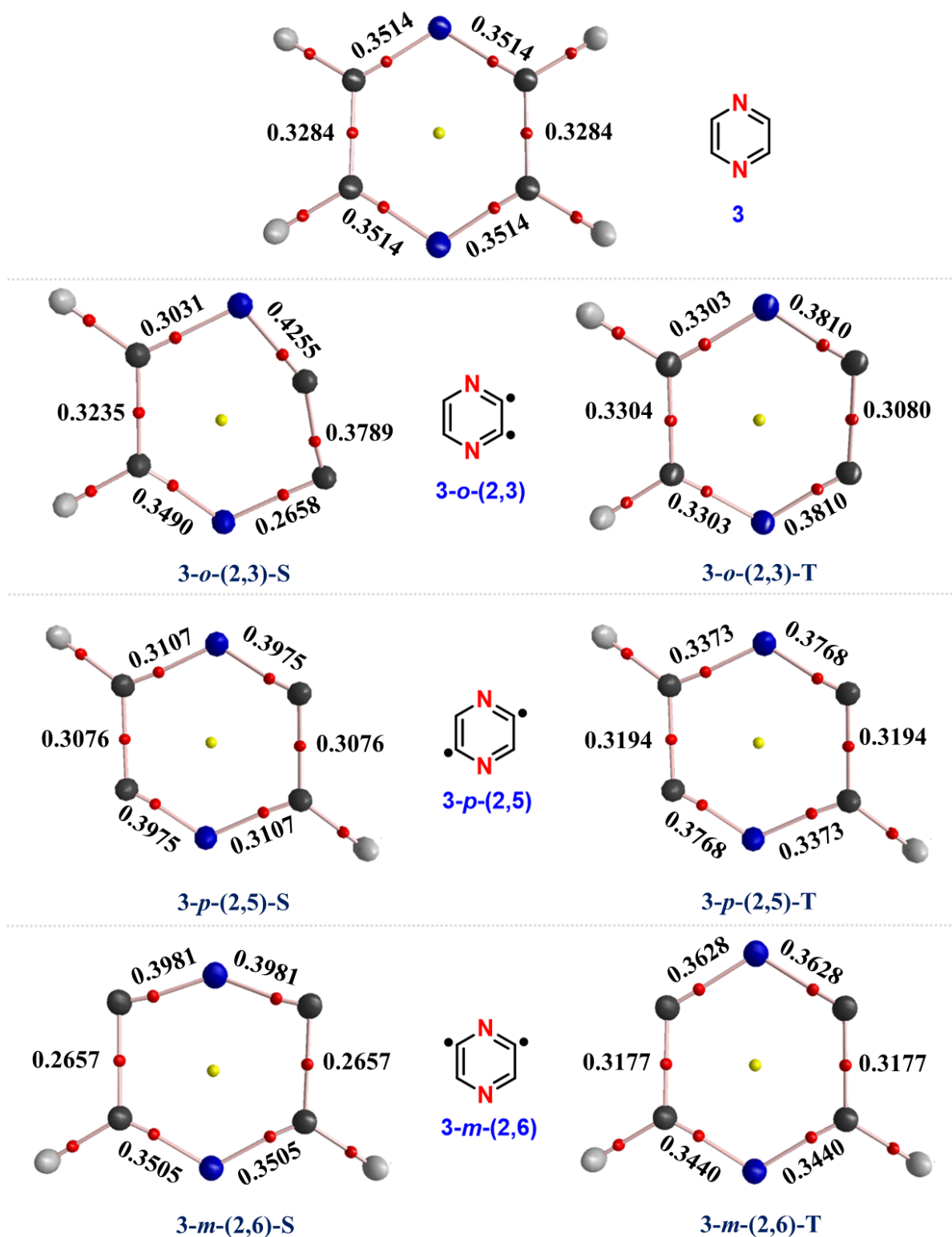
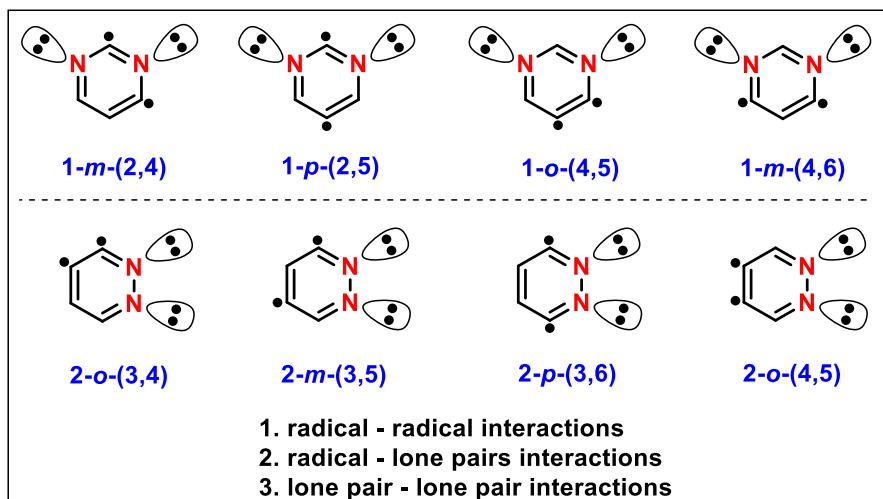


Figure 5.13 AIM analysis of the pyrazine and didehydropyrazine biradical isomers with bond critical and ring critical points. The corresponding charge/electron densities of each bond critical point are indicated at (U)B3LYP/cc-pVTZ level of theory.

In all the cases, we observed that, the increment in charge density between the nitrogen and radical centres, which further confirmed the role of nitrogen lone pairs and their interactions with radical centres. In the cases of 4,5-didehydropyrimidine **1-o-(4,5)**, 3,4-didehydropyridazine **2-o-(3,4)**, 4,5-didehydropyridazine **2-o-(4,5)**, and 2,3-didehydropyrazine **3-o-(2,3)** biradicals where two radicals are *ortho*- to each other, we observed the highest charge density in singlet states at the bond critical point that connects the two radical centres. Also, we have observed a significant increment in the charge densities at the bond critical points, which connects the radical centres with nitrogen atoms. This observation once again proved the open-shell nature of the singlet state.

On the other hand, charge densities at the bond critical points were the lowest in the triplet states of those biradicals mentioned above and also, the increment in the charge densities at those bond critical points which connects the radical with nitrogen atoms. In summary, we have observed a significant change in the charge densities at bond critical points between two radical centres and nitrogen-radical centres in the singlet and triplet states and these changes in the charge densities are the outcomes of through space and through bond interaction between radical-radical and nitrogen lone pair and radical centres.

5.9 Summary of electronic structure of didehydrodiazine biradicals



Scheme 5.3 Didehydropyrimidine and didehydropyridazine biradicals and possible interactions which influence the stability of singlet and triplet state.

In this part, we inspected the stability of didehydrodiazine biradicals singlet and triplet states using multireference calculations. Out of those eight biradicals (didehydropyrimidine and didehydropyridazine) six of them (4,5-didehydropyrimidine **1-o-(4,5)**, 3,4-didehydropyridazine **2-o-(3,4)**, 3,5-didehydropyridazine **2-m-(3,5)** and C_{2v} for 2,5-didehydropyrimidine **1-p-(2,5)**, 4,6-didehydropyrimidine **1-m-(4,6)**, 4,5-didehydropyridazine **2-o-(4,5)**) were found to have singlet as their ground state and two of them (2,4-didehydropyrimidine **1-m-(2,4)**, 3,6-didehydropyridazine **2-p-(3,6)**) were predicted to have a triplet ground state as they are not stable in singlet state. Multireference calculations based molecular orbitals analysis provided the evidence of various possible modes of interactions between radical–radical, radical–lone pairs and lone pair–lone pair. Further, the role of nitrogen lone pairs has been verified by atoms-in-molecule analysis in didehydrodiazine biradicals.

5.10 References

1. Scott, T.; Nieman, R.; Luxon, A.; Zhang, B.; Lischka, H.; Gagliardi, L.; Parish, C. A. A Multireference ab initio Study of the Diradical Isomers of pyrazine. *J. Phys. Chem. A* **2019**, *123*, 2049–2057.
2. Chattopadhyay, S. Simplified Treatment of Electronic Structures of the Lowest Singlet and Triplet States of Didehydropyrazines. *J. Phys. Chem. A* **2019**, *123*, 5980–5994.
3. Cioslowski, J.; Szarecka, A.; Moncrieff, D. Energetics, electronic structures and geometries of didehydroazines. *Mol. Phys.* **2003**, *101*, 839–858.
4. Saraswat, M.; Venkataramani, S. Through Bond and Through Space Interactions in Dehydro-Diazine Radicals: A Case Study of 3c-5e Interactions. *Phys. Chem. Chem. Phys.* **2018**, *20*, 4386–4395.
5. Sah, C.; Jacob, L.; Saraswat, M.; Venkataramani, S. Does a Nitrogen Lone Pair Lead to Two Centered–Three Electron (2c–3e) Interactions in Pyridyl Radical Isomers? *J. Phys. Chem. A* **2017**, *121*, 3781–3791.

Chapter 6. Summary and Outlook

6.1 Summary

Through these investigations, we explored the electronic structure and reactivity of isomeric dehydrodiazine radicals using various quantum chemical calculations. In addition, matrix-isolation infrared spectroscopy has been employed to study the generation and characterization of dehydro- and didehydrodiazine radicals and their photochemistry.

In the first part of the thesis work, we investigated the relative stability of six-isomeric dehydrodiazine radicals (2-dehydropyrimidine **1a**, 4-dehydropyrimidine **1b**, 5-dehydropyrimidine **1c**, 3-dehydropyridazine **2a**, 4-dehydropyridazine **2b** and 2-dehydropyrazine **3a**). We have used various quantum chemical calculations for describing the thermodynamic stability of these six isomeric dehydro-diazine radical isomers and the factors influencing their relative stability. The role of nitrogen lone pairs and their interaction with radical centre has been studied and confirmed using first C-H bond dissociation energies (BDE), radical stabilization energies (RSE), spin densities and electrostatic potential mapping followed by natural bond orbital analysis (NBO) and molecular orbitals analysis. Based on these calculations, we have found that **1b** (4-dehydropyrimidine) is the most stable radical isomer, and **1c** (5-dehydropyrimidine) is the least stable radical isomer among these six dehydro-diazines. Also, the two modes of orbital interaction between lone pairs and radical centre through bond and through space have been identified. To quantify the strength of through bond and through space interactions, we have estimated the proton affinities of nitrogen lone pairs in the presence and absence of the radical centre. Based on these studies, we have confirmed the decisive role of nitrogen lone pairs (through bond and through space interaction) and also the 3c-5e interaction in determining the thermodynamic stability of the six dehydrodiazine radical isomers.

After exploring the relative thermodynamic stability, we investigated the kinetic stability of the six dehydrodiazine radical isomers using isomerization pathways through 1,2-H shift and unimolecular decomposition channels under thermal conditions. The isomerization of dehydrodiazines through 1,2-H shift has been explored by locating the transition states on the PES and the energy barrier was found to be in the range of 60-75 kcal/mol. This isomerization through 1,2-H shift is restricted to only a limited number of radical isomers and the barriers are high (>60 kcal/mol). Therefore, the kinetic stability of these radicals is mainly controlled by the unimolecular dissociation channels. Based on these unimolecular dissociation channels, the resulting kinetic stability order of the diazine radicals is found to

be $2a < 2b < 1b < 1a < 3a < 1c$. Also, we compared the free energy changes associated with the ring-opening step (ΔG) and the free energy of activation (ΔG^\ddagger), which showed an excellent linear correlation. This confirms that the ring-opening step has a strong thermodynamic driving force. Since, all the dehydrodiazines are isoelectronic and have the same number of atoms, we have observed some common ring opening and fragmentation products in the unimolecular dissociation channels. Furthermore, we have observed the molecules such as HCCH, HCN, HNC, CNCN, CN, HCC, HCCCCCH, HCCCN, etc., as the end products in unimolecular dissociation channels, which have also been detected and observed in the interstellar medium.

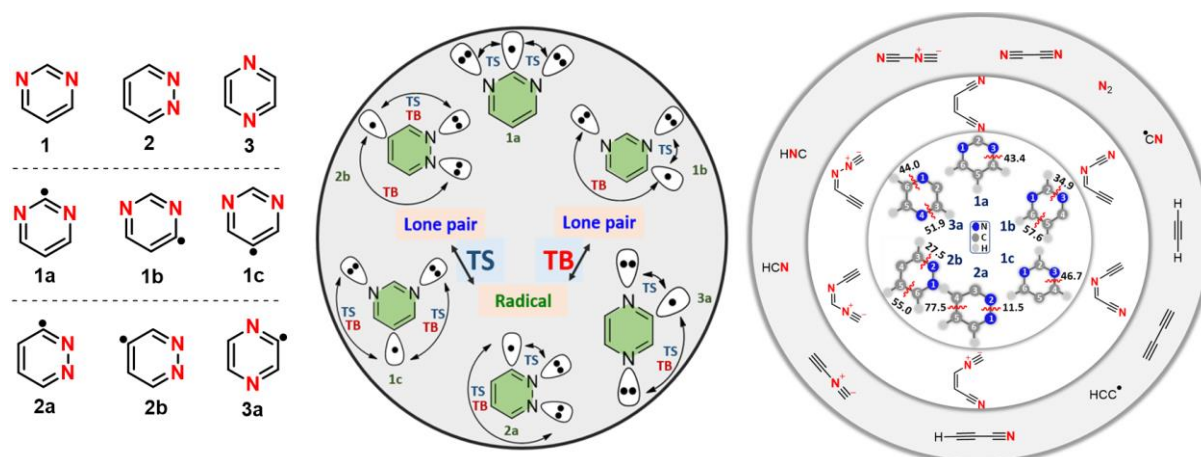


Figure 6.1. Diazines and possible radical isomers, the stabilizing and destabilizing interactions in diazine radicals; Summary of the unimolecular ring decomposition and fragmentation channels of six isomeric dehydro-diazine radicals (the free energy changes corresponding to the first ring-opening steps are given in kcal/mol).

During the initial phase of the thesis, along with computational work on diazine radicals, we were involved in setting up matrix-isolation infrared spectroscopic facility. After completion of the setup, we performed the experiments targeting a set of selected diazine radicals and biradicals.

Initially, the experimental studies, in particular photochemistry of two of the diazine radicals, namely, 2-dehydropyrazine **3a** and 2-dehydropyrimidine **1a** were carried out under matrix isolation conditions. Generally, iodo-precursor show excellent photochemistry in generating radical species under photochemical conditions. Hence, we have chosen commercially available 2-iodopyrazine **46** and 2-iodopyrimidine **48** as precursors using photolysis method. After successful deposition and isolation of 2-iodopyrazine **46** in inert gas matrices, we irradiated at 284 nm for generating the 2-dehydropyrazine radical **3a**. Upon changing the wavelength of irradiation to 350 nm, we observed the regeneration of the

precursor 2-iodopyrazine **46** with the disappearance of some of the signals which were formed at 284 nm irradiation. Based on this evidence, we ascertained the formation of 2-dehydropyrazine radical **3a** at 284 nm, which recombined with iodine radical to form back the precursor at 350 nm. This has been further confirmed by comparing the observed signals with the computed vibrational spectrum of the 2-dehydropyrazine radical **3a**. After successful generation and characterization of 2-dehydropyrazine radical **3a**, we have further irradiated the matrix containing photoproducts with shorter wavelength to understand the photochemistry of 2-dehydropyrazine radical **3a**. Upon irradiation at 254 nm, we observed that 2-dehydropyrazine radical **3a** led to various ring-opened products as well as ring fragmented products. Some of the small fragmented molecules have been identified using the literature assignments. Since some of the signals are new, we needed additional precursors and experiments to obtain insights for new species as well as to characterize them.

Similarly, we have done the experiment with the 2-iodopyrimidine **48**. 2-iodopyrimidine **48** has been synthesized using the 2-chloropyrimidine **49**. In this case also, a similar experimental procedure has been adopted to isolate the precursor in the matrix, and irradiated at 254 nm and 365 nm to generate and characterize the 2-dehydropyrimidine radical **1a**. Also, the photochemistry of 2-dehydropyrimidine radical **1a** has been explored at 254 nm irradiation and the ring-opening and fragmentation products have been identified using the computations and available literature. Upon comparing the experimentally obtained data and the possible photoproducts from 2-dehydropyrazine radical **3a** and 2-dehydropyrimidine radical **1a**, we identified and characterized various new ring-opened radical intermediates (**4**, **19**, **38**, **40**, **41** and **50**, **51**), ring-opened products (*Z/E*-**10**, *Z/E*-**17**, *Z/E*-**26**, *Z/E*-**37**, *Z/E*-**42** and *Z/E*-**66**) along with ring-fragmented small molecules such as HCCNC, HCCCN, HCCH, HCN, HNC and CN radical.

In order to further characterize some of the common ring-opened products from 2-dehydropyrazine radical **3a** and 2-dehydropyrimidine radical **1a**, and also to explore the possibility of diazine biradicals, we have performed the experiments with two of the diiodo derivatives. Firstly, we have chosen the 3,6-diiodopyridazine **52** as a precursor for generating the 3,6-didehydropyridazine **56**. A sample of 3,6-diiodopyridazine **52** in argon or nitrogen matrix at 4 K has been subjected to irradiation at 254 nm, and the photochemistry is followed at different intervals of time by infrared spectroscopy. We could not observe the targeted 3,6-didehydropyridazine biradical **56**, but ended up with some ring-opened products. Upon comparing the experimental data with the computed spectral data, we have assigned them as maleonitrile (*Z*)-**26**, and fumaronitrile (*E*)-**26**, respectively. Based on the computations, we

understood that 3,6-didehydropyridazine biradical is not stable in its singlet state, and so readily follows a barrierless ring opening step forming maleonitrile (**(Z)-26**). Upon further irradiation at 254 nm, maleonitrile (**(Z)-26**) was converted into fumaronitrile (**(E)-26**) under photochemical conditions. Furthermore, interesting *cis-trans* isomerization between maleonitrile to fumaronitrile has been explored with multireference calculations and the involvement of the S₁ state in isomerization has been confirmed through a minimum energy conical intersection (MECI). Also, we synthesized the 4,6-diiodopyrimidine **63** precursor from 4,6-dichloropyrimidine and subjected to matrix isolation experiments for generating 4,6-didehydropyrimidine biradical **65**. The matrix isolation infrared spectroscopic studies under photochemical conditions did not lead to the desired biradical. Instead, we ended up with similar ring fragmented and ring-opening products (**(Z)-66** and **(E)-66**) upon irradiation at 254 nm.

During the investigation of 3,6-didehydropyridazine **56**, 4,6-didehydropyrimidine **65** and 2-dehydropyrazine radical **3a** and their reactivity, we observed that the ring opening steps can involve diazine biradical intermediates. Although we could not isolate, trap and characterize the diradical intermediate in experiments, we have investigated the barrierless ring opening of 3,6-didehydropyridazine **56** to maleonitrile (**(Z)-26**). In order to understand the biradical electronic structure, we have performed computations on these systems using DFT and multireference methods. Since, the electronic structures of didehydrodiazine have 4c-6e interactions between two radical centres and the nitrogen lone pairs, the computational investigations with multireference methods provided great insights on ground state geometries and the stabilities of singlet and triplet states. We have estimated the singlet-triplet energy gaps for characterizing the ground state. The S-T energy gap has been estimated using the vertical energy (VE) and adiabatic energy (AE) gaps for didehydropyrimidine and didehydropyridazines biradicals and utilized the recent reported results on didehydropyrazines.

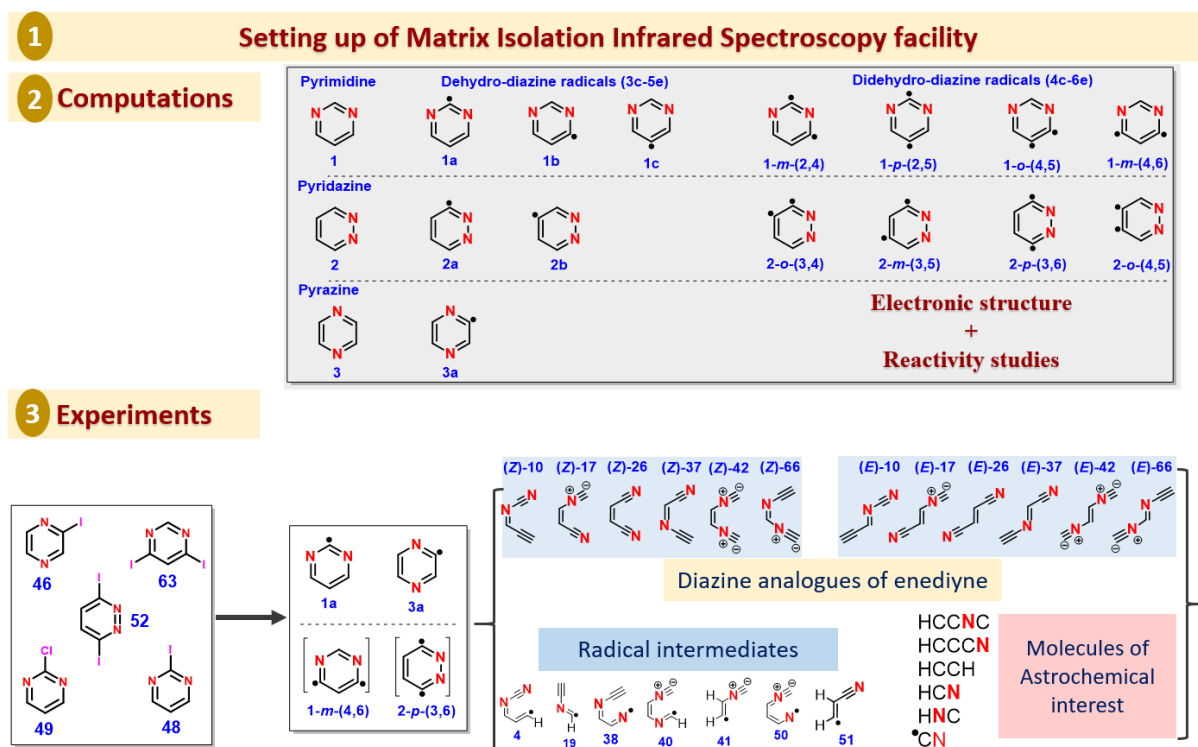


Figure 6.2 Overall summary of the work.

6.2 Outlook for future:

Through these investigations, we have successfully characterized two diazine radicals (2-dehydropyrazine **3a** and 2-dehydropyrimidine **1a**) using matrix isolation experiments among the six possible dehydrodiazine radicals and studied their photochemistry. We have characterized various new ring-opened stable species for the first time, which include diaza-analogues of enediyne with a molecular formula $C_4H_2N_2$. Several known ring-fragmented small molecules of astrochemical interest have also been characterized. Also, we have investigated the ring-opening channels of dehydrodiazine radicals computationally under thermal condition. However, we have not explored the ring-opening of diazine radical under photochemical condition using quantum chemical calculations. Understanding such reactions under photochemical condition demands a very detailed exploration of the excited states potential energy surfaces of all the diazine radicals. Particularly the interaction between nitrogen lone pairs and radical centres contributed to enormous complexity in exploring such reaction channels under photochemical conditions where ring-opening originated from the excited states. It is very challenging to characterize each diazine radical isomer owing to various limitations with respect to the availability of access to their suitable precursor, their kinetic stability and also timeline to the investigations. Attempts towards characterizing the

didehydrodiazine biradicals were unsuccessful and ended up with ring-opened and ring-fragmented molecules. However, these experiments provided supportive evidences to some of the ring-opened species that were observed in the photochemistry of 2-dehydropyrazine **3a** and 2-dehydropyrimidine **1a** radicals. In these experimental studies, we have only used the iodo-precursors for generating diazine radicals and biradicals. All these limitations (in generation and characterization of diazine radicals can be extended using the other possible methods such as flash vacuum pyrolysis or by using alternative precursors such as nitroso, oxalates, etc.

One of the important aspects that we observed during our photochemical experiments was the radical recombination with iodine to form the precursor back, particularly at longer wavelengths (365 nm irradiation). Such phenomena are known in the literature, however, the mechanism for the photo-induced recombination is not known so far. Indeed, we have observed such photoinduced radical recombination process repeatedly in our experiments with a better yield compared to the annealing type experiments. The understanding of exact mechanism of this process is an exciting problem to explore using theory and experiments.

Chapter 7. Materials and Methods

7.1 General Introduction of Matrix Isolation Infrared Spectroscopy

The matrix isolation technique involves the substance (in condensed phase) to be studied in inert medium with a large excess of inert gases (usually argon or nitrogen) at very low temperature. In this method, a sample molecule is trapped in a cavity surrounded by one or more layers of inert material (gases) and is thus “isolated” from the other substrate molecules in a “matrix” of the host gas. In general, the term matrix isolation (coined by George Pimentel) implies various techniques in which a molecule (guest) can be trapped in a rigid material (host) with restricted movement of guest molecules.^[1] This technique allows us to maintain and isolate molecules in a rigid solid (the inert matrix) at very low temperature for various spectroscopic studies. This method is very well suited for isolating and preserving highly reactive species in a solid environment (under matrix isolation condition). This isolation technique can be coupled with various spectroscopic methods to characterize the target species and is known as matrix isolation spectroscopy (MIS). Many new improvements and developments have been introduced in the past years and now matrix-isolation spectroscopy is established as one of the major and important methods used to investigate and characterize reactive intermediates and new species.^[2]

The matrix isolation technique was first developed and introduced by Pimentel and co-workers in 1954. The development of MIS technique was mainly directed towards the systematic studies of highly reactive free radicals and other unstable or transient species. The ability to stabilize reactive species at very low temperature by trapping them in a rigid matrix that results in the inhibition of various intermolecular interactions and reactions, is an important feature of matrix isolation technique.^[3]

Apart from the stabilization and isolation of reactive species, matrix isolation technique provides a number of advantages over more conventional spectroscopic techniques. The very low temperatures (typically 4-20 K) in MI helps in preventing the occurrence of side (any) processes with an activation energy of more than a few kJ mol^{-1} . Also, the isolation of solute (guest) molecules in an inert environment (in rigid matrix) reduces the intermolecular interactions which results in the sharpening of the solute absorption peaks compared to other condensed phases. Although this technique was developed to study reactive species by trapping (isolation) which inhibits intermolecular interactions, it has also provided the methods for studying these interactions (hydrogen bonding interaction) in various molecular complexes

formed under matrix isolation conditions.^[4] Overall, this technique allows us to study and characterized highly reactive molecular fragments, such as free radicals, carbenes, nitrenes and carbocations which are important intermediates for various chemical transformations used in laboratory and industrial reactions, weak molecular complexes that may be stable at low temperatures, and also molecular ions that are produced in plasma discharges or by high-energy radiation, using infrared absorption and laser-excitation spectroscopies.^[5]

7.1.1 Matrix-isolation experimental procedure and set-up

The procedure in matrix isolation experiment requires the solute (guest molecule in any form such as solid, liquid or vapor) to be mixed with a large excess of matrix gas (host inert gas) roughly in 1:1000 ratio of guest and host molecules for better isolation and to avoid molecular aggregation. The mixture is then allowed to deposit over a window (KBr or CsI) transparent in the spectral region to be studied, maintained at low temperature (4 K), and the spectrum is recorded. Different methods are required for the deposition of molecules depending on their vapor pressure. There are different methods available for generating and trapping unstable species under matrix isolation conditions at very low-temperature, depending upon whether the species is generated in the gas phase prior to deposition (over cold window) or in-situ generation after the deposition of suitable precursor(s). In the latter case, the "cage effect" or the choice of matrix host gas plays an important role in determining the products.^[6]

7.1.2 Gas phase generation of unstable species

- (a) Microwave discharge e.g., NCO from the discharge of N₂/CO/Ar
- (b) Flash vacuum pyrolysis (FVP) e.g., CH₃ radical from the pyrolysis of CH₃I or (CH₃)₂Hg

7.1.3 *In-situ* generation of unstable species

- (a) Photolysis e.g., CF₃ from the UV-photolysis of CF₃NNCF₃.
- (b) Atom-molecule reactions e.g., HCO formation from the reaction of H-atoms with CO produced by the photolysis of HI and CO in matrix isolation condition.
- (c) Proton beam irradiation e.g., CCl₃⁺ from the irradiation of CCl₄/Ar.

We have used the photolysis methods for our experiments. After successful deposition of the species without decomposition in the matrix, the trapped and isolated guest species can be activated by either suitable irradiation or by low-temperature annealing methods. The newly

formed species or intermediates due to photoirradiation can be characterized using various spectroscopic measurements like IR, UV-Vis, Raman, ESR, etc.^[7]

7.1.4 Host materials for matrix-isolation spectroscopy

In general, every substance that can be frozen at low temperature can be a potential host material for the matrix-isolation experiments. The examples include N₂, CO₂, SF₆, N₂O, CH₄ etc. All of them can be solidified at low temperatures (4–20 K) but they also have few disadvantages of relatively strong interactions with the guest species.^[8] The most commonly used host materials for the matrix isolation experiments are solid noble gases (Ne, Ar, Kr, and Xe) which are known to have very minor or almost negligible interactions with the trapped guest species. The aforementioned host gases were first employed by G. Pimentel in 1954 and offer three main advantages:

- they form clear glasses at very low temperature,
- they show transparency through the IR, Vis, and UV regions of the spectrum,
- they are, for most guests, chemically inert (not reactive with guest molecules).

7.1.5 Deposition of precursor (guest) molecules

The matrix has to be formed with the co-deposition of host (inert gases) and guest molecules (precursor for study) onto a cold window (at 4K) roughly in a ratio of 1:1000 (guest and host) for the very sharp features in the spectrum. Solids and liquids should have a sufficient vapor pressure (about 10⁻⁶ mbar) at low temperatures (4–10 K) so that it would not lead to decomposition. For the co-deposition, it is necessary to introduce the precursor molecules in the gas-phase to mix with inert gas to be trapped in the matrix.^[9]

These are some efficient ways of introducing the vapor of precursor (guest molecules) with the flow of inert gases for the co-deposition over the cold window during the matrix experiment:

(a) If the guest molecule (in solid and liquid form) has a significantly high vapour pressure under high vacuum condition, the vapour pressure can be controlled by thermal methods to evaporate the precursor molecules at a certain rate by extra cooling. This could be done by lowering the temperature of guest molecules using ice or liquid nitrogen.

(b) If the guest molecule (precursor) has low volatility compound, and also very low vapour pressure, this can be controlled by external heating. The rate of evaporation can be increased by heating the sample up to several hundred degrees.

(c) Laser ablation method is also useful in the deposition process especially for molecules containing transition metals.

7.1.6 Photochemistry and detection of unstable species

After the successful deposition of molecules (precursor), various reactive and unstable species can be generated via photochemically induced processes by irradiation at suitable wavelengths using high pressure mercury/xenon lamps or lasers or LEDs. Upon irradiation, these newly formed unstable species or intermediates can be trapped in the inert gas matrix at low temperature. Detection of these new species is possible with the help of various spectroscopic techniques such as NMR, ESR, IR, Raman, UV-Vis, Mossbauer, laser-excitation and photoelectron spectroscopies along with neutron scattering, circular dichroism and X-ray methods.^[10]

We have coupled this matrix-isolation technique with the infrared spectroscopic methods for characterizing free radicals. Infrared spectroscopy provides various advantages over other spectroscopies such as transparency of nitrogen and the rare gas matrices in entire infrared spectral region, typically sharp infrared absorptions in matrices with half bandwidths between 0.5 cm^{-1} and 2 cm^{-1} due to quenched rotational motion (by trapping) and Doppler broadening at low temperature. Also, the infrared spectroscopy is very sensitive towards the local environment, and is very useful for understanding the various possible molecular conformations and weak bimolecular complexes.

7.1.7 Matrix-Isolation FTIR Spectroscopy setup in our lab at IISER Mohali

Components of this set up and their uses:

- (a) **Glass oven:** A Buchi glass oven has been used for heating the sample for precursor deposition on to cold KBr window. (Figure 7.1a)
- (b) **Flow Controller:** MKS flow controller has been used for controlling the flow of inert gases during co-deposition of precursor with matrix host gas. This flow controller was connected with the mixing chamber which was filled with the inert gas. (Figure 7.1b and figure 7.3)
- (c) **Cryostat:** A closed cycle cryostat is the heart of matrix-isolation setup. This cryostat contains a transparent KBr window which cooled down to low temperature (4 K) with the help of closed cycle helium compressor connected to the cryostat by two lengths of high-pressure steel bellows tubing. (Figure 7.1c and figure 7.3)

- (d) **Compressor:** A close cycle He compressor has been used for cooling and maintaining the temperature of the cryostat throughout the experiment at 4 K. (Figure 7.1d and figure 7.3)
- (e) **Gas cylinders:** High purity (99.9995 %) gas cylinders of argon and nitrogen gases were used in experiments for trapping reactive species in inert matrices at low temperature. (Figure 7.1e)
- (f) **Rotary vane pump:** High vacuum pumps are required for evacuating the cryostat before cooling to 4 K as well as for evacuating the sample holder and mixing chamber. Rotary vane pump provides the initial vacuum in the order of 10^{-3} mbar. (Figure 7.1f and figure 7.3)
- (g) **Diffusion pump:** A conventional oil diffusion pump backed by a rotary vane pump provides the vacuum of up to the 10^{-6} mbar order for the experiments at low temperature. (Figure 7.1g and figure 7.3)
- (h) **UV-Light Source:** This light source (KiloArc Broadband Arc Lamp Light Source from HORIBA Scientific) has been used for inducing the photochemical process using different wavelengths. This light source is coupled with a monochromator and is suitable for irradiation between 254 nm to 900 nm range. (Figure 7.1h)
- (i) **Mixing Chamber:** Mixing chamber has been used for filling matrix host gases such as argon and nitrogen from the gas cylinders. Mixing chamber is also kept under a vacuum of 10^{-3} order mbar before filling the inert gases to minimize the water and carbon dioxide concentration. (Figure 7.1i and figure 7.3)
- (j) **Deposition Unit:** Deposition unit has been designed and fabricated for the solid and liquid samples and is also kept under high vacuum similar to cryostat. Sample (precursor) taken in a glass capillary is kept in the deposition unit and allowed to mix with the inert gases for co-deposition onto the cold KBr window by opening and closing the valve. (Figure 7.1j and figure 7.3)
- (k) **FTIR Spectrometer:** Bruker Tensor II Fourier transform infrared spectrometer (vibrational spectroscopy) has been used for the characterization of free radicals and intermediates in this work. (Figure 7.1k and figure 7.3)
- (l) **Chillers:** Two chillers are a part of this matrix-isolation setup. One chiller has been used with the diffusion pump and another chiller has been used with the He compressor. (Figure 7.1l)

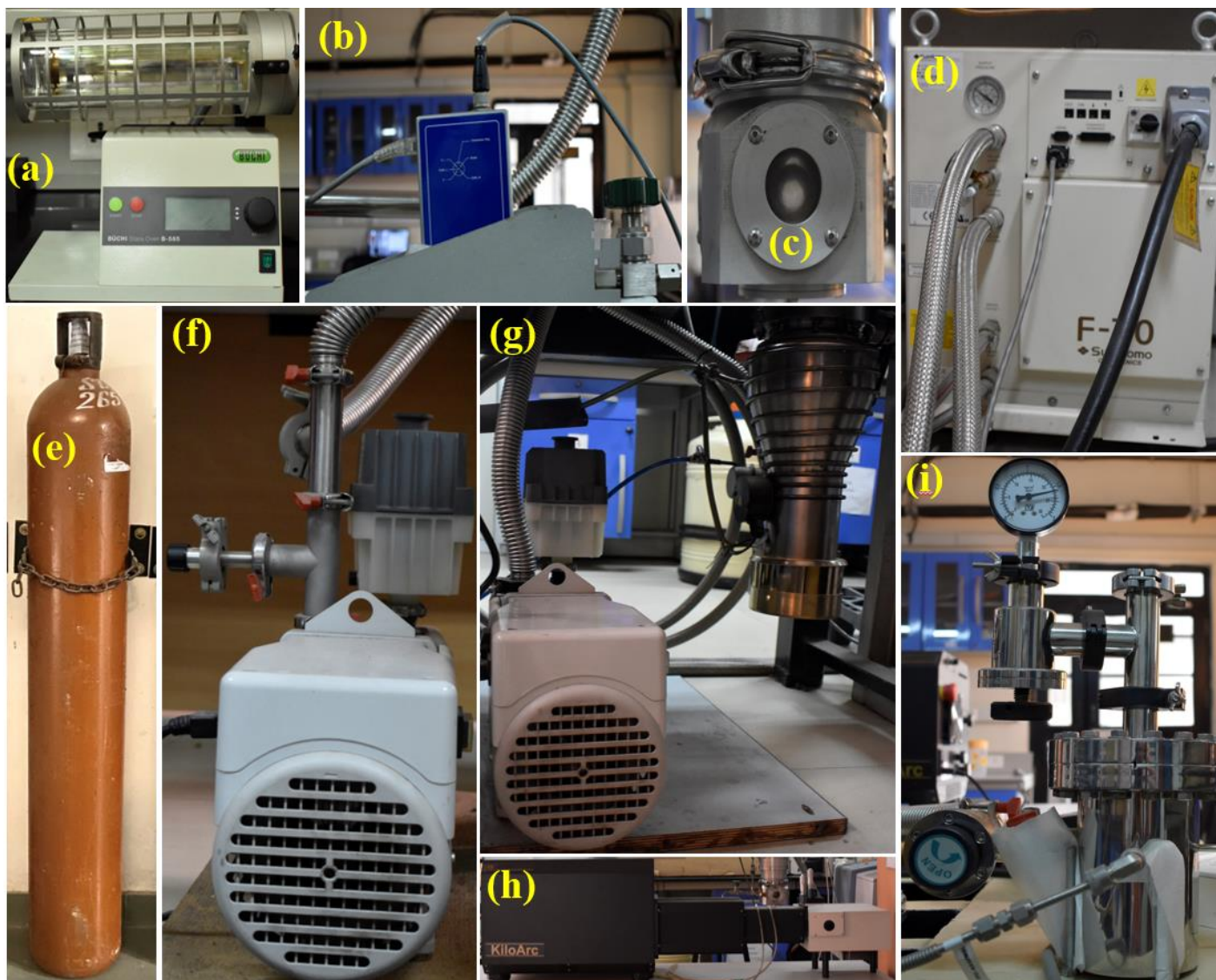


Figure 7.1 Images of each component of matrix-isolation setup.



Figure 7.2 Remaining parts of matrix-isolation setup (j) designed deposition unit; (k) FTIR spectrometer; (l) chiller.

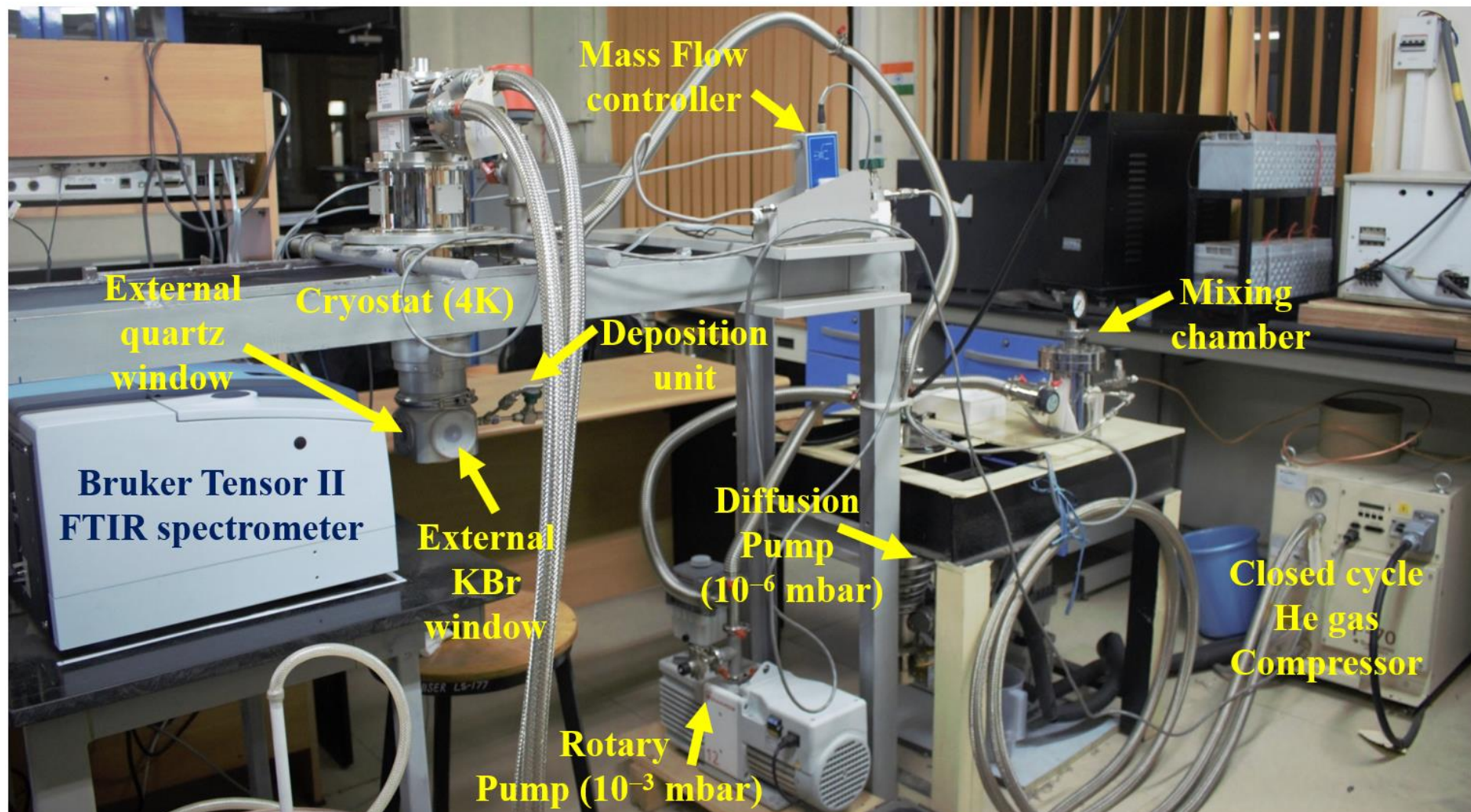


Figure 7.3 Matrix-isolation FTIR facility in our lab at IISER Mohali.

7.2 Computational details

The advancement of spectroscopic techniques joins hands with the quantum mechanics approaches and both of them are still improving to their maximum accuracy and measurements. Computational chemistry (originated from the calculations using quantum mechanics principles/methods) plays a major role in understanding the results obtained from the various spectroscopic methods. In this regard, we have also performed various quantum chemical calculations throughout this work to explain the results obtained from the matrix isolation infrared spectroscopy as well as to understand the electronic structures, relative stability, energies and reactivity aspects throughout the work.^[11]

7.2.1 Basic quantum chemistry approach

All the quantum chemistry approaches/methods are derived from the fundamental Schrödinger equation $H\psi = E\psi$.

Evolution is the basic tendency of nature which applies in this case too. In recent times, quantum chemical calculations have evolved like no other compared to where it started. All thanks to theoretical scientists around the globe for their prolific contributions in this area, starting from the basic Hartree-Fock methods to density functional theory to multireference methods by introducing various approximations to describe the electron correlation. The electron density is used in DFT as the fundamental property unlike Hartree-Fock theory which deals directly with the many-body wavefunction. The many-body electronic wavefunction is a function of $3N$ variables (the coordinates of all N atoms in the system) the electron density is only a function of x, y, z -only three variables. The Hohenburg-Kohn theorem emphasizes that the density of any system determines all ground-state properties of the system. By focusing on the electron density, it is possible to derive an effective one-electron-type Schrödinger equation.^[12]

7.2.2 Levels of theory (methods) used in this work

Density functional theory-based calculations have been used quite extensively in chemistry to investigate electronic properties, electronic structures and energies. We have used various DFT based computations/calculations for the dehydro-diazines electronic structure and reactivity studies as well as for comparison with matrix isolation infrared spectroscopy results. We mainly used B3LYP^[13] and M06-2X^[14] functionals extensively for various calculations (chapter 2). Apart from that, we used multireference or multiconfigurational methods (CASSCF)^[15] for describing the electronic structures of diazines biradicals (chapter 5) and to understand the various possible

orbital interactions. Also, we have used coupled cluster CCSD(T)^[16] methods for single point (only energy) calculations. In addition to that, we have used composite methods (CBS-QB3)^[17] for estimating the thermochemical data such as BDE, RSE and PA. This composite method (CBS-QB3) is known for better accuracy for estimating thermochemical data.

7.2.3 Basis sets used in this work

We have mainly used the cc-pVTZ basis set for electronic structure and reactivity studies of dehydro-diazines radicals throughout this work. Also, we have compared the obtained matrix isolated spectrum with the vibrational spectrum computed at DFT using cc-pVTZ^[18] basis set. However, we used DGTZVP^[19] basis set for the molecules containing iodine (iodo precursor). Apart for that, we have also used other basis sets such as 6-311++G(d,p), cc-pVDZ, aug-cc-pVDZ, aug-cc-pVTZ, cc-pVQZ and aug-cc-pVQZ to check the consistency of results in the relative stability of dehydro-diazines (chapter 2a).

Additionally, we have used the cc-pVDZ and cc-pVTZ basis set with CASSCF calculations for understanding the mechanism of cis-trans (*Z/E*) isomerization in maleonitrile to fumaronitrile (chapter 4) and in biradicals electronic structure (chapter 5) respectively.

7.2.4 Geometry optimization and frequency calculations

The first step towards exploring electronic structure is geometry optimization. Geometry optimization stands for the geometry at which the molecule possesses minimum energy or in other words, locating the minimum energy geometry is called geometry optimization. This is a necessary step because most of the molecules naturally exist in their lowest energy form. So, if we need to calculate certain energy related quantities, we have to estimate these quantities using the minimum energy geometry. In order to verify the minimum energy geometry, we have to perform frequency calculations. If all the frequencies are positive, it implies the minima over the potential energy surface (PES). One imaginary frequency provides an indication about the saddle point on the PES or the transition state. We can estimate all the energy terms like electronic energy, zero-point vibrational energy (ZPVE), enthalpy, Gibbs free energy and entropy along with heat capacity with the help of frequency calculations.

7.2.5 Spin density and Molecular orbitals

Spin density in a molecule is defined as the difference in the number of electrons occupying the α - and β - spin. One and two are the values of total spin density in monoradicals and biradicals (triplet state) respectively. Analysis of the spin density distribution provides insights on the

localization or delocalization of unpaired electrons (spin) within the molecule.^[20] As we know, delocalization of unpaired electrons (spin) provides the extra stability to the radical. Extent of spin delocalization to nearest atoms also provides indirect information about the possible interaction of nearby atoms with radical centres.

Additionally, we explored the molecular orbitals for a better understanding of the electronic structure and the interaction of radical centres (SOMO) with the heteroatom lone pair wherever necessary. We have performed the multireference calculation for analysing the molecular orbitals. Also, the orbital occupancies corresponding to molecular orbitals help in understanding the nature and multireference character of radical species.

7.2.6 Natural Bond Orbital (NBO) Analysis

We performed the natural bond orbital (NBO) calculations to understand the orbital interactions (between radical centre and nitrogen lone pairs) while exploring the electronic structures of dehydrodiazine radicals (Chapter 2). NBO calculations require two sets of orbitals named donor and acceptor orbitals in which one-centre is considered as the "lone pairs" or "radical centre" and two-centre is considered as "bonds".^[21] Using the second order perturbation theory, the orbital interaction energies can be estimated with the help of effective overlap between the donor and acceptor orbitals according to the formula as follows:

$$E(2) = \Delta E_{ij} = q_i \frac{F(i,j)^2}{\varepsilon_j - \varepsilon_i}$$

where q_i is the donor orbital occupancy, ε_i and ε_j are the diagonal elements (orbital energies) and $F(i,j)$ is the off-diagonal NBO Fock matrix element.

We have used the NBO calculations for estimating the interaction energies between the nitrogen lone pair orbitals and unpaired electron orbital (radical centre). Based on the NBO analysis, we estimated the orbital interaction energies corresponding to the direct overlap of nitrogen lone pair orbital with radical orbital which is defined as "Through space" (TS) interaction. Also, NBO calculations provide useful interaction energies in which radical centres interact with other atoms via an intervening bond known as "Through Bond" (TB) interaction. We have discussed the relative stability of dehydrodiazine radical isomers using TS and TB interaction energies estimated using NBO calculations.

7.2.7 Atoms in molecules (AIM) Analysis

Atoms in molecules (AIM) calculations have also been performed for understanding the electronic structures of dehydrodiazines radicals in chapter 2. AIM calculations help us in understanding the electronic charge density distribution within a molecule.^[22] Thus, it determines directly the shapes and sizes of molecules, their electrical moments and, most of their chemical and physical properties. Since the charge density describes the distribution of negative charge in real space, it is a physically measurable quantity. Consequently, when used as a basis for the discussion of chemistry, the charge density allows for a direct physical picture and interpretation. We have estimated the charge (electron) densities between two successive atoms within the ring in diazines. Also, we have estimated the electron density before and after creating the radicals and closely inspected the change in electron density which arises due to the interaction between the lone pairs and unpaired electrons in dehydro-diazines. AIM calculations further provided proof for the existence of nitrogen lone pair interactions with radical centres.

All these above-mentioned calculations were performed using the Gaussian09 suite of programs.^[23]

7.2.8 Multireference Methods

Multireference method is a general approach for describing a chemical system in which a single electron configuration is no longer appropriate for describing the electronic state. This commonly happens in reactions which involve breaking and formation of bonds, radicals, diradicals, triradicals or transition metals of first row.

A single determinant, RHF wave function does not dissociate properly for homolytically bond breaking in close shell molecule. UHF wave function provides a qualitatively good picture but results are often poor and the wave function is no longer an eigenfunction of spin operator $\langle S^2 \rangle$. Solution To keep a spin eigenfunction, we need to include at-least two determinants in our zeroth order wave function to homolytically break a single covalent bond for a close shell molecule, because of dissociation there should be two degenerate electron configuration σ and σ^* .

In this regard, multi reference methods and configuration interaction methods are needed to improve the description of the electron correlation.^[24] These methods are

- (i) MCSCF eg. CASSCF
- (ii) Multireference single and double Configuration Interaction (MRCISD)
- (iii) N-electron valence state perturbation theory (NEVPT)

We performed CASSCF calculation for understanding the nature of interaction between nitrogen lone pairs and radicals in dehydrodiazine radicals and didehydrodiazine biradicals. Also, to understand the electronic structure didehydrodiazine biradicals and their singlet-triplet energy gaps. In MCSCF, orbitals are obtained not as those which minimize the energy of a single determinant as in HF theory, but as those which minimize the Configuration Interaction energy of the MCSCF wave function.

$$\psi = \sum_{i=0} C_i \phi_i$$

or

$$\psi = C_0 \phi_0 + C_1 \phi_1 + C_2 \phi_2 + C_3 \phi_3 + \dots \dots \dots C_n \phi_n$$

Defining of active space in CASSCF calculations is the most crucial part as the obtained results depends on the choice of used active space. It is necessary to include at least those orbitals in active space which involved in the transformation. We performed CASSCF calculations using active space of 11 electrons and 9 orbitals for dehydrodiazine radicals, and 12 electrons and 10 orbitals for didehydrodiazine biradicals which includes both the nitrogen lone pairs, radical orbital(s) and benzene type six- π orbitals ($3-\pi$ and $3-\pi^*$). MCSCF calculations were performed for each dehydrodiazine radical, didehydrodiazine biradical using the MOLPRO program.^[25]

7.3 References

1. Whittle, E.; Dows, D. A.; Pimentel, G. C. Matrix Isolation Method for the Experimental Study of Unstable Species. *J. Chem. Phys.* **1954**, 22, 1943.
2. Pimentel, G. C.; Charles, S. W. Infrared Spectral Perturbations in Matrix Experiments. *Pure and Applied Chemistry*, **1963**, 7, 111–124.
3. Norman, I.; Porter, G. Trapped Atoms and Radicals in a Glass ‘Cage’. *Nature* **1954**, 174, 508–509.
4. Destexhe, A.; Smets, J.; Adamowicz, L.; Maes, G. Matrix Isolation FT-IR Studies and Ab Initio Calculations of HydrogenBonded Complexes of Molecules Modeling Cytosine or Isocytosine Tautomers. 1. Pyridine and Pyrimidine Complexes with Water in Argon Matrixes. *J. Phys. Chem.* **1994**, 98, 1506–1514.
5. Almond, M. J.; Wiltshire, K. S. Matrix Isolation. *Annu. Rep. Prog. Chem. Sect. C: Phys. Chem.* **2001**, 97, 3–60.
6. Dunkin, I. R. Matrix-Isolation Techniques: A Practical Approach. The Practical Approach in Chemistry Oxford Press, New York, **1998**.
7. Perutz, R. N. Photochemistry of small molecules in low-temperature matrixes. *Chem. Rev.* **1985**, 85, 97–127; (b) Rest A.J. Generation and Trapping of Unstable Solutes in Low Temperature Matrices. Springer, **1981**.
8. Meyer, B. ‘Low Temperature Spectroscopy’, Elsevier, New York, **1971**.
9. Cradock, S.; Hinchcliffe, A. J. Matrix Isolation Cambridge University Press, Cambridge, **1975**.

10. Dunkin, I. R. The matrix isolation technique and its application to organic chemistry. *Chem. Soc. Rev.* **1980**, 9, 1–23.
11. Chatfield, D.; Cramer, C. J. Essentials of Computational Chemistry: Theories and Models. *Theor. Chem. Acc.* **2002**, 108, 367–368.
12. Cheng, G.-J.; Zhang, X.; Chung, L. W.; Xu, L.; Wu, Y.-D. Computational Organic Chemistry - Bridging Theory and Experiment in Establishing the Mechanisms of Chemical Reactions. *J. Am. Chem. Soc.* **2015**, 137, 1706–1725.
13. Becke, A. D. Density-Functional Thermochemistry. III. The Role of Exact Exchange. *J. Chem. Phys.* **1993**, 98, 5648–5652; (b) Lee, C.; Yang, W.; Parr, R. G. Development of The ColleSalvetti Correlation-Energy Formula into A Functional of The Electron Density. *Phys. Rev. B: Condens. Matter Mater. Phys.* **1988**, 37, 785–789.
14. Zhao, Y.; Truhlar, D. G. The M06 Suite of Density Functionals for Main Group Thermochemistry, Thermochemical Kinetics, Noncovalent Interactions, Excited States, And Transition Elements: Two New Functionals and Systematic Testing of Four M06-Class Functionals and 12 Other Functionals. *Theor. Chem. Acc.* **2008**, 120, 215–241.
15. M. J. Frisch, I. N. Ragazos, M. A. Robb, and H. B. Schlegel, An Evaluation of 3 Direct MC-SCF Procedures. *Chem. Phys. Lett.* **1992**, 189, 524–28.
16. (a) Pople, J. A.; Krishnan, R.; Schlegel, H. B.; Binkley, J. S. Electron Correlation Theories and Their Application to the Study of Simple Reaction Potential Surfaces. *Int. J. Quantum Chem.* **1978**, 14, 545–560; (b) Purvis, G. D., III; Bartlett, R. J. A Full Coupled-Cluster Singles and Doubles Model - The Inclusion of Disconnected Triples. *J. Chem. Phys.* **1982**, 76, 1910–1918.
17. Montgomery Jr., J. A.; Frisch, M. J.; Ochterski, J. W.; Petersson, G. A. A complete basis set model chemistry. VII. Use of the minimum population localization method *J. Chem. Phys.* **2000**, 112, 6532–6542.
18. (a) Kendall, R. A.; Dunning, T. H., Jr; Harrison, R. J. Electron Affinities of The First-Row Atoms Revisited. Systematic Basis Sets and Wave Functions. *J. Chem. Phys.* **1992**, 96, 6796–6806; (b) Dunning Jr., T. H. Gaussian basis sets for use in correlated molecular calculations. I. The atoms boron through neon and hydrogen. *J. Chem. Phys.* **1989**, 90, 1007–1023.
19. Weigend, F.; Ahlrichs, R. Balanced basis sets of split valence, triple zeta valence and quadruple zeta valence quality for H to Rn: Design and assessment of accuracy. *Phys. Chem. Chem. Phys.* **2005**, 7, 3297–3305.
20. Glaser, R.; Choy, G. S. – C. Spin Polarization versus Spin Delocalization. Topological Electron and Spin Density Analysis of the Rotational Automerization of Allyl Radical Including Electron Correlation Effects. *J. Phys. Chem.* **1994**, 98, 11379–11393.
21. (a) Carpenter, J. E.; Weinhold, F. Analysis of the Geometry of the Hydroxymethyl Radical by the Different Hybrids for Different Spins Natural Bond Orbital Procedure. *J. Mol. Struct: THEOCHEM* **1988**, 169, 41–62; (b) Foster, J. P.; Weinhold, F. Natural Hybrid Orbitals. *J. Am. Chem. Soc.* **1980**, 102, 7211–7218.
22. Bader, R. F. W. A quantum theory of molecular structure and its applications. *Chem. Rev.* **1991**, 91, 893–928.
23. Frisch, M. J.; Trucks, G. W.; Schlegel, H. B.; Scuseria, G. E.; Robb, M. A.; Cheeseman, J. R.; Scalmani, G.; Barone, V.; Petersson, G. A.; Nakatsuji, H.; et al. Gaussian 09, revision C. 01; Gaussian, Inc.: Wallingford, CT, 2009.
24. (a) Eade, R. H. A.; Robb, M. A. Direct Minimization in MC SCF Theory - The Quasi-Newton Method. *Chem. Phys. Lett.* **1981**, 83, 362–368; (b) Frisch, M. J.; Ragazos, I. N.; Robb, M. A.; Schlegel, H. B. An Evaluation of Three Direct MC-SCF Procedures. *Chem. Phys. Lett.* **1992**, 189, 524–528.
25. Werner, H. J.; Knowles, P. J.; Knizia, G.; Manby, F. R.; Schütz, M.; Celani, P.; Györffy, W.; Kats, D.; Korona, T.; Lindh, R. MOLPRO, version 2012.1, A Package of Ab Initio Programs; 2012.

Appendix

Table A1: Electronic and thermodynamic parameters of all the species at (U)B3LYP/cc-pVTZ (bold) and (U)M06-2X/cc-pVTZ (normal) levels of theory.

Species	Zero-point corrected Electronic energy (E)	ZPVE (Hartree)	Lowest frequency (cm ⁻¹)	Spin Contamination		Point group	Electronic state	Free Energy (G) (Hartree)	Enthalpy (H) (Hartree)	Entropy (S) (Cal/Mol-Kelvin)
				Before annihilation	After annihilation					
1	-264.339234	0.076862	353.8	0.0000	0.0000	C _{2v}	¹ A ₁	-264.365926	-264.334112	66.958
	-264.228478	0.077622	359.4	0.0000	0.0000			-264.255154	-264.223379	66.877
1a	-263.669791	0.063775	382.1	0.7551	0.7500	C _{2v}	² A ₁	-263.697053	-263.664684	68.127
	-263.561618	0.064591	388.6	0.7588	0.7500			-263.588858	-263.556551	67.996
1b	-263.673622	0.063924	350.1	0.7547	0.7500	C _s	² A'	-263.701528	-263.668527	69.456
	-263.564174	0.064734	355.6	0.7580	0.7500			-263.592059	-263.559115	69.337
1c	-263.660972	0.063895	381.5	0.7568	0.7500	C _{2v}	² A ₁	-263.688232	-263.655876	68.099
	-263.551612	0.064724	383.5	0.7621	0.7500			-263.578850	-263.546555	67.972
2	-264.304312	0.076053	377.5	0.0000	0.0000	C _{2v}	¹ A ₁	-264.331032	-264.299144	67.113
	-264.191147	0.077012	385.0	0.0000	0.0000			-264.217839	-264.186022	66.965
2a	-263.634972	0.062825	355.0	0.7550	0.7500	C _s	² A'	-263.662944	-263.629767	69.826
	-263.523334	0.063783	363.7	0.7589	0.7500			-263.551265	-263.518203	69.584
2b	-263.631428	0.062843	375.9	0.7566	0.7500	C _s	² A'	-263.659350	-263.626301	69.557
	-263.518414	0.063771	379.0	0.7623	0.7500			-263.546318	-263.513327	69.435
3	-264.332819	0.076662	351.4	0.0000	0.0000	D _{2h}	¹ A _g	-264.358846	-264.327711	65.530
	-264.221159	0.077562	363.9	0.0000	0.0000			-264.247162	-264.216088	65.399
3a	-263.665757	0.063813	365.2	0.7553	0.7500	C _s	² A'	-263.693658	-263.660667	69.437
	-263.554966	0.064487	371.4	0.7589	0.7500			-263.582849	-263.549906	69.334
4	-263.618749	0.058714	128.6	0.7645	0.7501	C _s	² A'	-263.648754	-263.611941	77.481
	-263.507590	0.059776	115.6	0.7783	0.7502			-263.537535	-263.500849	77.211
5	-186.235630	0.025284	228.4	0.7544	0.7500	C _s	² A'	-186.261526	-186.230630	65.027
	-186.157254	0.025933	233.8	0.7563	0.7500			-186.183170	-186.152319	64.931
6	-77.336562	0.026990	653.2	0.0000	0.0000	D _{∞h}	¹ Σ _g	-77.355511	-77.332815	47.768
	-77.296981	0.027516	711.4	0.0000	0.0000			-77.315901	-77.293301	47.565
7	-186.185959	0.025749	249.9	0.7549	0.7500	C _s	² A'	-186.212147	-186.181036	65.479

Appendix

	-186.112306	0.026173	255.1	0.7570	0.7500			-186.138473	-186.107409	65.381
8	-93.423038	0.015618	470.1	0.0000	0.0000	$C_{\infty v}$	$^1\Sigma_g$	-93.442539	-93.419239	49.039
	-93.385897	0.016016	529.0	0.0000	0.0000			-93.405340	-93.382185	48.735
9	-92.740886	0.004905	2153.2	0.7579	0.750	$C_{\infty v}$	$^2\Sigma_g$	-92.760559	-92.737581	48.362
	-92.704593	0.005096	2237.0	0.7651	0.750			-92.724251	-92.701288	48.328
(Z)-10	-263.056271	0.048711	106.7	0.0000	0.0000	C_s	$^2A'$	-263.085521	-263.049658	75.479
	-262.950103	0.049568	111.5	0.0000	0.0000			-263.979262	-263.943569	75.123
(E)-10	-263.050686	0.048276	124.3	0.0000	0.0000	C_s	$^1A'$	-263.085475	-263.049742	75.206
	-262.943709	0.049224	124.7	0.0000	0.0000			-262.978428	-262.942765	75.059
11	-0.502156	0.0000	-	0.7500	0.7500	O_h	$^2A_{1g}$	-0.512810	-0.499796	27.392
	-0.498135	0.0000	-	0.7500	0.7500			-0.508789	-0.495774	27.392
12	-93.445026	0.016347	761.9	0.0000	0.0000	$C_{\infty v}$	$^1\Sigma_g$	-93.464384	-93.441541	48.079
	-93.406039	0.016621	782.8	0.0000	0.0000			-93.425388	-93.402568	48.030
13	-185.669826	0.015802	216.0	0.0000	0.0000	$C_{\infty v}$	$^1\Sigma_g$	-185.693098	-185.664971	59.198
	-185.603554	0.016212	220.8	0.0000	0.0000			-185.626788	-185.598738	59.035
14	-263.647452	0.058409	102.3	0.7726	0.7501	C_1	2A	-263.677802	-263.640420	78.678
	-263.531369	0.059247	99.8	0.7751	0.7501			-263.561742	-263.524354	78.690
15	-170.169195	0.036592	238.2	0.7623	0.7500	C_s	$^2A'$	-170.195539	-170.164072	66.227
	-170.094540	0.037244	241.0	0.7717	0.7501			-170.120867	-170.089461	66.101
16	-169.610753	0.027107	241.7	0.0000	0.0000	$C_{\infty v}$	$^1\Sigma_g$	-169.634039	-169.605791	59.453
	-169.540903	0.027681	242.4	0.0000	0.0000			-169.564169	-169.535991	59.306
(Z)-17	-263.082832	0.049358	108.1	0.0000	0.0000	C_s	$^1A'$	-263.112197	-263.076161	75.845
	-262.980488	0.050118	105.2	0.0000	0.0000			-263.009822	-262.973851	75.707
(E)-17	-263.078360	0.049090	128.7	0.0000	0.0000	C_s	$^1A'$	-263.113390	-263.077416	75.714
	-262.975685	0.049848	128.7	0.0000	0.0000			-263.010655	-262.974741	75.586
18	-263.591661	0.056893	100.9	0.7722	0.7502	C_1	2A	-263.622069	-263.584423	79.234
	-263.475072	0.058230	101.5	0.7723	0.7501			-263.505445	-263.467952	78.910
19	-170.130788	0.035258	210.0	0.7552	0.7500	C_s	$^2A'$	-170.156834	-170.125335	66.295
	-170.051562	0.036089	213.8	0.7556	0.7500			-170.077612	-170.046230	66.047
20	-170.081446	0.036327	229.0	0.7554	0.7500	C_s	$^2A'$	-170.107808	-170.076187	66.551
	-170.007847	0.036966	242.6	0.7582	0.7500			-170.034146	-170.002671	66.243
21	-76.623632	0.013985	293.6	0.7718	0.7502	$C_{\infty v}$	$^2\Sigma_g$	-76.644018	-76.619471	51.663
	-76.591378	0.015256	544.4	0.7747	0.7503			-76.611378	-76.587686	49.862
22	-263.026099	0.047721	102.1	0.0000	0.0000	C_s	$^1A'$	-263.055564	-263.019201	76.532
	-262.923291	0.048784	103.2	0.0000	0.0000			-262.952648	-262.916512	76.053

Appendix

23	-263.601236	0.057995	80.8	0.7597	0.7500	C_1	2A	-263.631803	-263.594128	79.293
	-263.486907	0.059085	83.5	0.7646	0.7501			-263.517336	-263.479906	78.778
24	-170.151380	0.036151	219.9	0.7632	0.7500	C_s	$^2A'$	-170.177827	-170.146138	66.693
	-170.073396	0.036846	231.2	0.7687	0.7501			-170.099793	-170.068225	66.442
25	-263.657271	0.059301	66.0	0.7654	0.7501	C_s	$^2A'$	-263.687958	-263.650310	79.235
	-263.543171	0.060126	74.1	0.7712	0.7501			-263.573673	-263.536271	78.719
(Z)-26	-263.114305	0.049885	108.6	0.0000	0.0000	C_{2v}	1A_1	-263.142903	-263.107795	73.891
	-263.008931	0.050591	106.4	0.0000	0.0000			-263.037529	-263.002425	73.884
(E)-26	-263.110549	0.049669	127.8	0.0000	0.0000	C_{2h}	1A_g	-263.144659	-263.109605	73.777
	-263.004991	0.050213	125.5	0.0000	0.0000			-263.039094	-263.004047	73.763
27	-263.590308	0.060269	214.4	0.7658	0.7500	C_s	$^2A'$	-263.618700	-263.584662	71.639
	-263.479403	0.061331	207.7	0.7868	0.7502			-263.507783	-263.473816	71.489
28	-263.613520	0.057581	105.7	0.7756	0.7503	C_s	$^2A''$	-263.643817	-263.606309	78.942
	-263.497829	0.058500	104.5	0.7841	0.7504			-263.528024	-263.490754	78.441
29	-154.060181	0.046938	224.5	0.7633	0.7500	C_s	$^2A'$	-154.086684	-154.054724	67.266
	-153.985100	0.047784	229.5	0.7723	0.7501			-154.011566	-153.979733	66.998
30	-109.562847	0.005582	2450.2	0.0000	0.0000	$D_{\infty h}$	$^1\Sigma_g$	-109.581273	-109.559542	45.735
	-109.527196	0.005726	2513.4	0.0000	0.0000			-109.545613	-109.523891	45.718
31	-153.507908	0.037481	239.1	0.0000	0.0000	$D_{\infty h}$	$^1\Sigma_g$	-153.530657	-153.502636	58.975
	-153.437823	0.038362	241.8	0.0000	0.0000			-153.460516	-153.432670	58.609
32	-263.567438	0.056481	113.6	0.7844	0.7505	C_1	2A	-263.597642	-263.560249	78.701
	-263.447847	0.057593	118.0	0.7933	0.7506			-263.477911	-263.440819	78.067
33	-262.996590	0.047787	114.3	0.0000	0.0000	C_s	$^1A'$	-262.025904	-262.989795	75.998
	-262.892679	0.048841	115.2	0.0000	0.0000			-262.921905	-262.885982	75.605
34	-263.610624	0.058156	89.4	0.7626	0.7500	C_1	2A	-263.640984	-263.603612	78.656
	-263.500503	0.059276	106.7	0.7683	0.7501			-263.530590	-263.493636	77.775
35	-186.254981	0.025548	236.7	0.7626	0.7500	C_s	$^2A'$	-186.281273	-186.250033	65.751
	-186.177458	0.026032	241.3	0.7683	0.7501			-186.203730	-186.172537	65.651
36	-185.706053	0.016389	253.4	0.0000	0.0000	$D_{\infty h}$	$^1\Sigma_g$	-185.728567	-185.701349	57.283
	-185.636276	0.016760	252.3	0.0000	0.0000			-185.658791	-185.631577	57.277
(Z)-37	-263.052006	0.048173	108.5	0.0000	0.0000	C_s	$^1A'$	-263.081283	-263.045291	75.753
	-262.945591	0.049208	109.4	0.0000	0.0000			-262.974808	-262.938960	75.448
(E)-37	-263.046830	0.047773	126.6	0.0000	0.0000	C_s	$1A'$	-263.081730	-263.045886	75.440
	-262.939744	0.048923	136.0	0.0000	0.0000			-262.974361	-262.938800	74.846
38	-263.599394	0.057657	129.9	0.7643	0.7501	C_s	$^2A'$	-263.629514	-263.592389	78.137

Appendix

	-263.483611	0.058888	136.5	0.7706	0.7501			-263.513536	-263.476765	77.393
39	-169.566597	0.026364	229.1	0.0000	0.0000	$C_{\infty v}$	$^1\Sigma_g$	-169.594112	-169.565653	59.896
	-169.500363	0.027030	235.6	0.0000	0.0000			-169.527707	-169.499419	59.536
40	-263.604630	0.057648	102.7	0.7716	0.7501	C_1	2A	-263.641514	-263.603686	79.615
	-263.491148	0.058428	68.7	0.7659	0.7500			-263.528658	-263.490204	80.933
41	-170.129842	0.036068	204.4	0.7619	0.7500	C_s	$^2A'$	-170.160667	-170.128898	66.865
	-170.057730	0.036872	218.7	0.7703	0.7501			-170.088401	-170.056786	66.540
(Z)- 42	-263.043727	0.048810	107.0	0.0000	0.0000	C_{2v}	1A_1	-263.078445	-263.042783	75.057
	-262.944258	0.049591	105.0	0.0000	0.0000			-262.978849	-262.943314	74.789
(E)- 42	-263.044115	0.048506	132.0	0.0000	0.0000	C_{2h}	1A_g	-263.078721	-263.043171	74.823
	-262.943299	0.049325	135.4	0.0000	0.0000			-262.978676	-262.943299	74.458
43	-	-	-	-	-	-	-	-	-	-
	-	-	-	-	-			-	-	-
44	-170.053653	0.034143	215.9	0.7562	0.7500	C_s	$^2A'$	-170.084866	-170.052709	67.679
	-	-	-	-	-			-	-	-
45	-169.490191	0.024782	187.1	0.0000	0.0000	$C_{\infty v}$	$^1\Sigma_g$	-169.518634	-169.489247	61.850
	-169.415234	0.025754	193.1	0.0000	0.0000			-169.443136	-169.414290	60.711
46	-7183.529914	0.066022	141.8	0.0000	0.0000	C_s	$^1A'$	-7183.567314	-7183.528970	80.701
	-7183.806784	0.067066	150.3	0.0000	0.0000			-7183.843986	-7183.805839	80.286
47-S	-262.970864	0.049547	115.5	0.0000	0.0000	C_{2v}	1A_1	-263.003144	-262.969920	69.927
	-262.867691	0.050705	182.7	0.0000	0.0000			-262.899483	-262.866747	68.900
47-T	-262.904062	0.048271	176.6	2.0178	2.0001	C_{2v}	3A_2	-262.936747	-262.903118	70.778
	-262.801185	0.047858	118.8	2.0182	2.0001			-262.834726	-262.800241	72.581
48	-7183.534389	0.065982	134.3	0.0000	0.0000	C_{2v}	1A_1	-7183.571106	-7183.533444	79.265
	-7183.812217	0.066992	143.1	0.0000	0.0000			-7183.848747	-7183.811273	78.870
49	-723.841690	0.067158	157.5	0.0000	0.0000	C_{2v}	1A_1	-723.875994	-723.840745	74.187
	-723.698017	0.068133	163.9	0.0000	0.0000			-723.732215	-723.697073	73.963
50	-263.619184	0.058840	95.7	0.7649	0.7501	C_s	$^2A'$	-263.655827	-263.618239	79.110
	-263.508118	0.059648	98.7	0.7708	0.7501			-263.544553	-263.507174	78.672
51	-170.165016	0.036592	238.2	0.7623	0.7500	C_s	$^2A'$	-170.195538	-170.164072	66.227
	-170.090405	0.037244	241.0	0.7717	0.7501			-170.120867	-170.089460	66.101
52	-14102.76202	0.054284	56.8	0.0000	0.0000	C_{2v}	1A_1	-14102.80463	-14102.761080	91.676
	-14103.43668	0.055381	62.4	0.0000	0.0000			-14103.47897	-14103.435740	90.999
53	-7182.828895	0.052022	155.7	0.7553	0.7500	C_s	$^2A'$	-7182.867017	-7182.827951	82.222
	-7183.109108	0.053092	162.1	0.7599	0.7500			-7183.146987	-7183.108164	81.709

Appendix

54	—	—	—	—	—	—	—	—	—	—
	—	—	—	—	—			—	—	—
55	−7182.760050	0.048304	156.6	0.7621	0.7501	C _s	² A'	−7182.799836	−7182.759106	85.723
	−7183.033798	0.049735	175.1	0.7672	0.7501			−7183.072824	−7183.032854	84.123
56-T	−262.954174	0.049871	302.8	2.0066	2.0000	C _{2v}	³ B ₂	−262.986244	−262.953230	69.483
	−262.845412	0.050930	317.2	2.0110	2.0000			−262.877283	−262.844467	69.065
(Z)−57	−262.948214	0.045907	118.6	0.0000	0.0000	C _{2v}	¹ A ₁	−262.982756	−262.947270	74.685
	−262.838943	0.047213	125.3	0.0000	0.0000			−262.873218	−262.837999	74.124
(E)−57	−262.953453	0.045776	124.8	0.0000	0.0000	C _{2h}	¹ A _g	−262.987726	−262.952509	74.121
	−262.843437	0.046824	126.5	0.0000	0.0000			−262.877546	−262.842493	73.776
58	−230.855487	0.071325	312.5	0.0000	0.0000	D _{2h}	¹ A _g	−230.886518	−230.854542	67.298
	−230.738867	0.070774	137.2	0.0000	0.0000			−230.771372	−230.737922	70.400
(Z)−59	−230.895870	0.070628	106.3	0.0000	0.0000	C _{2v}	¹ A ₁	−230.930973	−230.894926	75.868
	−230.790288	0.071842	108.1	0.0000	0.0000			−230.825141	−230.789344	75.341
60	−246.939751	0.061677	427.4	0.0000	0.0000	C _s	¹ A'	−246.971316	−246.938807	68.421
	−246.824667	0.061634	374.6	0.0000	0.0000			−246.856508	−246.823723	69.002
(Z)−61	−246.942438	0.058759	108.2	0.0000	0.0000	C _s	¹ A'	−246.977921	−246.941494	76.667
	−246.836209	0.059863	112.6	0.0000	0.0000			−246.871437	−246.835265	76.130
(Z)−62	−247.004546	0.060369	105.5	0.0000	0.0000	C _s	¹ A'	−247.039812	−247.003602	76.210
	−246.899326	0.061016	105.1	0.0000	0.0000			−246.934534	−246.898382	76.089
63	−14102.80284	0.055439	96.5	0.0000	0.0000	C _{2v}	¹ A ₁	−14102.84533	−14102.80189	91.417
	−14103.47862	0.056396	98.2	0.0000	0.0000			−14103.52083	−14103.47767	90.835
64	−7182.871629	0.053341	140.0	0.7555	0.7500	C _s	² A'	−7182.909577	−7182.870685	81.856
	−7183.151043	0.054210	145.4	0.7592	0.7500			−7183.188798	−7183.150098	81.450
65	−263.025403	0.050690	430.4	0.0000	0.0000	C _{2v}	¹ A ₁	−263.055863	−263.024459	66.095
	−262.913371	0.050810	426.8	0.0000	0.0000			−262.943913	−262.912426	66.270
(Z)−66	−263.020139	0.047720	102.0	0.0000	0.0000	C _s	¹ A'	−263.055561	−263.019195	76.539
	−262.917545	0.048671	104.5	0.0000	0.0000			−262.952738	−262.916601	76.056
(E)−66	−263.020043	0.047321	125.8	0.0000	0.0000	C _s	¹ A'	−263.055239	−263.019099	76.064
	−262.916736	0.048225	124.8	0.0000	0.0000			−262.951774	−262.915792	75.731
1-m-(2,4)-S	—	—	—	—	—	—	—	—	—	—
	—	—	—	—	—			—	—	—
1-m-(2,4)-T	−262.997863	0.051317	378.5	2.0120	2.000	C _s	³ A'	−263.030134	−262.996919	69.908
	−262.891705	0.051944	379.3	2.0212	2.000			−262.923926	−262.890761	69.801
1-p-(2,5)-S	−262.998456	0.049790	450.7	0.0000	0.0000	C _{2v}	¹ A ₁	−263.029207	−262.997512	66.707

Appendix

	-262.885732	0.050044	443.9	0.0000	0.0000			-262.916550	-262.884787	66.849
1-<i>p</i>-(2,5)-T	-262.979761	0.050889	339.6	2.0062	2.0000	C _{2v}	³ A ₁	-263.011589	-262.978816	68.976
	-262.874671	0.051785	353.7	2.0098	2.0000			-262.906393	-262.873727	68.750
1-<i>o</i>-(4,5)-S	-263.021261	0.051416	410.7	0.0000	0.0000	C _s	¹ A'	-263.052458	-262.020317	67.647
	-262.918413	0.052130	413.1	0.0000	0.0000			-262.949569	-262.917469	67.559
1-<i>o</i>-(4,5)-T	-262.988170	0.051421	382.9	2.0097	2.0000	C _s	³ A'	-263.020462	-262.987226	69.953
	-262.879477	0.052075	382.8	2.0151	2.0001			-262.911741	-262.878533	69.891
1-<i>m</i>-(4,6)-S	-263.025403	0.050690	430.4	0.0000	0.0000	C _{2v}	¹ A ₁	-263.055863	-263.024459	66.095
	-262.913371	0.050810	426.8	0.0000	0.0000			-262.943913	-262.912426	66.270
1-<i>m</i>-(4,6)-T	-262.990536	0.051104	320.0	2.0115	2.0000	C _{2v}	³ A ₁	-263.022343	-262.989592	68.930
	-262.885458	0.051814	332.0	2.0213	2.0000			-262.917150	-262.884514	68.688
2-<i>o</i>-(3,4)-S	-262.983459	0.050249	381.4	0.0000	0.0000	C _s	¹ A'	-263.014874	-262.982514	68.107
	-262.875912	0.051075	391.4	0.0000	0.0000			-262.907285	-262.874968	68.017
2-<i>o</i>-(3,4)-T	-262.956849	0.050651	395.6	2.0103	2.0000	C _s	³ A'	-262.989183	-262.955905	70.039
	-262.844227	0.051167	393.7	2.0162	2.0001			-262.876574	-262.843283	70.068
2-<i>m</i>-(3,5)-S	-262.974682	0.049577	371.4	0.0000	0.0000	C _s	¹ A'	-263.006224	-262.973738	68.374
	-262.871859	0.050668	284.2	0.0000	0.0000			-262.903116	-262.870915	67.773
2-<i>m</i>-(3,5)-T	-262.950449	0.049555	370.4	2.0164	2.0001	C _s	³ A'	-262.982962	-262.949505	70.415
	-262.840422	0.050720	364.5	2.0298	2.0004			-262.872822	-262.839478	70.179
2-<i>p</i>-(3,6)-S	—	—	—	—	—	—	—	—	—	—
	—	—	—	—	—			—	—	—
2-<i>p</i>-(3,6)-T	-262.954174	0.049871	302.8	2.0066	2.0000	C _{2v}	³ B ₂	-262.986244	-262.953230	69.483
	-262.845412	0.050930	317.2	2.0110	2.0000			-262.877283	-262.844467	69.065
2-<i>o</i>-(4,5)-S	-263.000307	0.051075	426.6	0.0000	0.0000	C _{2v}	¹ A ₁	-263.030817	-262.999363	66.201
	-262.889629	0.051724	423.5	0.0000	0.0000			-262.920164	-262.888685	66.255
2-<i>o</i>-(4,5)-T	-262.901703	0.050231	145.8	2.0102	2.0000	C _{2v}	³ A ₁	-262.934817	-262.900759	71.682
	-262.778450	0.058529	184.0	2.0113	2.0000			-262.811016	-262.777506	70.528
3-<i>o</i>-(2,3)-S	-262.981667	0.049280	87.4	0.0000	0.0000	C _s	¹ A'	-263.014422	-262.980723	70.926
	-262.874464	0.050795	144.7	0.0000	0.0000			-262.906082	-262.873520	68.533
3-<i>o</i>-(2,3)-T	-262.992985	0.051478	396.4	2.0095	2.0000	C _{2v}	³ B ₂	-263.024582	-262.992041	68.489
	-262.883605	0.052248	406.6	2.0146	2.0001			-262.915149	-262.882661	68.377
3-<i>p</i>-(2,5)-S	-263.009698	0.050598	442.3	0.0000	0.0000	C _{2h}	¹ A _g	-263.040122	-263.008754	66.020
	-262.891772	0.050807	447.3	0.0000	0.0000			-262.922201	-262.890827	66.032
3-<i>p</i>-(2,5)-T	-262.982930	0.051083	316.4	2.0063	2.0000	C _{2h}	³ B _u	-263.014750	-262.981986	68.957
	-262.875611	0.051816	333.9	2.0096	2.0000			-262.907317	-262.874667	68.717

Appendix

3-<i>m</i>-(2,6)-S	-262.994530	0.050709	452.9	0.0000	0.0000	C _{2v}	¹ A ₁	-263.025089	-262.993586	66.304
	-262.884370	0.051177	417.7	0.0000	0.0000			-262.914923	-262.883426	66.291
3-<i>m</i>-(2,6)-T	-262.991616	0.051311	415.1	2.0144	2.0000	C _{2v}	³ B ₂	-263.023157	-262.990671	68.373
	-262.882871	0.052066	419.2	2.0248	2.0002			-262.914359	-262.881926	68.260
TS1b-1c	-263.556904	0.056459	-2281.2	0.7656	0.7500	C ₁	² A	-263.585162	-263.551419	71.019
	-263.446141	0.057159	-2326.8	0.7642	0.7500			-263.474741	-263.440539	71.983
TS3a-3a	-263.540762	0.056060	-2433.3	0.7829	0.7502	C ₁	² A	-263.568808	-263.535426	70.257
	-263.428736	0.056706	-2806.7	0.7769	0.7502			-263.456875	-263.423336	70.590
TS2a-2b	-263.520927	0.055384	-2314.2	0.7678	0.7500	C ₁	² A	-263.549224	-263.515383	71.224
	-263.407480	0.056082	-2425.7	0.7651	0.7500			-263.436126	-263.401826	72.189
TS2b-2b	-263.532293	0.055845	-2233.3	0.7597	0.7500	C _{2v}	² B ₂	-263.560250	-263.526621	70.778
	-263.417939	0.056787	-2150.6	0.7599	0.7500			-263.445647	-263.412372	70.033
TS1a-4	-263.599144	0.058369	-533.4	0.7778	0.7504	C _s	² A'	-263.627783	-263.593294	72.589
	-263.484773	0.059063	-663.1	0.7896	0.7510			-263.513396	-263.478950	72.497
TS4-5,6	-263.564324	0.053027	-382.3	0.7677	0.7501	C _s	² A'	-263.596959	-263.556194	85.798
	-263.449334	0.054347	-408.5	0.7706	0.7502			-263.480683	-263.441574	82.311
TS4-10,11	-263.552384	0.049878	-625.5	0.7612	0.7500	C _s	² A'	-263.583610	-263.544810	81.662
	-263.439029	0.05068	-781.41	0.7632	0.7500			-263.470097	-263.431574	81.080
TS5-7	-186.133238	0.019291	-2009.1	0.7569	0.750	C _s	² A'	-186.159597	-186.127817	66.886
	-186.058376	0.019767	-1987.0	0.7561	0.750			-186.084926	-186.052908	67.387
TS5-12,9	-186.187319	0.021706	-278.9	0.7632	0.7501	C _s	² A'	-186.215469	-186.181412	71.679
	-186.109553	0.021961	-358.7	0.7652	0.7501			-186.137497	-186.103700	71.132
TS5-13,11	-186.171624	0.016052	-192.2	0.7517	0.7500	C _s	² A'	-186.198948	-186.165597	70.193
	-186.097284	0.016694	-567.2	0.7553	0.7500			-186.124021	-186.091487	68.472
TS7-8,9	-186.154466	0.021935	-406.6	0.7660	0.7501	C _s	² A'	-186.182488	-186.148618	71.287
	-186.078039	0.022382	-452.4	0.7679	0.7502			-186.105782	-186.072299	70.471
TS1b-14	-263.617515	0.058346	-520.7	0.7649	0.7501	C ₁	² A	-263.645974	-263.611768	71.992
	-263.502744	0.058941	-525.8	0.7657	0.7501			-263.531167	-263.497034	71.840
TS14-15,12	-263.600368	0.054344	-509.9	0.7695	0.7502	C ₁	² A	-263.631659	-263.592704	81.987
	-263.486168	0.055081	-624.5	0.7766	0.7504			-263.517168	-263.478623	81.124
TS14-17,11	-263.584795	0.049620	-104.9	0.7510	0.7500	C ₁	² A	-263.617878	-263.576488	87.112
	-263.474641	0.050583	-526.2	0.7556	0.7500			-263.506417	-263.466674	83.645
TS15-16,11	-170.104701	0.027896	-802.9	0.7687	0.7500	C _s	² A'	-170.131176	-170.099063	67.587
	-170.026692	0.028512	-947.5	0.7694	0.7501			-170.053088	-170.021153	67.213
	-263.581076	0.056997	-258.2	0.7647	0.7501	C _s	² A'	-263.609710	-263.575066	72.915

Appendix

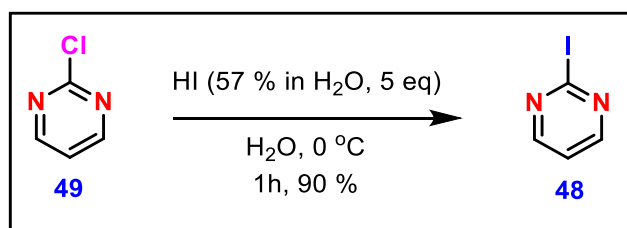
TS1b-18	-263.465281	0.057931	-259.6	0.7668	0.7501			-263.493895	-263.459338	72.732
TS18-19,12	-263.553971	0.053170	-590.7	0.7645	0.7501	C ₁	² A	-263.585139	-263.546195	81.964
	-263.436405	0.054305	-699.2	0.7677	0.7501			-263.466994	-263.428903	80.169
TS18-22,11	-263.528075	0.047969	-98.1	0.7510	0.7500	C ₁	² A	-263.561348	-263.519532	88.009
	-263.417411	0.049328	-529.0	0.7556	0.7500			-263.449033	-263.409334	83.554
TS19-20	-170.030568	0.029755	-2058.5	0.7582	0.7500	C _s	² A'	-170.057011	-170.024813	67.766
	-169.955443	0.030546	-2026.8	0.7567	0.7500			-169.981942	-169.949741	67.773
TS20-21,8	-170.039341	0.032058	-363.1	0.7648	0.7501	C _s	² A'	-170.067792	-170.033083	73.051
	-169.963485	0.032822	-479.7	0.7712	0.7503			-169.991592	-169.957394	71.975
TS1c-23	-263.585155	0.058337	-416.9	0.7784	0.7505	C _s	² A'	-263.613886	-263.579227	72.945
	-263.468314	0.059206	-531.3	0.7857	0.7508			-263.496962	-263.462465	72.606
TS23-24,12	-263.575740	0.054358	-548.5	0.7774	0.7504	C ₁	² A	-263.607479	-263.568115	82.849
	-263.458484	0.055266	-634.4	0.7843	0.7507			-263.489581	-263.451033	81.132
TS23-10,11	-263.549665	0.050067	-820.3	0.7670	0.7500	C ₁	² A	-263.580466	-263.542244	80.446
	-263.436389	0.051390	-950.6	0.7672	0.7500			-263.466751	-263.429265	78.895
TS24-16,11	-170.102612	0.028137	-902.8	0.7683	0.7500	C _s	² A'	-170.129020	-170.097040	67.309
	-170.024336	0.028843	-1011.3	0.7688	0.7501			-170.050664	-170.018866	66.925
TS2a-25	-263.616358	0.059792	-588.8	0.7825	0.7504	C _s	² A'	-263.644670	-263.610868	71.143
	-263.497844	0.060389	-702.4	0.7914	0.7509			-263.526161	-263.492350	71.161
TS25-15,12	-263.607918	0.054204	-384.4	0.7738	0.7503	C _s	² A'	-263.640097	-263.600048	84.290
	-263.494568	0.055173	-519.8	0.7846	0.7508			-263.526004	-263.486940	82.216
TS25-26,11	-263.607411	0.051121	-823.8	0.7663	0.7500	C ₁	² A	-263.638557	-263.599980	81.191
	-263.493988	0.051952	-933.2	0.7667	0.7500			-263.524978	-263.486664	80.639
TS2a-27	-263.510519	0.055659	-417.1	0.7731	0.7503	C _s	² A'	-263.539457	-263.504259	74.081
	-263.393614	0.056944	-496.4	0.7871	0.7508			-263.422399	-263.387523	73.403
TS27-28	-263.584816	0.057842	-479.6	0.7779	0.7502	C _s	² A'	-263.613500	-263.578925	72.769
	-263.466502	0.058280	-618.6	0.7888	0.7506			-263.495195	-263.460595	72.821
TS28-29,30	-263.598597	0.054568	-480.2	0.7676	0.7502	C ₁	² A	-263.630205	-263.590936	82.650
	-263.484869	0.055275	-571.3	0.7729	0.7503			-263.515883	-263.477375	81.045
TS29-31,11	-154.001400	0.038322	-841.3	0.7703	0.7500	C _s	² A'	-154.027980	-153.995457	68.451
	-153.923094	0.039132	-999.2	0.7706	0.7501			-153.949578	-153.917294	67.949
TS2b-28	-263.586120	0.057912	-446.7	0.7761	0.7503	C ₁	² A	-263.615486	-263.579948	74.795
	-263.468785	0.059046	-502.9	0.7822	0.7505			-263.497582	-263.462844	73.112
TS2b-32	-263.542720	0.055726	-442.0	0.7696	0.7501	C ₁	² A	-263.571747	-263.536426	74.340
	-263.424198	0.057534	-476.4	0.7634	0.7501			-263.452958	-263.418141	73.278

Appendix

TS _{32–24,12}	–263.548678	0.053926	–713.4	0.7756	0.7502	C _s	² A'	–263.579873	–263.541157	81.483
	–263.428996	0.054696	–837.4	0.7795	0.7504			–263.460058	–263.421555	81.035
TS _{32–33,11}	–	–	–	–	–	C ₁	² A	–	–	–
	–263.386968	0.049423	–502.5	0.7555	0.7500			–263.418729	–263.378913	83.800
TS _{3a–34}	–263.594672	0.058124	–424.7	0.7773	0.7504	C _s	² A'	–263.623511	–263.588704	73.258
	–263.480030	0.058851	–568.8	0.7890	0.7510			–263.508797	–263.474119	72.987
TS _{34–35,6}	–263.575525	0.054133	–503.0	0.7790	0.7504	C _s	² A'	–263.608048	–263.567779	84.753
	–263.458930	0.055130	–591.8	0.7852	0.7508			–263.490503	–263.451378	82.347
TS _{34–37,11}	–263.546862	0.049492	–707.4	0.7644	0.7500	C ₁	² A	–263.577547	–263.539355	80.380
	–263.433255	0.050971	–909.3	0.7669	0.7500			–263.463584	–263.426070	78.956
TS _{35–36,11}	–186.199320	0.017379	–839.6	0.7669	0.7500	C _s	² A'	–186.225638	–186.193989	66.612
	–186.121215	0.017856	–946.3	0.7675	0.7500			–186.147479	–186.115939	66.382
TS _{3a–38}	–263.582343	0.057992	–489.1	0.7778	0.7504	C _s	² A'	–263.610928	–263.576480	72.502
	–263.464864	0.058902	–574.3	0.7850	0.7508			–263.493387	–263.459080	72.205
TS _{38–19,12}	–263.563462	0.052795	–409.3	0.7654	0.7501	C _s	² A'	–263.595630	–263.555409	84.653
	–263.446335	0.054090	–430.8	0.7676	0.7502			–263.478005	–263.438529	83.084
TS _{38–37,11}	–263.546147	0.049374	–727.5	0.7646	0.7500	C ₁	² A	–263.577034	–263.538581	80.931
	–263.433262	0.050962	–852.3	0.7662	0.7500			–263.463564	–263.426086	78.879
TS _{19–39,11}	–170.072696	0.026592	–161.6	0.7515	0.7500	C ₁	² A	–170.100153	–170.066374	71.093
	–169.998380	0.027418	–526.0	0.7553	0.7500			–170.025183	–169.992333	69.139
TS _{58–(Z)–59}	–230.848282	0.069803	–510.7	0.0000	0.0000	C _{2v}	¹ A ₁	–230.875314	–230.842426	69.218
	–230.737504	0.070367	–531.6	0.0000	0.0000			–230.764488	–230.731698	69.011
TS _{60–(Z)–62}	–246.942482	0.060244	–479.1	0.0000	0.0000	C _s	¹ A'	–246.969783	–246.937223	68.528
	–246.829741	0.060807	–367.1	0.0000	0.0000			–246.856969	–246.824557	68.216
TS _{60–(Z)–61}	–246.909236	0.058594	–480.1	0.0000	0.0000	C _s	¹ A'	–246.936825	–246.903593	69.943
	–246.799356	0.059432	–495.1	0.0000	0.0000			–246.826875	–246.793800	69.612

A2. Synthesis of 2-iodopyrimidine and 4,6-diiodopyrimidine

2-Iodopyrimidine has been synthesized from the 2-chloropyrimidine using the standard literature procedure. Reaction condition for the synthesis of 2-iodopyrimidine has been mentioned in scheme A1 followed by the procedure.



Scheme A1. Synthesis of 2-iodopyrimidine (**48**).

Hydroiodic acid (3.2 mL, 57%), precooled to 0 °C, was added to solid 2-chloropyrimidine (800 mg, 3.90 mmol) in a 50 mL round-bottomed flask. The mixture was kept and vigorously stirred at 0 °C for 50 min. The light brownish green suspension was quickly neutralized at 0 °C with a saturated aqueous solution of potassium carbonate and decolorized with potassium disulfite at 0 °C. The aqueous solution was extracted with diethyl ether (5*6 mL), dried over desiccated magnesium sulphate, filtered, and evaporated under reduced pressure. The light-yellow oil was dissolved in a minimal amount of boiling petroleum ether (bp 30-50 °C) and crystallized at 0 °C to give 1.31 g (90%) of colourless 2-iodopyrimidine. mp 30-32 °C

¹H NMR (500 MHz, CDCl₃): δ 8.40 (d, J = 3.9 Hz, 2H), 7.30 (t, J = 3.9 Hz, 1H).

¹³C NMR (125 MHz, CDCl₃): δ 158.5, 129.5, 120.6.

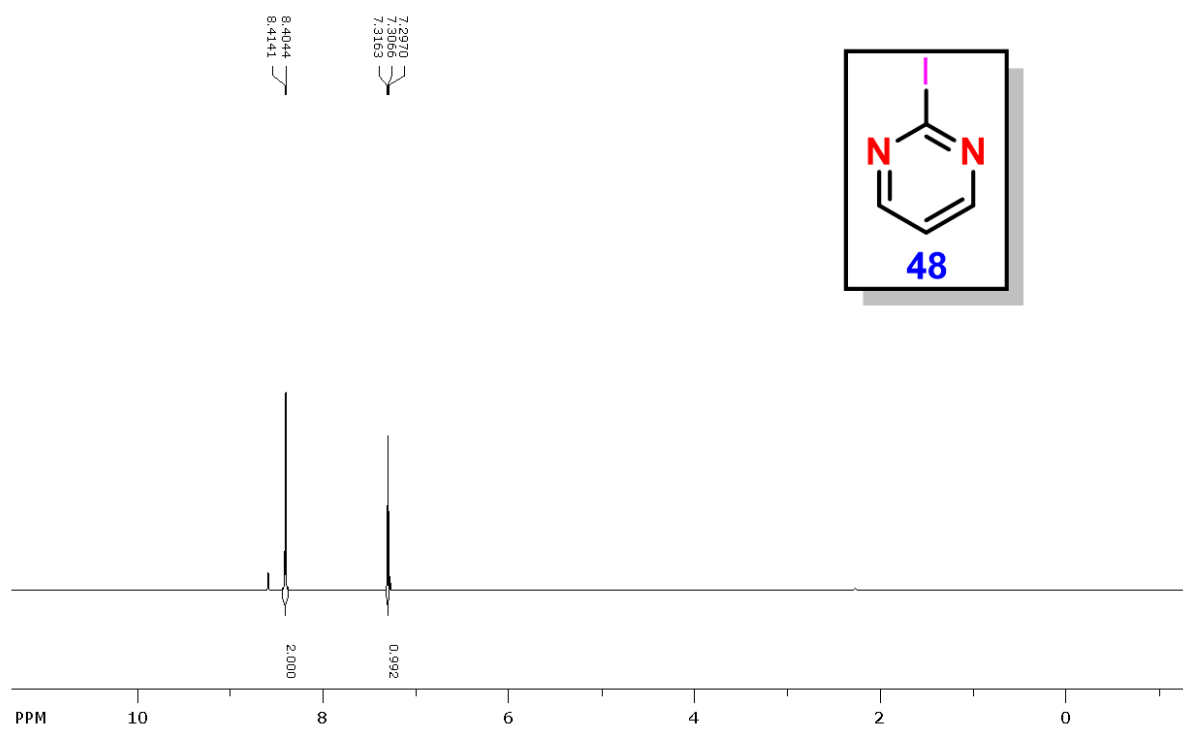


Figure A1. ¹H NMR spectrum of 2-iodopyrimidine (48).

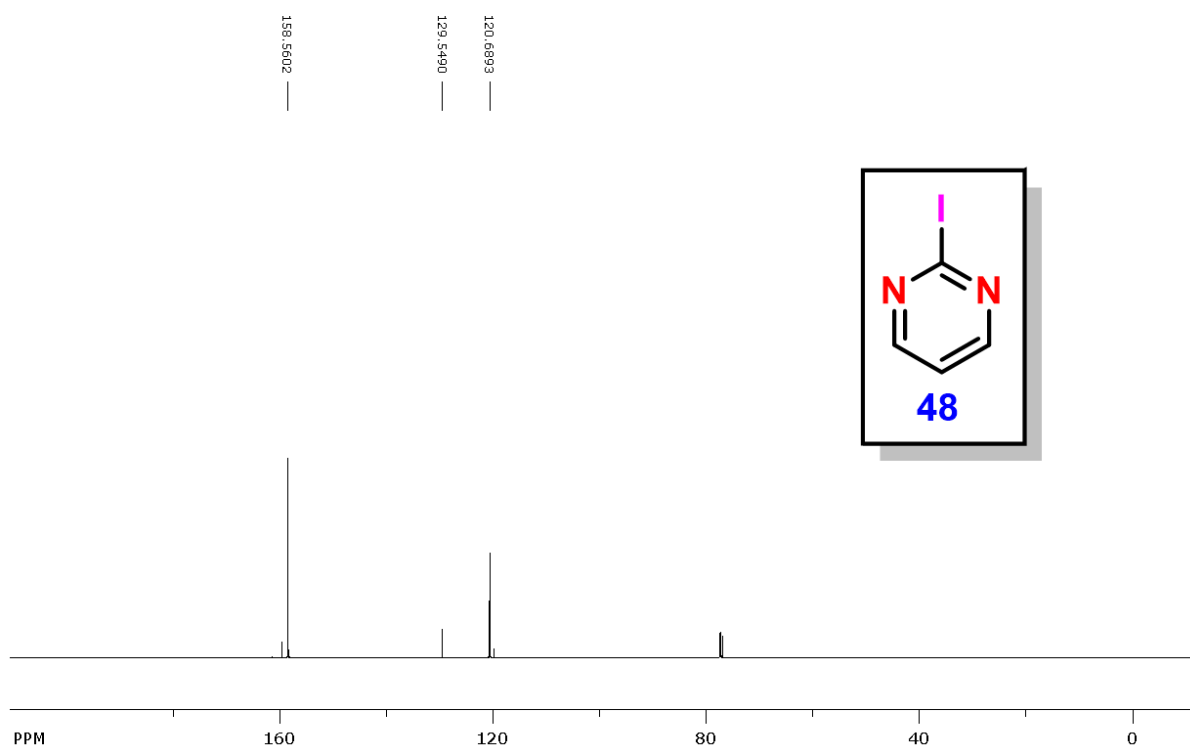
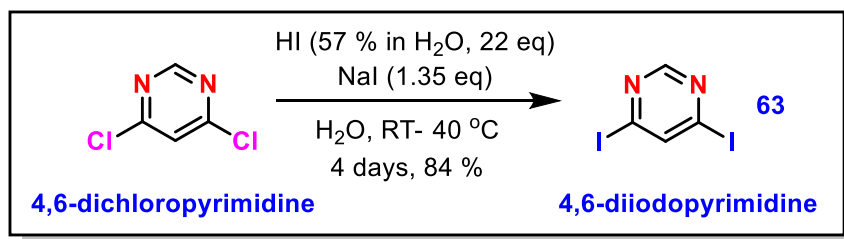


Figure A2. ¹³C NMR spectrum of 2-iodopyrimidine (48).

Synthesis of 4,6-diiodopyrimidine (63)



Scheme A2. Synthesis of 4,6-diiodopyrimidine (63).

A mixture of 4,6-dichloropyrimidine (1.00 g, 6.70 mmol), NaI (1.36 g, 9.00 mmol), and hydriodic acid (57 wt % in H₂O, 20 mL, 151.0 mmol) was heated at 40 °C with stirring for 1 h. The reaction mixture was stirred at room temperature for 30 h and basified with 10 N NaOH to pH = 10). The resulting precipitate was filtered, washed with H₂O, and dried to give 4,6-Diiodopyrimidine as a light-yellow solid (1.86 g, 84%).

¹H NMR (500 MHz, CDCl₃): δ 8.59 (d, $^5J = 0.84$ Hz, 1H), 8.57 (t, $^5J = 0.84$ Hz, 1H).

¹³C NMR (125 MHz, CDCl₃): δ 158.7, 142.5, 131.0.

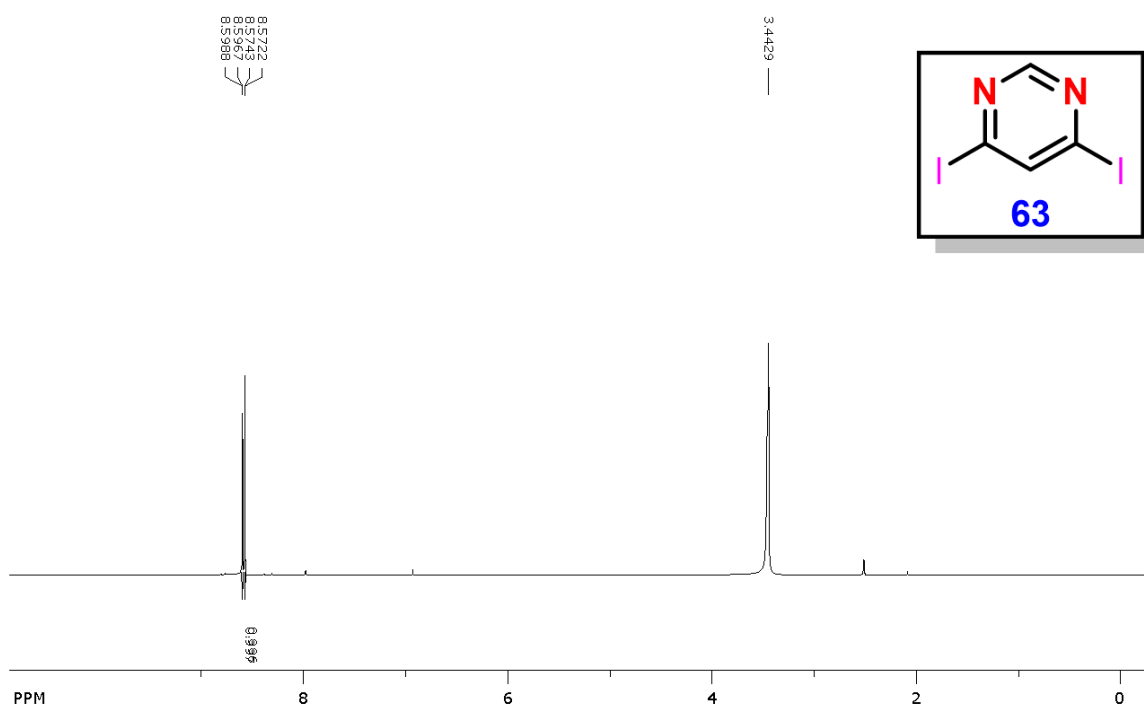


Figure A3. ¹H NMR spectrum of 4,6-diiodopyrimidine (**63**).

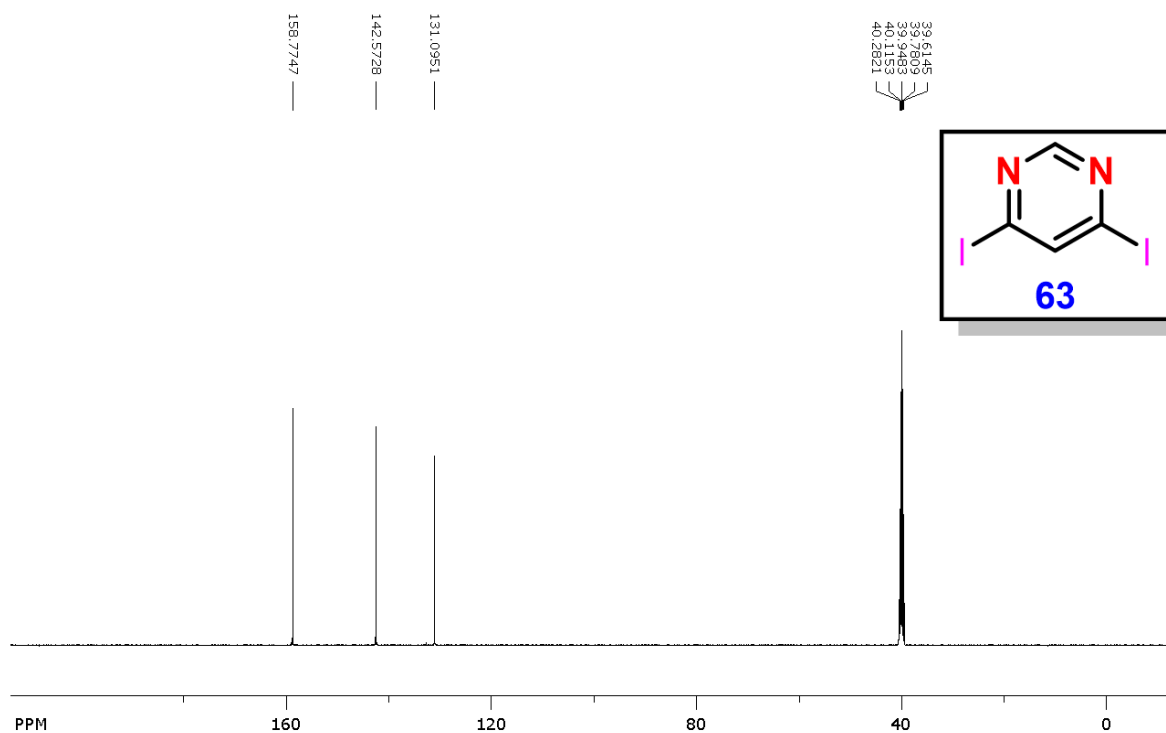


Figure A4. ¹³C NMR spectrum of 4,6-diiodopyrimidine (**63**).

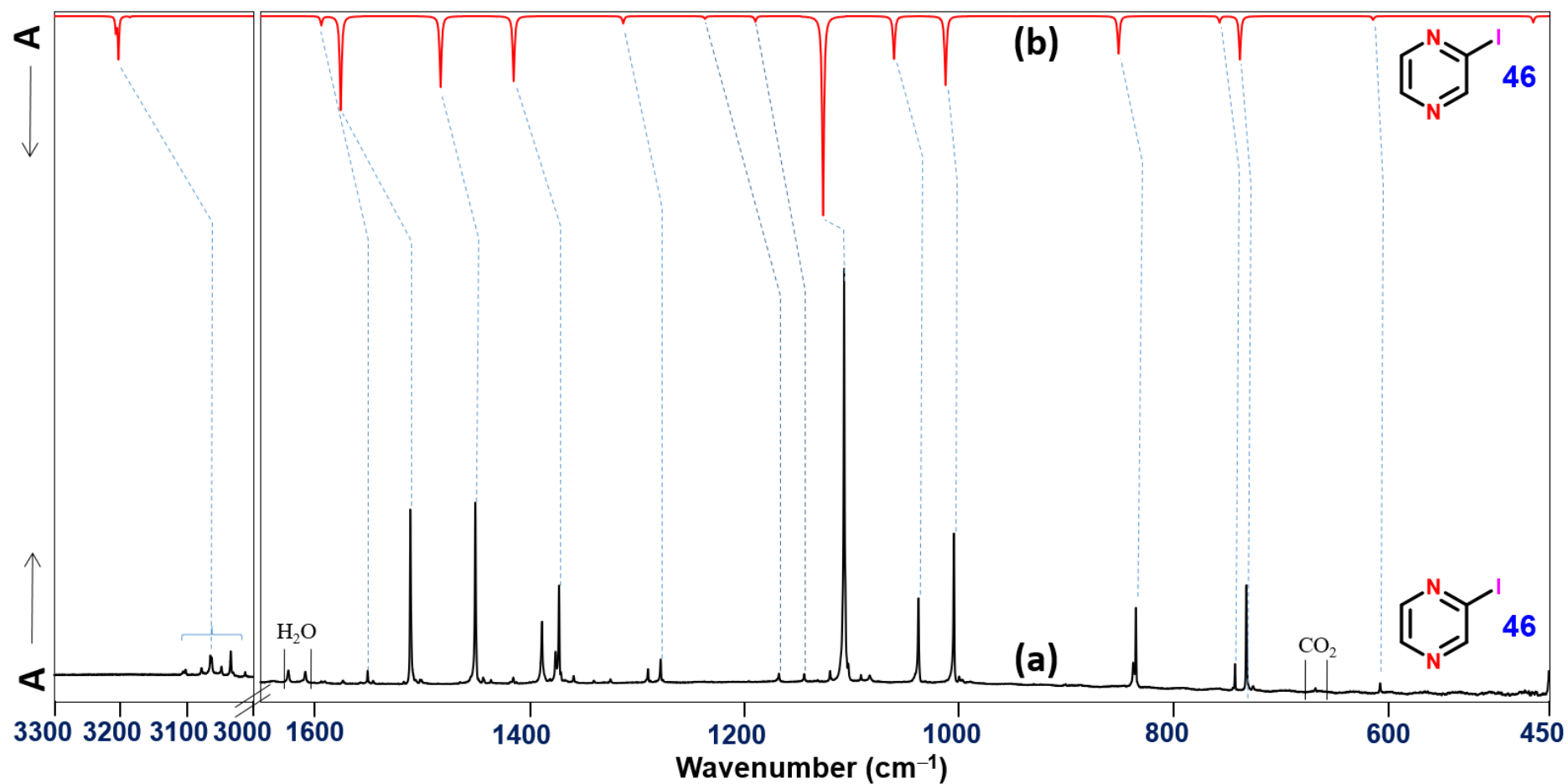


Figure A5. FTIR spectrum of 2-iodopyrazine (**46**). (a) Deposition spectrum of **46** (Ar, 4K) and (b) computed vibrational spectrum **46** (B3LYP/DGTZVP level of theory, unscaled).

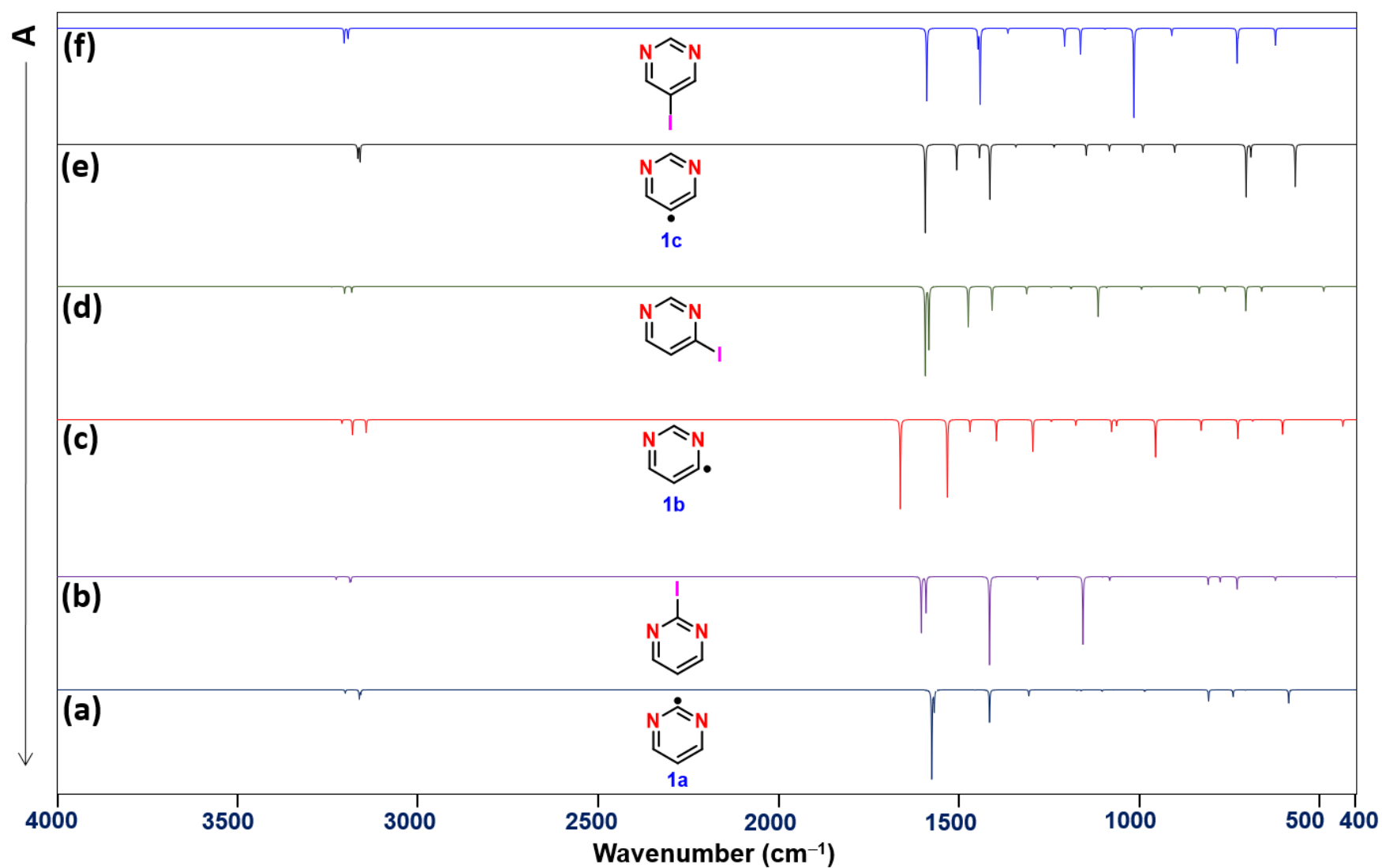


Figure A6. Computed vibrational spectrum of possible pyrimidine radicals and their iodo-precursor. ((U)B3LYP/cc-pVTZ level of theory for all the radicals and B3LYP/DGTZVP level of theory for all iodo-precursors, unscaled).

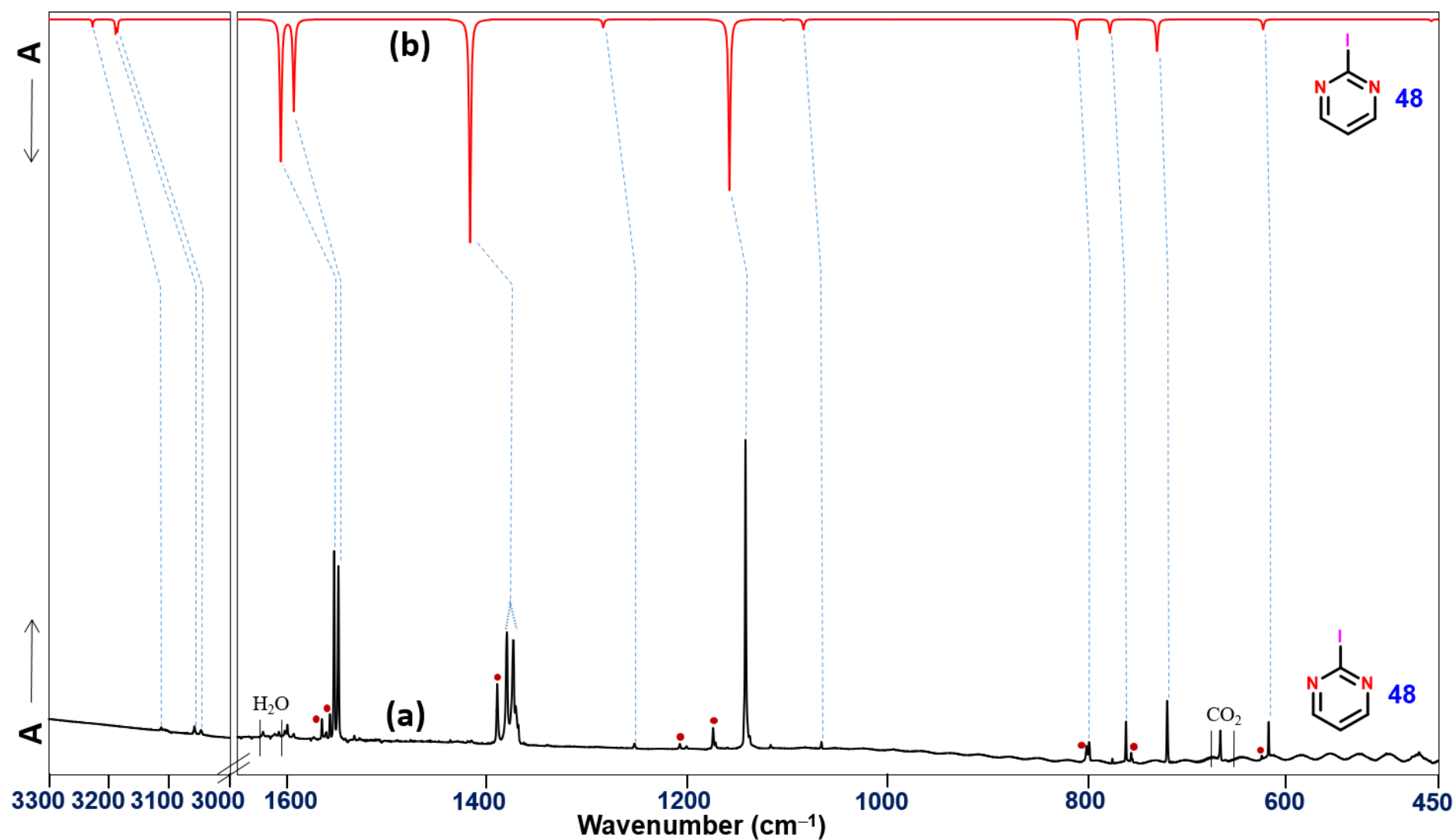


Figure A7. FTIR spectrum of 2-iodopyrimidine (**48**). (a) Deposition spectrum of **48** (Ar, 4K); The red dots indicate the signals due to 2-choropyrimidine (**49**), the synthetic precursor of **48**; (b) Computed vibrational spectrum of 2-iodopyrimidine (**48**) (B3LYP/DGTZVP level of theory, unscaled).

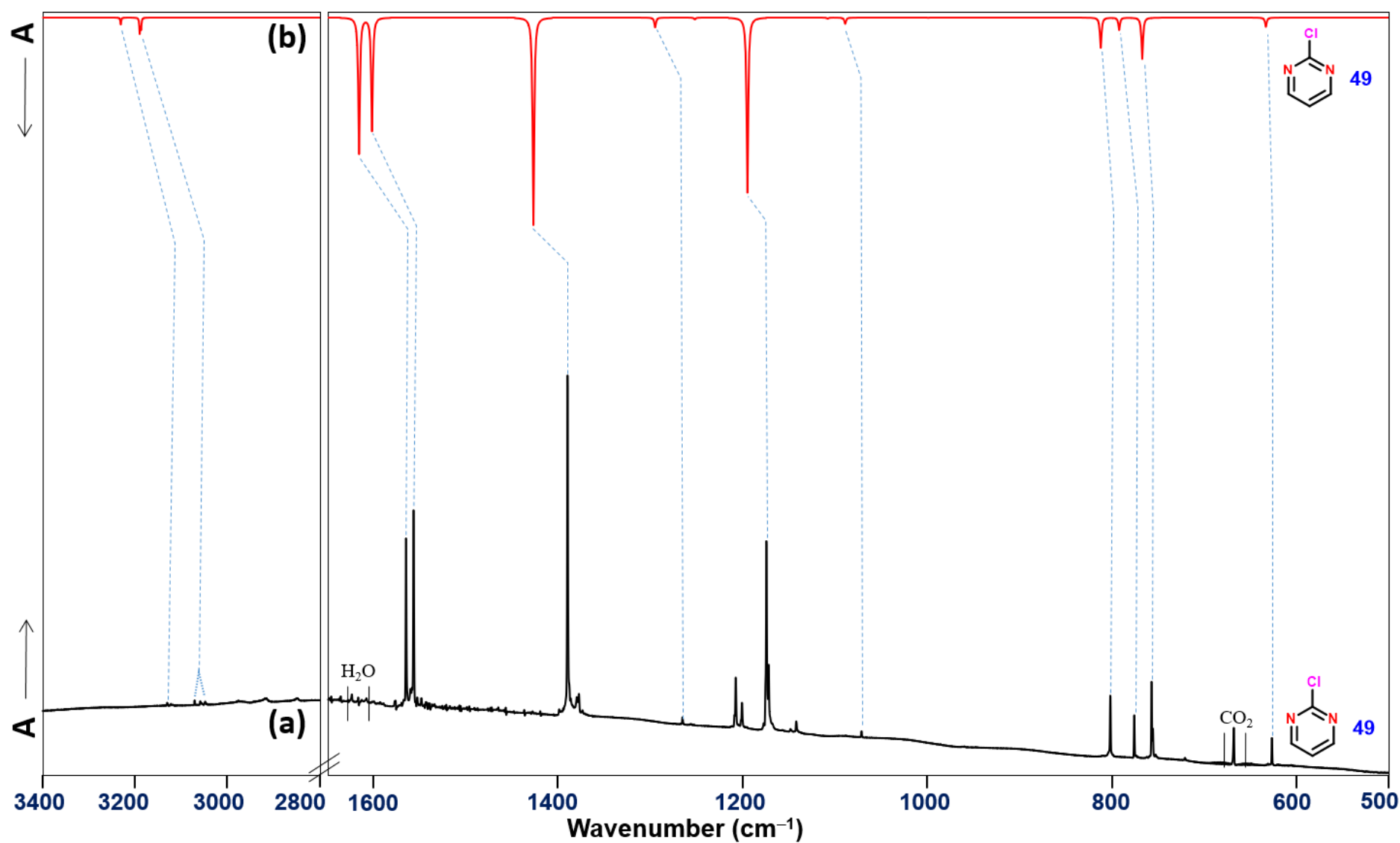


Figure A8. FTIR spectrum of 2-chloropyrimidine (**49**). (a) Deposition spectrum of **49** (Ar, 4K); (b) Computed vibrational spectrum of 2-chloropyrimidine (**49**) (B3LYP/DGTZVP level of theory, unscaled).

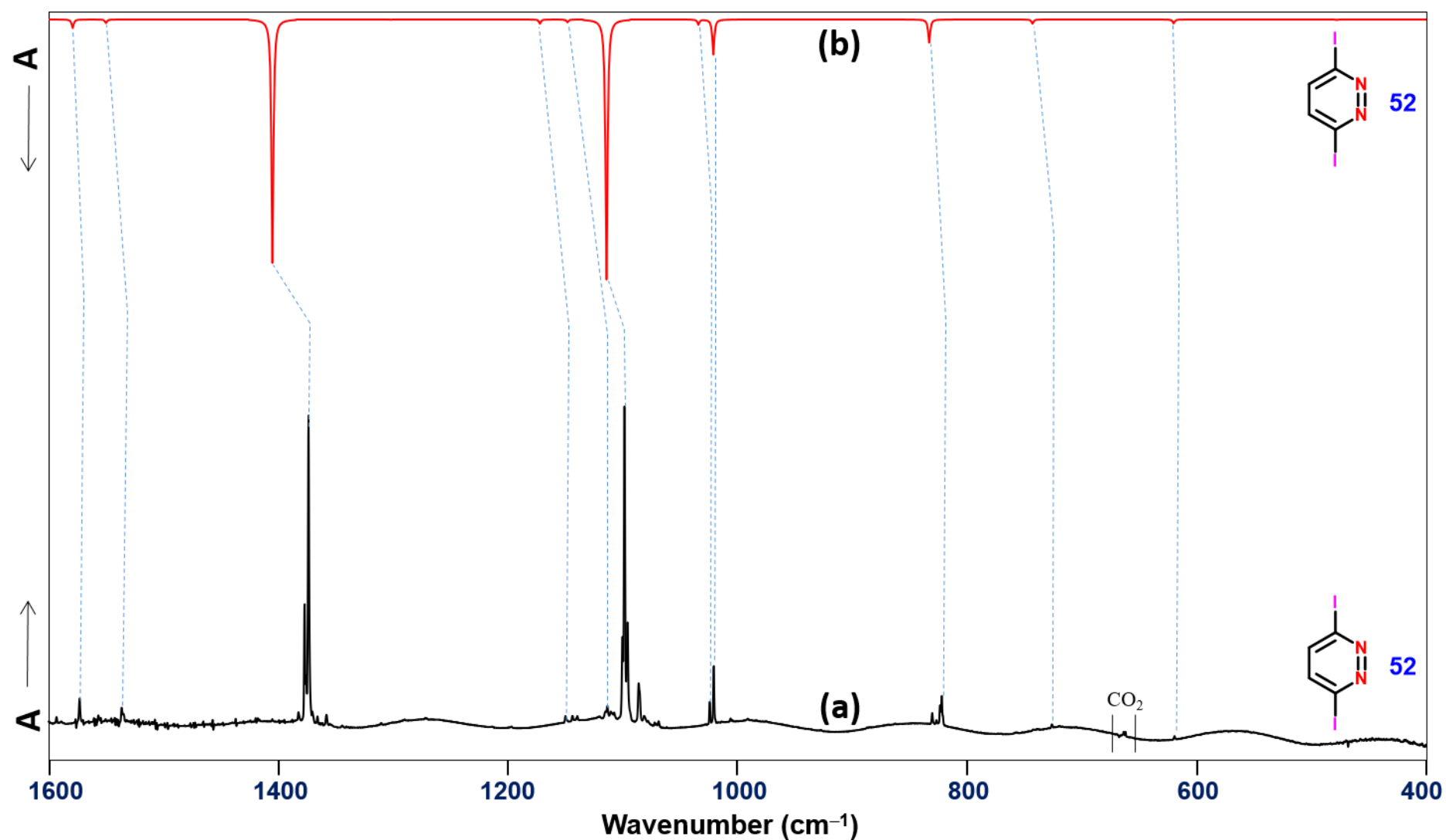


Figure A9. FTIR spectrum of 3,6-diiodopyridazine (**52**). (a) Deposition spectrum of **52** (Ar, 4K); (b) Computed vibrational spectrum of 3,6-diiodopyridazine (**52**) (B3LYP/DGTZVP level of theory, unscaled).

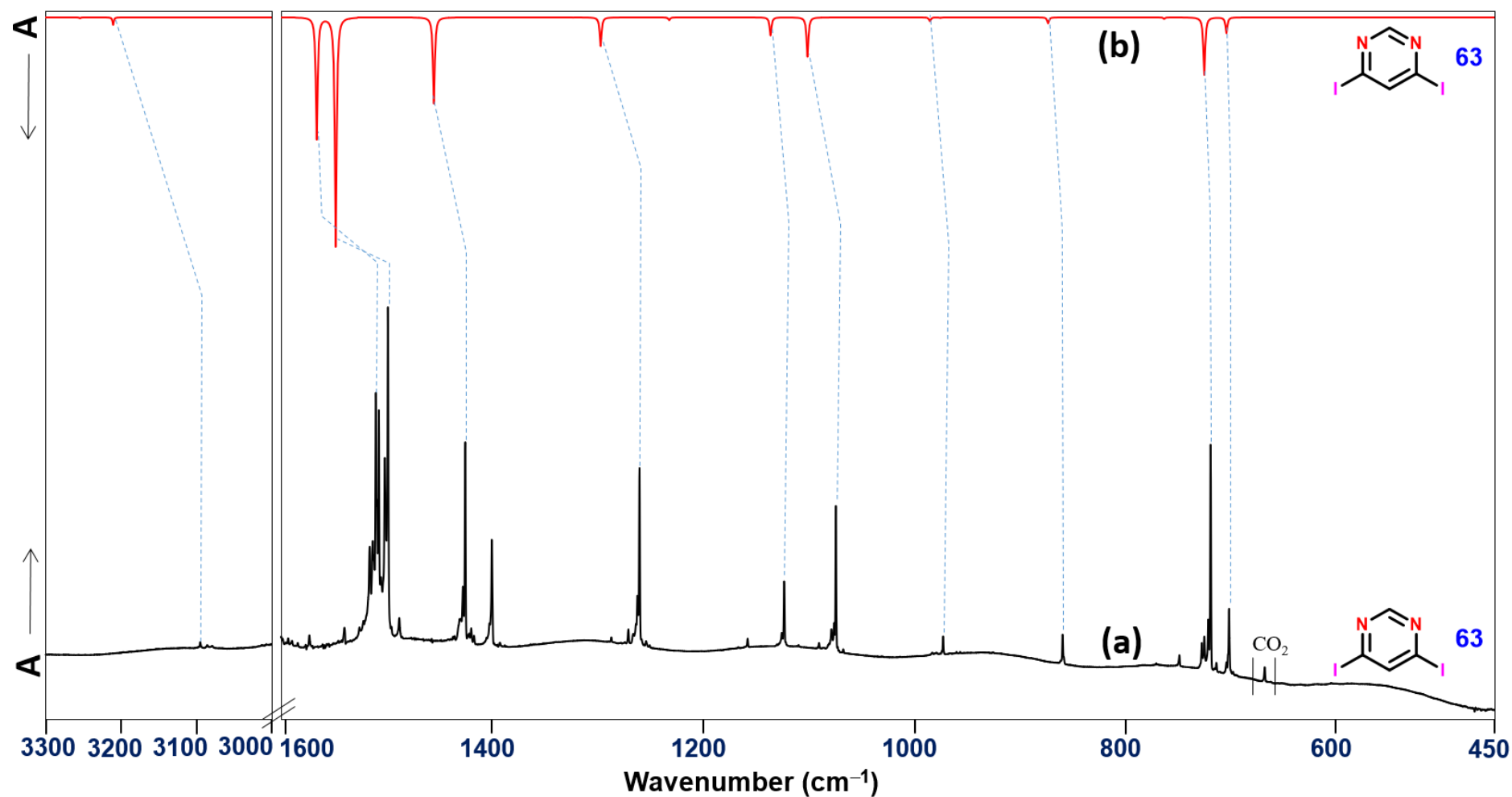
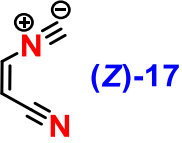
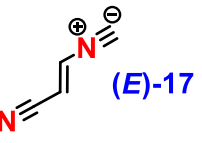


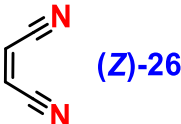
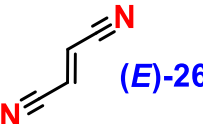
Figure A10. FTIR spectrum of 4,6-diiodopyrimidine (**63**). (a) Deposition spectrum of **63** (Ar, 4K); (b) Computed vibrational spectrum of 4,6-diiodopyrimidine (**63**) (B3LYP/DGTZVP level of theory, unscaled).

Table A2. Harmonic frequencies of ring-opened products (*Z*)-**17** and (*E*)-**17** in argon matrix at 4 K.

Normal mode										
	Symmetry	$\tilde{\nu}_{\text{calc}}$ / cm^{-1} [a]	I_{calc} [b]	$\tilde{\nu}_{\text{exp}}$ / cm^{-1} [c]	$I_{\text{rel, exp}}$	Symmetry	$\tilde{\nu}_{\text{calc}}$ / cm^{-1} [a]	I_{calc} [b]	$\tilde{\nu}_{\text{exp}}$ / cm^{-1} [c]	$I_{\text{rel, exp}}$
6	A ₂	598.4	<1 (1.8)	—	—	B _u	530.6	< 1 (0.4)	—	—
7	B ₂	746.5	1.7 (4.8)	—	—	A _u	542.0	< 1 (0.8)	—	—
8	B ₁	782.9	11.8 (32.8)	757.0	18	B _g	876.6	1.5 (4.8)	—	—
9	A ₁	904.1	2.9 (8.0)	—	—	A _u	964.3	14.5 (46.7)	929.5	11
10	A ₂	973.1	0 (0.0)	—	—	B _u	1036.7	< 1 (2.6)	—	—
11	B ₂	1061.5	5.6 (15.6)	—	—	A _g	1077.3	8.3 (26.7)	—	—
12	A ₁	1260.1	< 1 (2.5)	—	—	B _u	1299.3	< 1 (0.1)	—	—
13	B ₂	1422.6	< 1 (2.4)	—	—	A _g	1339.9	< 1 (0.2)	—	—
14	A ₁	1669.3	8.3 (23.2)	—	—	A _g	1675.5	9.1 (29.1)	—	—
15	A ₁	2183.3	100.0 (278.3)	2121.0	100	A _g	2184.6	100.0 (321.2)	2122.5	100
16	B ₂	2339.6	< 1 (1.7)	—	—	B _u	2338.8	< 1 (2.9)	—	—
17	B ₂	3186.7	2.9 (8.1)	—	—	A _g	3186.4	< 1 (0.9)	—	—
18	A ₁	3202.3	< 1 (0.1)	—	—	B _u	3191.8	2.5 (7.9)	—	—

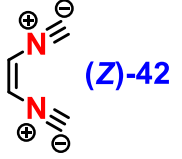
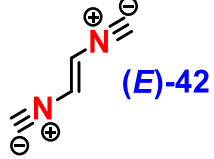
[a] B3LYP/cc-pVTZ; [b] Relative intensities in % and absolute intensities (in parentheses) are given in km/mol; [c] Experiment frequencies in argon matrix at 4 K.

Table A3. Harmonic frequencies of ring-opened products maleonitrile (*Z*)-**26** and fumaronitrile (*E*)-**26** in argon matrix at 4 K.

Normal mode	 (<i>Z</i>)- 26					 (<i>E</i>)- 26				
	Symmetry	$\tilde{\nu}_{\text{calc}}$ / cm^{-1} [a]	$I_{\text{calc}}^{[\text{b}]}$	$\tilde{\nu}_{\text{exp}}$ / cm^{-1} [c]	$I_{\text{rel,exp}}$	Symmetry	$\tilde{\nu}_{\text{calc}}$ / cm^{-1} [a]	$I_{\text{calc}}^{[\text{b}]}$	$\tilde{\nu}_{\text{exp}}$ / cm^{-1} [c]	$I_{\text{rel,exp}}$
5	A ₁	479.8	< 1 (0.3)	—	—	A _g	539.6	0 (0.0)	—	—
6	A ₂	617.2	0 (0.0)	—	—	B _u	544.9	1 (0.7)	—	—
7	B ₂	740.0	2 (0.9)	—	—	A _u	559.1	6 (2.7)	—	—
8	B ₁	786.6	100 (37.7)	760.0	100	B _g	879.8	0 (0.0)	—	—
9	A ₁	882.0	15 (5.5)	870.0	21	A _u	983.7	100 (48.8)	945.5	100
10	A ₂	996.4	0 (0.0)	—	—	B _u	1024.6	16 (7.7)	1011.5	18
11	B ₂	1029.6	18 (6.8)	1011.5	17	A _g	1026.4	0 (0.0)	—	—
12	A ₁	1244.4	2 (0.6)	—	—	B _u	1297.3	4 (1.8)	—	—
13	B ₂	1418.1	< 1 (0.1)	—	—	A _g	1326.7	0 (0.0)	—	—
14	A ₁	1660.4	2 (0.7)	—	—	A _g	1668.7	0 (0.0)	—	—
15	A ₁	2332.4	1 (0.4)	—	—	A _g	2329.1	0 (0.0)	—	—
16	B ₂	2345.0	2 (0.6)	—	—	B _u	2346.1	7 (3.3)	—	—
17	B ₂	3177.4	14 (5.2)	3066.5	12	A _g	3178.6	0 (0.0)	—	—
18	A ₁	3191.6	2 (0.6)	—	—	B _u	3186.0	12 (6.0)	3087.5	10

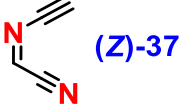
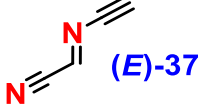
[a] B3LYP/cc-pVTZ; [b] Relative intensities in % and absolute intensities (in parentheses) are given in km/mol; [c] Experiment frequencies in argon matrix at 4 K.

Table A4. Harmonic frequencies of ring-opened products (*Z*)-42 and (*E*)-42 in argon matrix at 4 K.

Normal mode	 (<i>Z</i>)-42					 (<i>E</i>)-42				
	Symmetry	$\tilde{\nu}_{\text{calc}}$ / cm^{-1} [a]	I_{calc} ^[b]	$\tilde{\nu}_{\text{exp}}$ / cm^{-1} [c]	$I_{\text{rel, exp}}$	Symmetry	$\tilde{\nu}_{\text{calc}}$ / cm^{-1} [a]	I_{calc} ^[b]	$\tilde{\nu}_{\text{exp}}$ / cm^{-1} [c]	$I_{\text{rel, exp}}$
6	A ₂	564.4	0 (0.0)	—	—	B _u	465.7	< 1 (0.9)	—	—
7	B ₂	753.7	4.1 (11.5)	—	—	A _u	513.6	0 (0.0)	—	—
8	B ₁	778.1	10.3 (28.9)	755.0	12	B _g	872.7	0 (0.0)	—	—
9	A ₁	929.0	3.9 (10.8)	—	—	A _u	943.4	9.7 (51.0)	915.5	10
10	A ₂	944.9	0 (0.0)	—	—	B _u	1084.3	0 (0.0)	—	—
11	B ₂	1088.4	7.6 (21.2)	—	—	A _g	1086.6	8.8 (46.6)	—	—
12	A ₁	1274.4	< 1 (1.0)	—	—	B _u	1322.1	< 1 (4.0)	—	—
13	B ₂	1422.5	3.2 (9.0)	—	—	A _g	1328.2	0 (0.0)	—	—
14	A ₁	1680.2	1.1 (3.0)	—	—	A _g	1684.9	0 (0.0)	—	—
15	A ₁	2187.0	64.2 (179.2)	2117.5	40	A _g	2184.5	0 (0.0)	—	—
16	B ₂	2190.2	100.0 (279.0)	2119.5	100	B _u	2194.3	100.0 (527.8)	2121.5	100
17	B ₂	3195.5	3.7 (10.4)	—	—	A _g	3194.1	0 (0.0)	—	—
18	A ₁	3212.1	<1 (0.5)	—	—	B _u	3196.6	2.5 (13.2)	—	—

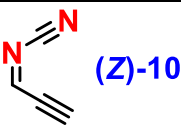
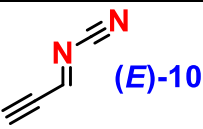
[a] B3LYP/cc-pVTZ; [b] Relative intensities in % and absolute intensities (in parentheses) are given in km/mol; [c] Experiment frequencies in argon matrix at 4 K.

Table A5. Harmonic frequencies of ring-opened products (*Z*)-**37** and (*E*)-**37** in argon matrix at 4 K.

Normal mode	 (<i>Z</i>)- 37					 (<i>E</i>)- 37				
	Symmetry	$\tilde{\nu}_{\text{calc}}$ / cm^{-1} [a]	$I_{\text{calc}}^{[\text{b}]}$	$\tilde{\nu}_{\text{exp}}$ / cm^{-1} [c]	$I_{\text{rel, exp}}$	Symmetry	$\tilde{\nu}_{\text{calc}}$ / cm^{-1} [a]	$I_{\text{calc}}^{[\text{b}]}$	$\tilde{\nu}_{\text{exp}}$ / cm^{-1} [c]	$I_{\text{rel, exp}}$
5	A'	496.6	2 (1.3)	—	—	A'	539.1	29 (27.7)	—	—
6	A'	553.7	67 (56.3)	504.5	41	A''	559.7	0 (0.0)	—	—
7	A''	639.9	1 (0.6)	—	—	A'	560.0	11 (10.5)	—	—
8	A''	702.5	39 (32.5)	674.5	35	A'	577.5	27 (25.6)	—	—
9	A'	730.7	1 (0.8)	—	—	A''	695.1	36 (34.2)	623.5	20
10	A''	910.1	7 (6.2)	—	—	A''	961.0	11 (10.4)	—	—
11	A'	934.0	6 (5.2)	—	—	A'	1010.3	29 (27.1)	—	—
12	A'	1019.7	48 (40.7)	—	—	A'	1065.9	8 (7.3)	—	—
13	A'	1404.1	5 (4.4)	—	—	A'	1371.7	11 (10.1)	—	—
14	A'	1633.3	8 (6.3)	—	—	A'	1645.4	6 (5.7)	—	—
15	A'	2178.2	9 (7.8)	—	—	A'	2180.7	6 (5.6)	—	—
16	A'	2327.0	6 (5.4)	—	—	A'	2399.1	0 (0.1)	—	—
17	A'	3162.0	0 (0.2)	—	—	A'	3088.9	8 (7.7)	—	—
18	A'	3473.1	100 (83.6)	3320.0	100	A'	3472.3	100 (94.0)	3312.0	100

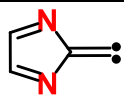
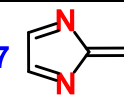
[a] B3LYP/cc-pVTZ; [b] Relative intensities in % and absolute intensities (in parentheses) are given in km/mol; [c] Experiment frequencies in argon matrix at 4 K.

Table A6. Harmonic frequencies of ring-opened products (*Z*)-**10** and (*E*)-**10** in argon matrix at 4 K.

Normal mode										
	Symmetry	$\tilde{\nu}_{\text{calc}}$ / cm^{-1} [a]	$I_{\text{calc}}^{[\text{b}]}$	$\tilde{\nu}_{\text{exp}}$ / cm^{-1} [c]	$I_{\text{rel, exp}}$	Symmetry	$\tilde{\nu}_{\text{calc}}$ / cm^{-1} [a]	$I_{\text{calc}}^{[\text{b}]}$	$\tilde{\nu}_{\text{exp}}$ / cm^{-1} [c]	$I_{\text{rel, exp}}$
5	A'	521.7	9 (8.9)	—	—	A'	548.9	3 (4.9)	—	—
6	A''	645.6	15 (15.8)	—	—	A''	576.7	0 (0.7)	—	—
7	A'	691.9	36 (37.3)	659.5	21	A'	603.0	3 (3.8)	—	—
8	A''	732.4	31 (32.1)	716.2	18	A'	693.6	29 (41.7)	663.0	8
9	A'	750.8	8 (8.6)	—	—	A''	726.0	24 (33.6)	713.5	10
10	A'	934.6	2 (2.2)	—	—	A''	995.7	3 (4.0)	—	—
11	A''	960.2	3 (2.7)	—	—	A'	1021.8	37 (52.8)	—	—
12	A'	1035.3	51 (52.9)	—	—	A'	1070.1	7 (10.5)	—	—
13	A'	1409.6	7 (7.6)	—	—	A'	1385.6	6 (7.9)	—	—
14	A'	1637.1	100 (103.1)	1593.5	100	A'	1647.4	100 (142.2)	1599.5	100
15	A'	2202.3	56 (57.5)	2133	64	A'	2208.2	60 (85.5)	2134	57
16	A'	2291.7	25 (25.9)	2197	19	A'	2296.0	18 (25.3)	2197	13
17	A'	3138.7	2 (1.8)	—	—	A'	3075.5	6 (8.8)	—	—
18	A'	3460.1	63 (65.0)	3318.0	52	A'	3461.9	53 (75.1)	3319.5	39

[a] B3LYP/cc-pVTZ; [b] Relative intensities in % and absolute intensities (in parentheses) are given in km/mol; [c] Experiment frequencies in argon matrix at 4 K.

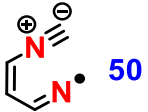
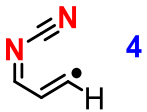
Table A7. Harmonic frequencies of **47** argon matrix at 4 K.

Normal mode	<div> 47  </div>					<div> 47  </div>		
	Symmetry	$\tilde{\nu}_{\text{calc}}$ / cm^{-1} [a]	I_{calc} ^[b]	$\tilde{\nu}_{\text{exp}}$ / cm^{-1} [c]	$I_{\text{rel, exp}}$	Symmetry	$\tilde{\nu}_{\text{calc}}$ / cm^{-1} [d]	I_{calc} ^[e]
3	A ₂	597.6	0 (0.0)	—	—	A ₂	575.8	0 (0.0)
4	B ₁	699.5	4 (5.8)	—	—	B ₁	665.7	3 (3.8)
5	A ₁	738.0	3 (3.8)	—	—	A ₁	740.7	4 (4.6)
6	B ₁	902.0	20 (27.4)	—	—	B ₁	898.5	25 (25.6)
7	A ₁	903.1	14 (19.1)	—	—	A ₁	908.0	12 (13.1)
8	B ₂	924.7	16 (21.8)	—	—	B ₂	920.8	0 (0.0)
9	A ₂	954.7	0 (0.0)	—	—	A ₂	922.8	18 (19.7)
10	A ₁	994.6	9 (12.0)	—	—	A ₁	1003.3	10 (10.7)
11	B ₂	1030.1	37 (52.0)	1004.5	20	B ₂	1071.0	46 (47.6)
12	B ₂	1259.9	0 (0.5)	—	—	B ₂	1280.9	0 (0.0)
13	A ₁	1328.4	2 (3.3)	—	—	A ₁	1349.0	4 (4.7)
14	A ₁	1453.2	17 (23.9)	1437.5	14	A ₁	1480.9	15 (15.9)
15	B ₂	1564.1	2 (3.3)	—	—	B ₂	1567.9	2 (2.2)
16	A ₁	1678.2	100 (139.8)	1639.5	100	A ₁	1694.1	100 (101.4)
17	B ₂	3194.0	1 (1.6)	—	—	B ₂	3209.0	1 (1.1)
18	A ₁	3207.7	4 (5.0)	—	—	A ₁	3224.4	3 (3.5)

[a] B3LYP/cc-pVTZ; [b] Relative intensities in % and absolute intensities (in parentheses) are given in km/mol;

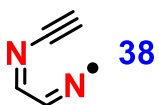
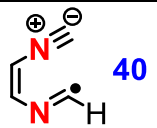
[c] Experiment frequencies in argon matrix at 4 K; [d,e] computed data at CCSD(T)/TZ2P level of theory.

Table A8. Harmonic frequencies of ring-opened radicals **50** and **4** in argon matrix at 4 K.

Normal mode	 50					 4				
	Symmetry	$\tilde{\nu}_{\text{calc}}$ / cm^{-1} [a]	$I_{\text{calc}}^{[\text{b}]}$	$\tilde{\nu}_{\text{exp}}$ / cm^{-1} [c]	$I_{\text{rel, exp}}$	Symmetry	$\tilde{\nu}_{\text{calc}}$ / cm^{-1} [a]	$I_{\text{calc}}^{[\text{b}]}$	$\tilde{\nu}_{\text{exp}}$ / cm^{-1} [c]	$I_{\text{rel, exp}}$
5	A'	452.3	11 (27.7)	—	—	A'	540.0	6 (5.5)	—	—
6	A''	464.9	5 (13.0)	—	—	A''	554.0	9 (8.5)	—	—
7	A''	762.0	11 (26.3)	—	—	A''	687.9	50 (49.5)	674.5	31
8	A'	800.8	3 (7.2)	—	—	A'	702.7	23 (22.8)	690.0	8
9	A''	888.6	0 (0.2)	—	—	A''	869.8	0 (0.2)	—	—
10	A'	899.2	6 (14.6)	—	—	A'	888.0	18 (17.3)	869.5	10
11	A''	979.3	0 (0.0)	—	—	A'	925.2	2 (1.5)	—	—
12	A'	1039.5	3 (8.4)	—	—	A''	995.4	0 (0.0)	—	—
13	A'	1250.6	1 (2.8)	—	—	A'	1037.2	34 (33.6)	1012.0	21
14	A'	1270.3	2 (4.3)	—	—	A'	1268.5	18 (18.2)	—	—
15	A'	1424.9	1 (1.5)	—	—	A'	1426.2	10 (10.0)	—	—
16	A'	1637.5	14 (33.7)	1585.5	10	A'	1592.9	100 (99.1)	1573.0	100
17	A'	1705.5	4 (10.8)	—	—	A'	1673.6	29 (28.5)	1612.0	30
18	A'	2180.9	100 (243.3)	2111.0	100	A'	2262.3	30 (29.3)	2182.0	38
19	A'	2964.8	6 (15.5)	—	—	A'	3052.3	5 (5.2)	—	—
20	A'	3178.2	1 (1.7)	—	—	A'	3140.9	14 (13.6)	—	—
21	A'	3198.8	1 (3.6)	—	—	A'	3264.3	4 (3.9)	—	—

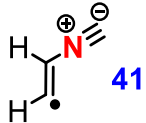
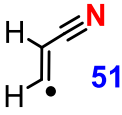
[a] B3LYP/cc-pVTZ; [b] Relative intensities in % and absolute intensities (in parentheses) are given in km/mol; [c] Experiment frequencies in argon matrix at 4 K.

Table A9. Harmonic frequencies of ring-opened radicals **38** and **40** in argon matrix at 4 K.

Normal mode	 38					 40				
	Symmetry	$\tilde{\nu}_{\text{calc}}$ / cm^{-1} [a]	$I_{\text{calc}}^{[\text{b}]}$	$\tilde{\nu}_{\text{exp}}$ / cm^{-1} [c]	$I_{\text{rel, exp}}$	Symmetry	$\tilde{\nu}_{\text{calc}}$ / cm^{-1} [a]	$I_{\text{calc}}^{[\text{b}]}$	$\tilde{\nu}_{\text{exp}}$ / cm^{-1} [c]	$I_{\text{rel, exp}}$
5	A'	516.0	12 (9.8)	—	—	A	382.3	1 (1.4)	—	—
6	A'	539.3	82 (64.6)	—	—	A	470.6	1 (3.1)	—	—
7	A''	549.7	0 (0.0)	—	—	A	614.0	9 (22.1)	—	—
8	A''	690.2	43 (33.8)	674.0	19	A	675.0	13 (30.7)	—	—
9	A''	799.7	13 (10.5)	—	—	A	772.6	9 (20.6)	—	—
10	A'	803.4	49 (38.7)	775.5	31	A	878.0	3 (7.2)	—	—
11	A'	886.3	7 (5.3)	—	—	A	924.8	27 (65.5)	—	—
12	A''	957.9	0 (0.1)	—	—	A	985.5	100 (239.1)	945.0	100
13	A'	1012.7	36 (28.5)	950.5	27	A	1108.6	18 (43.6)	—	—
14	A'	1226.6	20 (15.7)	1198.0	14	A	1240.7	5 (10.9)	—	—
15	A'	1402.9	7 (5.4)	—	—	A	1422.4	3 (6.9)	—	—
16	A'	1600.6	16 (12.4)	—	—	A	1532.5	5 (12.7)	—	—
17	A'	1712.0	4 (3.0)	—	—	A	1997.5	2 (4.7)	—	—
18	A'	2166.0	23 (17.9)	—	—	A	2149.0	36 (85.8)	2108.0	28
19	A'	2966.2	21 (16.9)	2970	12	A	3003.5	18 (41.8)	2984.0	20
20	A'	3141.8	15 (11.8)	—	—	A	3182.7	0 (0.9)	—	—
21	A'	3476.1	100 (79.3)	3318.0	100	A	3218.2	1 (3.6)	—	—

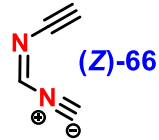
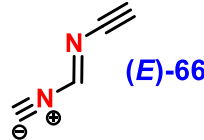
[a] B3LYP/cc-pVTZ; [b] Relative intensities in % and absolute intensities (in parentheses) are given in km/mol; [c] Experiment frequencies in argon matrix at 4 K.

Table A10. Harmonic frequencies of ring-opened radicals **41** and **51** in argon matrix at 4 K.

Normal mode										
	Symmetry	$\tilde{\nu}_{\text{calc}}$ / cm^{-1} [a]	I_{calc} [b]	$\tilde{\nu}_{\text{exp}}$ / cm^{-1} [c]	$I_{\text{rel, exp}}$	Symmetry	$\tilde{\nu}_{\text{calc}}$ / cm^{-1} [a]	I_{calc} [b]	$\tilde{\nu}_{\text{exp}}$ / cm^{-1} [c]	$I_{\text{rel, exp}}$
3	A'	513.8	2 (3.9)	—	—	A'	557.4	12 (6.3)	—	—
4	A''	685.4	23 (42.1)	659.0	18	A''	699.1	100 (49.2)	674.5	100
5	A'	776.4	17 (32.0)	739.5	7	A'	783.2	40 (19.6)	716.5	61
6	A''	830.0	0 (0.7)	—	—	A''	849.3	0 (0.0)	—	—
7	A'	1033.4	10 (18.8)	—	—	A'	1001.0	14 (7.1)	—	—
8	A'	1291.9	0 (0.5)	—	—	A'	1259.8	6 (3.1)	—	—
9	A'	1655.0	6 (12.0)	—	—	A'	1650.6	0 (1.0)	—	—
10	A'	2199.5	100 (187.2)	2129.0	100	A'	2341.4	13 (6.7)	—	—
11	A'	3084.5	2 (3.6)	—	—	A'	3058.5	0 (0.7)	—	—
12	A'	3276.8	5 (8.8)	—	—	A'	3257.3	11 (5.6)	—	—

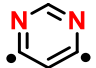
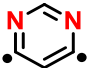
[a] B3LYP/cc-pVTZ; [b] Relative intensities in % and absolute intensities (in parentheses) are given in km/mol; [c] Experiment frequencies in argon matrix at 4 K.

Table A11. Harmonic frequencies of ring-opened products (Z)-66 and (E)-66 in argon matrix at 4 K.

Normal mode										
	Symmetry	$\tilde{\nu}_{\text{calc}}$ / cm^{-1} [a]	$I_{\text{calc}}^{[\text{b}]}$	$\tilde{\nu}_{\text{exp}}$ / cm^{-1} [c]	$I_{\text{rel, exp}}$	Symmetry	$\tilde{\nu}_{\text{calc}}$ / cm^{-1} [a]	$I_{\text{calc}}^{[\text{b}]}$	$\tilde{\nu}_{\text{exp}}$ / cm^{-1} [c]	$I_{\text{rel, exp}}$
5	A'	468.1	2 (3.5)	—	—	A'	528.3	1 (2.3)	—	—
6	A'	558.8	26 (55.4)	—	—	A''	529.4	0 (1.4)	—	—
7	A''	622.7	2 (4.7)	—	—	A'	546.5	5 (15.3)	—	—
8	A''	688.4	15 (33.9)	663.5	23	A'	576.9	16 (48.0)	—	—
9	A'	748.5	3 (7.5)	—	—	A''	676.1	12 (37.5)	—	—
10	A''	915.1	2 (3.2)	—	—	A''	961.4	2 (6.2)	—	—
11	A'	952.0	1 (2.4)	—	—	A'	1055.5	18 (54.6)	—	—
12	A'	1049.0	39 (85.8)	—	—	A'	1093.2	12 (36.3)	—	—
13	A'	1411.3	4 (8.8)	—	—	A'	1381.7	4 (11.4)	—	—
14	A'	1654.1	27 (59.5)	1593.5	40	A'	1661.7	25 (78.4)	1599.5	33
15	A'	2159.9	100 (216.9)	2091.0	100	A'	2170.1	100 (305.2)	2120.5	100
16	A'	2196.9	35 (78.1)	2128.5	31	A'	2205.3	31 (95.6)	2140.0	47
17	A'	3187.2	0 (1.3)	—	—	A'	3112.2	3 (9.7)	—	—
18	A'	3475.4	39 (84.6)	3310.0	28	A'	3475.5	32 (97.2)	3313.0	23

[a] B3LYP/cc-pVTZ; [b] Relative intensities in % and absolute intensities (in parentheses) are given in km/mol; [c] Experiment frequencies in argon matrix at 4 K.

Table A12. Harmonic frequencies of **65** at B3LYP/cc-pVTZ and CCSD(T)/TZ2P level of theory.

Normal mode	 65			 65		
	Symmetry	$\tilde{\nu}_{\text{calc}}$ / cm^{-1} [a]	$I_{\text{calc}}^{[b]}$	Symmetry	$\tilde{\nu}_{\text{calc}}$ / cm^{-1} [c]	$I_{\text{calc}}^{[d]}$
3	A ₁	613.5	9 (18.5)	A ₁	614.5	38 (55.4)
4	B ₂	621.8	33 (69.0)	B ₂	633.6	4 (5.9)
5	B ₁	646.5	2 (5.5)	B ₁	633.6	4 (5.9)
6	A ₁	821.9	31 (65.2)	A ₁	825.8	6 (8.8)
7	B ₁	833.5	3 (6.6)	B ₁	832.6	53 (78.7)
8	B ₂	886.5	58 (122.2)	B ₂	928.6	89 (129.8)
9	B ₁	958.7	1 (2.5)	B ₁	952.0	1 (2.3)
10	A ₁	1097.7	0 (0.0)	A ₁	1094.6	0 (0.0)
11	B ₂	1195.2	37 (76.6)	B ₂	1221.3	21 (30.9)
12	B ₂	1216.0	0 (0.0)	B ₂	1255.6	5 (7.3)
13	A ₁	1299.3	21 (43.7)	A ₁	1294.0	32 (46.9)
14	B ₂	1302.9	30 (63.0)	B ₂	1329.6	52 (77.3)
15	B ₂	1486.4	100 (208.3)	B ₂	1501.2	100 (146.0)
16	A ₁	1788.5	28 (57.5)	A ₁	1775.9	55 (80.7)
17	A ₁	3216.2	3 (6.7)	A ₁	3232.9	2 (5.4)
18	A ₁	3264.4	0 (0.0)	A ₁	3286.8	0 (0.5)

[a] B3LYP/cc-pVTZ; [b] Relative intensities in % and absolute intensities (in parentheses) are given in km/mol; [c,d] computed data at CCSD(T)/TZ2P level of theory.

Cartesian coordinates of all the species at (U)B3LYP/cc-pVTZ level of theory.

1				2				3			
C	0.00000000	0.00000000	-1.30665310	N	0.00000000	0.66434400	-1.22559610	C	0.00000000	1.13000400	0.69544900
N	0.00000000	1.19229100	-0.71243510	C	0.00000000	1.31868700	-0.06747410	C	-0.00000000	1.13000400	-0.69544900
C	0.00000000	1.18035200	0.62066490	C	0.00000000	0.68882600	1.17429990	N	0.00000000	0.00000000	-1.40025900
C	0.00000000	0.00000000	1.34943790	C	0.00000000	-0.68882600	1.17429990	C	-0.00000000	-1.13000400	-0.69544900
C	0.00000000	-1.18035200	0.62066490	C	0.00000000	-1.31868700	-0.06747410	C	0.00000000	-1.13000400	0.69544900
N	0.00000000	-1.19229100	-0.71243510	N	0.00000000	-0.66434400	-1.22559610	N	0.00000000	0.00000000	1.40025900
H	0.00000000	2.14554900	1.11501190	H	0.00000000	1.26548500	2.08906590	H	0.00000000	2.06047800	1.25141100
H	0.00000000	0.00000000	-2.39068710	H	0.00000000	2.39838100	-0.15084810	H	-0.00000000	2.06047800	-1.25141100
H	0.00000000	0.00000000	2.43006690	H	0.00000000	-1.26548500	2.08906590	H	-0.00000000	-2.06047800	-1.25141100
H	0.00000000	-2.14554900	1.11501190	H	0.00000000	-2.39838100	-0.15084810	H	0.00000000	-2.06047800	1.25141100
1a				1b				1c			
C	0.00000000	0.00000000	1.32154022	C	-0.37262894	-1.24473124	0.00000000	C	0.00000000	0.00000000	-1.23773178
N	0.00000000	1.18561100	0.78196522	N	0.95524367	-1.01850833	0.00000000	N	0.00000000	1.19413200	-0.64975878
C	0.00000000	1.18675000	-0.56038978	C	1.34652767	0.20119786	0.00000000	C	0.00000000	1.19833600	0.69283522
C	0.00000000	0.00000000	-1.28130778	C	0.50444635	1.30103968	0.00000000	C	0.00000000	0.00000000	1.35891722
C	0.00000000	-1.18675000	-0.56038978	C	-0.84668822	0.97108901	0.00000000	C	0.00000000	-1.19833600	0.69283522
N	0.00000000	-1.18561100	0.78196522	N	-1.28794407	-0.29131710	0.00000000	N	0.00000000	-1.19413200	-0.64975878
H	0.00000000	2.15268800	-1.05132778	H	-0.70500219	-2.27484979	0.00000000	H	0.00000000	2.16097900	1.18864422
H	0.00000000	0.00000000	-2.36157478	H	0.84810292	2.32416525	0.00000000	H	0.00000000	0.00000000	-2.32180078
H	0.00000000	-2.15268800	-1.05132778	H	-1.60413904	1.74789071	0.00000000	H	0.00000000	-2.16097900	1.18864422
2a				2b				3a			
N	-1.00162465	-0.97566171	0.00000000	N	-0.77937236	1.09946735	0.00000000	C	0.38809431	-1.20349775	0.00000000
C	0.21774307	-1.32721351	0.00000000	C	0.56027358	1.25983436	0.00000000	C	1.31166410	-0.16875902	0.00000000
C	1.32557897	-0.48375255	0.00000000	C	1.37087425	0.15228643	0.00000000	N	0.86767496	1.09843913	0.00000000
C	0.99772534	0.85480198	0.00000000	C	0.85093728	-1.10528671	0.00000000	C	-0.39458613	1.30316707	0.00000000
C	-0.36135657	1.20348639	0.00000000	C	-0.55031663	-1.17475337	0.00000000	C	-1.34763491	0.28251165	0.00000000
N	-1.35732993	0.33163187	0.00000000	N	-1.31717668	-0.09100984	0.00000000	N	-0.92846075	-0.97975547	0.00000000
H	2.34397587	-0.84340153	0.00000000	H	1.44697979	-2.00865383	0.00000000	H	0.71285203	-2.23680528	0.00000000
H	1.75788527	1.62532717	0.00000000	H	-1.06855697	-2.12609991	0.00000000	H	2.37972797	-0.34262756	0.00000000
H	-0.66732395	2.24234934	0.00000000	H	0.90680956	2.28306692	0.00000000	H	-2.41230362	0.46811555	0.00000000
4				5				6			
C	1.29401848	0.08312338	0.00000000	C	0.02931630	0.67555812	0.00000000	C	0.00000000	0.00000000	0.59801300
N	0.51294309	1.15567365	0.00000000	N	0.34781342	-0.60946958	0.00000000	C	0.00000000	0.00000000	1.65961800
C	-0.76821566	1.06010409	0.00000000	C	-0.31823362	-1.64922978	0.00000000	H	-0.00000000	0.00000000	-0.59801300
C	-1.57582669	-0.15790588	0.00000000	N	-0.11631319	1.82297977	0.00000000	H	-0.00000000	0.00000000	-1.65961800
C	-1.08296411	-1.37594300	0.00000000	H	0.11300230	-2.65254139	0.00000000				
N	2.08718075	-0.76459709	0.00000000								
H	-1.30874992	2.00189442	0.00000000								
H	-2.65639551	-0.00347474	0.00000000								
H	-1.43779351	-2.39222710	0.00000000								
7				8				9			
C	0.07399866	0.62227887	0.00000000	N	0.00000000	0.00000000	0.42795071	C	0.00000000	0.00000000	-0.62612685
N	0.37926034	-0.71198463	0.00000000	C	0.00000000	0.00000000	-0.73667329	N	0.00000000	0.00000000	0.53668015
C	-0.52228188	-1.67013962	0.00000000	H	0.00000000	0.00000000	1.42438471				
N	-0.19251297	1.74166928	0.00000000								
H	1.38246773	-0.92062803	0.00000000								
(Z)-10				(E)-10				11			
C	-1.41308595	-0.14936873	0.00000000	C	-1.79687338	-0.12017735	0.00000000	H	0.00000000	0.00000000	0.00000000
N	-2.07275103	-1.10093388	0.00000000	N	-2.93807560	0.07678091	0.00000000				
C	2.19074410	-0.91183257	0.00000000	C	2.95585965	-0.12765584	0.00000000				
C	1.41038394	0.00199848	0.00000000	C	1.77379663	0.08717199	0.00000000				
C	0.50502465	1.09205772	0.00000000	C	0.40050231	0.42979354	0.00000000				
N	-0.77858424	1.02128257	0.00000000	N	-0.51352705	-0.47249425	0.00000000				
H	2.86881180	-1.73002649	0.00000000	H	3.99691323	-0.33966602	0.00000000				
H	0.93213472	2.09045631	0.00000000	H	0.16459402	1.49486540	0.00000000				

Appendix

12 C 0.00000000 0.00000000 -0.49704314 H 0.00000000 0.00000000 -1.56232914 N 0.00000000 0.00000000 0.64922686	13 N -0.20291035 1.85024627 0.00000000 C 0.05603148 0.72759301 0.00000000 C 0.42815317 -0.65093078 0.00000000 N -0.43131327 -1.64098294 0.00000000	14 C 2.05444902 -1.00994035 -0.18321785 N -2.14791322 -1.09694610 0.01136683 C -1.50446121 -0.13543660 -0.00610945 C -0.73027015 1.03857571 -0.01806357 C 0.64172896 1.04595070 0.00994830 N 1.40313516 -0.03323077 0.08645340 H -1.24909017 1.98469759 -0.04465281 H 1.17479406 1.98785550 0.01483283 H 2.51906275 -1.69621180 0.52973377
15 N -0.20291035 1.85024627 0.00000000 C 0.05603148 0.72759301 0.00000000 C 0.42815317 -0.65093078 0.00000000 C -0.43131327 -1.64098294 0.00000000 H 1.50158220 -0.84830551 0.00000000 H -0.39843794 -2.71749414 0.00000000	16 C 0.00000000 0.00000000 -1.83178808 C 0.00000000 0.00000000 -0.63101108 C 0.00000000 0.00000000 0.73721592 N 0.00000000 0.00000000 1.89252392 H 0.00000000 0.00000000 -2.89416808	(Z)-17 C 0.59411435 1.03436440 0.00000000 H 1.06308006 2.00826809 0.00000000 C -0.74271395 0.96607760 0.00000000 H -1.34079648 1.86688802 0.00000000 C 1.45424322 -0.09331250 0.00000000 N 2.18393210 -0.98558965 0.00000000 N -1.45112687 -0.20083972 0.00000000 C -2.11429698 -1.16882127 0.00000000
(E)-17 C 0.45069402 0.47954424 0.00000000 H 0.21978668 1.53638991 0.00000000 C -0.52634506 -0.43431971 0.00000000 H -0.32223245 -1.49658842 0.00000000 C 1.82019415 0.10951343 0.00000000 N 2.93998374 -0.16475111 0.00000000 N -1.84945117 -0.09174216 0.00000000 C -2.99975683 0.13787060 0.00000000	18 C 0.66556001 1.04124709 0.00659427 N -0.63774042 1.10634008 -0.02581575 C -1.39827853 0.02985897 -0.00772303 C -2.17902665 -0.89347808 0.01156558 C 1.92613376 -1.11444790 -0.18597299 N 1.38046439 -0.07720240 0.09807432 H 1.23396706 1.96223009 0.00973758 H -2.86365744 -1.70223842 0.02421221 H 2.34429111 -1.84303597 0.51345722	19 C -0.30617344 -1.72988039 0.00000000 N 0.29826925 -0.65472825 0.00000000 C 0.03039517 0.63119369 0.00000000 C -0.07196106 1.83165242 0.00000000 H 0.20260962 -2.69831041 0.00000000 H -0.20405833 2.88361379 0.00000000
20 C -0.53918100 -1.71891192 0.00000000 N 0.36412096 -0.76942854 0.00000000 C 0.09510879 0.57451877 0.00000000 C -0.14590024 1.74590045 0.00000000 H -0.37012606 2.78286014 0.00000000 H 1.36111404 -1.00590424 0.00000000	21 C 0.00000000 0.00000000 0.72761985 C 0.00000000 0.00000000 -0.47183215 H 0.00000000 0.00000000 -1.53472615	22 C 2.20828371 0.79245449 0.00000000 C 1.35574724 -0.05760009 0.00000000 H 2.93806906 1.56196529 0.00000000 N -1.42690768 0.23912647 0.00000000 C -2.00979051 1.25835573 0.00000000 C -0.75079991 -0.95931902 0.00000000 N 0.51547410 -1.08551280 0.00000000 H -1.37867714 -1.84060767 0.00000000
23 C -1.49901323 -0.23532296 0.31655583 N -1.45568051 -1.26981120 -0.38351984 C 2.24354001 -0.71393892 0.11808207 C 1.35836640 0.08849306 -0.00519438 C 0.36798535 1.10310937 -0.15678381 N -0.89215675 0.99891095 0.00667063 H -2.13882573 -0.20174243 1.20551939 H 0.74154613 2.08867014 -0.42827142 H 3.00686920 -1.44466932 0.22473820	24 C -0.13436413 1.80559028 0.00000000 C 0.09227802 0.62733445 0.00000000 C 0.39657042 -0.76926527 0.00000000 N -0.46287896 -1.68268051 0.00000000 H 1.45855677 -1.04939867 0.00000000 H -0.34530991 2.84620551 0.00000000	25 N 2.20424348 -0.77724398 0.00000000 C 1.39320674 0.04281526 0.00000000 C 0.46744891 1.11915850 0.00000000 C -0.86720558 1.00236960 0.00000000 C -1.64022156 -0.25279309 0.00000000 N -1.18164750 -1.41538574 0.00000000 H 0.91084955 2.10676559 0.00000000 H -1.45532068 1.91051876 0.00000000 H -2.73307176 -0.13817792 0.00000000
(Z)-26 C 0.00000000 0.67006900 1.03389220 H 0.00000000 1.19986600 1.97731320 C 0.00000000 -0.67006900 1.03389220 H 0.00000000 -1.19986600 1.97731320 C 0.00000000 -1.47843000 -0.13387480 C -0.00000000 1.47843000 -0.13387480 N 0.00000000 -2.17259400 -1.05391680 N -0.00000000 2.17259400 -1.05391680	(E)-26 C -0.46032703 0.48664073 0.00000000 H -1.51737462 0.25406626 0.00000000 C 0.46032703 -0.48664073 0.00000000 H 1.51737462 -0.25406626 0.00000000 C 0.11223481 -1.86371340 0.00000000 C -0.11223481 1.86371340 0.00000000 N -0.14270152 -2.98789290 0.00000000 N 0.14270152 2.98789290 0.00000000	27 N -1.18549795 -0.08640398 0.00000000 C -0.01935606 0.78035876 0.00000000 C -0.11078573 2.09109065 0.00000000 C 1.14907176 -0.09107728 0.00000000 C 0.63843099 -1.33283519 0.00000000 N -0.78480248 -1.28077738 0.00000000 H 0.53435382 2.95314091 0.00000000 H 2.17847433 0.22086021 0.00000000 H 1.13510908 -2.28895330 0.00000000

Appendix

28 N -1.95436080 -1.19214699 0.00000000 C 1.48521266 0.03886275 0.00000000 C 2.26223563 -0.88931969 0.00000000 C 0.59103204 1.10370530 0.00000000 C -0.80288349 0.97723096 0.00000000 N -1.42778160 -0.18318138 0.00000000 H 2.94612272 -1.70015554 0.00000000 H 0.97756035 2.11299681 0.00000000 H -1.46226733 1.83158137 0.00000000	29 C 0.07630212 0.67915921 0.00000000 C -0.15763475 1.85755544 0.00000000 C 0.41084325 -0.70295969 0.00000000 C -0.44687362 -1.69835555 0.00000000 H -0.37866394 2.89529219 0.00000000 H 1.48024014 -0.93307976 0.00000000 H -0.39739818 -2.77460890 0.00000000	30 N 0.00000000 0.00000000 0.54569200 N -0.00000000 0.00000000 -0.54569200
31 C 0.00000000 0.00000000 0.68187500 C 0.00000000 0.00000000 1.88604800 C -0.00000000 0.00000000 -0.68187500 C -0.00000000 0.00000000 -1.88604800 H 0.00000000 0.00000000 2.94727200 H -0.00000000 0.00000000 -2.94727200	32 N -0.75438156 1.04491775 0.01336999 C 0.58565857 1.09804620 -0.01266865 C 1.44155363 -0.00459202 -0.00731763 C 2.18161200 -0.96061542 0.00686364 C -1.99713394 -1.03565489 -0.17044420 N -1.33791867 -0.06529456 0.07344202 H 2.83580911 -1.79610563 0.01283155 H -2.44911900 -1.74304663 0.51713968 H 0.98926989 2.09868670 -0.03625418	33 C 2.17811336 -0.84860833 0.00000000 C 1.36420055 0.03488445 0.00000000 C 0.42533199 1.09282378 0.00000000 N -0.85866858 0.99083941 0.00000000 H 2.88827078 -1.63881559 0.00000000 H 0.79704483 2.11058613 0.00000000 N -1.36197843 -0.24097746 0.00000000 C -1.99111032 -1.23256726 0.00000000
34 C -1.52398967 0.06919217 0.24465515 C -1.32333753 1.25260101 -0.28545677 N 2.13346451 0.86958549 0.14403546 C 1.35330097 0.03126616 0.01131493 C 0.46938982 -1.09755541 -0.14866197 N -0.79531008 -1.10007672 -0.01897937 H -2.38715570 -0.10530429 0.88799439 H -1.79687960 2.21819829 -0.30071586 H 0.96477277 -2.03247893 -0.39377914	35 N -0.17370224 1.80359869 0.00000000 C 0.06912672 0.67858527 0.00000000 C 0.41042485 -0.72019692 0.00000000 N -0.44847055 -1.62962835 0.00000000 H 1.47790005 -0.96812248 0.00000000	36 N 0.00000000 0.00000000 1.84013200 C 0.00000000 0.00000000 0.68762500 C -0.00000000 0.00000000 -0.68762500 N -0.00000000 0.00000000 -1.84013200
37 C 2.20289145 0.86818230 0.00000000 C 1.38805763 -0.01928076 0.00000000 H 2.89136545 1.67517143 0.00000000 C -0.67517369 -1.02971803 0.00000000 N 0.60347680 -1.08742318 0.00000000 H -1.23060241 -1.96053470 0.00000000 N -2.09716430 1.13115377 0.00000000 C -1.44993381 0.17735801 0.00000000	38 C -1.58020459 -0.34946999 0.00000000 C -0.90014684 0.97399534 0.00000000 N 0.36019394 1.18023399 0.00000000 C 1.26454055 0.21693984 0.00000000 C 2.19472350 -0.55245342 0.00000000 N -1.01842830 -1.46379419 0.00000000 H -2.67859873 -0.30866353 0.00000000 H -1.54858271 1.84458136 0.00000000 H 2.96134620 -1.28506712 0.00000000	39 C 0.00000000 0.00000000 1.92229377 N 0.00000000 0.00000000 0.74482277 C 0.00000000 0.00000000 -0.56099823 C 0.00000000 0.00000000 -1.76006323 H 0.00000000 0.00000000 -2.82115323
40 C -0.55990495 1.07052102 0.00749296 C 0.78371106 0.99300408 -0.05385185 N 1.44094611 -0.20911889 -0.00973767 C 1.99125015 -1.23905986 0.03785149 C -1.94564483 -0.96117706 -0.24441607 N -1.36512693 0.00762600 0.19362094 H -1.04527599 2.03603000 -0.01267518 H 1.39326603 1.87893610 -0.12485883 H -2.49519288 -1.68424503 0.36789191	41 C 0.41926925 -1.59336067 0.00000000 H 0.35310094 -2.66664695 0.00000000 C -0.41620227 -0.58461691 0.00000000 H -1.49423432 -0.73991458 0.00000000 C 0.22681843 1.88165535 0.00000000 N -0.03402558 0.74064213 0.00000000	(Z)-42 C 0.00000000 0.66863800 0.97433385 H 0.00000000 1.20916800 1.90963385 C 0.00000000 -0.66863800 0.97433385 H 0.00000000 -1.20916800 1.90963385 N 0.00000000 -1.42958900 -0.15894515 C 0.00000000 -2.11952700 -1.10717015 C -0.00000000 2.11952700 -1.10717015 N -0.00000000 1.42958900 -0.15894515
(E)-42 C -0.45315442 0.49083262 0.00000000 H -1.51546203 0.28982093 0.00000000 C 0.45315442 -0.49083262 0.00000000 H 1.51546203 -0.28982093 0.00000000 N 0.08756514 -1.80851447 0.00000000 C -0.16262712 -2.95388430 0.00000000 C 0.16262712 2.95388430 0.00000000 N -0.08756514 1.80851447 0.00000000	44 C -0.17577875 1.60885439 0.00000000 C -0.65899817 -1.62274028 0.00000000 C 0.44675206 -0.84081741 0.00000000 N 0.20383213 0.52060505 0.00000000 H -0.60172830 2.58410760 0.00000000 H 1.50305252 -1.10012314 0.00000000	45 C 0.00000000 0.00000000 0.74907408 C -0.00000000 -0.00000000 -1.68567353 H -0.00000000 -0.00000000 -2.74800770 C -0.00000000 -0.00000000 2.00805988 N 0.00000000 0.00000000 -0.52582213

Appendix

46				47-S				47-T			
C	-0.03335434	3.26545588	0.00000000	C	0.00000000	-0.72990983	-1.17573085	C	0.00000000	-0.74883433	-1.19906611
C	1.17163486	2.55993639	0.00000000	C	0.00000000	0.00000000	0.80165997	C	0.00000000	0.00000000	0.79515350
N	1.19856647	1.21757160	0.00000000	H	0.00000000	-1.39063624	-2.03160136	H	0.00000000	-1.40522048	-2.05908952
C	0.02857786	0.60415420	0.00000000	N	0.00000000	1.18445213	0.04087833	N	0.00000000	1.17671506	0.02088403
C	-1.19321276	1.30180777	0.00000000	N	0.00000000	-1.18445213	0.04087833	N	0.00000000	-1.17671506	0.02088403
N	-1.21761295	2.63571952	0.00000000	C	0.00000000	0.00000000	2.13161898	C	0.00000000	0.00000000	2.24061250
H	-0.04847247	4.35349744	0.00000000	C	-0.00000000	0.72990983	-1.17573085	C	-0.00000000	0.74883433	-1.19906611
H	2.13136580	3.07299733	0.00000000	H	-0.00000000	1.39063624	-2.03160136	H	-0.00000000	1.40522048	-2.05908952
H	-2.14596239	0.77792188	0.00000000								
I	0.00668907	-1.53897321	0.00000000								
48				49				50			
C	0.00000000	0.00000000	-0.61286374	C	0.00000000	0.00000000	0.44740481	C	0.77497379	-1.02184796	0.00000000
N	0.00000000	1.19629900	-1.19689974	N	0.00000000	1.19740000	-0.13375219	H	1.29854832	-1.96750713	0.00000000
C	0.00000000	1.18581800	-2.53875774	C	0.00000000	1.18540200	-1.47450619	C	-0.56236839	-1.06515602	0.00000000
C	0.00000000	0.00000000	-3.27483274	C	0.00000000	0.00000000	-2.21122919	H	-1.08327578	-2.01334322	0.00000000
C	0.00000000	-1.18581800	-2.53875774	C	0.00000000	-1.18540200	-1.47450619	C	1.61402266	0.18567079	0.00000000
N	0.00000000	-1.19629900	-1.19689974	N	0.00000000	-1.19740000	-0.13375219	H	2.69852955	0.00582125	0.00000000
H	0.00000000	2.15917200	-3.02732874	H	0.00000000	2.15855500	-1.96338019	N	1.23096535	1.37635442	0.00000000
H	0.00000000	0.00000000	-4.36049974	H	0.00000000	0.00000000	-3.29667219	C	-2.14099528	0.92197296	0.00000000
H	0.00000000	-2.15917200	-3.02732874	H	0.00000000	-2.15855500	-1.96338019	N	-1.37776517	0.03095850	0.00000000
I	0.00000000	0.00000000	1.52760426	CI	0.00000000	0.00000000	2.19841081				
51				52				53			
C	-0.43132357	-1.64104733	0.00000000	N	0.00000000	0.67354700	-1.09247482	N	-1.22627741	1.20550258	0.00000000
H	-0.39791745	-2.71755110	0.00000000	C	0.00000000	1.32177800	0.06171818	C	-0.02706254	0.65037734	0.00000000
C	0.42807671	-0.65093421	0.00000000	C	0.00000000	0.69107800	1.32049518	C	1.19872698	1.36000242	0.00000000
H	1.50151835	-0.84819726	0.00000000	C	0.00000000	-0.69107800	1.32049518	C	1.13345426	2.74362301	0.00000000
C	0.05594921	0.72760391	0.00000000	C	0.00000000	-1.32177800	0.06171818	C	-0.17343553	3.25410112	0.00000000
N	-0.20283071	1.85028773	0.00000000	N	0.00000000	-0.67354700	-1.09247482	N	-1.25391407	2.57453425	0.00000000
				H	0.00000000	1.26338400	2.24264018	H	2.14809842	0.83293333	0.00000000
				H	0.00000000	-1.26338400	2.24264018	H	2.01916024	3.37171981	0.00000000
				I	0.00000000	3.44937700	-0.05450182	I	0.00762231	-1.48516102	0.00000000
				I	0.00000000	-3.44937700	-0.05450182				
55				(Z)-57				(E)-57			
N	1.23161387	1.08906172	0.00000000	N	0.00000000	0.63402600	-1.11065165	N	-0.46843944	0.42787440	0.00000000
C	-0.03906798	0.66006474	0.00000000	C	0.00000000	1.33000200	0.03591335	C	-0.08685364	1.70978968	0.00000000
C	-1.24045855	1.35443935	0.00000000	C	0.00000000	2.10396800	0.96012435	C	0.07336785	2.90381901	0.00000000
C	-1.15116940	2.81551547	0.00000000	C	0.00000000	-2.10396800	0.96012435	C	-0.07336785	-2.90381901	0.00000000
C	0.18270331	3.05631625	0.00000000	C	0.00000000	-1.33000200	0.03591335	C	0.08685364	-1.70978968	0.00000000
N	1.34135435	2.69610519	0.00000000	N	0.00000000	-0.63402600	-1.11065165	N	0.46843944	-0.42787440	0.00000000
H	-2.20903185	0.86835857	0.00000000	H	0.00000000	2.75485600	1.79833535	H	0.25723686	3.94873289	0.00000000
H	-1.98087507	3.50610625	0.00000000	H	0.00000000	-2.75485600	1.79833535	H	-0.25723686	-3.94873289	0.00000000
I	-0.00628141	-1.47525751	0.00000000								
58				(Z)-59				60			
C	0.00000000	1.19011700	0.73911000	C	0.00000000	0.67372200	1.07563195	C	-1.39987461	-0.32807776	0.00000000
C	0.00000000	0.00000000	1.35076700	H	0.00000000	1.18437000	2.03144795	C	-0.44230910	-1.26561416	0.00000000
C	0.00000000	-1.19011700	0.73911000	C	0.00000000	1.49447600	-0.07423705	C	0.89379170	-0.96826534	0.00000000
C	-0.00000000	-1.19011700	-0.73911000	C	0.00000000	2.22853400	-1.02713605	C	1.36808620	0.37845310	0.00000000
C	-0.00000000	0.00000000	-1.35076700	H	0.00000000	2.86387800	-1.87700105	C	0.32281089	1.27112435	0.00000000
C	-0.00000000	1.19011700	-0.73911000	C	0.00000000	-1.49447600	-0.07423705	N	-0.86676286	0.99973967	0.00000000
H	0.00000000	2.16991900	1.19232600	C	0.00000000	-2.22853400	-1.02713605	H	1.66353462	-1.73130164	0.00000000
H	0.00000000	-2.16991900	1.19232600	H	0.00000000	-2.86387800	-1.87700105	H	-2.47302713	-0.39903737	0.00000000
H	-0.00000000	-2.16991900	-1.19232600	C	0.00000000	-0.67372200	1.07563195	H	2.42180201	0.60644014	0.00000000
H	-0.00000000	2.16991900	-1.19232600	H	0.00000000	-1.18437000	2.03144795				
(Z)-61				(Z)-62				63			
C	0.59574807	1.08120311	0.00000000	C	0.58574164	1.09098530	0.00000000	C	0.00000000	0.00000000	2.47904906
H	1.07978647	2.05307574	0.00000000	H	1.04161460	2.07426759	0.00000000	N	0.00000000	1.19630700	1.87735606
C	1.44195842	-0.05882435	0.00000000	C	1.46559005	-0.01270844	0.00000000	C	0.00000000	1.17944200	0.55060106
C	2.17961778	-1.00809059	0.00000000	C	2.24236767	-0.92996123	0.00000000	C	0.00000000	0.00000000	-0.20111194
H	2.82107676	-1.85436046	0.00000000	H	2.91430476	-1.75197117	0.00000000	C	0.00000000	-1.17944200	0.55060106
C	-1.41187105	-0.03623503	0.00000000	C	-1.49279925	-0.19352378	0.00000000	N	0.00000000	-1.19630700	1.87735606
C	-2.17873185	-0.96653922	0.00000000	C	-0.75703049	1.02044587	0.00000000	H	0.00000000	0.00000000	3.56702206
				H	-1.34108095	1.93083605	0.00000000	H	0.00000000	0.00000000	-1.28407694

Appendix

H	-2.82862964	-1.80402971	0.00000000	N	-2.12543658	-1.15779412	0.00000000	I	0.00000000	3.06186100	-0.46076194
N	-0.69036597	1.07660441	0.00000000					I	0.00000000	-3.06186100	-0.46076194
64				(Z)-66				(E)-66			
C	1.08415181	2.61594053	0.00000000	C	-0.75440163	0.97387041	0.00000000	C	-0.49299930	-0.40558642	0.00000000
N	-0.05477235	3.33930092	0.00000000	N	-1.38924547	-0.25254042	0.00000000	N	-1.82682762	-0.06432107	0.00000000
C	-1.16398650	2.67763431	0.00000000	C	-1.91212699	-1.30001777	0.00000000	C	-2.97807631	0.14329588	0.00000000
C	-1.28433022	1.29196681	0.00000000	C	2.13492061	-0.81132319	0.00000000	C	2.86067530	-0.08923896	0.00000000
C	-0.04029761	0.64186138	0.00000000	C	1.32922996	0.07671974	0.00000000	C	1.68418717	0.14188047	0.00000000
N	1.12387493	1.28290211	0.00000000	N	0.50149691	1.12917230	0.00000000	N	0.39147947	0.49738303	0.00000000
H	2.02985049	3.15264785	0.00000000	H	-1.41160288	1.83301604	0.00000000	H	-0.29668618	-1.47507519	0.00000000
H	-2.22975976	0.76219198	0.00000000	H	2.84011112	-1.60493435	0.00000000	H	3.90140207	-0.29846442	0.00000000
I	0.02156540	-1.50254112	0.00000000								
1-m-(2,4)-T				1-p-(2,5)-S				1-p-(2,5)-T			
C	-0.95074244	-0.91524653	0.00000000	C	0.00000000	0.00000000	-1.21338380	C	0.00000000	0.00000000	-1.24622900
N	-1.31456542	0.32971422	0.00000000	N	0.00000000	1.16245500	-0.76992680	N	0.00000000	1.19812000	-0.71739700
C	-0.30545110	1.22204565	0.00000000	C	0.00000000	1.17817300	0.66271520	C	0.00000000	1.20735800	0.62767700
C	1.03100764	0.83326979	0.00000000	C	0.00000000	0.00000000	1.32718820	C	0.00000000	0.00000000	1.28748500
C	1.23499806	-0.53976539	0.00000000	C	0.00000000	-1.17817300	0.66271520	C	0.00000000	-1.20735800	0.62767700
N	0.27021148	-1.39054768	0.00000000	N	0.00000000	-1.16245500	-0.76992680	N	0.00000000	-1.19812000	-0.71739700
H	-0.58234633	2.27006975	0.00000000	H	0.00000000	2.17601800	1.07178320	H	0.00000000	2.16561700	1.13194900
H	1.83395093	1.55394335	0.00000000	H	0.00000000	-2.17601800	1.07178320	H	0.00000000	-2.16561700	1.13194900
1-o-(4,5)-S				1-o-(4,5)-T				1-m-(4,6)-S			
C	-1.03411193	-0.70045412	0.00000000	C	-0.69732190	1.01876184	0.00000000	C	0.00000000	0.00000000	-1.32487418
N	0.16595247	-1.23008188	0.00000000	N	0.61547870	1.14629672	0.00000000	N	0.00000000	1.14317900	-0.62850517
C	1.25339174	-0.43423869	0.00000000	C	1.32554209	-0.00040703	0.00000000	C	0.00000000	1.09869800	0.63934883
C	1.13428169	0.98181186	0.00000000	C	0.70259437	-1.22379230	0.00000000	C	0.00000000	0.00000000	1.48673783
C	-0.12009791	1.18129584	0.00000000	C	-0.68192475	-1.27104294	0.00000000	C	0.00000000	-1.09869800	0.63934883
N	-1.26644337	0.67188450	0.00000000	N	-1.32879366	-0.16749038	0.00000000	N	0.00000000	-1.14317900	-0.62850517
H	2.21426646	-0.93363220	0.00000000	H	2.40543807	0.09381149	0.00000000	H	0.00000000	0.00000000	-2.40552117
H	-1.91161173	-1.32947551	0.00000000	H	-1.30557226	1.91342671	0.00000000	H	0.00000000	0.00000000	2.56122583
1-m-(4,6)-T				2-o-(3,4)-S				2-o-(3,4)-T			
C	0.00000000	0.00000000	-1.27088985	N	-1.41358926	0.41373407	0.00000000	N	-1.28913531	0.24107149	0.00000000
N	0.00000000	1.17852600	-0.63871285	C	-0.37186738	1.11657618	0.00000000	C	-1.02026013	-1.00396101	0.00000000
C	0.00000000	1.14630700	0.65313715	C	0.89824723	1.17324887	0.00000000	C	0.30221212	-1.39596382	0.00000000
C	0.00000000	0.00000000	1.42896315	C	1.37245007	-0.13527779	0.00000000	C	1.26525618	-0.43055053	0.00000000
C	0.00000000	1.14630700	0.65313715	C	0.35226003	-1.13093537	0.00000000	C	0.83518245	0.91438226	0.00000000
N	0.00000000	-1.17852600	-0.63871285	N	-0.94944021	-0.92004517	0.00000000	N	-0.44783387	1.24648159	0.00000000
H	0.00000000	0.00000000	-2.35248285	H	2.41915452	-0.41559230	0.00000000	H	2.32518320	-0.65298936	0.00000000
H	0.00000000	0.00000000	2.50837715	H	0.61551212	-2.18190128	0.00000000	H	1.53925732	1.73667644	0.00000000
2-m-(3,5)-S				2-m-(3,5)-T				2-p-(3,6)-T			
N	-0.57901754	1.16885473	0.00000000	N	-0.42445838	1.30127255	0.00000000	N	0.00000000	0.67862000	-1.21963015
C	0.65353375	1.00513101	0.00000000	C	0.83208536	1.02129344	0.00000000	C	0.00000000	1.27696700	-0.09957015
C	1.54041487	-0.07442158	0.00000000	C	1.40781704	-0.24772370	0.00000000	C	0.00000000	0.68809700	1.17548585
C	0.64734830	-1.08543130	0.00000000	C	0.49389657	-1.25769421	0.00000000	C	0.00000000	-0.68809700	1.17548585
C	-0.72868425	-1.03331929	0.00000000	C	-0.86779084	-0.99156510	0.00000000	C	0.00000000	-1.27696700	-0.09957015
N	-1.41261126	0.13002674	0.00000000	N	-1.29507339	0.27043909	0.00000000	N	0.00000000	-0.67862000	-1.21963015
H	-1.35106473	-1.91717637	0.00000000	H	-1.63880260	-1.74864954	0.00000000	H	0.00000000	-1.27676300	2.08191685
H	2.61679030	-0.04674694	0.00000000	H	2.47947616	-0.39919460	0.00000000	H	-0.00000000	1.27676300	2.08191685
2-o-(4,5)-S				2-o-(4,5)-T				3-o-(2,3)-S			
N	0.00000000	0.63603500	-1.07731195	N	0.00000000	0.60669800	-1.08293575	C	0.05424430	1.19085607	0.00000000
C	0.00000000	1.38469700	0.05967905	C	0.00000000	1.36327000	0.04030025	C	1.22631239	0.43240127	0.00000000
C	0.00000000	0.63008400	1.20686505	C	0.00000000	0.67276100	1.24214725	N	1.07081349	-0.92986564	0.00000000
C	0.00000000	-0.63008400	1.20686505	C	0.00000000	-0.67276100	1.24214725	C	-0.15168567	-1.13621582	0.00000000
C	0.00000000	-1.38469700	0.05967905	C	0.00000000	-1.36327000	0.04030025	C	-1.37961183	-0.72720546	0.00000000
N	0.00000000	-0.63603500	-1.07731195	N	0.00000000	-0.60669800	-1.08293575	N	-1.19090136	0.69223444	0.00000000
H	0.00000000	-2.45647200	-0.05808095	H	0.00000000	-2.43258200	-0.11413475	H	0.11576534	2.27238298	0.00000000
H	-0.00000000	2.45647200	-0.05808095	H	-0.00000000	2.43258200	-0.11413475	H	2.22929462	0.83201899	0.00000000

Appendix

3-o-(2,3)-T				3-p-(2,5)-S				3-p-(2,5)-T			
C	0.00000000	0.69151000	1.04594610	C	1.38620466	0.17939851	0.00000000	C	1.28444614	0.44014851	0.00000000
C	0.00000000	-0.69151000	1.04594610	C	0.47027008	1.22393666	0.00000000	C	0.17007806	1.27156949	0.00000000
N	0.00000000	-1.35475800	-0.12748790	N	-0.76881430	1.02983906	0.00000000	N	-1.06083925	0.88059649	0.00000000
C	0.00000000	-0.69647200	-1.22404290	C	-1.38620466	-0.17939851	0.00000000	C	-1.28444614	-0.44014851	0.00000000
C	-0.00000000	0.69647200	-1.22404290	C	-0.47027008	-1.22393666	0.00000000	C	-0.17007806	-1.27156949	0.00000000
N	-0.00000000	1.35475800	-0.12748790	N	0.76881430	-1.02983906	0.00000000	N	1.06083925	-0.88059649	0.00000000
H	0.00000000	1.26765300	1.96099610	H	2.46118282	0.24244518	0.00000000	H	2.30169073	0.80354863	0.00000000
H	0.00000000	-1.26765300	1.96099610	H	-2.46118282	-0.24244518	0.00000000	H	-2.30169073	-0.80354863	0.00000000
3-m-(2,6)-S				3-m-(2,6)-T							
C	0.00000000	1.16617700	0.61412107	C	0.00000000	1.14827800	-0.63082288				
C	0.00000000	1.18404100	-0.83467793	C	0.00000000	1.11059000	0.75886613				
N	0.00000000	0.00000000	-1.19062292	N	0.00000000	0.00000000	1.43076012				
C	0.00000000	-1.18404100	-0.83467793	C	0.00000000	-1.11059000	0.75886613				
C	0.00000000	-1.16617700	0.61412107	C	0.00000000	-1.14827800	-0.63082288				
N	0.00000000	0.00000000	1.23005808	N	0.00000000	0.00000000	-1.31027288				
H	0.00000000	2.08087200	1.18531808	H	0.00000000	2.07261200	-1.18996488				
H	0.00000000	-2.08087200	1.18531808	H	0.00000000	-2.07261200	-1.18996488				
TS1a-4				TS4-5,6				TS5-7			
C	-0.26124001	-1.25761240	0.00000000	C	1.37156796	-0.10865471	0.00000000	C	0.03538699	-0.67726992	0.00000000
N	-1.35003217	-0.48871731	0.00000000	N	0.83654886	1.10547524	0.00000000	N	-0.21710302	0.64051338	0.00000000
C	-1.04987916	0.77943491	0.00000000	C	-0.36561717	1.42582214	0.00000000	C	0.31609963	1.82168573	0.00000000
C	0.28739632	1.33924349	0.00000000	C	-2.01491503	-0.17579600	0.00000000	N	0.06273297	-1.83431098	0.00000000
C	1.39211384	0.59589844	0.00000000	C	-1.52769694	-1.28867396	0.00000000	H	-1.02832943	1.49008833	0.00000000
N	0.90648886	-1.43947946	0.00000000	N	1.96813005	-1.10128666	0.00000000				
H	-1.88920221	1.46703552	0.00000000	H	-0.68853626	2.46984211	0.00000000				
H	0.34588054	2.42731569	0.00000000	H	-2.78604610	0.55828193	0.00000000				
H	2.43777896	0.86123953	0.00000000	H	-0.93820286	-2.17362891	0.00000000				
TS5-12,9				TS5-13,11				TS7-8,9			
C	-0.24452135	0.90810020	0.00000000	C	0.00325729	-0.72564412	0.00000000	C	0.26627630	0.86454607	0.00000000
N	0.43608229	-0.84876151	0.00000000	N	-0.15395279	0.56862020	0.00000000	N	0.37987568	-1.03371976	0.00000000
C	-0.15146564	-1.84524457	0.00000000	C	-0.29023292	1.74032502	0.00000000	C	-0.63740441	-1.67767367	0.00000000
N	0.01215353	2.04073907	0.00000000	N	0.14074633	-1.87152764	0.00000000	N	-0.25855828	1.89800092	0.00000000
H	-0.76172878	-2.72097673	0.00000000	H	1.81429905	3.03226672	0.00000000	H	1.37754684	-1.17120251	0.00000000
TS4-10,11				TS1b-14				TS14-15,12			
C	-1.42306809	-0.05902518	0.00000000	C	-1.22017494	-0.86658440	-0.04572419	C	1.50109551	-1.25452222	0.02352876
N	-0.73206544	1.07751663	0.00000000	N	-1.18113710	1.17585474	-0.07471508	N	-1.87471147	-1.14149435	0.01153473
C	0.55294957	1.09299869	0.00000000	C	-0.01148860	1.31909184	0.02741795	C	-1.36395820	-0.10727248	-0.01174715
C	1.38585394	-0.06719757	0.00000000	C	1.23265970	0.66212920	0.06951294	C	-0.72815387	1.16841536	-0.05027700
C	1.76285272	-1.21880880	0.00000000	C	1.12250847	-0.69650718	-0.08635714	C	0.56786517	1.33184001	0.15994603
N	-2.12559266	-0.97960275	0.00000000	N	-0.07203831	-1.33084738	0.05524281	N	1.78594080	-0.13307227	-0.13472911
H	1.02881396	2.06618264	0.00000000	H	-2.13565256	-1.26170663	0.38344177	H	-1.37747965	2.01660655	0.25794392
H	3.10611367	0.94992219	0.00000000	H	2.17751393	1.16548050	0.18992998	H	1.15302140	2.23535286	0.13122214
H	2.19715023	-2.18930478	0.00000000	H	1.98933868	-1.32760213	-0.22616315	H	0.98476127	-2.16075711	0.26037865
TS14-17,11				TS15-16,11				TS1b-18			
C	2.12475726	-0.90459067	-0.31552059	N	0.11805230	-1.90613359	0.00000000	C	1.26674615	-0.51677244	-0.03650713
N	-2.16070272	-1.13705731	-0.03827279	C	0.02480399	-0.75548754	0.00000000	N	0.21911738	-1.34736275	0.05070469
C	-1.51502387	-0.18453119	0.02843407	C	-0.08273767	0.61774004	0.00000000	C	-0.93152179	-0.76804407	0.01403171
C	-0.76028307	1.01293995	0.11558189	C	0.20308202	1.79676983	0.00000000	C	-1.81586302	0.08909669	-0.00827321
C	0.57417792	1.07422315	0.02697795	H	-2.00382560	0.53410414	0.00000000	C	0.07432358	1.51269922	-0.10600889
N	1.38093111	-0.01057576	-0.15846880	H	0.30656940	2.85469707	0.00000000	N	1.08690778	0.79442550	0.02346706
H	-1.31219423	1.93055989	0.26307068					H	2.26487726	-0.91995015	-0.09507913
H	1.08891976	2.02222424	0.10124880					H	-2.76985014	0.53964344	-0.13657420
H	3.13990630	-1.90760009	1.88003166					H	-0.19931269	2.34899106	0.53299622
TS18-19,12				TS18-22,11				TS19-20			
C	-0.68957992	-1.22879297	0.20113118	C	-0.58079908	-1.07515613	0.04404515	C	-0.30947804	-1.87972694	0.00000000
N	0.52805403	-1.14464693	0.09120000	N	0.68880292	-1.07017914	0.13297425	N	0.20111353	-0.68845011	0.00000000
C	1.34374100	-0.11206890	-0.00790115	C	1.42730495	0.02889283	0.03825012	C	-0.02976273	0.62587681	0.00000000
C	2.16764797	0.77016814	-0.00250429	C	2.19472098	0.95394580	-0.03153297	C	-0.04724276	1.82983850	0.00000000
C	-1.48573905	1.35642999	0.02095924	C	-2.03788600	0.98311585	-0.33288128	H	1.02460098	-1.52539409	0.00000000
N	-1.76086503	0.23158997	0.14254369	N	-1.36416804	0.03703486	-0.15963708	H	-0.11349452	2.88861465	0.00000000

Appendix

H	-1.30055091	-2.10127300	-0.00194471	H	-1.12204211	-2.00821210	0.12985526				
H	2.89917694	1.53694417	0.01429358	H	2.84781800	1.78699577	-0.09691105				
H	-0.98536904	2.24131002	0.35374714	H	-3.01826513	2.10843622	1.84640947				
TS _{20-21,8}				TS _{1c-23}				TS _{23-24,12}			
C	-0.72041712	-1.64068898	0.00000000	C	0.66973479	1.17872901	0.00000000	C	-1.80709618	-0.39233113	0.15252713
N	0.36210815	-1.13919430	0.00000000	N	1.51387694	0.23886736	0.00000000	N	-1.25647214	-1.36900008	-0.19905594
C	0.42708074	0.85192170	0.00000000	C	0.46006301	-1.68048334	0.00000000	C	2.18716684	-0.79719185	0.07660977
C	-0.24245671	1.86387975	0.00000000	C	-0.66062265	-1.18670594	0.00000000	C	1.35123778	0.06206609	0.01391686
H	-0.67024333	2.83754456	0.00000000	C	-1.35832624	0.04776042	0.00000000	C	0.46700469	1.17326603	-0.05990704
H	1.35024478	-1.31385930	0.00000000	N	-0.74102865	1.17935142	0.00000000	N	-0.79364231	1.23973995	-0.03168493
				H	1.08049087	2.19466112	0.00000000	H	-2.69020818	0.07641380	0.53890121
				H	-2.44308501	0.07087762	0.00000000	H	0.96439062	2.14781307	-0.15172506
				H	1.28756259	-2.34887105	0.00000000	H	2.88673990	-1.59426080	0.12912969
TS _{23-10,11}				TS _{24-16,11}				TS _{2a-25}			
C	-1.39374108	-0.15278558	0.05042605	C	-0.07275610	1.85845871	0.00000000	N	-0.72398318	-1.40501882	0.00000000
N	-2.19096627	-0.97589936	-0.18415009	C	-0.01183711	0.65971467	0.00000000	C	0.46930773	-1.26669957	0.00000000
C	2.25998475	-0.89604837	-0.04893024	C	0.05954982	-0.71752931	0.00000000	C	1.40063591	-0.19511814	0.00000000
C	1.45803295	-0.00109619	-0.02716303	N	-0.22859695	-1.85013087	0.00000000	C	0.83797181	1.03066445	0.00000000
C	0.54619119	1.08413001	-0.02441578	H	1.88453145	-0.77187431	0.00000000	C	-0.60816456	1.16318983	0.00000000
N	-0.73403882	1.01786428	0.01744525	H	-0.13409251	2.91892601	0.00000000	N	-1.48871055	0.24231317	0.00000000
H	-0.67311918	-0.87980805	1.59955588					H	2.46720410	-0.36098633	0.00000000
H	0.97227641	2.08228092	-0.06818060					H	1.43941488	1.92975006	0.00000000
H	2.95307157	-1.70142651	-0.06394342					H	-1.01626829	2.17795645	0.00000000
TS _{25-15,12}				TS _{25-26,11}				TS _{2a-27}			
N	2.02749105	-1.18957754	0.00000000	N	-2.21168090	-1.00661491	0.08944670	N	-1.38962442	0.09162238	0.00000000
C	1.45925361	-0.18746989	0.00000000	C	-1.50232193	-0.10123188	0.01639480	C	-0.54919111	1.12076981	0.00000000
C	0.86341474	1.10710076	0.00000000	C	-0.67818495	1.05180215	-0.07380707	C	0.48251491	1.77043758	0.00000000
C	-0.42261026	1.38321417	0.00000000	C	0.66116305	1.03919419	-0.06663090	C	1.48168031	-0.38474994	0.00000000
C	-2.05485578	-0.22025229	0.00000000	C	1.45051108	-0.15359678	0.01785919	C	0.50003710	-1.28538507	0.00000000
N	-1.58547124	-1.28188568	0.00000000	N	1.91932114	-1.20334576	-0.16483877	N	-0.89296325	-1.08559660	0.00000000
H	1.57684462	1.93230159	0.00000000	H	-1.19546298	1.99928313	-0.15004313	H	1.21306136	2.54283058	0.00000000
H	-0.93478626	2.33426132	0.00000000	H	1.20418502	1.97176521	-0.12344781	H	2.54964874	-0.56096219	0.00000000
H	-2.80741087	0.53812307	0.00000000	H	2.45079287	0.48167024	1.43833933	H	0.72515628	-2.35048317	0.00000000
TS ₂₇₋₂₈				TS _{28-29,30}				TS _{29-31,11}			
N	-1.30893447	-0.26363387	0.00000000	N	1.35516074	-1.37581738	-0.13033429	C	0.01641102	-0.70640990	0.00000000
C	0.17031065	0.94180688	0.00000000	C	-1.38355286	0.07363048	0.00349087	C	0.09230630	-1.90690548	0.00000000
C	-0.01045145	2.18970151	0.00000000	C	-2.18171249	-0.82405085	0.03030285	C	-0.07497141	0.66400795	0.00000000
C	1.16092475	-0.08327082	0.00000000	C	-0.51250332	1.19243684	-0.02112209	C	0.21613420	1.84662617	0.00000000
C	0.66133523	-1.32779470	0.00000000	C	0.80899268	1.18167839	-0.04683613	H	0.16504613	-2.96561589	0.00000000
N	-0.76846598	-1.33189442	0.00000000	N	1.78429133	-0.37793622	0.16057375	H	-1.95267136	0.67543131	0.00000000
H	-0.74325080	2.96953863	0.00000000	H	-2.86501215	-1.63573914	0.05012682	H	0.28834458	2.90627212	0.00000000
H	2.21392763	0.14770115	0.00000000	H	-1.00318773	2.16677064	-0.01911602				
H	1.17841126	-2.27119892	0.00000000	H	1.50469134	2.00307467	-0.03770010				
TS _{2b-28}				TS _{2b-32}				TS _{32-24,12}			
N	-0.01959546	-1.52291497	-0.00927103	N	1.24550218	-0.60116147	-0.12076125	N	-0.62063237	1.14680525	0.00000000
C	-1.65530338	-0.19617741	0.01155102	C	0.16118129	-1.36134222	0.05056669	C	0.64465676	1.07141732	0.00000000
C	-1.08091766	0.90221769	-0.00941407	C	-1.09704900	-0.75374175	0.05947669	C	1.49402433	-0.07278688	0.00000000
C	0.25649505	1.35511060	-0.01268118	C	-1.71716276	0.30670198	-0.02658627	C	2.30438835	-0.95931551	0.00000000
C	1.25423463	0.44719604	0.03387480	C	0.23026268	1.54100671	-0.06926516	C	-2.42371820	-0.62315172	0.00000000
N	1.02265744	-0.94710460	-0.01905012	N	1.10749167	0.67879068	0.06182182	N	-1.24447809	-0.49205167	0.00000000
H	0.50122069	2.40986321	-0.05632124	H	-2.51478597	0.98107093	-0.23355925	H	2.99380911	-1.76649089	0.00000000
H	2.29964104	0.71209940	0.05547172	H	0.25148079	2.50400866	0.43799189	H	-3.21148627	-1.35050958	0.00000000
H	-2.46934745	-0.88190713	0.05911410	H	0.32895504	-2.42423242	0.12299163	H	1.15734296	2.03674613	0.00000000
TS _{32-33,11}				TS _{3a-34}				TS _{34-35,6}			
N	-0.72850216	1.11976289	0.02306612	C	-0.10447449	-1.36620668	0.00000000	C	-1.85803222	-0.22581765	0.00000000
C	0.55106783	1.12407799	0.09033518	C	1.16911262	-0.99633488	0.00000000	C	-1.34451185	-1.33869040	0.00000000
C	1.39358193	-0.01983194	0.02031413	N	1.28012300	1.17710255	0.00000000	N	1.99259885	-1.02008424	0.00000000
C	2.10506801	-0.98156288	-0.03746790	C	0.12060631	1.35116104	0.00000000	C	1.34114835	-0.06971154	0.00000000
C	-1.91762998	-1.05764819	-0.24303009	C	-1.17295905	0.72574247	0.00000000	C	0.62087823	1.17804648	0.00000000
N	-1.29753906	-0.07173614	-0.12706399	N	-1.24337584	-0.55405310	0.00000000	N	-0.62185291	1.37127860	0.00000000
H	2.73039308	-1.84063982	-0.08733693	H	-0.35258021	-2.42727310	0.00000000	H	-2.72061793	0.39964770	0.00000000
H	-2.34421098	-1.98559035	1.62212683	H	2.10077851	-1.53626052	0.00000000	H	-0.69899846	-2.18344193	0.00000000
H	1.00357975	2.09983302	0.21228726	H	-2.07914071	1.31601574	0.00000000	H	1.26749978	2.06247231	0.00000000

Appendix

TS_{34-37,11}				TS_{3a-38}				TS_{38-19,12}			
C	-1.38087805	-0.02349489	0.04614024	C	0.75719758	-1.13637958	0.00000000	C	-2.01482920	-0.33217519	0.00000000
C	-2.35723302	-0.72809194	-0.13789270	C	-0.72083569	-1.11435575	0.00000000	C	-0.55098915	1.32124878	0.00000000
N	2.24328800	-1.04812873	-0.08002085	N	-1.42575185	-0.03415374	0.00000000	N	0.65918561	1.08812485	0.00000000
C	1.51168196	-0.15889876	-0.01800485	C	-0.71735732	1.08954747	0.00000000	C	1.43135777	0.02636688	0.00000000
C	0.68663291	1.01573720	-0.00499786	C	0.36718261	1.66872660	0.00000000	C	2.27200214	-0.83760602	0.00000000
N	-0.58943910	1.04885514	0.01394018	N	1.54730490	-0.15104165	0.00000000	N	-1.50683291	-1.38243576	0.00000000
H	-0.48288895	-1.08796481	1.39784125	H	1.19687290	-2.14347991	0.00000000	H	-2.86621903	0.31892497	0.00000000
H	-3.07197199	-1.51005597	-0.21107065	H	-1.24223448	-2.06578578	0.00000000	H	-0.97283105	2.32940009	0.00000000
H	1.21669586	1.96142622	-0.03567491	H	1.07736720	2.46040096	0.00000000	H	2.94733176	-1.65515536	0.00000000
TS_{38-37,11}				TS_{19-39,11}				TS_{58-(Z)-59}			
C	1.42790211	-0.19960924	0.05718213	C	-0.28097195	1.79105391	0.00000000	C	0.00000000	0.96297200	1.20093505
C	0.62880418	1.00701581	0.03045428	N	-0.15328642	0.62020003	0.00000000	C	0.00000000	1.35689200	0.00384805
N	-0.64388081	1.07902790	-0.02625077	C	-0.00902834	-0.67706825	0.00000000	C	0.00000000	0.70001500	-1.21564395
C	-1.44535087	0.02436894	-0.03513897	C	0.12256446	-1.86902406	0.00000000	C	0.00000000	-0.70001500	-1.21564395
C	-2.28483292	-0.84082200	-0.05892214	H	1.83839883	3.11253686	0.00000000	C	0.00000000	-1.35689200	0.00384805
N	2.27764707	-0.96038425	-0.16790594	H	0.23922108	-2.92370666	0.00000000	C	0.00000000	-0.96297200	1.20093505
H	0.39623999	-1.07276039	1.43375795					H	0.00000000	1.23505100	2.23523405
H	1.19663123	1.93114378	0.03951545					H	0.00000000	1.20551200	-2.17006895
H	-2.98836997	-1.63460996	-0.07562829					H	0.00000000	-1.20551200	-2.17006895
								H	0.00000000	-1.23505100	2.23523405
TS_{60-(Z)-62}				TS_{60-(Z)-61}							
N	-0.90754724	1.10930387	0.00000000	C	0.53330839	1.12133234	0.00000000				
C	0.27888500	1.27420083	0.00000000	C	1.58106379	0.43909083	0.00000000				
C	-1.40762434	-0.48875135	0.00000000	C	0.57653425	-1.39168003	0.00000000				
C	-0.39583639	-1.28092570	0.00000000	C	-0.67050440	-1.21131926	0.00000000				
C	0.94954451	-0.94454393	0.00000000	C	-1.40775783	-0.01563032	0.00000000				
C	1.35734994	0.39676878	0.00000000	N	-0.74748604	1.14251118	0.00000000				
H	-2.47778682	-0.49013775	0.00000000	H	1.39534278	-2.07942854	0.00000000				
H	1.73738794	-1.68748230	0.00000000	H	2.64770353	0.39089467	0.00000000				
H	2.39931722	0.67200114	0.00000000	H	-2.48650919	0.04019424	0.00000000				

Mayank Saraswat

Address: Hathras, India **Phone:** +91 90419 86427 **Email:** saraswat.mayank20@gmail.com

EDUCATION

Ph.D., Indian Institute of Science Education and Research Mohali 2015- ongoing
2013 - 2015
M.S., Indian Institute of Science Education and Research Mohali
CGPA: 9.2/10
2010 - 2013
B.Sc., Saraswati Degree College (Agra University), India
Percentage: 77.8%
2009 - 2010
Class XII., Mahatma Gandhi Inter college, Hathras, India
Percentage: 80.4%

RESEARCH EXPERIENCE

05/2015 - 07/2015
Summer Internship, IISER Mohali

- Advisor: Dr. Sugumar Venkataramani
- Understanding the electronic structure and reactivity of Dehydro-diazine radicals

01/2015 - 05/2015
Masters project, IISER Mohali

- Advisor: Dr. Sugumar Venkataramani
- Synthesis and characterization of substituted phenylazo 1,3-cyclohexadione derivatives

05/2014 - 07/2014
Summer Internship, IISER Mohali

- Advisor: Dr. Angshuman Roy Choudhury
- In-situ crystallization of fluoro- phenols and anilines under cryogenic condition

ADDITIONAL SKILLS

Technical: Ultra-high Vacuum technology
Spectroscopy: Infrared spectroscopy, Matrix-Isolation technique
Computational: Gaussian, MOLPRO, CFOUR, GaussSum

AWARDS

- **Lindau Nobel Laureate Meeting:** Selected to attend the (postponed) meeting in 2021. Funded by DST, India
- **CSIR Fellowship (JRF/SRF):** All India Rank- 66
- **Best Poster Award:** ChemCYS- Chemistry Conference for Young Scientists, Belgium (February 2020)
- **Best Poster Award:** 1st CRIKC Chemistry Symposium, India (November 2019)
- **CSIR Travel Grant:** For attending International Symposium on Molecular Spectroscopy 2019, Illinois, U.S.
- **Certificate(s) of Academic Excellence:** Highest grade point for semesters January 2014- April 2014 and August 2014- November 2014

